

Detailed Stochastic Finite Element Simulation in Geotechnics



Theofilos Manitaras

Supervisor: **Professor Manolis Papadrakakis**

School of Civil Engineering
National Technical University of Athens

This dissertation is submitted for the degree of
Doctor of Engineering

April 2017



NATIONAL TECHNICAL UNIVERSITY OF ATHENS
SCHOOL OF CIVIL ENGINEERING

Detailed Stochastic Finite Element Simulation in Geotechnics

Theofilos-Ioannis Manitaras

A Thesis submitted for the Degree of
Doctor of Engineering

Athens, April 2017

Λεπτομερής Προσομοίωση Προβλημάτων Γεωτεχνικής Μηχανικής με Στοχαστικά Πεπερασμένα Στοιχεία

Θεόφιλος-Ιωάννης Μανιταράς

Η διατριβή υποβλήθηκε
στη Σχολή Πολιτικών Μηχανικών
του Εθνικού Μετσόβιου Πολυτεχνείου
προς εκπλήρωση των προϋποθέσεων
του τίτλου του Διδάκτορος Μηχανικού

Απρίλιος 2017

Επιβλέπων Καθηγητής:
Μανόλης Παπαδρακάκης

ΕΘΝΙΚΟ ΜΕΤΣΟΒΙΟ ΠΟΛΥΤΕΧΝΕΙΟ
ΣΧΟΛΗ ΠΟΛΙΤΙΚΩΝ ΜΗΧΑΝΙΚΩΝ
Τ.Κ. 15780 Πολυτεχνειούπολη Ζωγράφου, Αθήνα

I certify that I have read this thesis and that, in my opinion, it is fully adequate in scope and quality as a dissertation for the degree of Doctor of Philosophy.

Manolis Papadrakakis
Professor Emeritus
(Principal Advisor)
School of Civil Engineering
National Technical University of Athens

I certify that I have read this thesis and that, in my opinion, it is fully adequate in scope and quality as a dissertation for the degree of Doctor of Philosophy.

George Bouckovalas
Professor
(Member of Advisory Committee)
School of Civil Engineering
National Technical University of Athens

I certify that I have read this thesis and that, in my opinion, it is fully adequate in scope and quality as a dissertation for the degree of Doctor of Philosophy.

Vissarion Papadopoulos
Associate Professor
(Member of Advisory Committee)
School of Civil Engineering
National Technical University of Athens

I certify that I have read this thesis and that, in my opinion, it is fully adequate in scope and quality as a dissertation for the degree of Doctor of Philosophy.

Ioannis Psycharis
Professor
School of Civil Engineering
National Technical University of Athens

I certify that I have read this thesis and that, in my opinion, it is fully adequate in scope and quality as a dissertation for the degree of Doctor of Philosophy.

Konstantinos Spiliopoulos
Professor
School of Civil Engineering
National Technical University of Athens

I certify that I have read this thesis and that, in my opinion, it is fully adequate in scope and quality as a dissertation for the degree of Doctor of Philosophy.

Nikos Gerolymos
Associate Professor
School of Civil Engineering
National Technical University of Athens

I certify that I have read this thesis and that, in my opinion, it is fully adequate in scope and quality as a dissertation for the degree of Doctor of Philosophy.

George Stefanou
Assistant Professor
School of Civil Engineering
Aristotle University of Thessaloniki

Theofilos-Ioannis Manitaras
Institute of Structural Analysis & Antiseismic Research
School of Civil Engineering
National Technical University of Athens
Zografou Campus, 15780 Athens, Greece

Copyright © 2017

Ph.D. Thesis

Author e-mail: teojgor@gmail.com

All rights reserved. No part of this work may be translated, reproduced or utilized in any form or by any means, electronic or mechanical, without the prior permission of the author, except for brief excerpts in connection with references or scholarly analysis. Use in connection with any form of information storage and retrieval, electronic adaptation, computer software, or by similar or dissimilar methodology now known or hereafter developed is thus forbidden.

Dedicated to my parents and sister

“We know more about the movement of celestial
bodies than we know about the soil underfoot”
Leonardo da Vinci

“Every addition to true knowledge is an addition
to human power”
Horace Mann
Lectures on Education (1855)

«Γνωρίζουμε περισσότερα για την κίνηση των ουράνιων σωμάτων απ' ότι για το έδαφος κάτω από τα πόδια μας...» ισχυριζόταν ο Λεονάρντο ντα Βίντσι. Εύστοχη παρατήρηση που σίγουρα μας δίνει τροφή για σκέψη· τα εδάφη στη φυσική τους κατάσταση συγκαταλέγονται άλλωστε ανάμεσα στα πιο «αβέβαια» υλικά. Δυστυχώς, η έλλειψη διαθέσιμων δεδομένων σχετικά με τις ιδιότητές τους ώθησε τους μηχανικούς στην αναζήτηση τρόπων αντιμετώπισης της εν λόγω αβεβαιότητας. Ας αναλογιστούμε, για παράδειγμα, την εισαγωγή των συντελεστών ασφαλείας· η εκπληκτική υπολογιστική ισχύς των σύγχρονων παράλληλων υπολογιστών άνοιξε εντελώς νέους ορίζοντες, ειδικώς όσον αφορά την ενσωμάτωση της αβεβαιότητας των εδαφικών ιδιοτήτων στις αριθμητικές αναλύσεις. Μέχρι σήμερα, μερικές από τις πιο διαδεδομένες μεθόδους εντάσσονται στη λεγόμενη «οικογένεια» των Μεθόδων Στοχαστικών Πεπερασμένων Στοιχείων, οι οποίες νοούνται ως επέκταση της παραδοσιακής πια «ντετερμινιστικής» Μεθόδου των Πεπερασμένων Στοιχείων.

Η συγκεκριμένη Διατριβή ασχολείται ειδικά με την αξιοποίηση των Στοχαστικών Πεπερασμένων Στοιχείων για την προσομοίωση γεωτεχνικών προβλημάτων με στοχαστικές εδαφικές ιδιότητες, όπου η χωρική διακύμανση των ιδιοτήτων του υλικού, όπως το μέτρο ελαστικότητας ή η διαπερατότητα, λαμβάνεται υπόψη μέσω της χρήσης ομογενών τυχαίων πεδίων.

Στο πρώτο μέρος, εκτίθενται οι στοιχειώδεις θεωρητικές βάσεις· για το σκοπό αυτό, παρουσιάζονται η βασική θεωρία συνόλων και πιθανοτήτων, μαζί με εκείνη των τυχαίων διαδικασιών και πεδίων. Επιπλέον, επεξηγούνται οι βασικές παραλλαγές των Μεθόδων Στοχαστικών Πεπερασμένων Στοιχείων, ακολουθούμενες από μία σύντομη εισαγωγή στις γνωστές και ως Συναρτήσεις Διακύμανσης Απόκρισης ως εναλλακτική αξιόπιστη τεχνική για την ποσοτικοποίηση της αβεβαιότητας της εξεταζόμενης «απόκρισης».

Το δεύτερο μέρος συγκροτείται από μεμονωμένες αριθμητικές «μελέτες» της μεθοδολογίας Στοχαστικών Πεπερασμένων Στοιχείων με έμφαση σε προβλήματα γεωτεχνικής φύσης. Συγκεκριμένα, οι πρώτες εφαρμογές εξετάζουν την καθίζηση ενός θεμελίου σε στερεοποιήσιμο εδαφικό στρώμα με στοχαστικό μέτρο ελαστικότητας και διαπερατότητα. Στη δεύτερη εφαρμογή, το πρόβλημα διάδοσης διατμητικού κύματος σε εδαφικό στρώμα με χωρικά μεταβλητό μέτρο διάτμησης αποτελεί το κύριο αντικείμενο έρευνας. Αυτό ακριβώς επιλύεται με τη μεθοδολογία των Δυναμικών Συναρτήσεων Διακύμανσης Απόκρισης χρησιμοποιώντας την ταχεία προσομοίωση Monte Carlo, ενώ η όλη αξιοπιστία της μεθόδου ελέγχεται και πάλι μέσω παρεμφερών αποτελεσμάτων που έχουν προκύψει από προσομοιώσεις τύπου Monte Carlo. Τέλος, το πρόβλημα της στερεοποίησης επανεξετάζεται στη βάση των Δυναμικών Συναρτήσεων Διακύμανσης Απόκρισης, με σκοπό να αποδειχτεί το δυναμικό της εν λόγω εναλλακτικής μεθοδολογίας.

Εν ολίγοις, καθ' όλη την έκταση της παρούσας εργασίας, καταβάλλεται προσπάθεια να αναδειχτεί το πλήρες δυναμικό της Μεθόδου Στοχαστικών Πεπερασμένων Στοιχείων για τη διερεύνηση γεωτεχνικών προβλημάτων, κάτι που μέλλει να αποδειχτεί εργαλείο ανεκτίμητης αξίας για την ποσοτικοποίηση της αβεβαιότητας και την αξιολόγηση κινδύνων στα χέρια των σύγχρονων μηχανικών. Ας μη λησμονούμε το απόφθεγμα που ο Οράτιος Μανν, Αμερικανός

ανθρωπιστής και κατεξοχήν μεταρρυθμιστής του αμερικανικού εκπαιδευτικού συστήματος, έγραφε το 1855 στις «Διαλέξεις περί Εκπαιδευσεως» (διάλεξη I): «Κάθε προσθήκη στην αληθινή γνώση είναι προσθήκη στην ανθρώπινη δύναμη».

Λέξεις-κλειδιά:

Εδαφική στερεοποίηση – μέθοδος στοχαστικών πεπερασμένων στοιχείων – καθίζηση θεμελίου – προσομοίωση Monte Carlo – διάδοση διατμητικού κύματος – χωρική διακύμανση ιδιοτήτων εδαφικού υλικού – ομοιογενή τυχαία πεδία – αβεβαιότητα απόκρισης – αβεβαιότητα εδαφικών παραμέτρων – δυναμικές συναρτήσεις διακύμανσης απόκρισης.

Declaration

The following dissertation is submitted for the degree of Ph.D. (Doctor of Philosophy) at the National Technical University of Athens (NTUA). Specifically, the research described herein has been conducted in the School of Civil Engineering under the supervision of professor Manolis Papadrakakis. As the sole author, I affirm that the present work is original, except where acknowledgments or references are made to previous or relevant research. Furthermore, I declare that no part has already been or is currently submitted for any such degree, diploma or other qualification, though selected parts of this work have been, will be presented at the conferences and/or are included in the publications cited below:

- T. Manitaras, V. Papadopoulos, M. Papadrakakis
Title: "Simulation of stochastic wave propagation in soil using Dynamic Variability Response Functions"
ICOSSAR 2017 (12th International Conference on Structural Safety Reliability): August 6-10, 2017 Vienna, Austria IASSAR (International Association for Structural Safety and Reliability)
- T. Manitaras, M. Papadrakakis
Title: "Simulation of stochastic soil consolidation using Dynamic Variability Response Functions"
COUPLED PROBLEMS 2017 (VII International Conference on Coupled Problems in Sciences and Engineering): June 12-14, 2017, Rhodes Island, Greece ECCOMAS (European Community on Computational Methods in Applied Sciences) and CIMNE (International Center for Numerical Methods in Engineering – Barcelona, Spain)
- T. Manitaras, V. Papadopoulos, M. Papadrakakis (2017)
Title: "Dynamic Variability Response Functions for Stochastic Wave Propagation in Soils" (in press)

(DOI: 10.1016/j.soidy.2017.02.004)

Journal: "Soil Dynamics and Earthquake Engineering", ISSN 0267-7261, Elsevier

- T. Manitaras, M. Papadrakakis (2017)
Title: "Footing Settlement on a Consolidating Soil Layer with Stochastic Properties" (in press)
(DOI: 10.1007/s11242-017-0844-x)
Journal: "Transport in Porous Media", ISSN: 0169-3913 (print version), ISSN: 1573-1634 (electronic version), Springer
- T. Manitaras, M. Papadrakakis
Title: "Consolidation of soil with stochastic properties" (ID E12124)
ECCOMAS Congress 2016 (European Congress on Computational Methods in Applied Sciences and Engineering): June 5-10, 2016 Crete Island, Greece ECCOMAS (European Community on Computational Methods in Applied Sciences), GRACM (Greek Association for Computational Mechanics), NTUA (National Technical University of Athens) and ICMES (Institute of Research & Development for Computational Methods in Engineering Sciences)
- T. Manitaras, M. Papadrakakis
Title: "Finite Element Simulation of Wave Propagation in Nonlinear Soils" (ID C2076)
COMPDYN 2015 (5th International Conference on Computational Methods in Structural Dynamics and Earthquake Engineering): May 27-28, 2015 Crete Island, Greece ECCOMAS (European Community on Computational Methods in Applied Sciences) and IACM (International Association for Computational Mechanics)

Theofilos Manitaras
April 2017

Acknowledgements

"The process of pursuing a Ph.D. can be compared to a long journey passing through many storms. Being able to arrive safe and sound at your destination is simply impossible without help from others."

Theofilos-Ioannis Manitaras

As a Ph.D. graduate having successfully completed his dissertation, the author acknowledges support from the European Research Council Advance Grant "MASTER –Mastering the challenges in numerical modelling and optimum design of CNT reinforced composites", as well as the Bodossaki Foundation; their financial and moral support has been of utter importance.

Personal Acknowledgements

First of all, I would like to express my sincere gratitude towards my supervisor, professor Manolis Papadrakakis, who introduced me to the amazing world of Finite Elements and Computational Mechanics; he has always been so supportive since the early years of my diploma thesis back in 2009. Right from the start, he was the one who believed in me and insisted on following this path, and as time goes by, I can't feel but grateful realizing how clear-sighted he was.

I was equally fortunate to have George Bouckovalas as a professor in Geotechnical Engineering during both my bachelor and master studies at the National Technical University of Athens; his ability to motivate has been one of the reasons for choosing Geotechnical Engineering as my main area of study. Fruitful discussions between us have helped me focus on my target and solve any problem of geotechnical nature along the way.

I would also like to especially thank assistant professor Vissarion Papadopoulos for making the overall study of Stochastic Finite Element Analysis an enjoyable experience;

he has always been willing to discuss any potential problems I faced and propose functional solutions or alternative paths.

Having confronted many challenges, I of course cannot forget Alexander Karatarakis, the lead developer up to 2015 of "Solverize", our in-house finite element code used throughout my dissertation; he has been a true friend, our midnight online discussions on how to extend the code are simply unforgettable.

At this point, I feel indebted to George Stavroulakis for offering the "AnalyzerSharp" code, the foundation stone on which "Solverize" has been built; his talent of tackling problems related to programming has proved valuable whenever things were stuck.

All in all, the journey was much easier having Manolis Georgioudakis as companion; his help since my bachelor thesis and throughout my further studies definitely affected my choices. He is a great friend and I am very happy I had the chance to meet him.

Last but not least, I would like to thank my parents Dimitri and Katerina, as well as my sister Evangelina; their support and encouragement has been decisive. They have always been there believing in me, never hesitating to go to extremes in order to enable me to study.

Abstract

"We know more about the movement of celestial bodies than we know about the soil underfoot" claimed once Leonardo da Vinci; a clever quotation that certainly gives us food for thought. Soils in their natural state are by far among the most variable materials. Unfortunately, lack of available data on their properties has led engineers to seek new ways of dealing with this uncertainty. Let us consider, for example, the adoption of safety factors; the astounding computing power of today's parallel computers has opened completely new paths for engineers, especially on how to incorporate uncertain soil parameters directly in their numerical analyses. Up to now, some of the most widely used methods lay under the umbrella of stochastic finite element methods (SFEM), consisting of the alternative extension of the classical deterministic finite element method (FEM).

This thesis, in particular, deals with the application of SFEM for the simulation of geotechnical problems with uncertain soil parameters, while the spatial variability of material properties such as elasticity or permeability is taken into account via the use of homogeneous random fields.

In the first part, essential theoretical concepts are established; to this purpose, basic set and probability theory, together with random processes and fields, are analyzed. Furthermore, the basic variants of SFEM are discussed, followed by a brief introduction to variability response functions (VRF) as an alternative, trustworthy technique for quantifying response uncertainty.

The second part consists of numerical case studies of the SFEM methodology with a special regard to problems of a clearly geotechnical nature. Specifically, the first application consists of the settlement of a footing resting on a consolidating soil layer with stochastic Young's modulus and permeability. In the second application, the problem of shear wave propagation in a soil layer with spatially variable shear-modulus is studied; this is tackled with the DVRF methodology using the fast Monte Carlo simulation (FMCS), whereas again the accuracy of the FMCS is compared with the results obtained via the MCS. Next, the footing problem is revisited on the basis of

dynamic variability response functions (DVRF), in order to prove the potential of this alternative methodology.

To conclude, throughout the present work, the potential of SFEM is fully demonstrated, something which will definitely prove to be of immense value for uncertainty quantification and risk assessment in the hands of modern engineers. After all, we must never forget what Horace Mann wrote in 1855: "Every addition to true knowledge is an addition to human power" (Lectures on Education, Lecture 1).

Keywords: geotechnical, soil consolidation, stochastic finite element method, Monte Carlo simulation, shear wave propagation, footing settlement, variability response functions, response uncertainty, homogeneous random fields, uncertain soil parameters, spatial variability of soil properties.

Εκτενής Περίληψη

0.1 Εισαγωγή

Τα εδάφη στη φυσική τους κατάσταση συγκαταλέγονται ανάμεσα στα πιο μεταβλητά υλικά, ενώ η χωρική διακύμανση και αβεβαιότητα των ιδιοτήτων τους είναι παρούσες ακόμη και σε εδαφικά στρώματα που θεωρούνται ομογενή στις γεωτεχνικές εφαρμογές. Η έλλειψη ωστόσο επαρκών δεδομένων που απαιτούνται για την εκτίμηση των εδαφικών παραμέτρων όσον αφορά γεωτεχνικά προβλήματα οδήγησε στην υιοθέτηση ντετερμινιστικών μεθόδων ανάλυσης, βασιζόμενων σε συντελεστές ασφαλείας ώστε να λαμβάνεται υπόψη η αβεβαιότητα και διακύμανση των εδαφικών ιδιοτήτων. Είναι γεγονός πως η υπολογιστική ισχύς που παρέχουν οι σύγχρονοι πολυπύρρηνοι επεξεργαστές ανοίγει νέους δρόμους στην ενσωμάτωση της αβεβαιότητας σε προβλήματα μηχανικού. Σε αυτή την κατεύθυνση, όλο και αυξανόμενο ποσοστό έρευνας είναι αφιερωμένο στην επίλυση στοχαστικών προβλημάτων με στόχο την ποσοτικοποίηση των συνεπειών της αβεβαιότητας τόσο των ιδιοτήτων υλικού και γεωμετρίας, όσο και φόρτισης και συνοριακών συνθηκών.

Ιδιαίτερα τα τελευταία χρόνια, η επιρροή της εγγενούς εδαφικής διακύμανσης σε γεωτεχνικά προβλήματα έχει προσελκύσει διεθνώς το ενδιαφέρον. Μεγάλος πράγματι αριθμός ερευνητών έχει μελετήσει την επιρροή της χωρικής διακύμανσης διαφόρων εδαφικών ιδιοτήτων όπως το μέτρο ελαστικότητας, η γωνία τριβής και η διαπερατότητα σε σχετικές εφαρμογές. Μελέτες φέρουσας ικανότητας θεμελίων (Al-Bittar and Soubra, 2013; Cho and Park, 2010; Griffiths et al., 2002, 2006; Simões et al., 2014) και καθίζησης (Fenton and Griffiths, 2005; Maheshwari and Kumar, 2011; Paice et al., 1996), ευστάθειας πρανών (Griffiths and Fenton, 2004; Griffiths et al., 2009), καθώς και διήθησης (Griffiths and Fenton, 1997), αποτελούν μερικές μόνο χαρακτηριστικές περιπτώσεις. Επιπλέον, το φαινόμενο της στερεοποίησης υπό πιθανοτική σκοπιά έχει μελετηθεί από διάφορους ερευνητές. Στα άρθρα (Badaoui et al., 2007; Houmadi et al., 2012), για παράδειγμα, η επιρροή της διακύμανσης της διαπερατότητας και του μέτρου ελαστικότητας στην κατακόρυφη διεύθυνση εξετάζεται για το πρόβλημα της μονοδιάστατης στερεοποίησης. Επίσης, στο άρθρο (Bong et al., 2014) διερευνάται η επιρροή της χωρικής διακύμαν-

σης των συντελεστών στερεοποίησης κατά την οριζόντια και κατακόρυφη διεύθυνση στο βαθμό στερεοποίησης του φορτιζόμενου εδάφους. Στο δε άρθρο (Huang et al., 2010) μελετάται η επιρροή της συσχέτισης μεταξύ της στοχαστικής διαπερατότητας του εδάφους, αλλά και του συντελεστή ογκομετρικής συμπίεστικότητας σε συζευγμένα μονοδιάστατα και διδιάστατα προβλήματα στερεοποίησης. Δυναμικά προβλήματα με στοχαστικές εδαφικές παραμέτρους έχουν επιπρόσθετα διερευνηθεί στα άρθρα (Ho Lee et al., 2013; Johari and Khodaparast, 2015; Johari and Momeni, 2015; Wang and Sett, 2016). Τέλος, μια εκτενής κάλυψη των πιθανοτικών μεθόδων προσομοίωσης στη γεωτεχνική μηχανική, συνοδευόμενη από πλήθος πρακτικών εφαρμογών, παρουσιάζεται στο σύγγραμμα (Fenton and Griffiths, 2008).

Η πιο εύρωστη υπολογιστική μέθοδος για τη διερεύνηση της επιρροής της χωρικής διακύμανσης των ιδιοτήτων των υλικών στην απόκριση διαφόρων προβλημάτων είναι η μέθοδος των στοχαστικών πεπερασμένων στοιχείων (ΜΣΠΣ) (Stefanou, 2009). Οι δε τρεις πιο σημαντικές παραλλαγές αυτής είναι: η μέθοδος διαταραχής, η μέθοδος των φασματικών στοχαστικών πεπερασμένων στοιχείων (ΜΦΣΠΣ) και η μέθοδος Monte Carlo. Η μέθοδος διαταραχής συνίσταται από το ανάπτυγμα σε σειρά Taylor του στοχαστικού μητρώου στιβαρότητας, καθώς και του διανύσματος απόκρισης του υπό μελέτη συστήματος. Στο πλαίσιο της ΜΦΣΠΣ, το στοχαστικό μητρώο στιβαρότητας των πεπερασμένων στοιχείων συνίσταται από το άθροισμα μίας ντετερμινιστικής και μίας στοχαστικής συνιστώσας, η οποία δίδεται μέσω του αναπτύγματος Karhunen-Loève (K-L), ενώ το μητρώο απόκρισης εκφράζεται ως ανάπτυγμα πολυωνύμων Hermite. Σημειώνεται βεβαίως πως στην ανάλυση πολύπλοκων προβλημάτων, οι δύο ανωτέρω τεχνικές μπορεί να είναι δύσκολα υλοποιήσιμες, ενώ πολλές φορές αποδεικνύονται και υπολογιστικά δαπανηρές (Stavroulakis et al., 2014). Γι' αυτούς τους λόγους, η απευθείας ανάλυση Monte Carlo παραμένει η μόνη αξιόπιστη και καθολική, μολονότι υπολογιστικά ακριβή, μέθοδος για την αντιμετώπιση τέτοιου είδους προβλημάτων, ειδικά σε περιπτώσεις όπου παρατηρείται μεγάλη διακύμανση των στοχαστικών παραμέτρων (Stavroulakis et al., 2014).

Ένα από τα σημαντικότερα στάδια της προσομοίωσης Monte Carlo είναι η γένεση δειγματοσυναρτήσεων των τυχαίων πεδίων (Vanmarcke, 2010) που περιγράφουν με ακρίβεια τη μεταβλητότητα της υπό μελέτη ιδιότητας. Στην πραγματικότητα, διάφορες μέθοδοι έχουν προταθεί για τη γένεση των παραπάνω δειγματοσυναρτήσεων. Η μέθοδος φασματικής αναπαράστασης (Shinozuka and Deodatis, 1996), είναι μία από τις πιο διαδεδομένες μεθόδους για τη γένεση ομοιογενών Γκαουσιανών τυχαίων πεδίων σε μία, δύο και τρεις χωρικές διαστάσεις. Κάνοντας μάλιστα χρήση της μεθόδου φασματικής αναπαράστασης και στη συνέχεια έναν μετασχηματισμό χωρίς μνήμη (Grigoriu, 1995, 2002), δειγματοσυναρτήσεις μη-Γκαουσιανών πεδίων είναι εύκολο να υπολογιστούν.

Στις περισσότερες μελέτες, τα γεωτεχνικά προβλήματα αναλύονται με τη μέθοδο των στοχαστικών πεπερασμένων στοιχείων, ενσωματώνοντας με διάφορες τεχνικές τη στοχαστική ιδιότητα του εδάφους. Συνήθως, κάποια παραλλαγή της μεθόδου Monte Carlo υιοθετείται με σκοπό την ποσοτικοποίηση της αβεβαιότητας της υπό μελέτη στοχαστικής ιδιότητας. Πέρα όμως από τις όποιες πρακτικές δυσκολίες που παρουσιάζει η εν λόγω μέθοδος λόγω του υψηλού υπολογιστικού κόστους, το μεγάλο της μειονέκτημα έγκειται στο ότι η δομή συσχέτισης των υπό μελέτη ιδιοτήτων οφείλει να είναι εκ των προτέρων γνωστή, γεγονός πολύ σπάνιο στην πράξη. Ως εκ τούτου, η διερεύνηση της ευαισθησίας της απόκρισης του μοντέλου ως προς τα διαφορετικά χαρακτηριστικά συσχέτισης καθιστά τη μέθοδο σχεδόν απαγορευτική για την επίλυση ρεαλιστικών προβλημάτων.

Για την αντιμετώπιση αυτών των δυσκολιών, η έννοια των συναρτήσεων διακύμανσης της απόκρισης (ΣΔΑ) παρουσιάστηκε σε μία σειρά από άρθρα (Bucher and Shinozuka, 1988; Kardara et al., 1989; Shinozuka, 1987). Υπενθυμίζεται πως η ΣΔΑ είναι μια συνάρτηση Green που συσχετίζει τη διακύμανση της απόκρισης του συστήματος με το φάσμα ισχύος των αβέβαιων παραμέτρων (Arwade et al., 2016). Ως τέτοια, εξαρτάται από ντετερμινιστικές ιδιότητες σχετικές με τη γεωμετρία, τις συννοριακές συνθήκες και τις συνθήκες φόρτισης, τη μέση τιμή των ιδιοτήτων των υλικών, αλλά και την τυπική απόκλιση σ_{ff} της στοχαστικής ιδιότητας που μελετάται. Αρχικά, εκφράστηκε σε κλειστή μορφή για ισοστατικούς και υπερστατικούς φορείς δοκών και δικτυωμάτων υπό ντετερμινιστική φόρτιση, ενώ αργότερα επεκτάθηκε και στην επίλυση προβλημάτων στοχαστικής κάμψης πλακών (Graham and Deodatis, 1998). Όπως αναφέρεται στο άρθρο (Papadopoulos et al., 2005), στα περισσότερα προβλήματα, η εύρεση μιας αναλυτικής σχέσης για τη ΣΔΑ είναι πολύ δύσκολη, αν όχι αδύνατη. Παρ' όλα αυτά, δύναται εναλλακτικά να υπολογιστεί αριθμητικά με τη λεγόμενη ταχεία μέθοδο Monte Carlo, κάνοντας χρήση της μεθόδου των πεπερασμένων στοιχείων όπως επεξηγείται στο άρθρο (Papadopoulos et al., 2005, 2006). Επιπλέον εφαρμογές της αποτελούν η μελέτη ιδιοτήτων υλικού για ετερογενή τυχαία υλικά (Arwade et al., 2016), καθώς και ο εύρωστος βέλτιστος σχεδιασμός όπου λαμβάνονται υπόψη οι στοχαστικές παράμετροι του συστήματος (Kokkinos and Papadopoulos, 2016). Θα πρέπει ασφαλώς να σημειωθεί πως η αρχική εκδοχή της ΣΔΑ αφορούσε στοχαστικά στατικά προβλήματα. Η επέκταση της μεθόδου για δυναμικά συστήματα, που οδήγησε στη δυναμική συνάρτηση διακύμανσης της απόκρισης (ΔΣΔΑ), παρουσιάστηκε σχετικά πρόσφατα στο άρθρο (Papadopoulos and Kokkinos, 2012). Παράλληλα, αποδείχτηκε πως η ΔΣΔΑ και η αντίστοιχη δυναμική συνάρτηση μέσης τιμής της απόκρισης (ΔΣΜΑ) διατηρούν το πλεονέκτημα της μητρικής μεθόδου για δυναμικά φορτία. Την ανεξαρτησία τους δηλαδή από το φάσμα ισχύος, επιτρέποντας την εμβάθυνση

στην ευαισθησία της απόκρισης δυναμικών συστημάτων ως προς τις στοχαστικές αυτών ιδιότητες (Papadopoulos and Kokkinos, 2015).

0.2 Σκοπός της διατριβής

Η φύση της ερευνητικής εργασίας που απαιτείται για την ολοκλήρωση της παρούσας διατριβής υπήρξε διττή ή, όπως κανείς εύστοχα θα παρατηρούσε, το μέγεθος αυτής δύναται να θεωρηθεί διπλό σε όγκο, εφόσον περιλάμβανε: α) τη διερεύνηση, αξιολόγηση και επαλήθευση νέων υπολογιστικών μεθόδων για την εξέταση της συμπεριφοράς του εδάφους με τη χρήση αβέβαιων παραμέτρων και β) τη δημιουργία του κατάλληλου πλαισίου λογισμικού για την υποστήριξη των εν λόγω εφαρμογών. Οφείλει βεβαίως να σημειωθεί πως το δεύτερο ήταν το προαπαιτούμενο, και όχι ο βασικός στόχος, ούτε το κύριο θέμα της διατριβής, κάτι που σίγουρα εξηγεί γιατί η σημασία του παραβλέπεται ή επισκιάζεται από τα επιτεύγματα του πρώτου. Εάν όμως ληφθεί υπόψη, αυτή η λεπτομέρεια είναι καθοριστική, αποκαλύπτοντας ταυτόχρονα τόσο τη δυσκολία, όσο και πολυπλοκότητα του όλου εγχειρήματος. Υπήρχε πάραυτα λόγος για τη συγκεκριμένη επιλογή, τη μη συμβατική αυτή πορεία. Σύμφωνα με όσα γνωρίζουμε, δεν υπάρχουν, τουλάχιστον μέχρι σήμερα, διαθέσιμα εμπορικά πακέτα λογισμικού με βάση τα πεπερασμένα στοιχεία, τα οποία θα μπορούσαν να υποστηρίξουν την ανάλυση με στοχαστικά πεπερασμένα στοιχεία. Ως εκ τούτου, η ανάπτυξη ενός κατάλληλου αριθμητικού πακέτου φαινόταν η μόνη λύση για την επίτευξη του στόχου. Αφού λοιπόν η υλοποίηση αυτού κρίθηκε εφικτή, το εν λόγω εξειδικευμένο λογισμικό χρησιμοποιήθηκε για την ποσοτικοποίηση της αβεβαιότητας και διακύμανσης των εδαφικών παραμέτρων στα μεγέθη απόκρισης που παρουσιάζουν ενδιαφέρον σε γεωτεχνικά προβλήματα. Στο σημείο αυτό θα πρέπει ασφαλώς να επισημάνουμε το εξής: ακριβώς επειδή τα εδάφη συγκαταλέγονται ανάμεσα στα πιο αβέβαια υλικά, η ενσωμάτωση της διακύμανσης των ιδιοτήτων τους σε αριθμητικές προσομοιώσεις κρίνεται εξέχουσας σημασίας.

0.2.1 Ανάπτυξη λογισμικού

Όπως προαναφέρθηκε, ζητούμενο για τη διεκπεραίωση της διατριβής ήταν η ανάπτυξη των κατάλληλων αριθμητικών μεθόδων που απαιτούνταν για την επιτυχή εκτέλεση αναλύσεων με στοχαστικά πεπερασμένα στοιχεία. Προκειμένου δε να επιτευχθεί ο εν λόγω στόχος, ο αντικειμενοστραφής κώδικας πεπερασμένων στοιχείων *Solverize* έπρεπε επανειλημμένα να διευρυνθεί με τη μορφή νέων κλάσεων, διεπαφών και μεθόδων. Δεδομένου αυτού, η όλη διαδικασία ανάπτυξης λογισμικού μπορεί να χωριστεί σε δύο φάσεις:

1. Η πρώτη, αποτελούμενη από όλα τα στοιχεία που αναπτύχθηκαν με σκοπό την επίλυση προβλημάτων με ντετερμινιστικές ιδιότητες υλικού, περιλάμβανε τα ακόλουθα:
 - Εμπλουτισμός με διδιάστατα τετραπλευρικά και τριγωνικά ισοπαραμετρικά στοιχεία με ποικίλες επιλογές ως προς τον αριθμό των κόμβων, ώστε να καταστεί δυνατή η επίλυση προβλημάτων υπό συνθήκες επίπεδης έντασης και παραμόρφωσης. Επιπλέον, εισήχθησαν εξαεδρικά και τετραεδρικά πεπερασμένα στοιχεία τριών διαστάσεων με υποστήριξη εναλλακτικών τάξεων συναρτήσεων σχήματος.
 - Προσθήκη μονοδιάστατων διατμητικών στοιχείων για την προσομοίωση της δυναμικής απόκρισης εδάφους σε μία χωρική διάσταση.
 - Ανάπτυξη τετραπλευρικών και εξαεδρικών στοιχείων τύπου u-p για την προσομοίωση πορώδων υλικών. Εδώ θα πρέπει να υπογραμμιστεί πως η ανεξάρτητη επιλογή συναρτήσεων σχήματος για τους βαθμούς ελευθερίας μετατόπισης και πίεσης πόρων επιτρέπει πρόσθετη ευελιξία προσομοίωσης.
 - Εισαγωγή της γενικευμένης μεθόδου αριθμητικής ολοκλήρωσης Newmark (GN11) για την προσομοίωση του φαινομένου εδαφικής στερεοποίησης.
 - Προσθήκη ιξωδών αποσβεστήρων τύπου Lysmer ως απορροφητικές συνοριακές συνθήκες για την προσομοίωση διάδοσης κύματος.
 - Προγραμματισμός απευθείας μεθόδων ολοκλήρωσης της εξίσωσης κίνησης και συγκεκριμένα των Newmark, HHT-α και Bathe, για την προσομοίωση δυναμικών προβλημάτων.
 - Προσθήκη ειδικής κλάσης που αναλαμβάνει τη μετατροπή δεδομένης σεισμικής καταγραφής σε ισοδύναμα επικόμβια φορτία επιβαλλόμενα στη βάση του αριθμητικού εδαφικού προσομοιώματος.
2. Η δεύτερη φάση, περιλάμβανε τους απαιτούμενους αριθμητικούς αλγόριθμους που θα επέτρεπαν στον κώδικα να εκτελεί προσομοιώσεις με στοχαστικά πεπερασμένα στοιχεία. Για το σκοπό αυτό αναπτύχθηκαν τα ακόλουθα τμήματα λογισμικού:
 - Ανάπτυξη της πολυδιάστατης μεθόδου φασματικής αναπαράστασης για τη γένεση ομογενών Γκαουσιανών τυχαίων πεδίων σε μία, δύο και τρεις διαστάσεις. Επίσης, προστέθηκαν ποικίλες δομές συσχέτισης καθώς και μετασχηματισμοί υπό τη μορφή πεδίων μεταφοράς για τη γένεση λογαριθμικανονικών πεδίων, ενώ ξεχωριστή φροντίδα δόθηκε ώστε να εξασφαλιστεί η

αξιοποίηση πολυπύρηνων επεξεργαστών για την επιτάχυνση της όλης διαδικασίας.

- Προγραμματισμός της μεθόδου στοχαστικών πεπερασμένων στοιχείων τύπου Monte Carlo με υποστήριξη παράλληλης εκτέλεσης σε πολυπύρηνους επεξεργαστές, αλλά και αποτελεσματική αποθήκευση των αποτελεσμάτων υπό τη μορφή αρχείων Hdf5 .
- Ανάπτυξη της ταχείας μεθόδου Monte Carlo για τον υπολογισμό των ΔΣΜΑ και ΔΣΔΑ γενικευμένων προσομοιωμάτων πεπερασμένων στοιχείων, όπου και πάλι η υποστήριξη πολυπύρηνων επεξεργαστών και η αποτελεσματικότητα αποθήκευσης υπήρξαν πρωταρχικής σημασίας.
- Δημιουργία των απαραίτητων τμημάτων λογισμικού για τον υπολογισμό των στατιστικών απόκρισης μέσω των ΔΣΜΑ και ΔΣΔΑ και των παρεχόμενων δομών συσχέτισης.
- Ανάπτυξη κώδικα σε γλώσσα προγραμματισμού Python για την επεξεργασία των στατιστικών απόκρισης, αλλά και τη γραφική αυτών αναπαράσταση.

0.2.2 Γεωτεχνικές εφαρμογές

Έπειτα από την επιτυχή ενσωμάτωση των επιμέρους αναγκαίων τμημάτων λογισμικού, ο κώδικας *Solverize* χρησιμοποιήθηκε για την προσομοίωση προβλημάτων γεωτεχνικής φύσης, στα οποία λήφθηκε υπόψη η χωρική διακύμανση και αβεβαιότητα των εδαφικών παραμέτρων. Η πρώτη εφαρμογή αφορά τη μελέτη της καθίζησης άκαμπτου θεμελίου επί στερεοποιήσιμου εδαφικού στρώματος, όπου η χρήση των στοχαστικών πεπερασμένων στοιχείων επιτρέπει την ενσωμάτωση της αβεβαιότητας τόσο του μέτρου ελαστικότητας, όσο και της διαπερατότητας του εδάφους στην προσομοίωση. Οι δε αναλύσεις ευαισθησίας προσφέρουν στη συνέχεια μια λεπτομερέστερη εικόνα, όσον αφορά την επιρροή της δομής συσχέτισης της υπό μελέτη ιδιότητας στην απόκριση ως προς τις καθιζήσεις, αλλά και τις υπερπιέσεις πόρων.

Ακολουθεί η μελέτη του προβλήματος της διάδοσης διατμητικού κύματος σε έδαφος με στοχαστικό μέτρο διάτμησης, όπου αξιοποιήθηκε η μεθοδολογία των δυναμικών συναρτήσεων διακύμανσης της απόκρισης (ΔΣΔΑ), οι οποίες και υπολογίστηκαν μέσω της ταχείας μεθόδου Monte Carlo. Σημειώνεται πως οι αναλύσεις που εκτελέστηκαν αφορούσαν τη διάδοση διατμητικού κύματος σε εδαφικά προσομοιώματα μίας και δύο διαστάσεων, επιβεβαιώνοντας την εγκυρότητα, καθώς και ανεξαρτησία των ΔΣΔΑ ως προς το φάσμα ισχύος των ιδιοτήτων υλικού. Αποδείχθηκε επίσης πως τα στατιστικά μεγέθη απόκρισης της εδαφικής επιφάνειας είναι ευαίσθητα σε ισχυρά συσχετισμένα πεδία

ή, για την ακρίβεια, πως το διατμητικό κύμα επηρεάζεται μόνο από ομαλή διακύμανση των πεδίων που προσομοιώνουν το μέτρο διάτμησης.

Τέλος, το πρόβλημα της εδαφικής στερεοποίησης επανεξετάζεται υπό το πρίσμα της μεθοδολογίας των ΔΣΔΑ, όπου η έννοια των ΔΣΔΑ επιβεβαιώνεται για άλλη μια φορά ως προς την ακρίβειά της. Παράλληλα, αναδείχθηκε περαιτέρω η αξία των ΔΣΔΑ, δεδομένου πως αυτές αποκαλύπτουν τους μηχανισμούς που ελέγχουν τη διακύμανση της απόκρισης.

0.3 Στοιχεία θεωρίας πιθανοτήτων

Στην ενότητα αυτή παρουσιάζονται οι βασικές έννοιες των συνόλων, καθώς και η θεωρία πιθανοτήτων και τυχαίων μεταβλητών. Ο ενδιαφερόμενος μπορεί βέβαια να ανατρέξει στα συγγράμματα (Bertsekas and Tsitsiklis, 2008; Papoulis and Pillai, 2002), όπου οι εν λόγω έννοιες εξετάζονται σε βάθος.

0.3.1 Θεωρία συνόλων

Ως *σύνολο* ορίζεται μια συλλογή αντικειμένων που συνιστούν τα *μέλη* του συνόλου. Λέμε ότι το x ανήκει στο σύνολο A χρησιμοποιώντας το συμβολισμό $x \in A$, ενώ για την αντίθετη περίπτωση χρησιμοποιείται ο συμβολισμός $x \notin A$. Το δε σύνολο που δεν έχει κανένα στοιχείο ονομάζεται *κενό σύνολο* και συμβολίζεται με \emptyset . Αν κάθε στοιχείο x του A είναι και στοιχείο του B , τότε το A καλείται *υποσύνολο* του B και συμβολίζεται ως $A \subseteq B$. Τέλος, ορίζεται το σύνολο Ω , το οποίο περιέχει όλα τα υπό μελέτη στοιχεία ως *καθολικό σύνολο* και κάθε άλλο σύνολο είναι υποσύνολο αυτού. Μεταξύ δύο συνόλων A και B ορίζονται οι εξής σχέσεις:

- Το *συμπληρωματικό* ενός συνόλου A , που συμβολίζεται με A^c , είναι το σύνολο για το οποίο αν $x \in A$, τότε $x \notin A^c$.
- Η *ένωση* των συνόλων A, B , που συμβολίζεται ως $A \cup B$, είναι το σύνολο για το οποίο αν $x \in A \cup B$, τότε $x \in A$ ή $x \in B$.
- Η *τομή* των συνόλων A, B , που συμβολίζεται ως $A \cap B$, είναι το σύνολο για το οποίο αν $x \in A \cap B$, τότε $x \in A$ και $x \in B$.
- Η *διαφορά* των συνόλων A, B , που συμβολίζεται ως $A - B$, είναι το σύνολο για το οποίο αν $x \in A - B$, τότε $x \in A$ και $x \notin B$.
- Η *συμμετρική διαφορά* των συνόλων A, B , που συμβολίζεται ως $A \Delta B$, είναι το σύνολο για το οποίο αν $x \in A \Delta B$, τότε $x \in A$ ή $x \notin B$, αλλά $x \notin A \cap B$.

- Δύο σύνολα A, B λέγονται *ξένα* αν $A \cap B = \emptyset$.

0.3.2 Νόμοι πιθανοτήτων

Τα βασικά συστατικά της θεωρίας πιθανοτήτων είναι η έννοια του πειράματος, αλλά και των δυνατών αποτελεσμάτων, ενώ το σύνολο όλων των δυνατών αποτελεσμάτων ονομάζεται δειγματικός χώρος Ω . Ένα υποσύνολο του Ω , το οποίο συνιστά μία συλλογή από πιθανά αποτελέσματα ονομάζεται *ενδεχόμενο*. Ο *νόμος πιθανότητας* αναθέτει σε ένα ενδεχόμενο E έναν αριθμό, ο οποίος ονομάζεται *πιθανότητα* του ενδεχομένου E , που ικανοποιεί $0 \leq P(E) \leq 1$ και εκφράζει το πόσο πιθανό είναι να λάβει χώρα το εν λόγω ενδεχόμενο. Υπάρχουν δύο τρόποι να περιγράψουμε τη σημασία της πιθανότητας $P(E)$. Αρχικά, ως αναλογιστούμε τη ρίψη ενός εξαέδρου δίκαιου ζαριού. Έστω A το ενδεχόμενο πως το αποτέλεσμα της ρίψης είναι ο αριθμός 6. Για ένα δίκαιο ζάρι είναι λογικό να θεωρήσουμε πως η πιθανότητα του A είναι $P(A) = 1/6$, η οποία και είναι κοινή για όλα τα δυνατά αποτελέσματα της ρίψης. Ας θεωρήσουμε τώρα ότι το πείραμα επαναλαμβάνεται n φορές, όπου με n_A συμβολίζουμε το πλήθος των ρίψεων με αποτέλεσμα τον αριθμό 6. Τότε, η πιθανότητα $P(A)$ δύναται να ερμηνευτεί ως ο λόγος n_A/n , ως δηλαδή η σχετική συχνότητα με την οποία το αποτέλεσμα της ρίψης δίνει 6 όταν ο συνολικός αριθμός ρίψεων n είναι αρκετά μεγάλος. Υπάρχουν πάραυτα περιπτώσεις όπου το πείραμα δεν μπορεί να επαναληφθεί και η ερμηνεία βάσει της συχνότητας δεν είναι έγκυρη. Για παράδειγμα, έστω το γεγονός G της αστοχίας ενός κτιρίου κατά τη διάρκεια ενός ισχυρού σεισμού τα επόμενα 50 χρόνια. Στην περίπτωση αυτή, η πιθανότητα $P(G)$ χρησιμοποιείται για να εκφράσει την υποκειμενική μας πεποίθηση σχετικά με το πόσο πιθανό είναι να λάβει χώρα το γεγονός G .

Η θεωρία πιθανοτήτων είναι θεμελιωμένη στα εξής αξιώματα των πιθανοτήτων:

1. Για κάθε ενδεχόμενο A , $P(A) \geq 0$.
2. Αν τα ενδεχόμενα A και B είναι ξένα, δηλαδή $A \cap B = \emptyset$, τότε $P(A \cup B) = P(A) + P(B)$.
3. Η πιθανότητα του δειγματικού χώρου Ω είναι $P(\Omega) = 1$.

0.3.3 Τυχαίες μεταβλητές

Αν το αποτέλεσμα ενός πειράματος είναι αριθμητική τιμή, η τιμή αυτή ονομάζεται *τυχαία μεταβλητή*. Μιλώντας με μαθηματικούς όρους, η τυχαία μεταβλητή είναι μία συνάρτηση που αντιστοιχεί ενδεχόμενα του δειγματικού χώρου σε αριθμητικές τιμές. Διακρίνονται διαφορετικές περιπτώσεις, ανάλογα με τη φύση των αριθμητικών τιμών που μπορεί να

λάβει η τυχαία μεταβλητή. Ως εκ τούτου, οι τυχαίες μεταβλητές που μπορούν να λάβουν μόνο διακριτές αριθμητικές τιμές ονομάζονται *διακριτές τυχαίες μεταβλητές*. Ο δε όρος *συνεχής τυχαία μεταβλητή* αναφέρεται στην περίπτωση των μεταβλητών που λαμβάνουν τιμές στην ευθεία των πραγματικών αριθμών. Διευκρινίζεται ασφαλώς πως, στην παρούσα διατριβή, ασχολούμαστε αποκλειστικά με περιπτώσεις συνεχών τυχαίων μεταβλητών.

0.3.3.1 Συνάρτηση πυκνότητας πιθανότητας και αθροιστική συνάρτηση κατανομής

Για την πλήρη περιγραφή μίας συνεχούς τυχαίας μεταβλητής X , απαιτείται μόνο η γνώση της *συνάρτησης πυκνότητας πιθανότητας* (ΣΠΠ) που συμβολίζεται ως $f_X(x)$. Κάνοντας χρήση αυτής, η πιθανότητα μία τυχαία μεταβλητή X να βρίσκεται μεταξύ των τιμών a , b υπολογίζεται ως εξής:

$$P(a \leq X \leq b) = \int_a^b f_X(x) dx \quad (1)$$

Προκειμένου να εξασφαλίζονται τα αξιώματα των πιθανοτήτων, η ΣΠΠ ικανοποιεί τις ακόλουθες σχέσεις:

$$f_X(x) \geq 0 \quad (2)$$

$$\int_{-\infty}^{\infty} f_X(x) dx = 1 \quad (3)$$

Η δε *αθροιστική συνάρτηση κατανομής* (ΑΣΚ) μίας τυχαίας μεταβλητής X , που συμβολίζεται ως $F_X(x)$, σχετίζεται με τη ΣΠΠ μέσω της ακόλουθης σχέσης:

$$F_X(x) = \int_{-\infty}^x f_X(u) du \quad (4)$$

και εκφράζει την πιθανότητα η τιμή μίας τυχαίας μεταβλητής X να είναι μικρότερη ή ίση ενός αριθμού x :

$$F_X(x) = P(X \leq x) \quad (5)$$

Τέλος η ΣΠΠ υπολογίζεται από την ΑΣΚ με παραγωγήιση ως εξής:

$$f_X(x) = \frac{dF_X(x)}{dx} \quad (6)$$

0.3.3.2 Μέση τιμή και διασπορά

Οι ΣΠΠ και ΑΣΚ παρέχουν μεγάλο όγκο πληροφορίας σχετικά με την τυχαία μεταβλητή X . Για πρακτικούς λόγους, είναι κρίσιμο να συνοψίσουμε όλη αυτή την πληροφορία, ο-

ρίζοντας αντιπροσωπευτικές ποσότητες που χαρακτηρίζουν μία τυχαία μεταβλητή. Ειδικά για το σκοπό αυτό, ορίζεται η προσδοκία $E[X]$ ή μέση τιμή μ_X μίας τυχαίας μεταβλητής X ως το κέντρο βάρους όλων των δυνατών τιμών που λαμβάνει η X και δίνεται από τη σχέση:

$$E[X] = \mu_X = \int_{-\infty}^{+\infty} x f_X(x) dx \quad (7)$$

Η $E[X]$ εκφράζει μία αντιπροσωπευτική τιμή για την τυχαία μεταβλητή X . Εναλλακτικές σημαντικές ποσότητες που προσφέρουν πληροφορία για μία τυχαία μεταβλητή X είναι οι λεγόμενες ροπές. Ειδικότερα, η n -οστή ροπή της X είναι η προσδοκία της τυχαίας μεταβλητής X^n και δίνεται από τη σχέση:

$$E[X^n] = \mu_X = \int_{-\infty}^{+\infty} x^n f_X(x) dx \quad (8)$$

Μία ακόμη σημαντική ποσότητα της τυχαίας μεταβλητής X είναι η διασπορά που ορίζεται ως:

$$Var(X) = E[(X - E[X])^2] \quad (9)$$

και αποτελεί μέτρο της διακύμανσης της τυχαίας μεταβλητής X γύρω από τη μέση τιμή της μ_X . Η δε τετραγωνική ρίζα της διασποράς ονομάζεται τυπική απόκλιση σ_X :

$$\sigma_X = \sqrt{Var(X)} \quad (10)$$

και αποτελεί ένα πιο φυσικό μέτρο της διακύμανσης της X , δεδομένου πως και οι δύο έχουν τις ίδιες μονάδες μέτρησης. Σημειώνεται πως τόσο η διασπορά, όσο και η τυπική απόκλιση είναι εξ ορισμού μη-αρνητικές. Τέλος, ένα εναλλακτικό μέτρο της διακύμανσης της τυχαίας μεταβλητής X είναι ο συντελεστής διακύμανσης, που περιγράφει το μέγεθος της διακύμανσης σε σχέση με τη μέση τιμή και ορίζεται ως εξής:

$$COV_X = \frac{\sigma_X}{\mu_X} \quad (11)$$

0.3.4 Συνήθεις κατανομές πιθανότητας

Σε αυτή την υποενότητα παρουσιάζονται οι τρεις πιο συνήθεις συνεχείς κατανομές πιθανότητας που χρησιμοποιούνται στην πράξη:

1. Η πιο απλή συνεχής κατανομή είναι η *ομοιόμορφη κατανομή*, σύμφωνα με την οποία η πιθανότητα η τυχαία μεταβλητή να λάβει τιμή στο κλειστό διάστημα $[a, b]$ είναι σταθερή. Η ομοιόμορφη κατανομή έχει τις εξής ιδιότητες:

- Συνάρτηση πυκνότητας πιθανότητας:

$$f_X(x) = \begin{cases} \frac{1}{b-a}, & \text{αν } a \leq x \leq b \\ 0, & \text{διαφορετικά} \end{cases} \quad (12)$$

- Μέση τιμή: $E[X] = \frac{b-a}{2}$
- Διασπορά: $Var(X) = \frac{(b-a)^2}{12}$

2. Η *κανονική ή Γκαουσιανή κατανομή* είναι η σημαντικότερη συνεχής κατανομή πιθανότητας. Η συνάρτηση πυκνότητας πιθανότητας της κανονικής κατανομής είναι η εξής:

$$f_X(x) = \frac{1}{\sqrt{2\pi}\sigma} \exp\left(-\frac{(x-\mu)^2}{2\sigma^2}\right) \quad (13)$$

όπου μ η μέση τιμή της τυχαίας μεταβλητής X και σ η τυπική απόκλιση.

3. Η *λογαριθμοκανονική κατανομή*, σύμφωνα με την οποία ο φυσικός λογάριθμος της τυχαίας μεταβλητής X ακολουθεί κανονική κατανομή. Η συνάρτηση πυκνότητας πιθανότητας είναι:

$$f_X(x) = \frac{1}{\sqrt{2\pi}\sigma_{\ln X}} \exp\left(-\frac{(\ln x - \mu_{\ln X})^2}{2\sigma_{\ln X}^2}\right) \quad (14)$$

όπου $\mu_{\ln X}$ και $\sigma_{\ln X}^2$ η μέση τιμή και διασπορά του φυσικού λογάριθμου της τυχαίας μεταβλητής X αντίστοιχα.

0.3.5 Από κοινού συνεχείς τυχαίες μεταβλητές

Σε πολλές περιπτώσεις, ενδιαφερόμαστε για δύο ή περισσότερες τυχαίες μεταβλητές που ανήκουν στον ίδιο δειγματικό χώρο, καθώς και τη σχέση που τις συνδέει. Για το λόγο αυτό, στην παρούσα υποενότητα μελετώνται οι *από κοινού συνεχείς τυχαίες μεταβλητές*. Σε αναλογία με την περίπτωση του χώρου μίας τυχαίας μεταβλητής, διερευνούμε την πιθανότητα δύο τυχαίες μεταβλητές X και Y να λάβουν συγκεκριμένες τιμές. Τότε, ορίζεται η *από κοινού αθροιστική συνάρτηση κατανομής* που έχει ως εξής:

$$F_{XY}(x, y) = P[(X \leq x) \cap (Y \leq y)] \quad (15)$$

Εκτενής Περίληψη

ενώ η από κοινού συνάρτηση πυκνότητας πιθανότητας ως:

$$f_{XY}(x, y) = \frac{\partial^2 F_{XY}}{\partial x \partial y}(x, y) \quad (16)$$

η οποία ικανοποιεί την ακόλουθη συνθήκη:

$$\int_{-\infty}^{+\infty} \int_{-\infty}^{+\infty} f_{XY}(x, y) dx dy = 1 \quad (17)$$

Με βάση την από κοινού συνάρτηση πυκνότητας πιθανότητας, μπορούν να υπολογιστούν οι λεγόμενες οριακές συναρτήσεις πυκνότητας πιθανότητας των X και Y ως εξής:

$$f_X(x) = \int_{-\infty}^{+\infty} f_{XY}(x, y) dy \quad (18)$$

$$f_Y(y) = \int_{-\infty}^{+\infty} f_{XY}(x, y) dx \quad (19)$$

που αντιστοιχούν στις συναρτήσεις πυκνότητας πιθανότητάς τους, εφόσον αυτές αντιμετωπιστούν ως ξεχωριστές τυχαίες μεταβλητές. Δύναται να οριστεί η από κοινού ροπή δύο τυχαίων μεταβλητών X και Y ως $E[X^n \cdot Y^m]$, όπου το άθροισμα των n και m ονομάζεται συνολική τάξη της ροπής. Ειδικότερα, η δεύτερη ροπή των X, Y γύρω από το κεντροειδές τους ονομάζεται συνδιασπορά, συμβολίζεται ως σ_{XY} και υπολογίζεται από την ακόλουθη σχέση:

$$\sigma_{XY} = E[(X - \mu_X)(Y - \mu_Y)] = \int_{-\infty}^{+\infty} \int_{-\infty}^{+\infty} (x - \mu_x)(y - \mu_y) f_{XY}(x, y) dx dy \quad (20)$$

Αν $\sigma_{XY} = 0$, οι τυχαίες μεταβλητές X, Y είναι ασυσχέτιστες. Τονίζεται δε πως δύο ανεξάρτητες τυχαίες μεταβλητές είναι πάντα ασυσχέτιστες, ενώ το αντίστροφο δεν είναι πάντοτε αληθές. Με σκοπό τώρα την καλύτερη κατανόηση του βαθμού συσχέτισης δύο τυχαίων μεταβλητών X, Y , η συνδιασπορά μπορεί να κανονικοποιηθεί ως προς το γινόμενο των τυπικών αποκλίσεών τους, από όπου προκύπτει ο συντελεστής συσχέτισης:

$$\rho_{XY} = \frac{\sigma_{XY}}{\sigma_X \sigma_Y} \quad (21)$$

Ο συντελεστής συσχέτισης ορίζεται μόνο στην περίπτωση που $\sigma_X \neq 0$ και $\sigma_Y \neq 0$, ενώ ικανοποιεί $-1 \leq \rho_{XY} \leq +1$. Δύο τυχαίες μεταβλητές X, Y είναι ανεξάρτητες, αν η από κοινού συνάρτηση πυκνότητας πιθανότητας ισούται με το γινόμενο των οριακών

συναρτήσεών τους, ή αλλιώς:

$$f_{XY}(x, y) = f_X(x)f_Y(y) \quad (22)$$

Η έννοια της ανεξαρτησίας μπορεί επίσης να γενικευτεί και στην περίπτωση περισσότερων της μίας τυχαίων μεταβλητών ως εξής:

$$f_{XYZ}(x, y, z) = f_X(x)f_Y(y)f_Z(z) \quad (23)$$

για τις τυχαίες μεταβλητές X, Y, Z .

0.4 Στοχαστικές διαδικασίες και τυχαία πεδία

0.4.1 Βασικές έννοιες

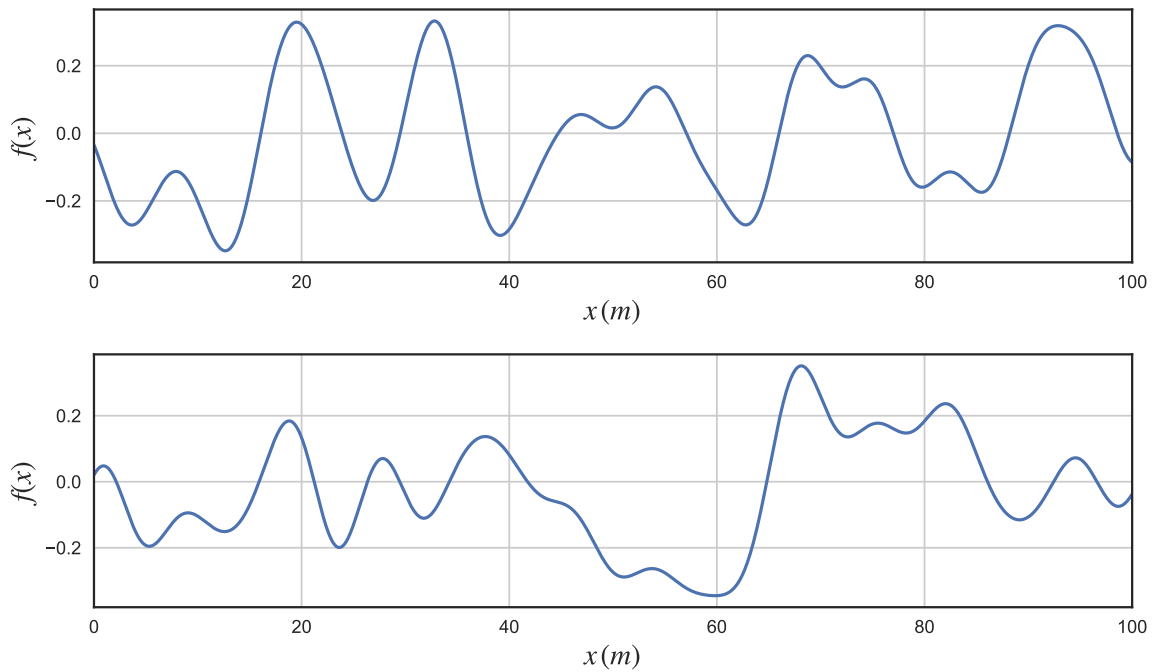
Οι στοχαστικές ή τυχαίες διαδικασίες αποτελούν ακολουθίες τυχαίων μεταβλητών. Γενικά, ο όρος αναφέρεται είτε στη διαδικασία, είτε στην παραγόμενη ακολουθία. Έστω $Y(t)$ μια στοχαστική διαδικασία. Το σύνολο όλων των δυνατών τυχαίων μεταβλητών αποτελεί το χώρο κατάστασης αυτής, ενώ το σύνολο των τιμών του t συνιστά το χώρο δεικτών της. Στη διεθνή βιβλιογραφία, ο όρος στοχαστική διαδικασία χρησιμοποιείται όταν ο χώρος δεικτών αποτελείται από χρονικά σημεία, ενώ ο όρος τυχαίο πεδίο υιοθετείται όταν εκείνος αποτελείται από σημεία στο χώρο.

Ειδικά στην παρούσα διατριβή, μελετώνται πραγματικά βαθμωτά τυχαία πεδία με συνεχή χώρο δεικτών, όπου οι τυχαίες μεταβλητές είναι πραγματικοί αριθμοί, ενώ οι δείκτες αναφέρονται σε χωρικά σημεία τόσο σε μία, όσο και σε δύο και τρεις διαστάσεις. Όσο για τις δειγματοσυναρτήσεις των τυχαίων πεδίων που θεωρούνται ανεξάρτητες με κοινή συνάρτηση κατανομής, αυτές ονομάζονται πραγματοποιήσεις του τυχαίου πεδίου. Στα σχήματα 1, 2 και 3 απεικονίζονται πραγματοποιήσεις τυχαίων πεδίων μίας, δύο και τριών διαστάσεων αντίστοιχα.

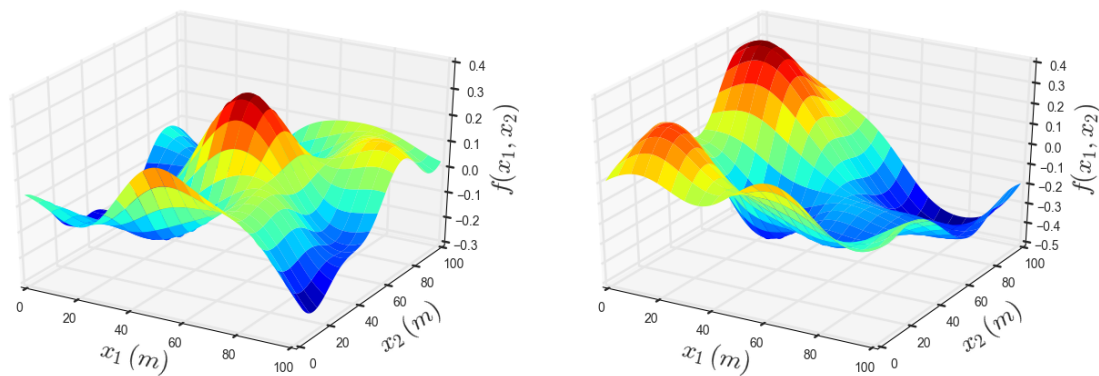
0.4.2 Εν συνόλω μέση τιμή και διασπορά

Για ένα τυχαίο πεδίο Y , ο συμβολισμός $Y(\mathbf{x})$ χρησιμοποιείται για το τυχαίο πεδίο όσον αφορά τη θέση \mathbf{x} στο χώρο. Συνεπώς, σε κάθε σημείο \mathbf{x} , η κατανομή της μεταβλητής $f(\mathbf{x})$ είναι η οριακή συνάρτηση κατανομής της διαδικασίας $f_{Y(\mathbf{x})}(y)$. Οι δε εν συνόλω

Εκτενής Περίληψη



Σχήμα 1. Πραγματοποιήσεις τυχαίων πεδίων μίας διάστασης.

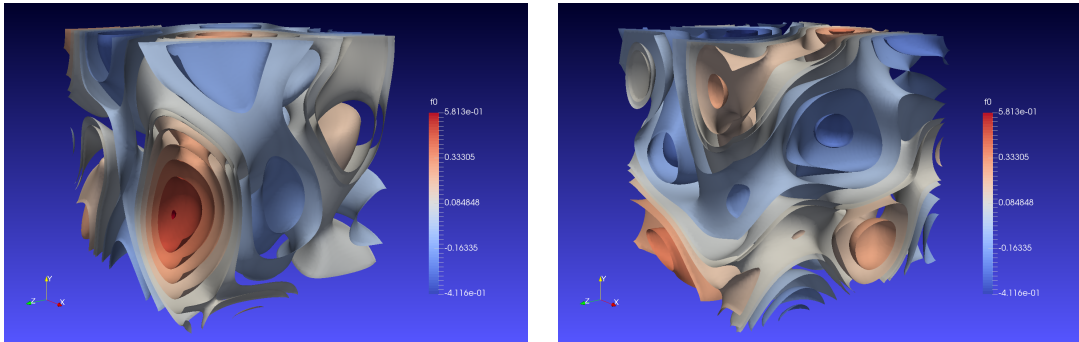


Σχήμα 2. Πραγματοποιήσεις τυχαίων πεδίων δύο διαστάσεων.

μέση τιμή και διασπορά υπολογίζονται σε κάθε χωρικό σημείο σύμφωνα με τις σχέσεις:

$$\mu_Y(\mathbf{x}) = E[Y(\mathbf{x})] = \int_{-\infty}^{+\infty} y f_{Y(\mathbf{x})}(y) dy \quad (24)$$

$$\sigma_{Y(\mathbf{x})}^2 = E[(Y(\mathbf{x}) - \mu_Y(\mathbf{x}))^2] = \int_{-\infty}^{+\infty} (y - \mu_Y(\mathbf{x}))^2 f_{Y(\mathbf{x})}(y) dy \quad (25)$$



Σχήμα 3. Πραγματοποιήσεις τυχαίων πεδίων τριών διαστάσεων.

0.4.3 Στάσιμες στοχαστικές διαδικασίες και ομογενή τυχαία πεδία

Σε γενικές περιπτώσεις, η κατανομή που περιγράφει μία χρονική στοχαστική διαδικασία μεταβάλλεται με το χρόνο, γεγονός που συνεπάγεται πως η μέση τιμή, διασπορά και συνάρτηση συσχέτισης εξαρτώνται από το χρόνο t . Οι στοχαστικές διαδικασίες, των οποίων η κατανομή παραμένει σταθερή με το χρόνο, ονομάζονται *στάσιμες διαδικασίες*. Για την ακρίβεια, μία στοχαστική διαδικασία είναι *αυστηρά στάσιμη*, αν η από κοινού συνάρτηση κατανομής παραμένει σταθερή με το χρόνο. Επισημαίνεται ασφαλώς πως στην πράξη, η απαίτηση αυτή είναι δύσκολο να αποδειχθεί και μία πιο χαλαρή συνθήκη χρησιμοποιείται. Μία στοχαστική διαδικασία αντιθέτως ονομάζεται *στάσιμη με την ευρεία έννοια*, αν η μέση τιμή της είναι σταθερή και η συνάρτηση συσχέτισης εξαρτάται μόνο από τη σχετική χρονική απόσταση μεταξύ δύο χρονικών σημείων. Έτσι, η συνάρτηση αυτοσυσχέτισης μεταξύ δύο χρονικών σημείων t_1 και t_2 εξαρτάται μόνο από τη διαφορά $\tau = t_1 - t_2$. Στην περίπτωση τώρα των τυχαίων πεδίων στο χώρο, ο όρος *ομογενής* χρησιμοποιείται για το χαρακτηρισμό ενός πεδίου, του οποίου η συνάρτηση κατανομής είναι σταθερή στο χώρο. Υπό αυτές τις συνθήκες, η συνάρτηση συσχέτισης μεταξύ δύο χωρικών σημείων με διανύσματα θέσης \mathbf{x} και \mathbf{y} εξαρτάται μόνο από τη διανυσματική διαφορά $\boldsymbol{\tau} = \mathbf{x} - \mathbf{y}$.

0.4.4 Εργοδικές στοχαστικές διαδικασίες και τυχαία πεδία

Έστω $X(t)$ μία χρονική στοχαστική διαδικασία και $X_m(t)$ μία δειγματοσυνάρτησή της. Η διαδικασία $X(t)$ ονομάζεται *εργοδική ως προς τη μέση τιμή*, εφόσον η χρονική μέση τιμή οποιασδήποτε πραγματοποίησης της $X_m(t)$ ισούται με την εν συνόλω μέση τιμή $\mu_X(t)$. Είναι φανερό πως, για να είναι μία διαδικασία εργοδική, θα πρέπει να είναι στάσιμη, ενώ το αντίστροφο δεν είναι πάντα αληθές. Με τον ίδιο τρόπο ορίζεται και η εργοδικότητα ως

προς τη διασπορά, τη συνάρτηση συσχέτισης, αλλά και τις ροπές ανώτερης τάξης. Μία διαδικασία αποκαλείται *ισχυρά εργοδική*, αν όλες οι χρονικές μέσες τιμές της είναι ίσες με τις αντίστοιχες εν συνόλω. Ονομάζεται δε *ασθενώς εργοδική*, αν είναι εργοδική ως προς τη μέση τιμή, τη διασπορά και τη συνάρτηση συσχέτισης.

Στην περίπτωση των τυχαίων πεδίων $f(\mathbf{x})$, όπου ο δείκτης \mathbf{x} αντιστοιχεί σε ένα σημείο του χώρου, η εργοδικότητα ως προς τη μέση τιμή αναφέρεται στην περίπτωση που η χωρική μέση τιμή είναι ίση με την εν συνόλω. Όπως και στην περίπτωση των στοχαστικών διαδικασιών, έτσι και για τα τυχαία πεδία έχουμε εργοδικότητα ως προς τη διασπορά, τη συνάρτηση συσχέτισης, αλλά και τις ροπές ανώτερης τάξης.

0.4.5 Στοχαστικές διαδικασίες και τυχαία πεδία στο πεδίο συχνοτήτων

Στην υποενότητα αυτή παρουσιάζεται μία εναλλακτική διατύπωση των ιδιοτήτων δευτέρας τάξης ενός στατιστικά ομογενούς τυχαίου πεδίου, γνωστή ως *φασματική αναπαράσταση*. Σε αυτή την περίπτωση, η συνάρτηση αυτοσυσχέτισης μπορεί να εκφραστεί στο πεδίο των συχνοτήτων με τη μορφή του *φάσματος ισχύος*. Το ζεύγος μετασχηματισμού Fourier $g(x)$ και $G(\kappa)$ ορίζεται ως:

$$G(\kappa) = \frac{1}{2\pi} \int_{-\infty}^{+\infty} g(x) e^{-i\kappa x} dx \quad (26)$$

$$g(x) = \int_{-\infty}^{+\infty} G(\kappa) e^{i\kappa x} d\kappa \quad (27)$$

όπου η συνάρτηση $G(\kappa)$ καλείται μετασχηματισμός Fourier της συνάρτησης $g(x)$. Αναλυτικότερα, η εξίσωση (26) είναι ο *εμπρός μετασχηματισμός Fourier* και η (27) ο *αντίστροφος μετασχηματισμός Fourier*.

0.4.6 Σχέσεις Wiener-Khinchine

Εδώ παρουσιάζονται οι σχέσεις Wiener-Khinchine για ομογενή τυχαία πεδία μίας διάστασης:

$$S_X(\kappa) = \frac{1}{2\pi} \int_{-\infty}^{+\infty} R_X(\tau) e^{-i\kappa\tau} d\tau \quad (28)$$

$$R_X(\tau) = \int_{-\infty}^{+\infty} S_X(\kappa) e^{i\kappa\tau} d\kappa \quad (29)$$

όπου $S_X(\kappa)$ το *φάσμα ισχύος*, κ ο *κυματικός αριθμός* και $R_X(\tau)$ η συνάρτηση αυτοσυσχέτισης που είναι συνάρτηση της σχετικής απόστασης τ .

Για ομογενή τυχαία πεδία, το φάσμα ισχύος είναι πραγματική και συμμετρική συνάρτηση, με αποτέλεσμα οι εξισώσεις (28) και (29) να δύνανται να οριστούν χωρίς τη χρήση φανταστικών αριθμών ως:

$$S_X(\kappa) = \frac{1}{2\pi} \int_{-\infty}^{+\infty} R_X(\tau) \cos(\kappa\tau) d\tau \quad (30)$$

$$R_X(\tau) = \int_{-\infty}^{+\infty} S_X(\kappa) \cos(\kappa\tau) d\kappa \quad (31)$$

Οι δε σχέσεις Wiener-Khinchine για διδιάστατα πεδία είναι οι εξής:

$$S_X(\kappa_1, \kappa_2) = \frac{1}{4\pi^2} \int_{-\infty}^{+\infty} \int_{-\infty}^{+\infty} R_X(\tau_1, \tau_2) \cos(\kappa_1\tau_1 + \kappa_2\tau_2) d\tau_1 d\tau_2 \quad (32)$$

$$R_X(\tau_1, \tau_2) = \int_{-\infty}^{+\infty} \int_{-\infty}^{+\infty} S_X(\kappa_1, \kappa_2) \cos(\kappa_1\tau_1 + \kappa_2\tau_2) d\kappa_1 d\kappa_2 \quad (33)$$

0.4.7 Προσομοίωση Γκαουσιανών τυχαίων πεδίων με τη μέθοδο της φασματικής αναπαράστασης

Στην ενότητα αυτή αναλύεται η μέθοδος της φασματικής αναπαράστασης για την παραγωγή Γκαουσιανών ομοιογενών πεδίων. Σύμφωνα με αυτή, το στοχαστικό πεδίο $f(\mathbf{x})$ αναπτύσσεται ως άθροισμα τριγωνομετρικών συναρτήσεων με τυχαίες γωνίες φάσης.

0.4.7.1 Μέθοδος φασματικής αναπαράστασης για την προσομοίωση Γκαουσιανών τυχαίων πεδίων μίας διάστασης

Η σχέση που χρησιμοποιείται για την προσομοίωση ομογενούς τυχαίου πεδίου $\hat{f}(\mathbf{x}_1)$ μίας διάστασης, μετά τη διατήρηση μόνο των πρώτων N_1 όρων, έχει ως εξής:

$$\hat{f}(\mathbf{x}_1) = \sqrt{2} \sum_{i=1}^{N_1} A_i \cos(\kappa_{1i} \mathbf{x}_1 + \phi_i) \quad (34)$$

όπου $\phi_i (i = 1, \dots, N_1)$ είναι ανεξάρτητες τυχαίες γωνίες φάσης, ομοιόμορφα κατανοημένες στο διάστημα $[0, 2\pi]$. Οι δε κυματικοί αριθμοί κ_{1i} αντιστοιχούν στον πρώτο χωρικό άξονα ως εξής:

$$\kappa_{1i} = i\Delta\kappa_1 = i \frac{\kappa_{1u}}{N_1} \quad \text{για } i = 1, \dots, N_1 \quad (35)$$

όπου κ_{1u} είναι ο άνω κυματικός αριθμός αποκοπής. Οι ντετερμινιστικοί συντελεστές A_i ορίζονται ως:

$$A_0 = 0 \quad A_i = \sqrt{2S_{f_0}(\kappa_{1i})\Delta\kappa_1} \quad \text{για} \quad i = 1, \dots, N_1 \quad (36)$$

όπου S_{f_0} είναι το φάσμα ισχύος, μη-αρνητική συνάρτηση του κυματικού αριθμού κ_i . Τονίζεται πως ο συντελεστής A_0 επιλέγεται μηδενικός ώστε να εξασφαλίζεται πως η μέση τιμή, υπολογισμένη σε όλο το μήκος $T_0 = 2\pi/\Delta\kappa_1$ του πεδίου $\hat{f}(\mathbf{x}_1)$, παραμένει μηδενική. Λόγω του κεντρικού οριακού θεωρήματος, το παραγόμενο τυχαίο είναι ασυμπτωτικά Γκαουσιανό καθώς $N_1 \rightarrow \infty$. Η δε μέση τιμή και η συνάρτηση αυτοσυσχέτισης είναι ίσες με τις αντίστοιχες που έχουν τεθεί ως στόχος για $N_1 \rightarrow \infty$. Επιπρόσθετα, το παραγόμενο τυχαίο πεδίο $\hat{f}(\mathbf{x}_1)$ είναι περιοδικό με περίοδο T_0 . Ένας επιπλέον περιορισμός οφείλει να εφαρμοστεί στο χωρικό βήμα Δx_1 , όποτε γεννώνται δειγματοσυναρτήσεις τυχαίων πεδίων στη μία διάσταση:

$$\Delta x_1 \leq \frac{2\pi}{2\kappa_{1u}} \quad (37)$$

και αυτό, γιατί η συνθήκη (37) είναι απαραίτητη για την αποφυγή του φαινομένου των επικαλύψεων.

0.4.8 Μη-Γκαουσιανές στοχαστικές διαδικασίες και τυχαία πεδία

Οι περισσότερες ιδιότητες των υλικών που προσομοιώνονται ως τυχαία πεδία είναι μη-Γκαουσιανές. Αυτός είναι και ο λόγος που η μελέτη των μη-Γκαουσιανών τυχαίων πεδίων έχει ιδιαίτερη σημασία για τη σωστή προσομοίωση της χωρικής διακύμανσης των ιδιοτήτων του υπό εξέταση υλικού. Ειδικότερα στην παρούσα διατριβή, θα ασχοληθούμε με μία ειδική κατηγορία στοχαστικών διαδικασιών και τυχαίων πεδίων, τις *διαδικασίες μεταφοράς και τα πεδία μεταφοράς*, που προσφέρουν μία απλή μεθοδολογία για τη μετατροπή κανονικών διαδικασιών και πεδίων σε μη-κανονικά.

0.4.8.1 Διαδικασίες και πεδία μεταφοράς

Στο σημείο αυτό μελετάται η περίπτωση βαθμωτών πραγματικών διαδικασιών $X(t)$ και $Y(t)$. Έστω g μία μονοτονική συνάρτηση και $Y(t)$ μία στάσιμη Γκαουσιανή στοχαστική διαδικασία με μοναδιαία διασπορά και συνάρτηση συσχέτισης $\rho(\tau) = E[Y(t+\tau)Y(t)]$. Η διαδικασία που προκύπτει από τον ακόλουθο μετασχηματισμό χωρίς μνήμη:

$$X(t) = g(Y(t)) \quad (38)$$

ονομάζεται διαδικασία μεταφοράς. Με ανάλογο τρόπο, έστω $Y(\mathbf{t})$, όπου $\mathbf{t} \in \mathbb{R}^d$ ένα βαθμωτό πραγματικό Γκαουσιανό ομογενές τυχαίο πεδίο με μοναδιαία διασπορά και συνάρτηση συσχέτισης $\rho(\boldsymbol{\tau}) = E[Y(\mathbf{t} + \boldsymbol{\tau})Y(\mathbf{t})]$. Το τυχαίο πεδίο που προκύπτει από τον ακόλουθο μετασχηματισμό:

$$X(\mathbf{t}) = g(Y(\mathbf{t})) \quad (39)$$

ονομάζεται πεδίο μεταφοράς.

0.5 Στοχαστικά πεπερασμένα στοιχεία

Τις δύο τελευταίες δεκαετίες, η μέθοδος των στοχαστικών πεπερασμένων στοιχείων (ΜΣΠΣ), επέκταση της κλασικής ντετερμινιστικής μεθόδου, έχει αναδειχθεί ως η κυρίαρχη μέθοδος για την επίλυση στοχαστικών προβλημάτων στην υπολογιστική μηχανική. Οι κύριες παραλλαγές αυτής είναι οι εξής:

1. Η μέθοδος διαταραχής, που έχει εφαρμοστεί με επιτυχία σε πλήθος γραμμικών και μη γραμμικών στατικών, καθώς και δυναμικών προβλημάτων. Όσον αφορά ένα στατικό ελαστικό πρόβλημα υπό ντετερμινιστική φόρτιση, αυτή συνίσταται στο ανάπτυγμα του καθολικού μητρώου στιβαρότητας, αλλά και του διανύσματος μετακινήσεων, κάνοντας χρήση ενός τυχαίου διανύσματος $\boldsymbol{\epsilon}$ με μηδενική μέση τιμή και γνωστό μητρώο συνδιασποράς ως:

$$\mathbf{K} = \mathbf{K}^{(0)} + \sum_{i=1}^n \mathbf{K}_i^{(1)} \boldsymbol{\epsilon}_i + \sum_{i=1}^n \sum_{j=1}^n \mathbf{K}_{ij}^{(2)} \boldsymbol{\epsilon}_i \boldsymbol{\epsilon}_j + \dots \quad (40)$$

$$\mathbf{U} = \mathbf{U}^{(0)} + \sum_{i=1}^n \mathbf{U}_i^{(1)} \boldsymbol{\epsilon}_i + \sum_{i=1}^n \sum_{j=1}^n \mathbf{U}_{ij}^{(2)} \boldsymbol{\epsilon}_i \boldsymbol{\epsilon}_j + \dots \quad (41)$$

Αντικαθιστώντας τις παραπάνω σχέσεις στην εξίσωση ισορροπίας και εξισώνοντας τους όρους βάσει του $\boldsymbol{\epsilon}$, προκύπτει στη συνέχεια σειρά από εξισώσεις προς επίλυση. Διατηρώντας δε τους όρους μέχρι και δεύτερης τάξης και απαλείφοντας τους υπόλοιπους από τις ανωτέρω εξισώσεις, η μέση τιμή της απόκρισης προκύπτει από τη σχέση:

$$E[\mathbf{U}] = \mathbf{U}^{(0)} + \sum_{i=1}^n \sum_{j=1}^n \mathbf{U}_{ij}^{(2)} E[\boldsymbol{\epsilon}_i \boldsymbol{\epsilon}_j] \quad (42)$$

2. Η μέθοδος φασματικών στοχαστικών πεπερασμένων στοιχείων, όπως παρουσιάστηκε από τους Ghanem & Spanos (Ghanem and Spanos, 2003), βασίζεται στο α-

νάπτυγμα Karhunen-Loève (K-L) του μητρώου στιβαρότητας, ενώ το τυχαίο διάνυσμα μετακινήσεων εκφράζεται ως ανάπτυγμα πολυωνυμικού χάους. Ως εκ τούτου προκύπτουν οι σχέσεις:

$$\mathbf{K}^{(e)}(\theta) = \mathbf{K}_0^{(e)} + \sum_{i=1}^{\infty} \mathbf{K}_i^{(e)} \xi_i(\theta) \quad (43)$$

$$\mathbf{U}(\theta) = \sum_{j=0}^{\infty} \mathbf{U}_j \Psi_j(\theta) \quad (44)$$

όπου στην εξίσωση (43), το \mathbf{K}_0 εκφράζει τη μέση τιμή του μητρώου στιβαρότητας $\mathbf{K}^{(e)}(\theta)$, ενώ το $\mathbf{K}_i^{(e)}$ δίνεται από τη σχέση:

$$\mathbf{K}_i^{(e)} = \sqrt{\lambda_i} \int_{\Omega_e} \phi_i(\mathbf{x}) \mathbf{B}^T \mathbf{D}_0 \mathbf{B} d\Omega_e \quad (45)$$

Η δε τελική εξίσωση ισορροπίας προκύπτει ως:

$$\left(\sum_{i=0}^{\infty} \mathbf{K}_i(\theta) \right) \cdot \left(\sum_{j=0}^{\infty} \mathbf{U}_j \psi_j(\theta) \right) - \mathbf{F} = 0 \quad (46)$$

ενώ ο αριθμός αγνώστων στην εξίσωση (46) εξαρτάται από τον αριθμό των όρων που διατηρούνται στα αναπτύγματα των εξισώσεων (43) και (44).

3. Η μέθοδος *Monte Carlo*, η οποία είναι δυνατόν να εφαρμοστεί σε οποιοδήποτε στοχαστικό πρόβλημα πεπερασμένων στοιχείων συνίσταται από τα εξής τρία βήματα:

- Γένεση δειγματοσυναρτήσεων τυχαίων πεδίων που περιγράφουν την υπό μελέτη στοχαστική ιδιότητα.
- Εκτέλεση ντετερμινιστικής ανάλυσης πεπερασμένων στοιχείων για κάθε ένα από τα παραπάνω πεδία.
- Στατιστική επεξεργασία των αποτελεσμάτων όλων των παραπάνω αναλύσεων, με σκοπό τον υπολογισμό των στατιστικών χαρακτηριστικών των υπό μελέτη μεγεθών απόκρισης.

Υπενθυμίζεται πως κύριο μειονέκτημα της μεθόδου είναι το μεγάλο υπολογιστικό κόστος λόγω του πλήθους των αναλύσεων που απαιτούνται.

0.5.1 Μέθοδοι σημειακής διακριτοποίησης

Οι δημοφιλέστερες μέθοδοι σημειακής διακριτοποίησης που παριστάνουν ένα συνεχές στοχαστικό πεδίο σε συγκεκριμένα σημεία του χώρου είναι:

1. Η μέθοδος του κομβικού σημείου, όπου οι τιμές του τυχαίου πεδίου υπολογίζονται στους κόμβους του πλέγματος των πεπερασμένων στοιχείων.
2. Η μέθοδος του σημείου ολοκλήρωσης, όπου οι τιμές του τυχαίου πεδίου υπολογίζονται στα σημεία ολοκλήρωσης του κάθε στοιχείου.
3. Η μέθοδος του κεντρικού σημείου, όπου το τυχαίο πεδίο υπολογίζεται στο κεντρικό σημείο κάθε πεπερασμένου στοιχείου, ενώ η τιμή που προκύπτει θεωρείται αντιπροσωπευτική και σταθερή σε όλο το πεπερασμένο στοιχείο.

0.6 Συναρτήσεις διακύμανσης της απόκρισης

Η ιδέα των συναρτήσεων διακύμανσης της απόκρισης (ΣΔΑ) εισήχθη από τον Shinozuka σε μία σειρά από πρωτοποριακά άρθρα (Bucher and Shinozuka, 1988; Kardara et al., 1989; Shinozuka, 1987). Αρχικά, η μέθοδος εφαρμόστηκε σε στατικά προβλήματα, ενώ η επέκτασή της για δυναμικά προβλήματα που οδηγεί στην εδραίωση της δυναμικής συνάρτησης διακύμανσης απόκρισης (ΔΣΔΑ) παρουσιάστηκε στα άρθρα (Papadopoulos and Kokkinos, 2012, 2015). Αν και είναι δύσκολο ή αδύνατον να παραχθεί κλειστή σχέση για τις ΣΔΑ και ΔΣΔΑ, αυτές δύνανται πάραυτα να υπολογιστούν αριθμητικά με χρήση της ταχείας μεθόδου Monte Carlo (FMCS).

0.6.1 Ορισμός δυναμικής συνάρτησης μέσης τιμής/διακύμανσης της απόκρισης

Για μονοδιάστατα προβλήματα, οι συναρτήσεις μέσης τιμής/διακύμανσης της απόκρισης ορίζονται σύμφωνα με τις σχέσεις:

$$E[u(t)] = \int_{-\infty}^{+\infty} DMRF(t, \kappa, \sigma_{ff}) S_{ff}(\kappa) d\kappa \quad (47)$$

$$Var[u(t)] = \int_{-\infty}^{+\infty} DVRF(t, \kappa, \sigma_{ff}) S_{ff}(\kappa) d\kappa \quad (48)$$

όπου $u(t)$ είναι η υπό μελέτη απόκριση, ενώ ως S_{ff} δηλώνεται το φάσμα ισχύος του τυχαίου πεδίου που παριστάνει τη στοχαστική ποσότητα που εξετάζεται. Εδώ πρέπει να επισημανθεί και το κύριο χαρακτηριστικό των ΔΣΜΑ/ΔΣΔΑ, δηλαδή η ανεξαρτησία τους από το φάσμα ισχύος άρα και τη δομή συσχέτισης του τυχαίου πεδίου που χρησιμοποιείται για την περιγραφή της υπό μελέτη στοχαστικής ιδιότητας του συστήματος. Αυτό άλλωστε το πλεονέκτημα είναι που επιτρέπει την ανάλυση ευαισθησίας της μέσης τιμής

και της διασποράς της απόκρισης ως προς τα χαρακτηριστικά συσχέτισης των τυχαίων πεδίων.

Όσον αφορά διδιάστατα προβλήματα, οι αντίστοιχες σχέσεις για τις ΔΣΜΑ/ΔΣΔΑ έχουν ως εξής:

$$E[u(t)] = \int_{-\infty}^{+\infty} \int_{-\infty}^{+\infty} DMRF(t, \kappa_1, \kappa_2, \sigma_{ff}) S_{ff}(\kappa_1, \kappa_2) d\kappa_1 d\kappa_2 \quad (49)$$

$$Var[u(t)] = \int_{-\infty}^{+\infty} \int_{-\infty}^{+\infty} DVRF(t, \kappa_1, \kappa_2, \sigma_{ff}) S_{ff}(\kappa_1, \kappa_2) d\kappa_1 d\kappa_2 \quad (50)$$

0.6.2 Υπολογισμός άνω ορίων μέσης τιμής/διασποράς της απόκρισης

Η μεθοδολογία των ΔΣΜΑ/ΔΣΔΑ επιτρέπει τον άμεσο υπολογισμό άνω ορίων της μέσης τιμής, αλλά και διασποράς της απόκρισης, όλα συναρτήσεις του χρόνου t . Για στοχαστικά συστήματα σε μία διάσταση, τα ανωτέρω όρια υπολογίζονται βάσει των σχέσεων:

$$E[d(t)] = \int_{-\infty}^{+\infty} DMRF(t, \kappa, \sigma_{ff}, t) S_{ff}(\kappa) d\kappa \leq DMRF(t, \kappa^{max}(t), \sigma_{ff}) \sigma_{ff}^2 \quad (51)$$

$$Var[d(t)] = \int_{-\infty}^{+\infty} DVRF(t, \kappa, \sigma_{ff}, t) S_{ff}(\kappa) d\kappa \leq DVRF(t, \kappa^{max}(t), \sigma_{ff}) \sigma_{ff}^2 \quad (52)$$

όπου $\kappa^{max}(t)$ είναι ο κυματικός αριθμός που μεγιστοποιεί τις ΔΣΜΑ/ΔΣΔΑ αντίστοιχα για κάθε χρονική στιγμή t . Για μια πλήρη εικόνα, δίνονται στη συνέχεια και οι αντίστοιχες σχέσεις για τον υπολογισμό των άνω ορίων σε διδιάστατα στοχαστικά συστήματα:

$$\begin{aligned} E[d(t)] &= \int_{-\infty}^{+\infty} \int_{-\infty}^{+\infty} DMRF(t, \kappa_x, \kappa_y, \sigma_{ff}) S_{ff}(\kappa_x, \kappa_y) d\kappa_x d\kappa_y \\ &\leq DMRF(t, \kappa_x^{max}(t), \kappa_y^{max}(t), \sigma_{ff}) \sigma_{ff}^2 \end{aligned} \quad (53)$$

$$\begin{aligned} Var[d(t)] &= \int_{-\infty}^{+\infty} \int_{-\infty}^{+\infty} DVRF(t, \kappa_x, \kappa_y, \sigma_{ff}) S_{ff}(\kappa_x, \kappa_y) d\kappa_x d\kappa_y \\ &\leq DVRF(t, \kappa_x^{max}(t), \kappa_y^{max}(t), \sigma_{ff}) \sigma_{ff}^2 \end{aligned} \quad (54)$$

όπου $(\kappa_x^{max}(t), \kappa_y^{max}(t))$ είναι τα ζεύγη των κυματικών αριθμών στους άξονες κ_x και κ_y που μεγιστοποιούν τις ΔΣΜΑ/ΔΣΔΑ τη χρονική στιγμή t .

0.6.3 Ταχεία μέθοδος Monte Carlo

Όπως αναφέρθηκε παραπάνω, είναι εξαιρετικά δύσκολο, αν όχι ανέφικτο, να βρεθεί μία κλειστή σχέση για τις $\Delta\Sigma\text{MA}/\Delta\Sigma\text{DA}$. Παρ' όλα αυτά, οι ανωτέρω συναρτήσεις είναι δυνατόν να υπολογιστούν αριθμητικά με τη χρήση της ταχείας μεθόδου Monte Carlo (FMCS). Η βασική σύλληψη έγκειται στη γένεση τυχαίων πεδίων $f(x)$ για μονοδιάστατα προβλήματα που αντιστοιχούν σε τυχαία ημίτονα με μονοχρωματικά φάσματα ισχύος. Συγκεκριμένα, υπολογίζοντας τη μέση τιμή και τη διασπορά της υπο μελέτη απόκρισης για καθένα από τα παραπάνω ημίτονα, οι $\Delta\Sigma\text{MA}/\Delta\Sigma\text{DA}$ υπολογίζονται ξεχωριστά για κάθε κυματικό αριθμό. Η δε FMCS συνοψίζεται στα εξής βήματα:

1. Για την τυπική απόκλιση σ_{ff} της υπό μελέτη απόκρισης, γίνεται γένεση $N(5-10)$, δειγματοσυναρτήσεων ημιτόνων για κάθε κυματικό αριθμό κ ως εξής:

$$f_j(x) = \sqrt{2}\sigma_{ff} \cos(\kappa \cdot x + \phi_j) \quad (55)$$

όπου ϕ_j είναι το κέντρο των διαστημάτων $\left(\frac{2\pi j}{N}, \frac{2\pi(j+1)}{N}\right)$ για $j = 0, 1, \dots, N-1$. Τονίζεται φυσικά πως, λόγω της συμμετρίας των $\Delta\Sigma\text{MA}/\Delta\Sigma\text{DA}$ σε μονοδιάστατα στοχαστικά συστήματα, μόνο μη αρνητικές τιμές του κυματικού αριθμού χρησιμοποιούνται. Για την ακρίβεια, ένας άνω κυματικός αριθμός αποκοπής κ_u επιλέγεται κάθε φορά, ενώ ο άξονας κυματικών αριθμών χωρίζεται σε M υποδιαστήματα. Δεδομένων των παραπάνω, η διακριτοποιημένη μορφή της εξίσωσης (55) έχει ως εξής:

$$f_{ij}(x) = \sqrt{2}\sigma_{ff} \cos(\kappa_i \cdot x + \phi_j) \quad (56)$$

όπου $\kappa_i = i\Delta\kappa$ για $i = 0, 1, \dots, M$ και το $\Delta\kappa = \kappa_u/M$ συμβολίζει το πλάτος του διαστήματος στον άξονα των κυματικών αριθμών.

2. Για κάθε διακριτό κυματικό αριθμό κ_i , υπολογίζεται κατόπιν η μέση τιμή και διασπορά της απόκρισης για τις αντίστοιχες N δειγματοσυναρτήσεις των τυχαίων ημιτόνων, όπου f_{ij} για $j = 1, 2, \dots, N$.
3. Υπολογισμός των τιμών των $\Delta\Sigma\text{MA}/\Delta\Sigma\text{DA}$ για κάθε κυματικό αριθμό κ_i κάνοντας χρήση των σχέσεων:

$$DMRF(t, \kappa_i, \sigma_{ff}) = \frac{E[d(t)]_{\kappa_i}}{\sigma_{ff}^2} \quad (57)$$

$$DVRF(t, \kappa_i, \sigma_{ff}) = \frac{Var[d(t)]_{\kappa_i}}{\sigma_{ff}^2} \quad (58)$$

4. Συγκέντρωση όλων των τιμών των $\Delta\Sigma\Lambda/\Delta\Sigma\Delta\Lambda$ για κάθε κυματικό αριθμό k_i σε κάθε χρονικό βήμα για τη δεδομένη τυπική απόκλιση σ_{ff} . Η όλη διαδικασία δύναται επίσης να επαναληφθεί για εναλλακτικές τιμές της τυπικής απόκλισης σ_{ff} . Με ανάλογο τρόπο, η παραπάνω μέθοδος επεκτείνεται για την αντιμετώπιση στοχαστικών προβλημάτων σε δύο και τρεις χωρικές διαστάσεις.

0.7 Στερεοποίηση εδάφους με στοχαστικές ιδιότητες

Στην ενότητα αυτή μελετάται το φαινόμενο της στερεοποίησης κορεσμένου εδαφικού στρώματος με στοχαστική διαπερατότητα k και μέτρο ελαστικότητας E . Για την ενσωμάτωση της χωρικής διακύμανσης των εδαφικών ιδιοτήτων υιοθετείται η μέθοδος των στοχαστικών πεπερασμένων στοιχείων με τη μορφή της απευθείας ανάλυσης Monte Carlo. Συγκεκριμένα, η αριθμητική εφαρμογή που εξετάζεται συνίσταται από άκαμπτο τραχύ λωριδωτό θεμέλιο επί στοχαστικού εδαφικού στρώματος. Η δε υπό μελέτη απόκριση περιλαμβάνει τόσο την καθίζηση του θεμελίου, όσο και τις εδαφικές υπερπίεσεις πόρων.

0.7.1 Αριθμητική επίλυση των εξισώσεων στερεοποίησης

Κατά το φαινόμενο της εδαφικής στερεοποίησης συντελείται σταδιακή αποτόνωση των υπερπίεσεων των πόρων, συνοδευόμενη από παραμόρφωση του εδαφικού σκελετού. Αναλυτικότερα, ένα φορτίο, που εφαρμόζεται σε κορεσμένο εδαφικό στρώμα, παραλαμβάνεται αρχικά από το υγρό των πόρων του εδάφους υπό τη μορφή υπερπίεσης και σταδιακά μεταβιβάζεται στον εδαφικό σκελετό. Η θεωρία της μονοδιάστατης στερεοποίησης παρουσιάστηκε από τον Terzaghi, ενώ η επέκτασή στις τρεις διαστάσεις πραγματοποιήθηκε από τον Biot (Maurice A. Biot, 1941). Στην πραγματικότητα, το κλειδί για την κατανόηση του φαινομένου είναι η έννοια της ενεργούς τάσης, η οποία αναφέρεται στο ποσοστό της ολικής τάσης που παραλαμβάνεται από τον εδαφικό σκελετό. Συνδυάζοντας δε τις εξισώσεις ισορροπίας και διατήρησης μάζας με το νόμο του Darcy, που περιγράφει τη ροή υγρού μέσω πορώδους μέσου, οδηγούμαστε στο συζευγμένο σύστημα των εξισώσεων στερεοποίησης.

Στην παρούσα διατριβή, η χωρική διακριτοποίηση των εξισώσεων στερεοποίησης επιτυγχάνεται με τη μέθοδο πεπερασμένων στοιχείων μετατόπισης-πίεσης πόρων (u-p), ενώ για την ολοκλήρωση ως προς το χρόνο χρησιμοποιείται η γενικευμένη μέθοδος Newmark

0.7 Στερεοποίηση εδάφους με στοχαστικές ιδιότητες

πρώτης τάξης. Βάσει των παραπάνω, η τελική μητρική εξίσωση προκύπτει ως εξής:

$$\begin{bmatrix} \mathbf{K}_m & s\mathbf{C} \\ s\mathbf{C}^T & -s^2\Delta t\mathbf{K}_c \end{bmatrix} \begin{Bmatrix} \mathbf{u}^{(n+1)} \\ \frac{1}{s}\mathbf{u}_w^{(n+1)} \end{Bmatrix} = \begin{Bmatrix} \mathbf{f}^{(n+1)} \\ s\mathbf{C}^T\mathbf{u}^{(n+1)} \end{Bmatrix} \quad (59)$$

όπου \mathbf{K}_m το μητρώο στιβαρότητας των εδαφικών στοιχείων, \mathbf{C} το μητρώο σύζευξης, \mathbf{K}_c το μητρώο υδραυλικής αγωγιμότητας, ενώ \mathbf{u} και \mathbf{u}_w τα διανύσματα μετακινήσεων βαθμών ελευθερίας και πίεσης πόρων αντίστοιχα. Επιπλέον, το Δt δηλώνει το χρονικό βήμα ολοκλήρωσης και s ένας βαθμωτός συντελεστής που βελτιώνει το δείκτη κατάστασης του μητρώου στο αριστερό μέλος, όπως προτείνεται στο άρθρο (Reed, 1984). Τα δε μητρώα που προκύπτουν στην εξίσωση (59) μορφώνονται σύμφωνα με τις συναρτήσεις σχήματος που χρησιμοποιούνται για την παρεμβολή των βαθμών ελευθερίας μετακίνησης και πίεσης πόρων. Σημειώνεται πως οι τεχνικές που χρησιμοποιούνται για το σκοπό αυτό αναλύονται σε βάθος στα συγγράμματα (Lewis et al., 1998; O. C. Zienkiewicz et al., 1999; Smith and Griffiths, 2004). Οφείλει να σημειωθεί πως, στην παρούσα διατριβή, ο συντελεστής διαπερατότητας k ορίζεται σε μονάδες $[\text{μήκος}]^3[\text{χρόνος}]/[\text{μάζα}]$ ή ισοδύναμα $[\text{μήκος}]^4[\text{δύναμη}]^{-1}/[\text{χρόνος}]$, διαφορετικές από τη μονάδα ταχύτητας που χρησιμοποιείται στη γεωτεχνική. Ωστόσο, τα δύο διαφορετικά μεγέθη διαπερατότητας συνδέονται μέσω της σχέσης $k = k'/\gamma_w$, όπου k' ο συντελεστής διαπερατότητας εκφρασμένος σε όρους ταχύτητας και γ_w το ειδικό βάρος του νερού. Επιπρόσθετα, υιοθετείται ισοτροπική διαπερατότητα και έτσι ο τανυστής διαπερατότητας \mathbf{k} εκφράζεται ως $\mathbf{k} = k\mathbf{I}$, όπου \mathbf{I} ο μοναδιαίος τανυστής δεύτερης τάξης.

0.7.2 Ανάλυση με στοχαστικά πεπερασμένα στοιχεία

Στην εν λόγω μελέτη, ο συντελεστής διαπερατότητας k και το μέτρο ελαστικότητας E προσομοιώνονται ως βαθμωτά ομογενή λογαριθμοκανονικά τυχαία πεδία (2D-1V) με χωρική διακύμανση στις δύο διαστάσεις. Η επιρροή των k και E μελετάται ανεξάρτητα σε ξεχωριστές αναλύσεις Monte Carlo, ενώ η μέθοδος κεντρικού σημείου χρησιμοποιείται για τη μόρφωση των στοχαστικών μητρώων υδραυλικής αγωγιμότητας και στιβαρότητας. Συμφωνα με αυτή, η χωρικά συνεχής εδαφική ιδιότητα, π.χ. k , προσεγγίζεται από μία μοναδική τυχαία μεταβλητή $\hat{k}(x)$ που ορίζεται ως η τιμή του τυχαίου πεδίου στο κεντρικό σημείο x_c κάθε στοιχείου Ω_e ως:

$$\hat{k}(x) = k(x_c) \quad \forall x \in \Omega_e \quad (60)$$

Καταρχήν, η μέθοδος φασματικής αναπαράστασης χρησιμοποιείται για τη γένεση ομογενών Γκαουσιανών τυχαίων πεδίων μηδενικής μέσης τιμής και μοναδιαίας διασποράς στο κεντρικό σημείο κάθε πεπερασμένου στοιχείου. Έπειτα, οι λογαριθμοκανονικές παράμετροι υπολογίζονται ως εξής:

$$v_k = \frac{\sigma_k}{\mu_k} \quad (61)$$

$$\sigma_{\ln(k)}^2 = \ln(1 + v_k^2) \quad (62)$$

$$\mu_{\ln(k)} = \ln(\mu_k) - \frac{1}{2}\sigma_{\ln(k)}^2 \quad (63)$$

ενώ οι τελικές τιμές k_i (αντίστοιχα για E_i) υπολογίζονται μετασχηματίζοντας τα στοιχεία του Γκαουσιανού πεδίου G_i μέσω της ακόλουθης σχέσης:

$$k_i = \exp(\mu_{\ln(k)} + \sigma_{\ln(k)} G_i) \quad (64)$$

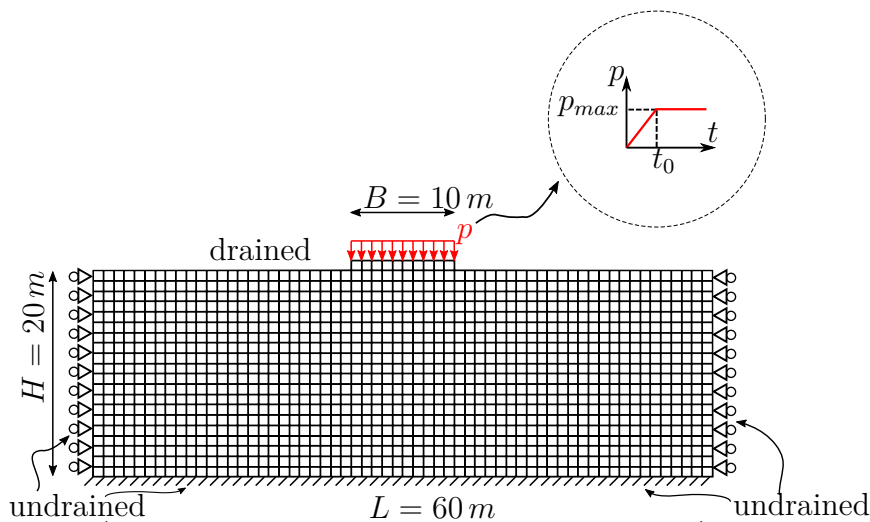
0.7.3 Αριθμητική εφαρμογή

0.7.3.1 Περιγραφή του αριθμητικού προσομοιώματος

Όπως αναφέρθηκε παραπάνω, η αριθμητική εφαρμογή αποτελείται από ένα άκαμπτο τραχύ λωριδωτό θεμέλιο επί κορεσμένου εδάφους. Αυτό φορτίζεται με ομοιόμορφο φορτίο αυξανόμενο με το χρόνο, μέχρι να φτάσει μία μέγιστη τιμή όπου και παραμένει έπειτα σταθερό. Το σχετικό προσομοίωμα των πεπερασμένων στοιχείων απεικονίζεται στο σχήμα 6.3, όπου το πάχος του εδαφικού στρώματος είναι $H = 20 \text{ m}$ και το πλάτος του θεμελίου $B = 10 \text{ m}$. Ως προς την οριζόντια διεύθυνση, το συνολικό μήκος $L = 60 \text{ m}$ θεωρείται επαρκές για την προσομοίωση του προβλήματος. Ισοπαραμετρικά τετρακομβικά τετραγωνικά στοιχεία επίπεδης παραμόρφωσης χρησιμοποιούνται επίσης για τη διακριτοποίηση εδάφους και θεμελίου με μήκος ακμής 1 m . Υπογραμμίζεται πως τα στοιχεία που αντιστοιχούν στο έδαφος διαθέτουν βαθμούς ελευθερίας μετακίνησης και πίεσης πόρων, που παρεμβάλλονται με διγραμμικές συναρτήσεις σχήματος, ενώ τα στοιχεία του θεμελίου διαθέτουν μόνο βαθμούς ελευθερίας μετακίνησης. Όσον αφορά τις συνοριακές συνθήκες, η βάση του μοντέλου πακτώνεται, την ίδια στιγμή που στις δύο κατακόρυφες πλευρές οι οριζόντιες μετακινήσεις δεσμεύονται. Συγχρόνως, στους κόμβους της βάσης και των κατακόρυφων πλευρών χρησιμοποιούνται αδιαπέρατες υδραυλικές συνοριακές συνθήκες, ενώ στην επιφάνεια του εδάφους επιτρέπεται ελεύθερη ροή, ή αλλιώς μηδενική υπερπίεση πόρων. Το δε ομοιόμορφο επιφανειακό φορτίο p , που εφαρμόζεται

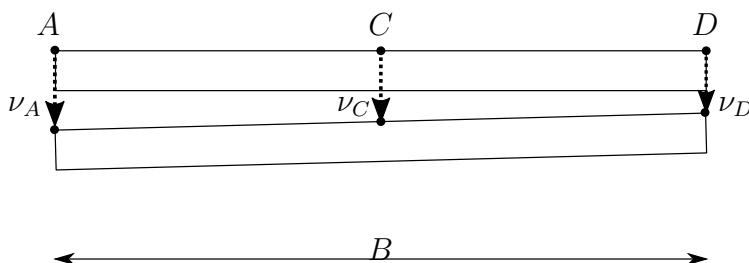
0.7 Στερεοποίηση εδάφους με στοχαστικές ιδιότητες

στο θεμέλιο, αυξάνεται γραμμικά από το χρόνο 0 έως το χρονικό σημείο $t_0 = 25$ ημέρες, οπότε και παραμένει σταθερό με τιμή $p_{max} = 1.0 \text{ kN/m}^2$. Εφόσον το πρόβλημα είναι γραμμικώς ελαστικό, η επιλογή του μοναδιαίου φορτίου επιτρέπει τη γενίκευση των αποτελεσμάτων για εναλλακτικά μεγέθη φορτίου. Στην προκειμένη εφαρμογή ο συντε-



Σχήμα 4. Δίκτυο πεπερασμένων στοιχείων.

λεστής διαπερατότητας k και το μέτρο ελαστικότητας E είναι οι στοχαστικές παράμετροι του προβλήματος, ενώ οι υπόλοιπες ιδιότητες των υλικών είναι χωρικά και χρονικά σταθερές. Ο λόγος Poisson του εδάφους είναι $\nu = 0.3$, ενώ το υλικό του θεμελίου έχει τις ιδιότητες $E = 20 \text{ GPa}$ και $\nu = 0.4$. Ο συντελεστής διαπερατότητας k και το μέτρο ελαστικότητας E προσομοιώνονται ως λογαριθμοκανονικά ομογενή τυχαία πεδία με μέση τιμή $\mu_k = 1.22 \cdot 10^{-5} \text{ m}^4 \cdot \text{kN}^{-1}/\text{day}$ και $\mu_E = 622.7 \text{ kPa}$ αντίστοιχα. Πλήθος διαφορετικών συντελεστών διακύμανσης $COV = \{0.25, 0.5, 1.0, 2.0, 5.0\}$ χρησιμοποιείται και για τις δύο εδαφικές ιδιότητες. Επιπρόσθετα, τα μήκη συσχέτισης $b_{1\ln(k)} = b_{2\ln(k)} = b_{\ln(k)}$ για k και $b_{1\ln(E)} = b_{2\ln(E)} = b_{\ln(E)}$ για E κυμαίνονται μεταξύ 4.0 m και 100.0 m . Στο



Σχήμα 5. Καθίζηση θεμελίου.

σχήμα 5, τα σημεία A και D αντιστοιχούν στις άνω αριστερά και δεξιά κορυφές του θεμε-

λίου, ενώ το C στο κέντρο της άνω ακμής του. Οι δε κατακόρυφες μετακινήσεις των A , C και D συμβολίζονται ως ν_A , ν_B και ν_C αντίστοιχα. Τονίζεται πως στη συγκεκριμένη ενότητα ο όρος *διαφορική καθίζηση* χρησιμοποιείται για να εκφράσει την απόλυτη τιμή της διαφοράς της κατακόρυφης μετακίνησης των A και D , ή αλλιώς $\Delta\nu = |\nu_A - \nu_D|$.

0.7.4 Μελέτη στατιστικών απόκρισης

0.7.4.1 Καθίζηση θεμελίου

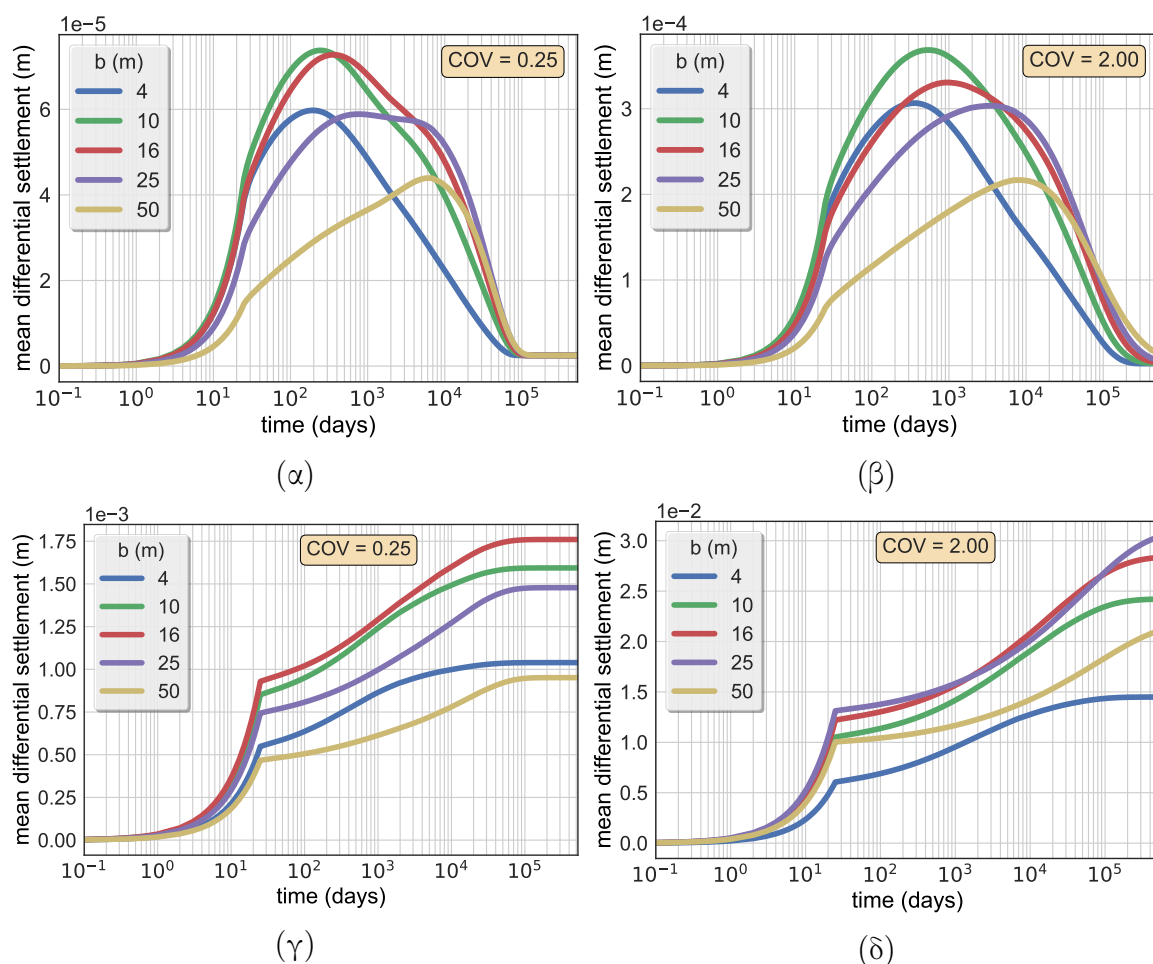
Στην παρούσα υποενότητα μελετάται η απόκριση του θεμελίου σε όρους καθίζησης. Αρχικά, η επιρροή του μήκους συσχέτισης $b_{\ln(k)} = b_{1\ln(k)} = b_{2\ln(k)}$ και $b_{\ln(E)} = b_{1\ln(E)} = b_{2\ln(E)}$, το οποίο λαμβάνεται ως ισοτροπικό, όπως και του συντελεστή διακύμανσης στη μέση διαφορική καθίζηση απεικονίζονται στο σχήμα 6. Από εκεί γίνεται φανερό πως μεγαλύτερες τιμές του συντελεστή διακύμανσης αυξάνουν τη διαφορική καθίζηση. Συγκρίνοντας δε τα αποτελέσματα για τις στοχαστικές ιδιότητες k και E , προκύπτει το συμπέρασμα πως η διαφορική καθίζηση είναι αρκετά μεγαλύτερη στην περίπτωση της διακύμανσης του μέτρου ελαστικότητας. Επιπλέον, η μορφή της καμπύλης εξέλιξης της διαφορικής καθίζησης είναι διαφορετική στις δύο περιπτώσεις. Όσον αφορά την περίπτωση του στοχαστικού k , η διαφορική καθίζηση λαμβάνει μία μέγιστη τιμή και έπειτα φθίνει προς μηδενικές τιμές. Αντίθετα, στην περίπτωση του E , οι διαφορικές καθιζήσεις παραμένουν καθ' όλη τη διάρκεια της στερεοποίησης, ενώ αυξάνονται μονοτονικά με το χρόνο. Έτσι, η τελική διαφορική καθίζηση είναι μη μηδενική μόνο για την περίπτωση της διακύμανσης του μέτρου ελαστικότητας. Σημειώνεται πως η καθίζηση μεμονωμένων σημείων του θεμελίου δεν παρουσιάζει το ίδιο ενδιαφέρον και για το λόγο αυτό παραλείπεται.

Η μελέτη λοιπόν της ευαισθησίας της μέσης τιμής και τυπικής απόκλισης της μέγιστης διαφορικής καθίζησης ως προς το κανονικοποιημένο μήκος συσχέτισης των τυχαίων πεδίων οδηγεί στο πιο ενδιαφέρον συμπέρασμα της εν λόγω εφαρμογής. Και αυτό γιατί, παρατηρώντας το σχήμα 7, είναι ξεκάθαρο πως η μέση τιμή και τυπική απόκλιση μεγιστοποιούνται για τιμή του λόγου $b_{\ln(k)}/B$ κοντά στη μονάδα για την περίπτωση του k , ανεξαρτήτως της τιμής του συντελεστή συσχέτισης. Όσον αφορά δε την περίπτωση του E , η εν λόγω μεγιστοποίηση πραγματοποιείται για τιμές του λόγου $b_{\ln(E)}/B$ μεταξύ των 1.5 και 2.5.

0.7.4.2 Υπερπίεση πόρων

Σε αυτή την υποενότητα διερευνάται η υπερπίεση πόρων του εδαφικού στρώματος. Συγκεκριμένα, εξετάζεται υπερπίεση του σημείου που βρίσκεται σε βάθος $B/2$ από την

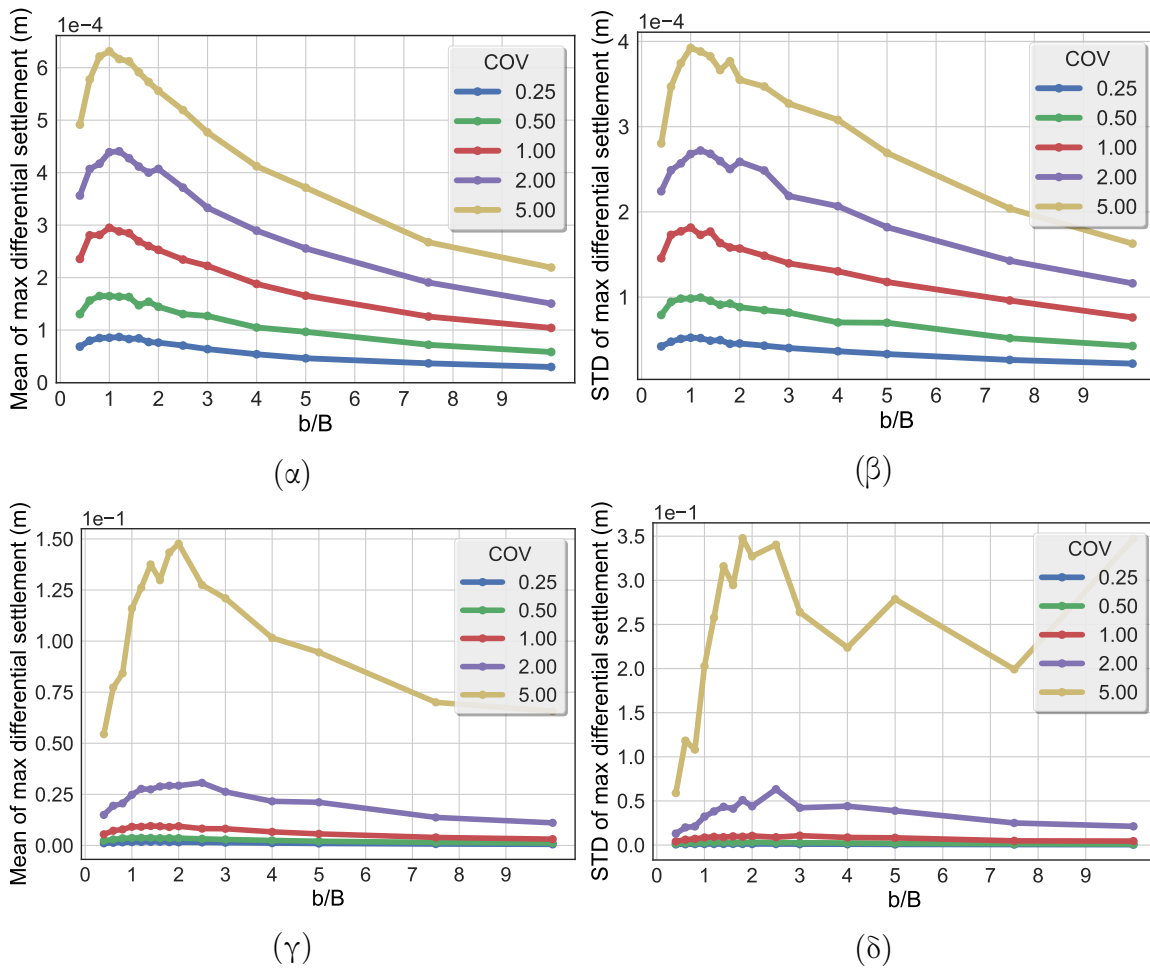
0.7 Στερεοποίηση εδάφους με στοχαστικές ιδιότητες



Σχήμα 6. Μέση τιμή της διαφορικής καθίζησης ν_{AD} για : (α) στοχαστικό k και $COV = 0.25$, (β) στοχαστικό k και $COV = 2.00$, (γ) στοχαστικό E και $COV = 0.25$ και (δ) στοχαστικό E και $COV = 2.00$.

εδαφική επιφάνεια επί της κατακόρυφου που διέρχεται από το κέντρο του θεμελίου. Παρατηρώντας το σχήμα 8, είναι ολοφάνερο πως η μέση τιμή της υπερπίεσης πόρων παραμένει ανεπηρέαστη από το μήκος συσχέτισης b , καθώς και την τιμή του συντελεστή διακύμανσης (COV) τόσο για τη χωρική διακύμανση του k , όσο και του E . Παρ' όλα αυτά, σύμφωνα και με το σχήμα 9, για μεγάλες τιμές του συντελεστή διακύμανσης παρουσιάζεται σημαντική διακύμανση της πίεσης γύρω από τη μέση τιμή για την περίπτωση του στοχαστικού E . Τέλος, μελετώντας τη μέγιστη τιμή της μέσης τιμής και τυπικής απόκλισης της υπερπίεσης συναρτήσει του κανονικοποιημένου μήκους συσχέτισης που απεικονίζονται στο σχήμα 10, είναι ξεκάθαρο πως δεν παρουσιάζεται συγκεκριμένο σχήμα των καμπυλών για την περίπτωση του k . Τουναντίον, στην περίπτωση του E ,

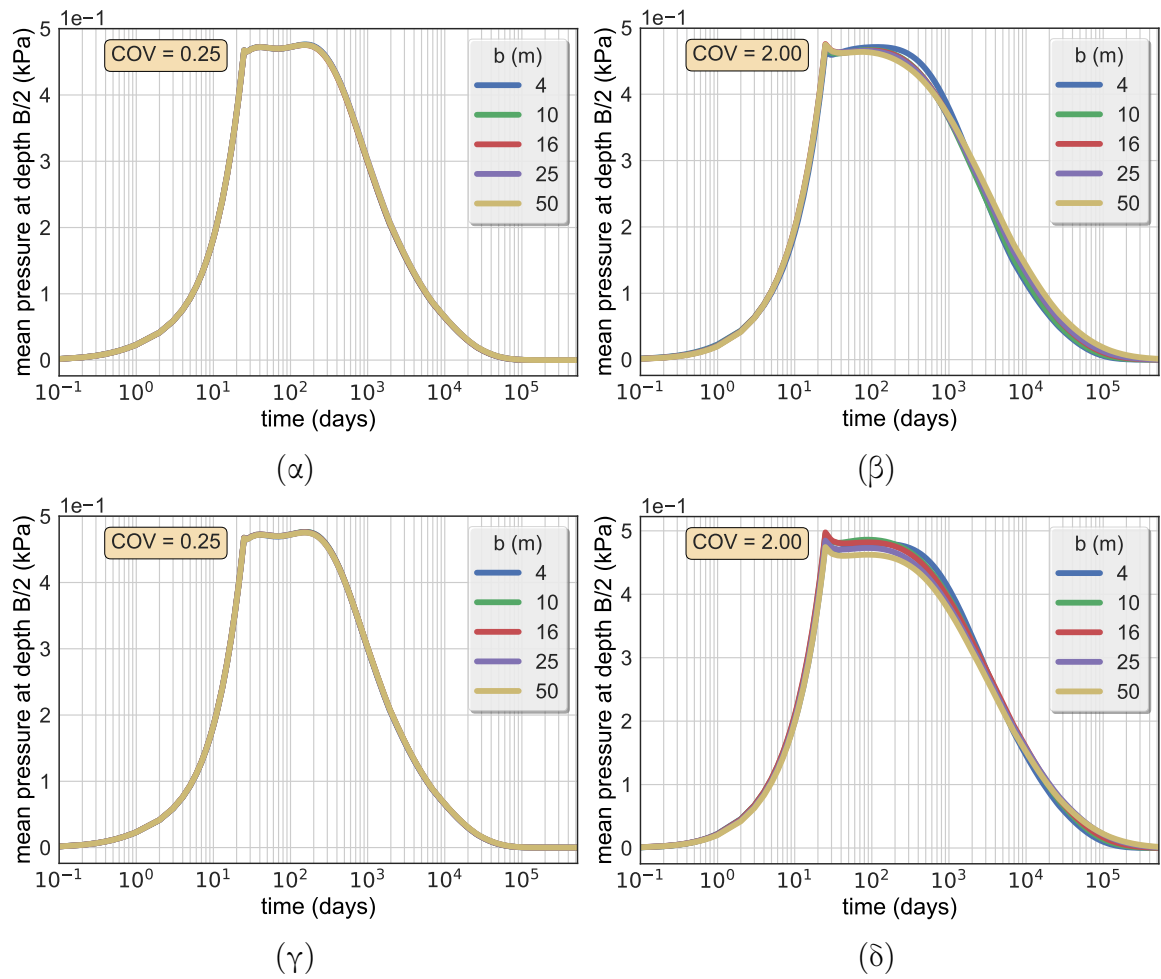
Εκτενής Περίληψη



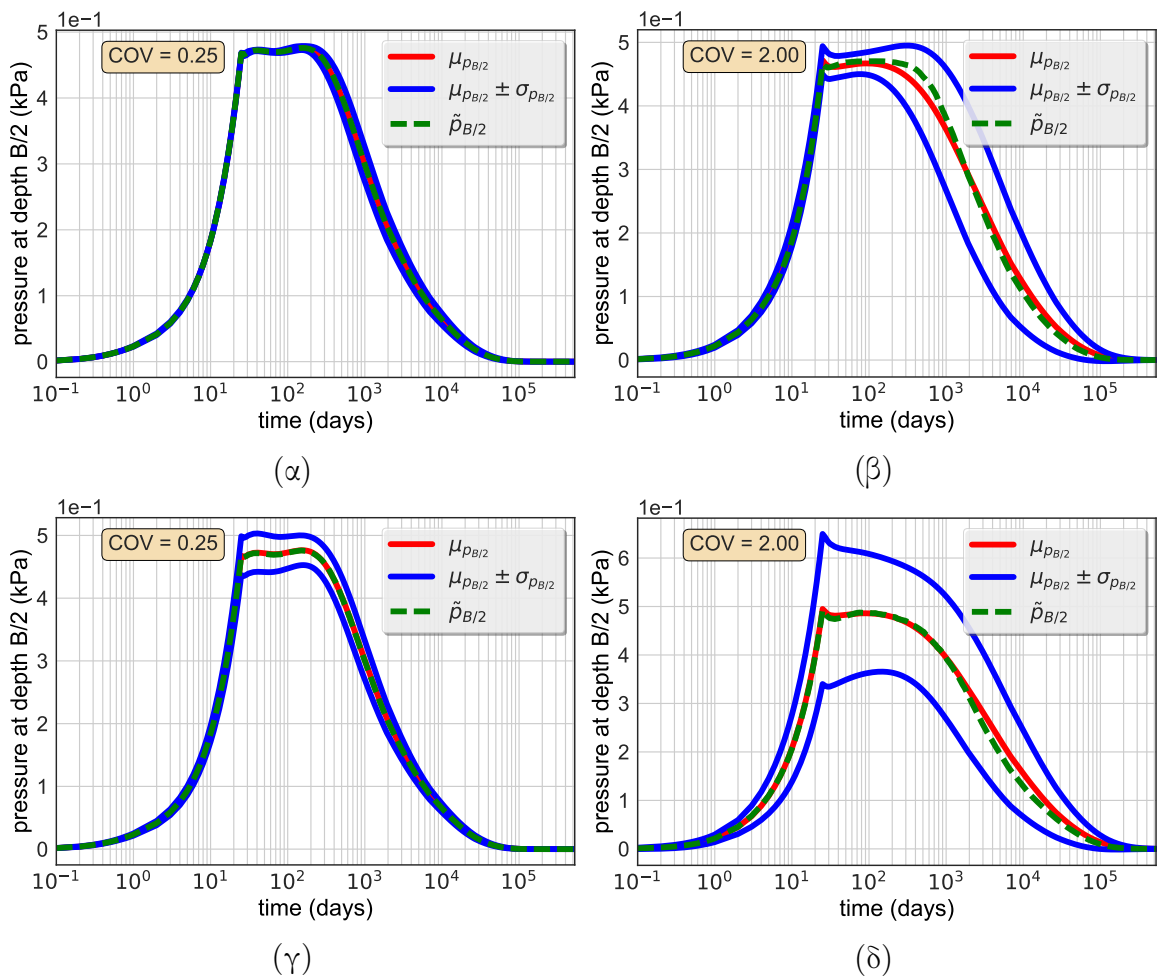
Σχήμα 7. Μέση τιμή και τυπική απόκλιση της μέγιστης διαφορικής καθίζησης ν_{AD} συναρτήσει του μήκους συσχέτισης: (α) μέση τιμή για στοχαστικό k , (β) τυπική απόκλιση για στοχαστικό k , (γ) μέση τιμή για στοχαστικό E και (δ) τυπική απόκλιση για στοχαστικό E .

οι τιμές μεγιστοποιούνται για μικρά μήκη συσχέτισης, ενώ σταθεροποιούνται όσο αυτά αυξάνονται.

0.7 Στερεοποίηση εδάφους με στοχαστικές ιδιότητες

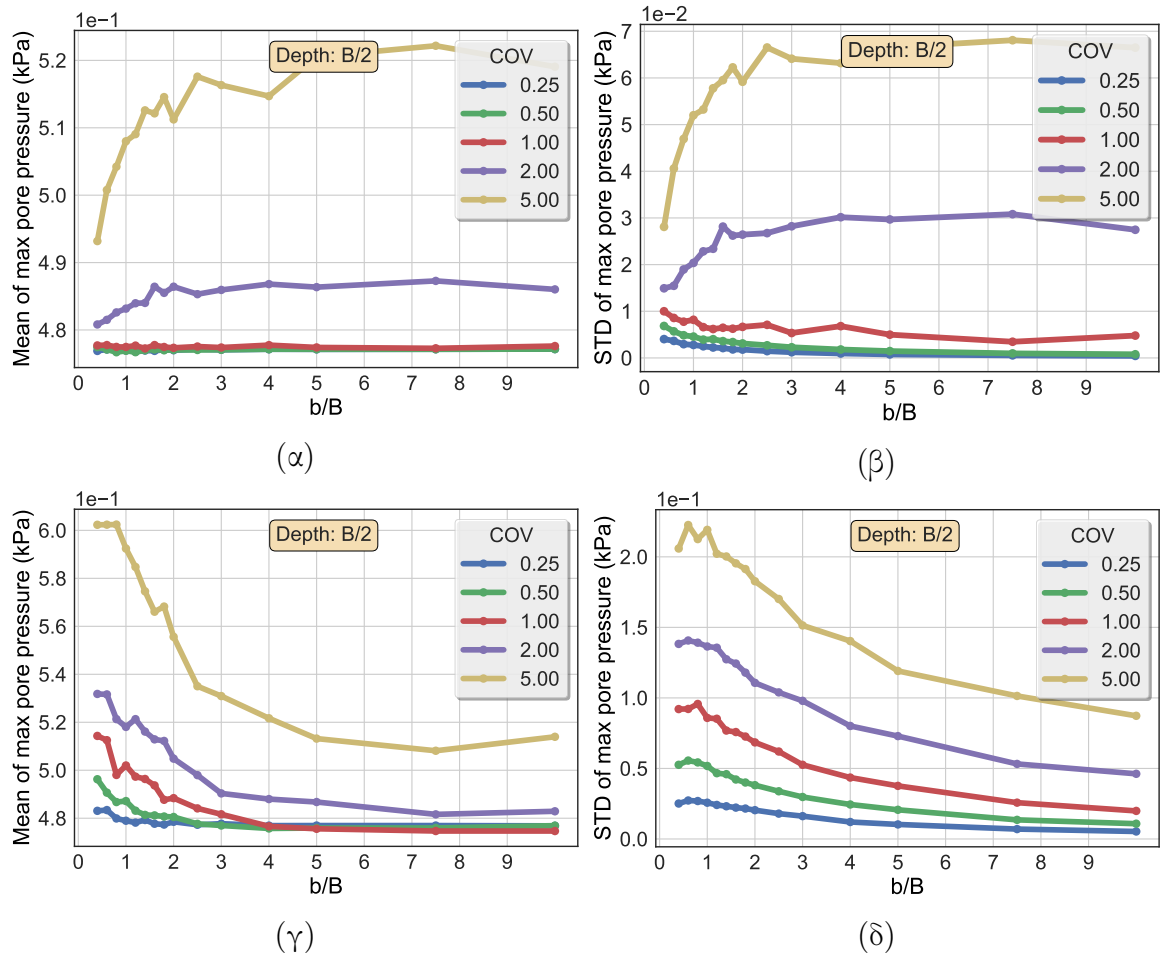


Σχήμα 8. Μέση τιμή της υπερπίεσης πόρων $p_{B/2}$ για: (α) στοχαστικό k και $COV = 0.25$, (β) στοχαστικό k και $COV = 2.00$, (γ) στοχαστικό E και $COV = 0.25$ και (δ) στοχαστικό E και $COV = 2.00$.



Σχήμα 9. Υπερπίεση πόρων $B/2$ για μήκος συσχέτισης $b = b_{\ln(k)} = b_{\ln(E)} = 10.0 \text{ m}$ για: (α) στοχαστικό k και $COV = 0.25$, (β) στοχαστικό k και $COV = 2.00$, (γ) στοχαστικό E και $COV = 0.25$ και (δ) στοχαστικό E και $COV = 2.00$.

0.7 Στερεοποίηση εδάφους με στοχαστικές ιδιότητες



Σχήμα 10. Μέση τιμή και τυπική απόκλιση της μέγιστης τιμής της $p_{B/2}$ συναρτήσει του μήκους συσχέτισης: (α) μέση τιμή για στοχαστικό k , (β) τυπική απόκλιση για στοχαστικό k , (γ) μέση τιμή για στοχαστικό E και (δ) τυπική απόκλιση για στοχαστικό E .

0.8 ΔΣΔΑ για τη διάδοση κύματος σε στοχαστικό έδαφος

Στην εν λόγω ενότητα εξετάζεται το πρόβλημα της διάδοσης διατμητικού κύματος σε έδαφος με χωρική διακύμανση του μέτρου διάτμησης G υπό το πρίσμα των ΔΣΜΑ/ΔΣΔΑ. Σημειώνεται πως η ανεξαρτησία αυτών από το φάσμα ισχύος της υπό μελέτη ιδιότητας υλικού καθιστά τη μεθοδολογία κατάλληλη για προβλήματα που περιλαμβάνουν εδάφη, όπου η έλλειψη επαρκών δεδομένων είναι συνήθης. Ειδικότερα, αποδεικνύεται πως, μέσω των ΔΣΜΑ/ΔΣΔΑ, η χρονοϊστορία της μέσης τιμής και διασποράς των μεγεθών απόκρισης δύνανται να υπολογιστούν με ακρίβεια για προβλήματα διάδοσης διατμητικού κύματος σε εδαφικά προσομοιώματα μίας και δύο διαστάσεων. Για τον αριθμητικό υπολογισμό των ΔΜΣΑ/ΔΣΔΑ μετατόπισης, ταχύτητας και επιτάχυνσης της εδαφικής επιφάνειας, υιοθετείται η ταχεία μέθοδος Monte Carlo (FMCS). Η εφαρμογή συνίσταται από αναλύσεις πεπερασμένων στοιχείων για τη διάδοση συνθετικών κυματιδιακών συναρτήσεων, καθώς και πραγματικής σεισμικής καταγραφής με σκοπό την επικύρωση του δυναμικού της μεθόδου. Η δε ακρίβεια της μεθόδου ελέγχεται με σύγκριση των αποτελεσμάτων με αντίστοιχα που προκύπτουν από απευθείας αναλύσεις Monte Carlo.

0.8.1 Προσομοίωση διάδοσης διατμητικού κύματος σε στοχαστικό έδαφος

Η στοχαστική εδαφική παράμετρος που μελετάται είναι το αντίστροφο του μέτρου διάτμησης του εδάφους $1/G$, του οποίου η χωρική διακύμανση συντελείται στον κατακόρυφο άξονα y για μονοδιάστατα μοντέλα, ενώ για μοντέλα επίπεδης παραμόρφωσης τόσο ο οριζόντιος άξονας x , όσο και ο κατακόρυφος y λαμβάνονται υπόψη. Γενικά, στη διδιάστατη περίπτωση ισχύει η εξής σχέση:

$$\frac{1}{G(x, y)} = F_0 \cdot (1 + f(x, y)) \quad (65)$$

όπου $G(x, y)$ το μέτρο διάτμησης στο σημείο με χωρικές συντεταγμένες (x, y) και $f(x, y)$ ένα ομογενές τυχαίο πεδίο μηδενικής μέσης τιμής που αναπαριστά τη διακύμανση του $1/G$ γύρω από τη μέση τιμή του $F_0 = 1/G_0$.

Το διατμητικό κύμα διαδίδεται μέσω ενός βραχώδους στρώματος που θεωρείται ομογενές στο εδαφικό στρώμα επί αυτού. Προκειμένου να ληφθεί υπόψη η ενδοσιμότητα του βραχώδους υποβάθρου, ιξώδεις αποσβεστήρες προστίθενται στους κόμβους της βάσης

0.8 ΔΣΔΑ για τη διάδοση κύματος σε στοχαστικό έδαφος

του μοντέλου, όπως απεικονίζεται στα σχήματα 11 και 12 για μία και δύο διαστάσεις αντίστοιχα.

Όσον αφορά τη διάδοση διατμητικού κύματος σε μία διάσταση, η διατμητική τάση δίνεται από τη σχέση:

$$\tau_{xy} = G \frac{\partial u}{\partial y} \quad (66)$$

όπου u η οριζόντια μετακίνηση κατά τον άξονα x . Οι δε επικόμβιες δυνάμεις για ένα μονοδιάστατο στοιχείο με μοναδιαία επιφάνεια διατομής και μήκος h_{el} , όπως αυτές απεικονίζονται στο σχήμα 11, υπολογίζονται ως εξής:

$$\begin{Bmatrix} F_i \\ F_j \end{Bmatrix} = \frac{1}{h_{el}} \begin{bmatrix} G & -G \\ -G & G \end{bmatrix} \begin{Bmatrix} u_i \\ u_j \end{Bmatrix} \quad (67)$$

όπου το μητρώο στο δεξί μέλος της εξίσωσης (67) αντιστοιχεί στο μητρώο στιβαρότητας για τη μονοδιάστατη περίπτωση. Για την προσομοίωση της διάδοσης κύματος στις δύο διαστάσεις χρησιμοποιούνται ισοπαραμετρικά τετρακομβικά τετραπλευρικά στοιχεία επίπεδης παραμόρφωσης.

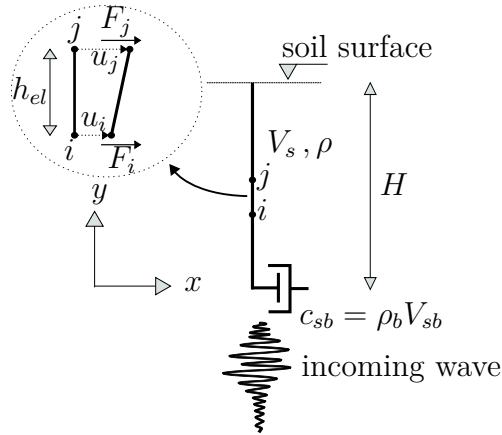
Οφείλει να σημειωθεί πως, για την περίπτωση προσομοίωσης διάδοσης δεδομένης εδαφικής κίνησης τόσο σε μία, όσο και σε δύο διαστάσεις, το προσπίπτον κύμα που διαδίδεται από το βραχώδες υπόστρωμα θα πρέπει να μετασχηματιστεί σε ισοδύναμες επικόμβιες δυνάμεις που εφαρμόζονται στη βάση του μοντέλου. Για το σκοπό αυτό υιοθετείται η ακόλουθη σχέση:

$$F_{wave}(t) = 2\rho_b \cdot V_{sb} \cdot V_I(t) \cdot A \quad (68)$$

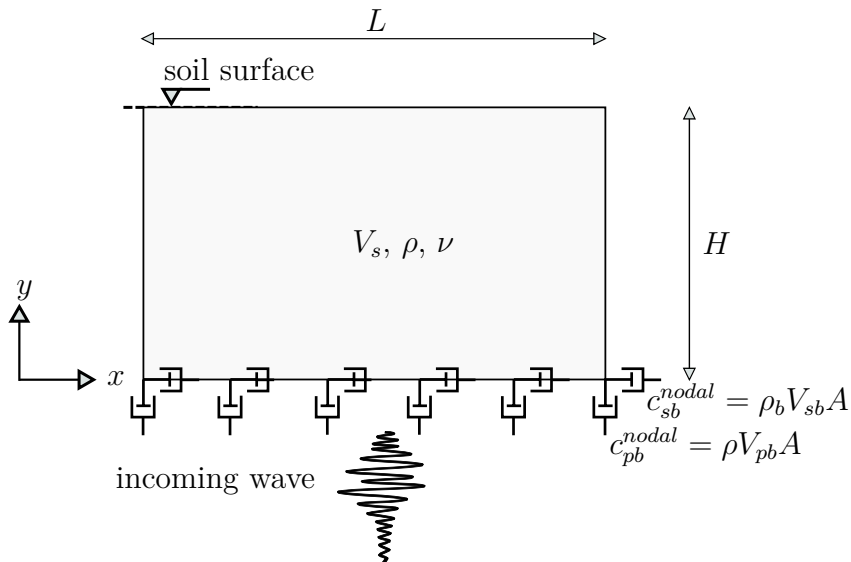
όπου ρ_b η πυκνότητα του βράχου, V_{sb} η ταχύτητα διάδοσης διατμητικού κύματος του βράχου, V_I η χρονοϊστορία ταχύτητας του διερχόμενου κύματος και A η επιφάνεια που αντιστοιχεί στον κόμβο όπου εφαρμόζεται η δύναμη.

0.8.1.1 Αριθμητική εφαρμογή

Σε αυτή την υποενότητα, η μέθοδος των ΔΣΜΑ/ΔΣΔΑ εφαρμόζεται στην προσομοίωση διατμητικού κύματος σε μονοδιάστατα και διδιάστατα εδαφικά μοντέλα. Αποσαφηνίζεται πως και στις δύο περιπτώσεις, οι εδαφικές ιδιότητες είναι οι ίδιες. Η υπό μελέτη στοχαστική ιδιότητα είναι το αντίστροφο του μέτρου διάτμησης G , η χωρική διακύμανση του οποίου και ενσωματώνεται στις προσομοιώσεις. Και τα δύο μοντέλα αποτελούνται από εδαφικό στρώμα που φορτίζεται από ομογενές βραχώδες υπόστρωμα. Οι δε ντετερμινιστικές παράμετροι είναι οι εξής: πυκνότητα $\rho = 1.8 \text{ Mg/m}^3$, λόγος Poisson $\nu = 0.3$,



Σχήμα 11. Μονοδιάστατο προσομοίωμα διάδοσης διατμητικού κύματος σε έδαφος.



Σχήμα 12. Προσομοίωμα επίπεδης παραμόρφωσης για τη διάδοση διατμητικού κύματος σε έδαφος.

ενώ οι αντίστοιχες ιδιότητες του βράχου: $V_{sb} = 760 \text{ m/s}$, $\rho_b = 2.4 \text{ Mg/m}^3$ και $\nu_b = 0.3$. Τέλος, η επιλεγείσα μέθοδος χρονικής αριθμητικής ολοκλήρωσης είναι η HHT – α με παράμετρο $\alpha = -0.02$. Η μέση τιμή της ταχύτητα διάδοσης διατμητικού κύματος του εδάφους είναι $V_{s0} = 240 \text{ m/s}$ ή μί μέ μή μέ άμ ά ί: $G_0 = \rho \cdot V_s^2 = 103.68 \text{ MPa}$, ενώ το μέτρο διάτμησης του βράχου υπολογίζεται ως $G_b = \rho_b \cdot V_{sb}^2 = 1386.24 \text{ MPa}$. Όπως προαναφέρθηκε, το αντίστροφο του μέτρου διάτμησης προσομοιώνεται ως τυχαίο πεδίο, η τιμή του οποίου δίνεται από τη σχέση:

$$\frac{1}{G(x, y)} = \frac{1}{G_0} \cdot (1 + f(x, y)) \quad (69)$$

0.8 ΔΣΔΑ για τη διάδοση κύματος σε στοχαστικό έδαφος

όπου $f(x, y)$ ένα ομογενές τυχαίο πεδίο μηδενικής μέσης τιμής. Για τον υπολογισμό των συναρτήσεων ΔΜΣΑ/ΔΣΔΑ χρησιμοποιείται η FMCS, σύμφωνα με την οποία το πεδίο f αντιστοιχεί στο τυχαίο ημίτονο όπως ορίστηκε στην εξίσωση (55). Αντίθετα, για την απευθείας μέθοδο Monte Carlo το f αντιστοιχεί σε ένα ομογενές πεδίο μηδενικής μέσης τιμής, οι πραγματοποιήσεις του οποίου γεννώνται με χρήση της μεθόδου φασματικής αναπαράστασης.

0.8.1.2 Διάδοση κύματος σε μία διάσταση

Για την προσομοίωση της διάδοσης του διατμητικού κύματος στη μία διάσταση, το μοντέλο πεπερασμένων στοιχείων, όπως απεικονίζεται στο σχήμα 11, αποτελείται από 100 στοιχεία ύψους $h_{el} = 1.0 m$ και έτσι το συνολικό πάχος του εδαφικού στρώματος είναι $H = 100 m$. Επιπλέον, κάθε στοιχείο έχει μοναδιαία διατομή $A = 1.0 m^2$, ενώ χρησιμοποιείται απόσβεση Rayleigh με λόγους απόσβεσης $\xi_1 = \xi_2 = 0.05$ που αντιστοιχούν στις δύο πρώτες ιδιομορφές με γωνιακές συχνότητες $\omega_1 = (\pi V_{s0})/(2H)$ και $\omega_2 = (3\pi V_{s0})/(2H)$. Ένας ιξώδης αποσβεστήρας προστίθεται επίσης στον κόμβο της βάσης του μοντέλου με απόσβεση $c_{sb}^{nodal} = \rho_b \cdot V_{sb} A = 1824.0 kN \cdot s/m$. Ενδεικτικά μελετάται η διάδοση μοναδιαίου παλμού της μορφής που προτάθηκε από τους Mavroeidis & Papageorgiou. Το δε αντίστροφο του μέτρου διάτμησης υπολογίζεται στο κεντρικό σημείο κάθε στοιχείου από τη σχέση:

$$\frac{1}{G} = \frac{1}{G_0} (1 + f(y)) \quad (70)$$

όπου το $f(y)$ αντιστοιχεί σε ομογενές μονοδιάστατο τυχαίο πεδίο μηδενικής μέσης τιμής. Ειδικά για τη σύγκριση των μεθόδων FMCS και απευθείας ανάλυσης Monte Carlo, θεωρείται πως το φάσμα ισχύος του ανωτέρω τυχαίου πεδίου είναι το εξής:

$$S_{ff}(\kappa) = \frac{1}{4} \sigma_{ff}^2 b^3 \kappa^2 \exp(-b|\kappa|) \quad (71)$$

Όπως έχει επανειλημμένα αναφερθεί, η μέθοδος FMCS χρησιμοποιείται για τον υπολογισμό των ΔΜΣΑ/ΔΣΔΑ. Στο σχήμα 7.4 απεικονίζονται οι ΔΜΣΑ/ΔΣΔΑ για τον παλμό Mavroeidis & Papageorgiou για τυπική απόκλιση τυχαίου πεδίου $\sigma_{ff} = 0.2$, απ' όπου και προκύπτει πως η ΔΣΜΑ είναι σταθερή ως προς τον άξονα των κυματικών αριθμών. Τουναντίον, η ΔΣΔΑ επηρεάζεται μόνο από μικρούς κυματικούς αριθμούς, η διασπορά δηλαδή της απόκρισης εμφανίζει ευαισθησία σε ισχυρά συσχετισμένες τιμές του $1/G$. Στη συνέχεια, στο σχήμα 14, παρουσιάζονται οι καμπύλες μέσης τιμής και διασποράς της μετακίνησης, ταχύτητας και επιτάχυνσης της εδαφικής επιφάνειας που υ-

πολογίστηκαν τόσο με τη μέθοδο FMCS, όσο και την απευθείας ανάλυση Monte Carlo για την περίπτωση Γκαουσιανού τυχαίου πεδίου με μήκος συσχέτισης $b = 40.0 \text{ m}$. Συγκρίνοντας δε τις εν λόγω μεθόδους, αποδεικνύεται πως, στην περίπτωση της μέσης τιμής, τα αποτελέσματα συμπίπτουν, ενώ, όσον αφορά τη διασπορά απόκλιση της μεθόδου FMCS, παρατηρείται μόνο στις μέγιστες τιμές της απόκρισης, με το σφάλμα να παραμένει εντός αποδεκτών ορίων.

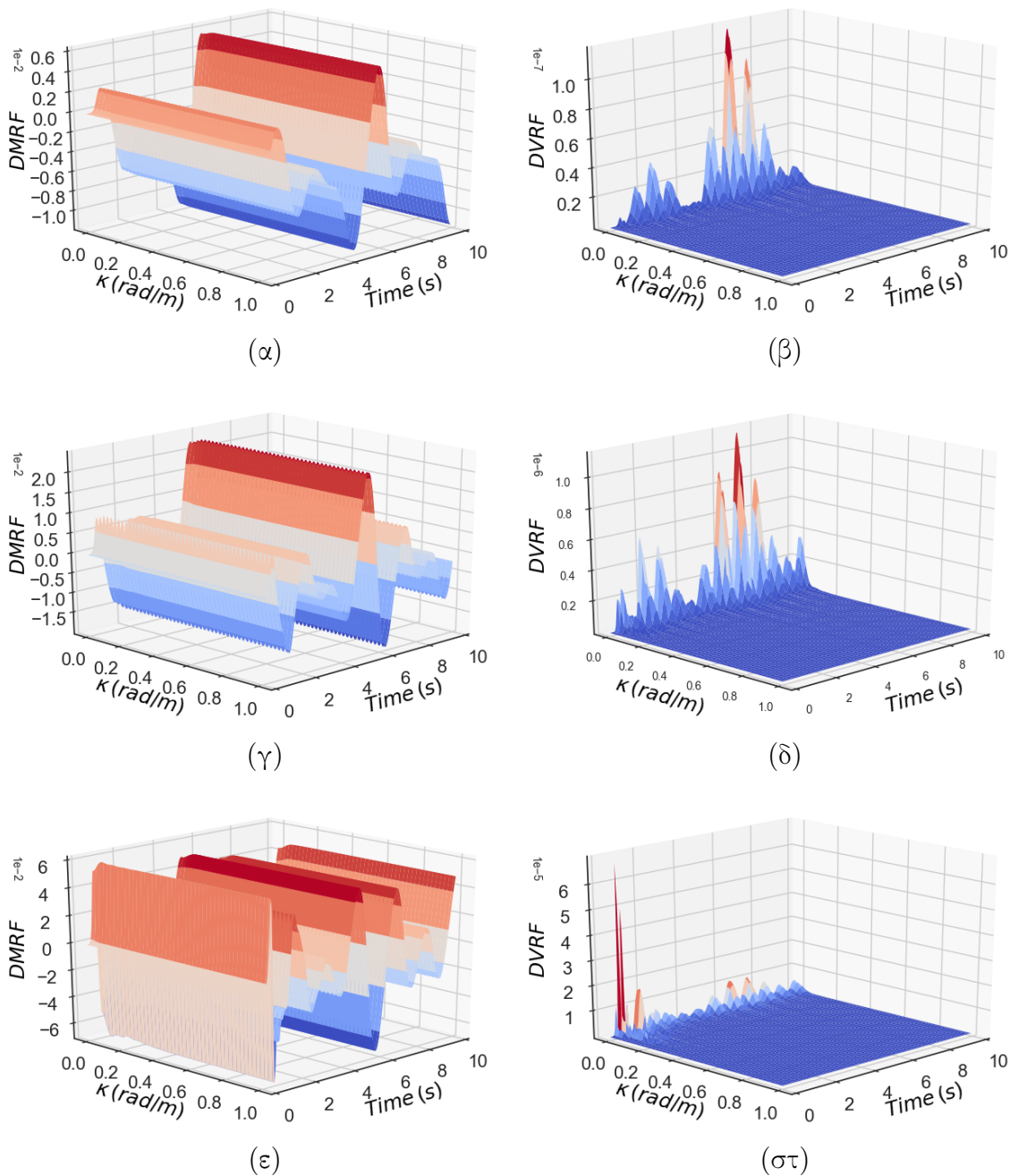
0.8.1.3 Διάδοση κύματος σε δύο διαστάσεις

Το μοντέλο που χρησιμοποιείται για την προσομοίωση διάδοσης διατμητικού κύματος σε δύο διαστάσεις απεικονίζεται στο σχήμα 12. Σύμφωνα με αυτό, το αριθμητικό προσομοίωμα αποτελείται από εδαφικό στρώμα με διαστάσεις $L = 200 \text{ m}$ και $H = 40 \text{ m}$. Όπως δε και στην περίπτωση της μίας διάστασης, έτσι και εδώ ιξώδεις αποσβεστήρες προστίθενται στους κόμβους της βάσης. Το μέτρο διάτμησης του βράχου είναι $G_b = 1386.24 \text{ MPa}$ και ο λόγος Poisson $\nu = 0.3$, ενώ οι τιμές της απόσβεσης για τους αποσβεστήρες είναι $c_{sb} = \rho_b \cdot V_{sb} = 1824.0 \text{ kN} \cdot \text{s}/\text{m}^3$ στην οριζόντια και $c_{pb} = \rho_b \cdot V_{pb} = 3412.39 \text{ kN} \cdot \text{s}/\text{m}^3$ στην κατακόρυφη διεύθυνση, όπου $V_{pb} = 1421.83 \text{ m}/\text{s}$ η ταχύτητα διάδοσης του διαμήκους κύματος στο βραχώδες υπόστρωμα. Οι τελικές τιμές που χρησιμοποιούνται σε κάθε αποσβεστήρα λαμβάνονται από το γινόμενο των αποσβέσεων c_{pb} και c_{sb} με την αντίστοιχη επιφάνεια A του κόμβου στον οποίο εφαρμόζονται, ή αλλιώς $c_{sb}^{nodal} = c_{sb}A$ και $c_{pb}^{nodal} = c_{pb}A$. Επισημαίνεται φυσικά πως οι ιδιότητες του εδαφικού στρώματος είναι ίδιες με εκείνες στην περίπτωση της μίας διάστασης. Για τη διακριτοποίηση του προσομοιώματος χρησιμοποιούνται ισοπαραμετρικά τετρακομβικά τετραγωνικά πεπερασμένα στοιχεία επίπεδης παραμόρφωσης με μήκος ακμής 1 m , με αποτέλεσμα το μοντέλο να αποτελείται από 8000 στοιχεία συνολικά. Ενδεικτικά μελετάται η διάδοση της καταγραφής Gilroy No1 EW του σεισμού Loma Prieta το 1989. Για τη σύγκριση των μεθόδων FMCS και απευθείας ανάλυσης Monte Carlo, το φάσμα ισχύος του τυχαίου πεδίου λαμβάνεται ως:

$$S_{ff}(\kappa_x, \kappa_y) = \sigma_{ff}^2 \frac{b_x b_y}{4\pi} \exp \left(- \left(\frac{b_x \kappa_x}{2} \right)^2 - \left(\frac{b_y \kappa_y}{2} \right)^2 \right) \quad (72)$$

Στο σημείο αυτό μελετώνται τα στατιστικά της απόκρισης για τον κεντρικό κόμβο της εδαφικής επιφάνειας. Στο σχήμα 15 απεικονίζονται οι ΔΣΔΑ της απόκρισης του κεντρικού κόμβου της εδαφικής επιφάνειας για την περίπτωση της σεισμικής καταγραφής με τυπική απόκλιση του τυχαίου πεδίου $\sigma_{ff} = 0.2$. Μία και μόνο ματιά αποκαλύπτει πως μόνο μικροί κυματικοί αριθμοί συμμετέχουν στη διασπορά της απόκρισης όσον αφορά τον άξονα κ_x , ενώ αντίθετα, μεγάλο εύρος τιμών του κατακόρυφου κυματικού άξονα κ_y συνει-

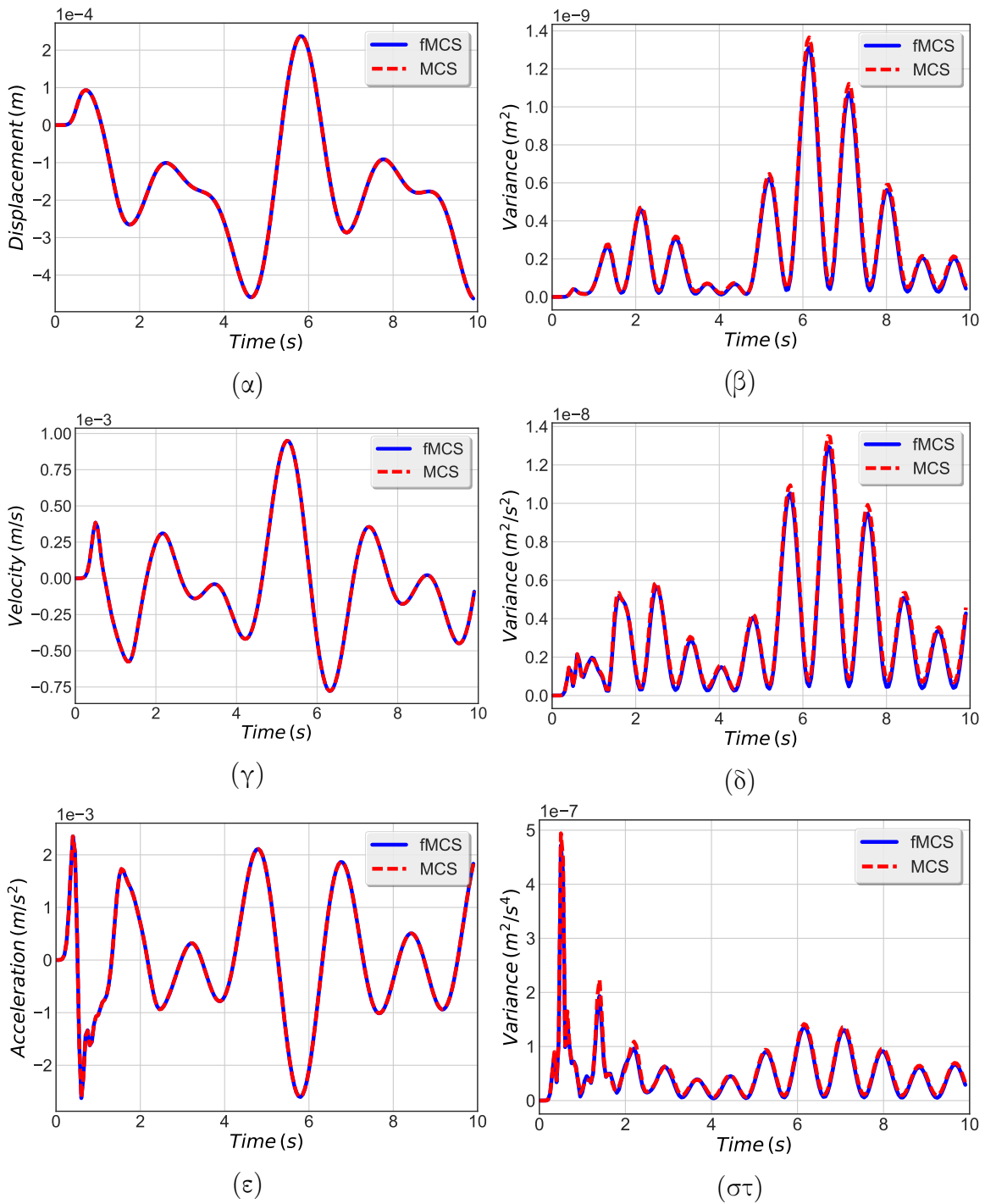
0.8 ΔΣΔΑ για τη διάδοση κύματος σε στοχαστικό έδαφος



Σχήμα 13. ΔΜΣΑ/ΔΣΔΑ της εδαφικής επιφάνειας για τη διάδοση μοναδιαίου παλμού τύπου Mavroidis & Papageorgiou για $\sigma_{ff} = 0.2$: (α) ΔΜΣΑ μετακίνησης, (β) ΔΣΔΑ μετακίνησης, (γ) ΔΜΣΑ ταχύτητας, (δ) ΔΣΔΑ ταχύτητας, (ε) ΔΜΣΑ επιτάχυνσης και (στ) ΔΣΔΑ επιτάχυνσης.

σφέρει σημαντικά στην εν λόγω διασπορά. Στην περίπτωση λοιπόν των δύο διαστάσεων, το φαινόμενο της διάδοσης διατμητικού κύματος εμφανίζει ευαισθησία στη διακύμανση

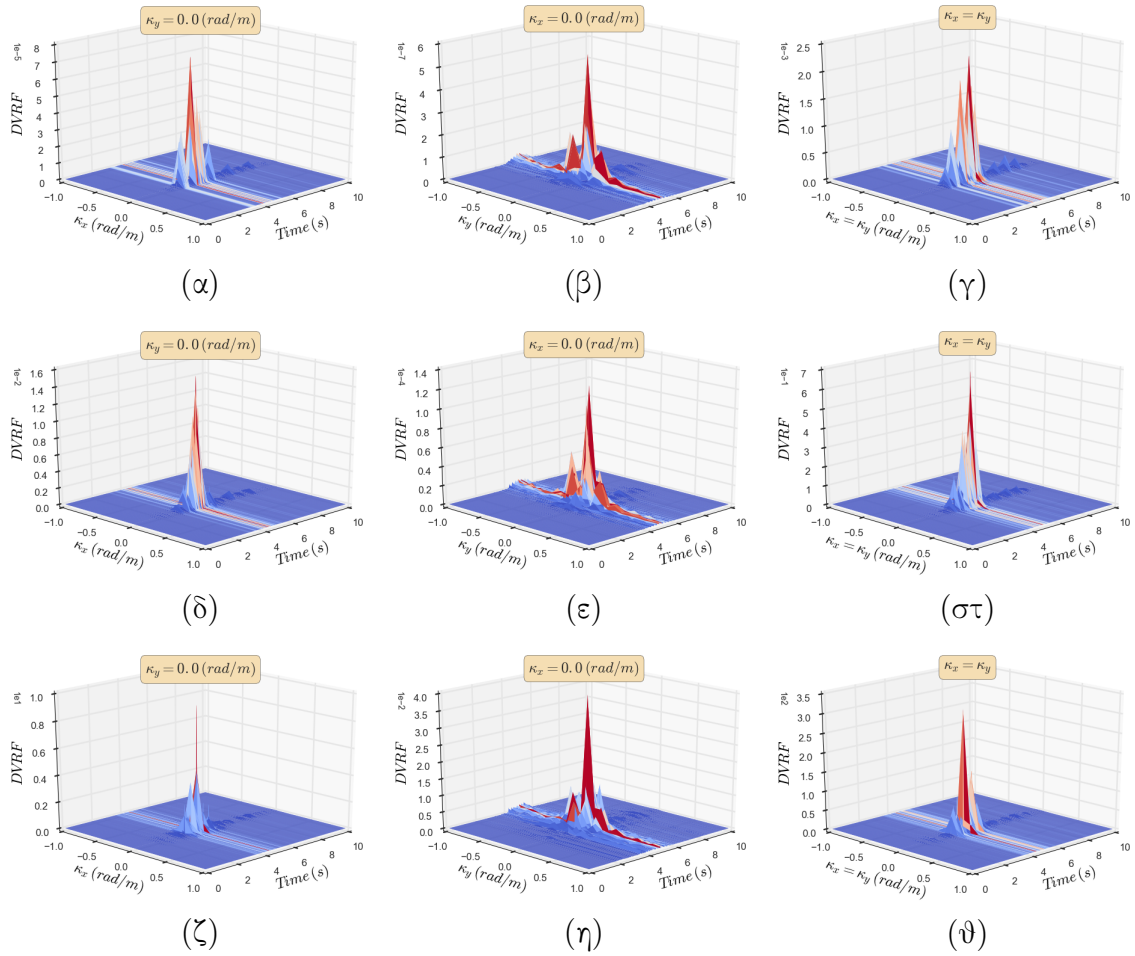
Εκτενής Περίληψη



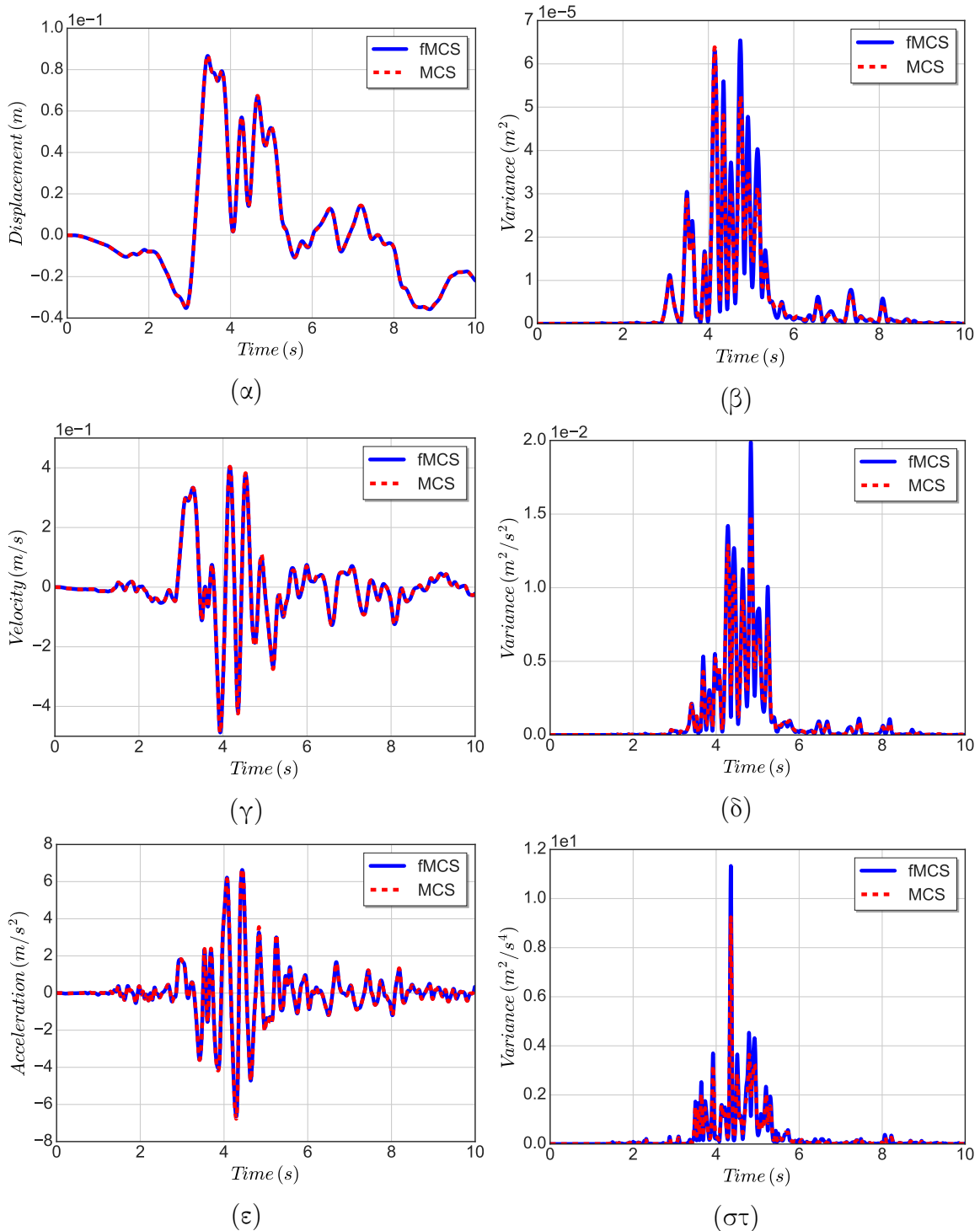
Σχήμα 14. Στατιστικά απόκρισης για μοναδιαίο παλμό τύπου Mavroudis & Papageorgiou για Γκαουσιανό τυχαίο πεδίο με $\sigma_{ff} = 0.2$ και μήκος συσχέτισης $b = 40 \text{ m}$: (α) μέση τιμή μετακίνησης, (β) διασπορά μετακίνησης, (γ) μέση τιμή ταχύτητας, (δ) διασπορά ταχύτητας, (ε) μέση τιμή επιτάχυνσης και (στ) διασπορά επιτάχυνσης.

0.8 ΔΣΔΑ για τη διάδοση κύματος σε στοχαστικό έδαφος

του μέτρου διάτμησης κατά την κατακόρυφη διεύθυνση. Τέλος, στο σχήμα 16 δίνονται η μέση τιμή και διασπορά των μεγεθών απόκρισης για τις μεθόδους FMCS και απευθείας ανάλυσης Monte Carlo. Οι δε παράμετροι του τυχαίου πεδίου στην περίπτωση αυτή είναι $\sigma_{ff} = 0.2$ και $b_x = b_y = 100$ m. Με λίγα λόγια, αποδεικνύεται πως, και στην προκειμένη περίπτωση, η μέση τιμή είναι κοινή και για τις δύο μεθοδολογίες, ενώ, όσον αφορά τη διασπορά, η απόκλιση της FMCS παρατηρείται μόνο για απότομες μεταβολές στην απόκριση που, παρ' όλα αυτά, κυμαίνεται εντός ανεκτών ορίων.



Σχήμα 15. ΔΣΔΑ απόκρισης εδαφικής επιφάνειας για $\sigma_{ff} = 0.2$: (α) ΔΣΔΑ μετατόπισης για $\kappa_y = 0.0$ (rad/m), (β) ΔΣΔΑ μετατόπισης για $\kappa_x = 0.0$ (rad/m), (γ) ΔΣΔΑ μετατόπισης για $\kappa_x = \kappa_y$, (δ) ΔΣΔΑ ταχύτητας για $\kappa_y = 0.0$ (rad/m), (ε) ΔΣΔΑ ταχύτητας για $\kappa_x = 0.0$ (rad/m), (στ) ΔΣΔΑ ταχύτητας για $\kappa_x = \kappa_y$, (ζ) ΔΣΔΑ επιτάχυνσης για $\kappa_y = 0.0$ (rad/m), (η) ΔΣΔΑ επιτάχυνσης για $\kappa_x = 0.0$ (rad/m) και (θ) ΔΣΔΑ επιτάχυνσης για $\kappa_x = \kappa_y$.



Σχήμα 16. Στατιστικά απόκρισης για διάδοση καταγραφής Gilroy No1 EW για Γκαουσιανό τυχαίο πεδίο με $\sigma_{ff} = 0.2$ και μήκος συσχέτισης $b_x = b_y = 100 \text{ m}$: (α) μέση τιμή μετακίνησης, (β) διασπορά μετακίνησης, (γ) μέση τιμή ταχύτητας, (δ) διασπορά ταχύτητας, (ε) μέση τιμή επιτάχυνσης και (στ) διασπορά επιτάχυνσης.

0.9 Εφαρμογή ΔΣΔΑ στη στοχαστική στερεοποίηση εδάφους

Στην εν λόγω ενότητα, η εφαρμογή της στοχαστικής εδαφικής στερεοποίησης, όπως αυτή μελετήθηκε στην ενότητα 0.7, επανεξετάζεται υπό το πρίσμα των δυναμικών συναρτήσεων μέσης τιμής/διακύμανσης της απόκρισης (ΔΣΜΑ/ΔΣΔΑ). Συγκεκριμένα, η ταχεία μέθοδος Monte Carlo (FMCS) χρησιμοποιείται για την εύρεση των ΔΣΜΑ/ΔΣΔΑ, οι οποίες κατόπιν υιοθετούνται για τον υπολογισμό της μέσης τιμής και διασποράς τόσο της καθίζησης του θεμελίου, όσο και της εδαφικής υπερπίεσης πόρων. Η δε σύγκριση με τα αντίστοιχα στατιστικά μεγέθη που λαμβάνονται με εφαρμογή της απευθείας μεθόδου Monte Carlo επικυρώνει την αποτελεσματικότητα και ορθότητα της προτεινόμενης μεθοδολογίας.

0.9.1 Επανεξέταση του προβλήματος της στοχαστικής στερεοποίησης

Όπως προαναφέρθηκε, το πρόβλημα αποτελείται από ένα άκαμπτο τραχύ λωριδωτό θεμέλιο σε στερεοποιήσιμο εδαφικό στρώμα με αβέβαιη διαπερατότητα k και μέτρο ελαστικότητας E . Οι ανωτέρω εδαφικές ιδιότητες υπολογίζονται στο κεντρικό σημείο κάθε πεπερασμένου στοιχείου με συντεταγμένες (x, y) ως εξής:

$$k(x, y) = k_0(1 + f(x, y)) \quad (73)$$

$$E(x, y) = E_0(1 + f(x, y)) \quad (74)$$

όπου k_0 και E_0 είναι η μέση τιμή της διαπερατότητας και του μέτρου ελαστικότητας αντίστοιχα. Επισημαίνεται πως, όπως και στην ενότητα 0.8, το $f(x, y)$ αντιστοιχεί στο τυχαίο ημίτονο για την περίπτωση της FMCS, ενώ αναπαριστά ένα ομογενές Γκαουσιανό τυχαίο πεδίο μηδενικής μέσης τιμής στην απευθείας προσομοίωση Monte Carlo. Τονίζεται δε πως η γεωμετρία και η διακριτοποίηση του μοντέλου, όπως και οι ιδιότητες των υπό μελέτη υλικών, παραμένουν ίδιες με την ενότητα 0.7. Παρ' όλα αυτά, η μέση τιμή των στοχαστικών k και E αναφέρεται εκ νέου εδώ, δηλαδή $k_0 \equiv \mu_k = 1.22 \cdot 10^{-5} m^4 \cdot kN^{-1}/day$ και $E_0 \equiv \mu_E = 622.7 kPa$.

Στη συνέχεια μελετώνται τόσο τα στατιστικά των καθιζήσεων του θεμελίου, όσο και των εδαφικών υπερπίεσεων. Όσον αφορά την καθίζηση, εξετάζονται αυτή του κέντρου του θεμελίου ν_C , καθώς και η διαφορική καθίζηση $\nu_{AD} = \nu_A - \nu_D$, ενώ, όσον αφορά την υπερπίεση πόρων, εκείνη μελετάται σε διάφορα βάθη από την εδαφική επιφάνεια.

Με στόχο την επικύρωση της ακρίβειας της μεθοδολογίας των ΔΣΜΑ/ΔΣΔΑ, τα παραγόμενα αποτελέσματα συγκρίνονται με τα αντίστοιχα που προκύπτουν με χρήση της απευθείας προσομοίωσης Monte Carlo. Ειδικότερα, η σύγκριση γίνεται συγκεκριμένα για τιμή της τυπικής απόκλισης $\sigma_k = \sigma_E = 0.2$, ενώ το φάσμα ισχύος των τυχαίων πεδίων έχει την εξής μορφή:

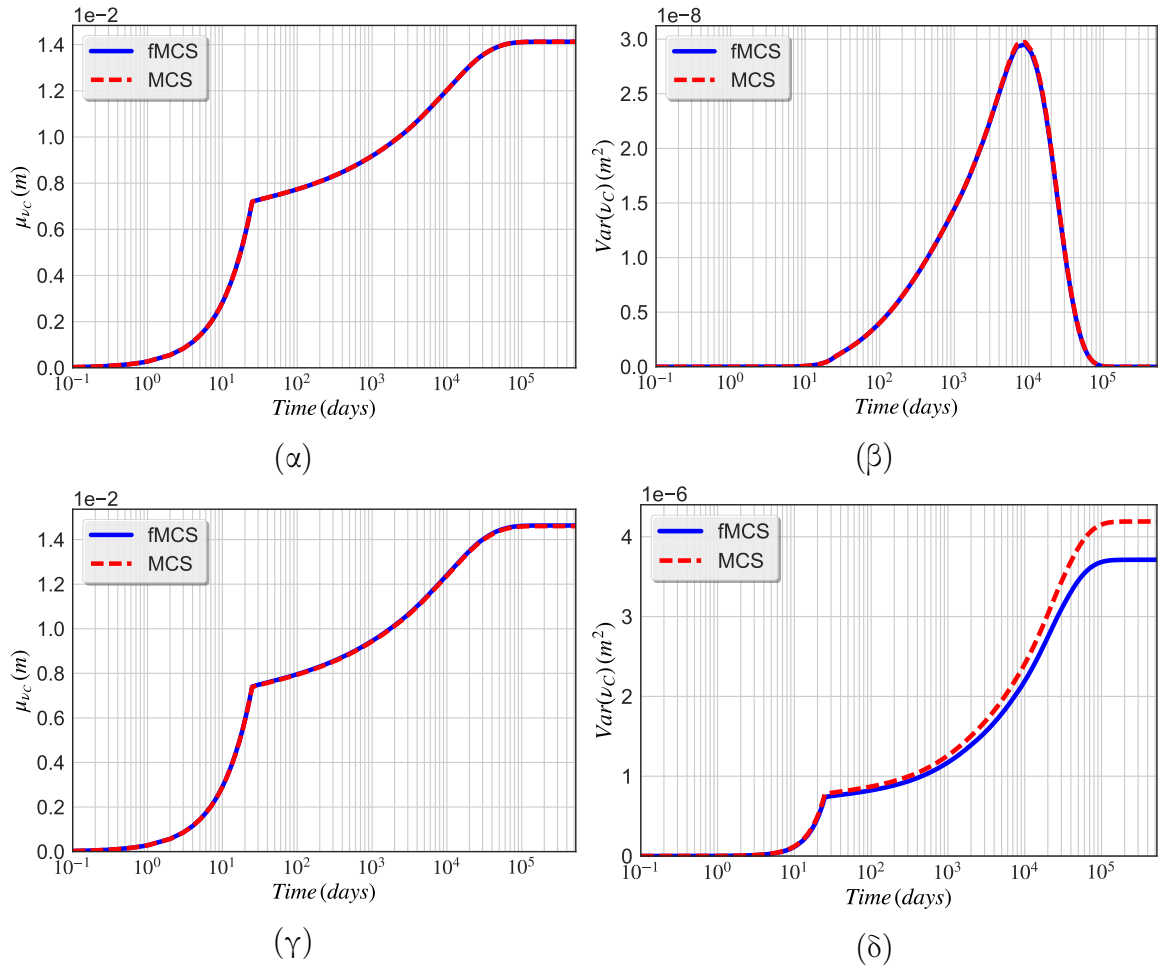
$$S_{ff}(\kappa_x, \kappa_y) = \frac{\sigma^2 b_1 b_2}{4\pi} \exp \left(- \left(\frac{b_1 \kappa_x}{2} \right)^2 - \left(\frac{b_2 \kappa_y}{2} \right)^2 \right) \quad (75)$$

Τέλος, το μήκος συσχέτισης είναι $b_{1k} = b_{2k} = b_{1E} = b_{2E} = 10.0 \text{ m}$. Ειδικά στην περίπτωση της ανάλυσης Monte Carlo, η μέθοδος φασματικής αναπαράστασης χρησιμοποιείται για τη γένεση των απαιτούμενων τυχαίων πεδίων.

0.9.1.1 Στατιστικά καθίζησης του θεμελίου

Στο σχήμα 17 απεικονίζεται η μέση τιμή και διασπορά της καθίζησης ν_C του κέντρου του θεμελίου. Είναι ολοφάνερο πως η μέση τιμή για την FMCS, αλλά και την απευθείας ανάλυση Monte Carlo βρίσκονται σε πλήρη ταύτιση τόσο στην περίπτωση της στοχαστικής διαπερατότητας όσο και του μέτρου ελαστικότητας. Όσον αφορά δε τη διασπορά, μόνο για μεγάλες τιμές αυτής παρατηρείται μικρή απόκλιση μεταξύ των δύο μεθόδων, η οποία παρά ταύτα παραμένει εντός αποδεκτών ορίων. Στο σχήμα 18 δίνεται η διασπορά της διαφορικής καθίζησης ν_{AD} για στοχαστική διαπερατότητα και μέτρο ελαστικότητας. Και σε αυτή την περίπτωση, η διασπορά που υπολογίζεται μέσω της FMCS εμφανίζει μικρή απόκλιση από την αντίστοιχη της απευθείας μεθόδου Monte Carlo και είναι εντονότερη στην περίπτωση του στοχαστικού μέτρου ελαστικότητας. Αξίζει δε να σημειωθεί πως οι τιμές της διασποράς είναι της τάξης του 10^{-6} για το στοχαστικό E , σε σχέση με τις αντίστοιχες της στοχαστικής διαπερατότητας 10^{-8} , επιβεβαιώνοντας τη μεγαλύτερη επιρροή του μέτρου ελαστικότητας όσον αφορά τη διαφορική καθίζηση. Ακριβώς επειδή η μέση τιμή της διαφορικής καθίζησης είναι μηδενική, λόγω συμμετρίας στη γεωμετρία και το φορτίο, η απεικόνισή της παραλείπεται. Τέλος, στο σχήμα 19 απεικονίζονται οι ΔΣΔΑ για την καθίζηση ν_{AD} . Εξετάζοντας αυτές σε όρους των κυματικών αριθμών κ_x and κ_y , καταλήγουμε στο συμπέρασμα πως οι τιμές που αντιστοιχούν στον κ_x έχουν πολύ μεγαλύτερη επιρροή σε σύγκριση με τον κ_y και για τις δύο περιπτώσεις των εδαφικών ιδιοτήτων. Σύμφωνα δε και με τα διαγράμματα, είναι ενδιαφέρον να επισημάνουμε πως η διακύμανση της διαφορικής καθίζησης επηρεάζεται κυρίως από τη διακύμανση των ιδιοτήτων στην οριζόντια διεύθυνση, με κρίσιμο κυματικό αριθμό $\kappa_x = 0.25 \text{ (rad/m)}$.

0.9 Εφαρμογή ΔΣΔΑ στη στοχαστική στερεοποίηση εδάφους



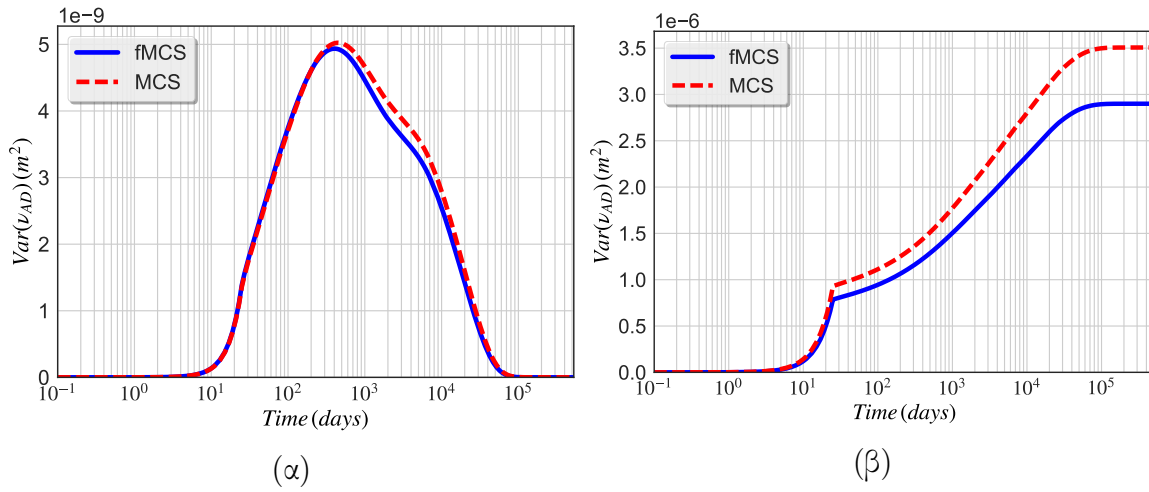
Σχήμα 17. Μέση τιμή και διασπορά της καθίζησης ν_C για στοχαστική διαπερατότητα και μέτρο ελαστικότητας με $\sigma_k = \sigma_E = 0.2$ και μήκος συσχέτισης $b = 10 \text{ m}$: (α) μ_{ν_C} για στοχαστικό k , (β) $Var(\nu_C)$ για στοχαστικό k , (γ) μ_{ν_C} για στοχαστικό E και (δ) $Var(\nu_C)$ για στοχαστικό E .

0.9.1.2 Στατιστικά υπερπίεσης πόρων

Στην υποενότητα αυτή μελετώνται τα στατιστικά της εδαφικής υπερπίεσης πόρων. Συγκεκριμένα, παρουσιάζεται η υπερπίεση σε βάθος $B/2$ από την εδαφική επιφάνεια στην κατακόρυφο που διέρχεται από το κέντρο του θεμελίου και συμβολίζεται ως $p_{B/2}$.

Στο σχήμα 20 απεικονίζεται η μέση τιμή και διασπορά της $p_{B/2}$ για τις δύο στοχαστικές εδαφικές ιδιότητες που λαμβάνονται υπόψη. Είναι ξεκάθαρο πως οι τιμές που υπολογίζονται με χρήση των ΔΣΜΑ/ΔΣΔΑ ταυτίζονται με τις αντίστοιχες της απευθείας μεθόδου Monte Carlo.

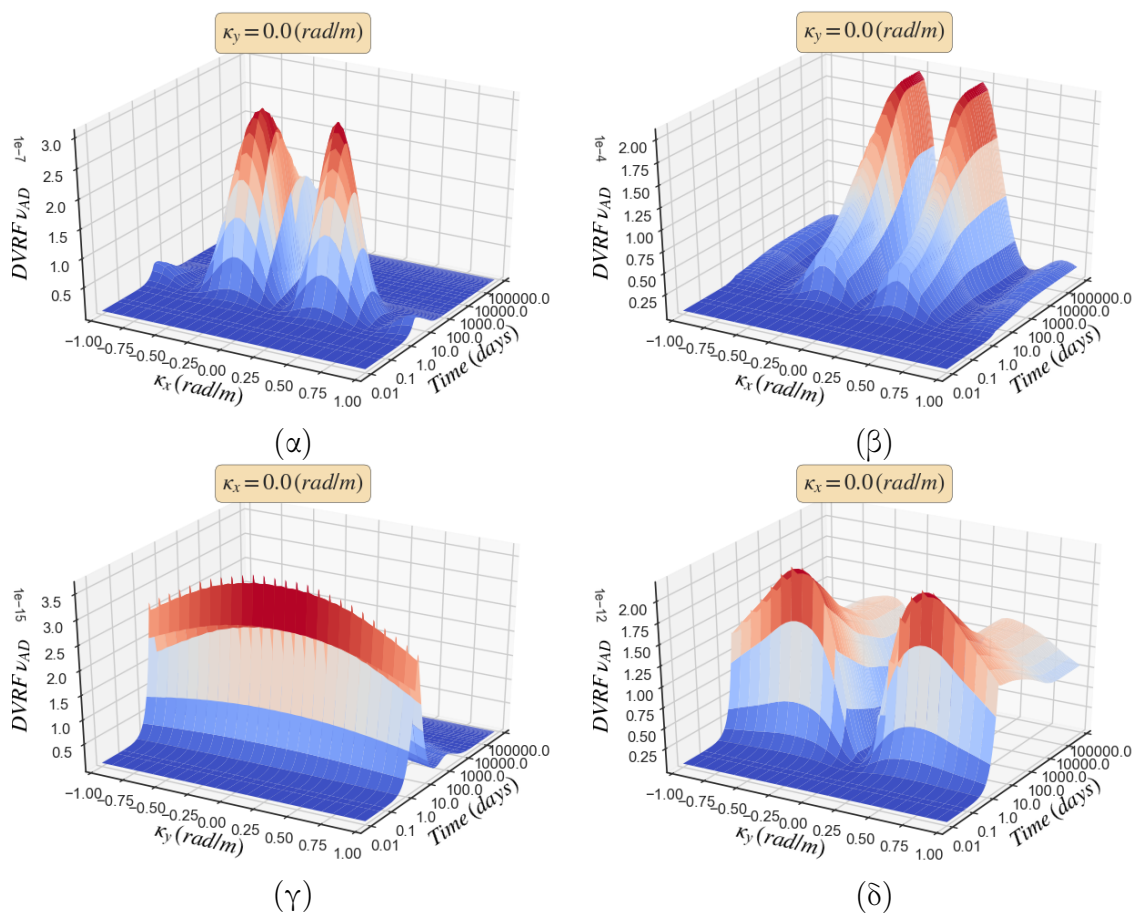
Τα σχήματα 21 και 22 παρουσιάζουν τις ΔΣΜΑ/ΔΣΔΑ αντίστοιχα για την υπερπίεση πόρων $p_{B/2}$. Στην προκειμένη περίπτωση, ο κύριος όγκος της ΔΣΔΑ είναι συ-



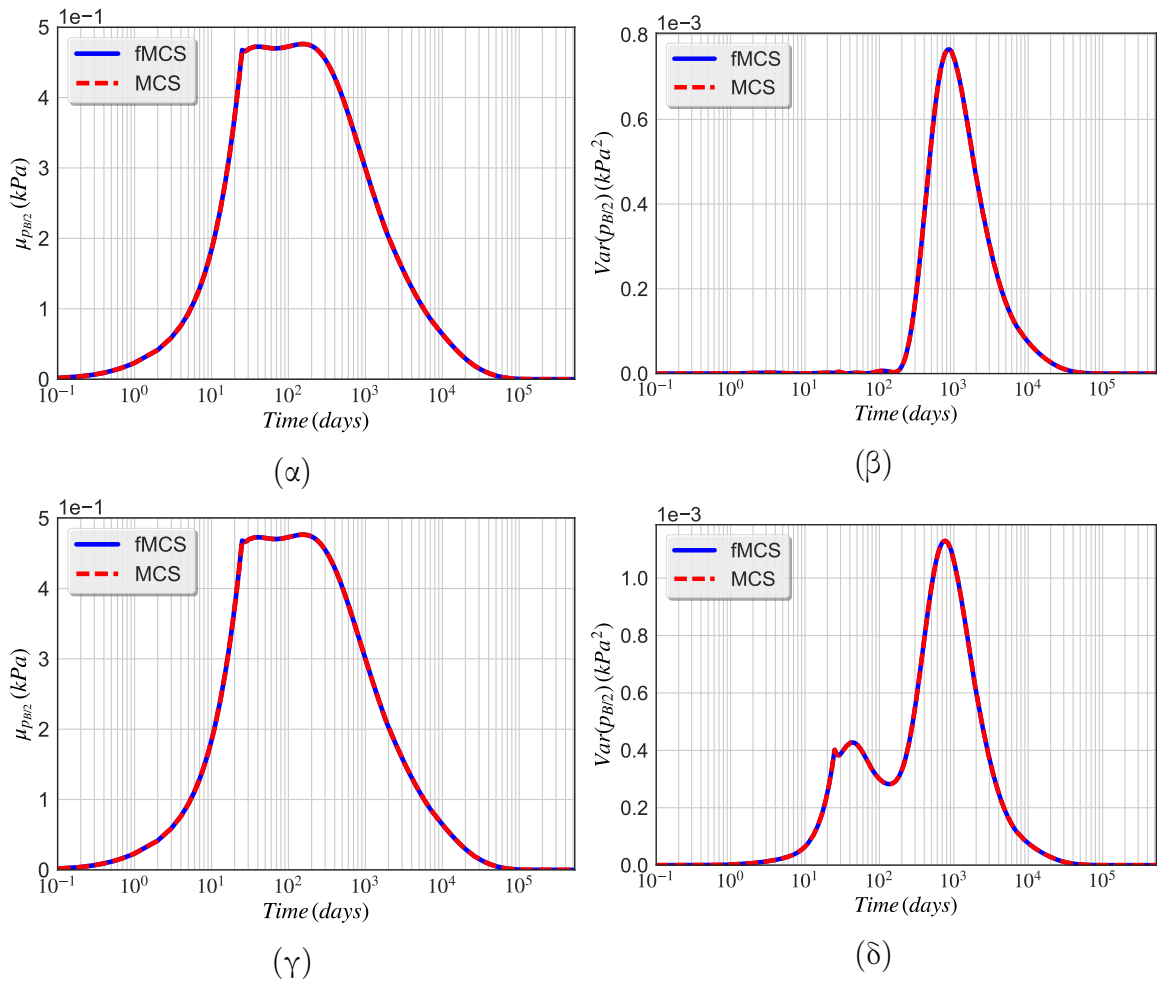
Σχήμα 18. Διασπορά της καθίζησης ν_{AD} για στοχαστική διαπερατότητα και μέτρο ελαστικότητας με $\sigma_k = \sigma_E = 0.2$ και μήκος συσχέτισης $b = 10 \text{ m}$: (α) $Var(\nu_{AD})$ για στοχαστικό k και (β) $Var(\nu_{AD})$ για στοχαστικό E .

γκεντρωμένος γύρω από μικρούς κυματικούς αριθμούς κ_x και κ_y , η διακύμανση δηλαδή επηρεάζεται από ισχυρά συσχετισμένες τιμές της διαπερατότητας. Αντίθετα, στην περίπτωση του μέτρου ελαστικότητας, οι κρίσιμοι κυματικοί αριθμοί αντιστοιχούν σε τιμές $\kappa_x = -0.75 \text{ (rad/m)}$, $\kappa_x = 0.75 \text{ (rad/m)}$ και $(-1.0, -0.75) \cup (0.75, 1.00) \text{ (rad/m)}$ όσον αφορά το κ_y .

0.9 Εφαρμογή ΔΣΔΑ στη στοχαστική στερεοποίηση εδάφους

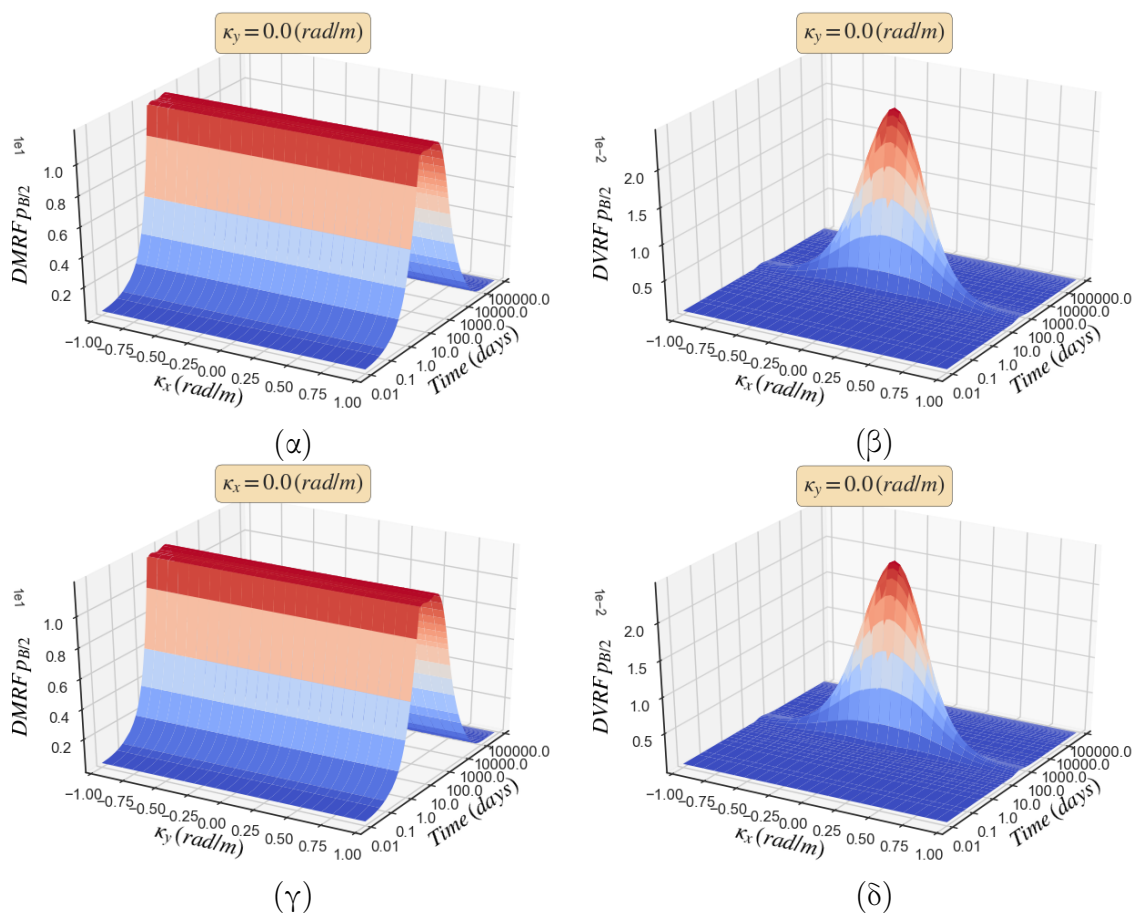


Σχήμα 19. ΔΣΔΑ της καθίζησης ν_{AD} για στοχαστική διαπερατότητα και μέτρο ελαστικότητας: (α) ΔΣΔΑ για στοχαστική διαπερατότητα και $\kappa_y = 0.0$ (rad/m), (β) ΔΣΔΑ για στοχαστικό μέτρο ελαστικότητας και $\kappa_y = 0.0$ (rad/m), (γ) ΔΣΔΑ για στοχαστική διαπερατότητα και $\kappa_x = 0.0$ (rad/m) και (δ) ΔΣΔΑ για στοχαστικό μέτρο ελαστικότητας και $\kappa_x = 0.0$ (rad/m).

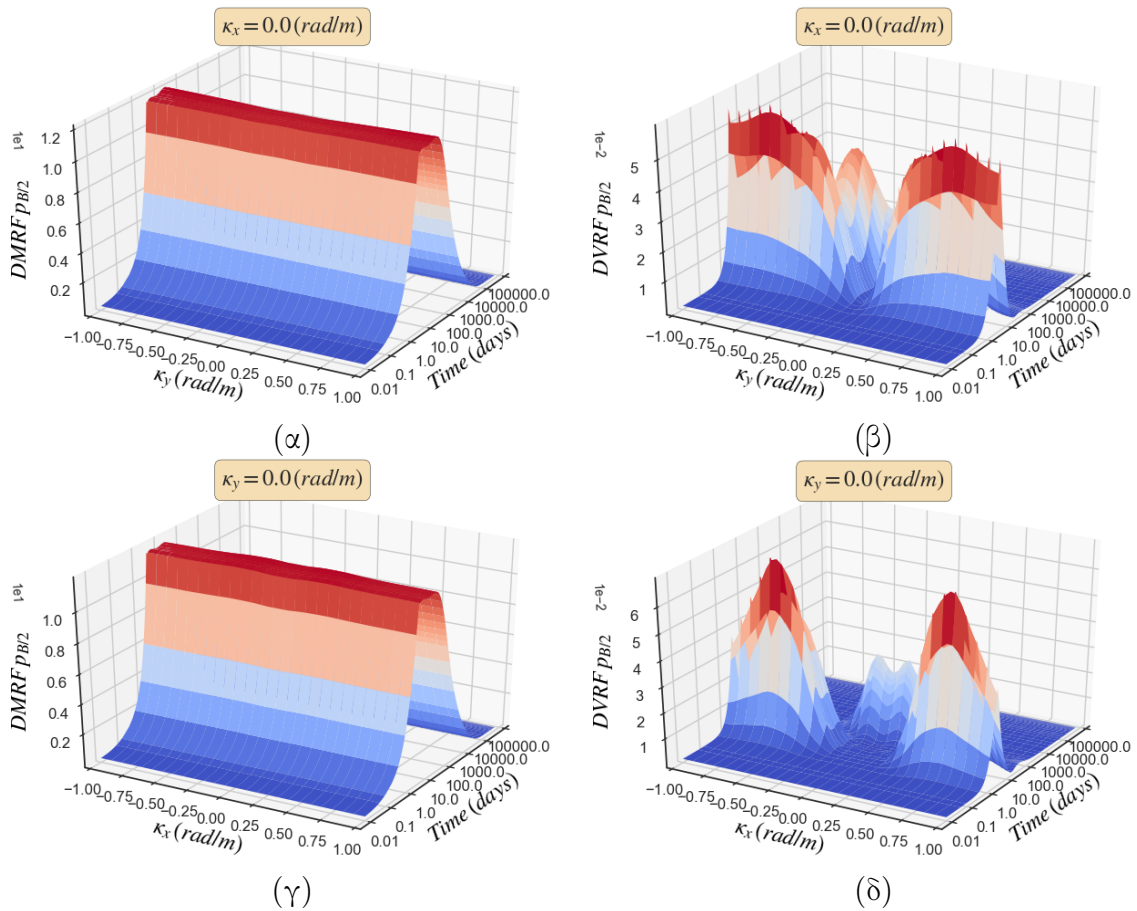


Σχήμα 20. Μέση τιμή και διασπορά της υπερπίεσης πόρων $p_{B/2}$ για στοχαστική διαπερατότητα και μέτρο ελαστικότητας με $\sigma_k = \sigma_E = 0.2$ και μήκος συσχέτισης $b = 10 \text{ m}$: (α) $\mu_{p_{B/2}}$ για στοχαστικό k , (β) $Var(p_{B/2})$ για στοχαστικό k , (γ) $\mu_{p_{B/2}}$ για στοχαστικό E και (δ) $Var(p_{B/2})$ για στοχαστικό E .

0.9 Εφαρμογή ΔΣΔΑ στη στοχαστική στερεοποίηση εδάφους



Σχήμα 21. ΔΣΜΑ/ΔΣΔΑ της υπερπίεσης πόρων $p_{B/2}$ για στοχαστική διαπερατότητα με $\sigma_k = 0.2$: (α) ΔΣΜΑ για $\kappa_y = 0.0$ (rad/m), (β) ΔΣΔΑ για $\kappa_y = 0.0$ (rad/m), (γ) ΔΣΜΑ για $\kappa_x = 0.0$ (rad/m) και (δ) ΔΣΔΑ για $\kappa_x = 0.0$ (rad/m).



Σχήμα 22. ΔΣΜΑ/ΔΣΔΑ της υπερπίεσης πόρων $B/2$ για στοχαστικό μέτρο ελαστικότητας με $\sigma_k = 0.2$: (α) ΔΣΜΑ για $\kappa_y = 0.0$ (rad/m), (β) ΔΣΔΑ για $\kappa_y = 0.0$ (rad/m), (γ) ΔΣΜΑ για $\kappa_x = 0.0$ (rad/m) και (δ) ΔΣΔΑ για $\kappa_x = 0.0$ (rad/m).

0.10 Συμπεράσματα και συνεισφορά της διατριβής

Στην παρούσα διδακτορική διατριβή προωθήθηκε η μέθοδος των στοχαστικών πεπερασμένων στοιχείων (ΜΣΠΣ) ως απαραίτητο εργαλείο για την ποσοτικοποίηση της επιρροής της διακύμανσης των εδαφικών ιδιοτήτων σε γεωτεχνικά προβλήματα. Η δε αξιοποίηση αυτή αποτελεί ρεαλιστικό στόχο, δεδομένης της συνεχώς αυξανόμενης υπολογιστικής ισχύος που είναι διαθέσιμη στους μηχανικούς. Με αυτό το σκεπτικό, η εν λόγω εργασία δύναται να θεωρηθεί ως ένα σημαντικό βήμα στη λεπτομερή επεξήγηση των απαιτούμενων μεθόδων για την επιτυχή ενσωμάτωση αβέβαιων εδαφικών ιδιοτήτων σε γεωτεχνικές μελέτες. Ιδιαίτερη έμφαση δόθηκε στις πρόσφατα εδραιωμένες έννοιες των δυναμικών συναρτήσεων μέσης τιμής/διακύμανσης της απόκρισης, οι οποίες προσφέρουν μια αξιόπιστη εναλλακτική μεθοδολογία για τον υπολογισμό στατιστικών της υπό μελέτης απόκρισης. Για το σκοπό αυτό, η ταχεία μέθοδος Monte Carlo, όπως αποδείχθηκε από τις εφαρμογές που μελετήθηκαν, συνιστά την κατεξοχήν μεθοδολογία για την αποτελεσματική εκτίμηση των συναρτήσεων $\Delta\Sigma\text{MA}/\Delta\Sigma\text{DA}$ γενικών προβλημάτων πεπερασμένων στοιχείων.

0.10.1 Κύρια σημεία συνεισφοράς της διατριβής

Η συνεισφορά της παρούσας διατριβής συνοψίζεται στα εξής κύρια σημεία:

- Τεκμηρίωση της σημασίας υιοθέτησης της μεθόδου των στοχαστικών πεπερασμένων στοιχείων σε προβλήματα γεωτεχνικής μηχανικής. Συγκεκριμένα, η ενσωμάτωση της διακύμανσης των εδαφικών παραμέτρων στην αριθμητική προσομοίωση αναδεικνύει χαρακτηριστικά της απόκρισης, όπως για παράδειγμα η διαφορική καθίζηση στην περίπτωση του θεμελίου σε στερεοποιήσιμο έδαφος, τα οποία δεν συναντώνται στην περίπτωση που το έδαφος θεωρηθεί ομογενές.
- Επικύρωση της ακρίβειας και της ευκολίας εφαρμογής των $\Delta\Sigma\text{MA}/\Delta\Sigma\text{DA}$ για τον υπολογισμό των στατιστικών της απόκρισης σε προβλήματα με πορώδη υλικά, καθώς και σε περιπτώσεις διάδοσης διατμητικού κύματος για την ανάλυση απόκρισης της εδαφικής επιφάνειας.
- Εκ νέου επιβεβαίωση της ταχείας μεθόδου Monte Carlo ως κατεξοχήν αξιόπιστη μεθοδολογία υπολογισμού των συναρτήσεων $\Delta\Sigma\text{MA}/\Delta\Sigma\text{DA}$ για γενικά προσομοιώματα πεπερασμένων στοιχείων ανεξαρτήτως πολυπλοκότητας.

- Εστίαση στη σπουδαιότητα της ανεξαρτησίας των ΔΣΜΑ/ΔΣΔΑ από τη δομή συσχέτισης, αλλά και την πιθανοτική κατανομή των τυχαίων πεδίων που περιγράφουν τη χωρική διακύμανση των εδαφικών ιδιοτήτων. Ειδικά αυτή τους η ιδιότητα επιτρέπει την εύκολη και υπολογιστικά αποδοτική ανάλυση ευαισθησίας του υπό μελέτη μοντέλου ως προς τις στοχαστικές παραμέτρους των υλικών, χωρίς να απαιτούνται επιπλέον αναλύσεις πεπερασμένων στοιχείων.

Contents

List of Figures	lxxvii
List of Tables	lxxxv
1 Introduction	1
1.1 Motivation and Scope	1
1.2 Dissertation Objective	3
1.2.1 Software Development	4
1.2.2 Geotechnical Applications	5
1.3 Thesis Outline	6
2 Basic probability theory	9
2.1 Sets	9
2.1.1 Terminology	9
2.1.2 Set operations	10
2.2 Probability law	12
2.2.1 Probability axioms	12
2.2.2 Conditional probability	13
2.2.3 Total probability theorem and Bayes' rule	13
2.2.4 Independence of events	14
2.3 Random variables	14
2.3.1 Probability density and cumulative distribution functions	15
2.3.2 Measures of central tendency and dispersion	15
2.4 Common probability distributions	16
2.4.1 Uniform distribution	16
2.4.2 Normal distribution	17
2.4.3 Lognormal distribution	17
2.5 Jointly distributed continuous random variables	19

Contents

2.5.1	Joint and marginal distributions	19
2.5.2	Covariance and correlation coefficient	20
2.5.3	Independent random variables	20
3	Random processes and random fields	23
3.1	Basic definitions	23
3.1.1	Ensembles and ensemble averages	24
3.1.2	Stationary random processes and homogeneous random fields . .	26
3.1.3	Ergodic random processes and fields	27
3.1.4	Random processes and fields in the frequency domain	28
3.1.4.1	Wiener-Khinchine relations	28
3.2	Simulation of Gaussian random fields by the spectral representation method	29
3.2.1	Spectral representation method for simulation of 1D fields . . .	29
3.2.2	Spectral representation method for simulation of 2D fields . . .	31
3.2.3	Spectral representation method for simulation of 3D fields . . .	35
3.3	Non-Gaussian random processes and fields	39
3.3.1	Memoryless transformations	39
3.3.1.1	Translation processes and fields	40
3.3.1.2	Lognormal random processes and fields	40
4	The Stochastic Finite Element Method	43
4.1	Main variants of the Stochastic Finite Element Method	43
4.1.1	The Perturbation method	43
4.1.1.1	Main aspects of the Perturbation method	44
4.1.1.2	The Perturbation-based stochastic finite element method	46
4.1.2	The Spectral Stochastic Finite Element Method	48
4.1.3	The Monte Carlo Simulation Method	49
4.2	Discretization methods	50
4.2.1	The nodal point method	50
4.2.2	The integration point method	51
4.2.3	The Midpoint method	51
5	Variability response functions	53
5.1	Definition of VRF and MRF	53
5.2	Definition of DVRF and DMRF	54
5.3	Upper bounds of the response variance and mean value	55

5.3.1	Time independent response	55
5.3.2	Transient response	57
5.4	The fast Monte Carlo simulation method	58
5.4.1	Problems in 1D	58
5.4.2	Problems in 2D	59
5.4.3	Problems in 3D	60
5.5	Symmetries of the DMRF and DVRF functions	62
5.5.1	Symmetry in the 1D case	62
5.5.2	Symmetry in the 2D case	62
6	Consolidation of a soil layer with stochastic material properties	65
6.1	The Consolidation Equation and its Numerical Solution	65
6.2	Representation of uncertain soil properties	67
6.2.1	Stochastic finite element analysis	68
6.3	Case Study	70
6.3.1	Description of the numerical example	70
6.3.2	On the choice of finite elements and model dimensions	72
6.3.3	Discussion of results	73
6.3.3.1	Footing settlement	73
6.3.3.2	Pore pressures	83
6.3.4	Foundation design guidelines	96
6.4	Concluding remarks	96
7	Dynamic variability response functions for shear wave propagation in soils	99
7.1	Time integration of equations of motion	100
7.1.1	The Newmark algorithm	100
7.1.2	Bathe algorithm	102
7.1.3	Hilber-Hughes-Taylor α method	105
7.2	Simulation of stochastic shear wave propagation in soils	107
7.3	Dynamic Variability Response Function	108
7.4	Numerical application	109
7.4.1	Synthetic wavelets used	110
7.4.2	Wave propagation in 1D	111
7.4.3	Wave propagation in 2D	123
7.5	Concluding remarks	129

Contents

8	Dynamic variability response functions for stochastic consolidation of soils	131
8.1	Revisiting the stochastic consolidation problem	131
8.2	Footing settlement statistics	132
8.3	Excess pore pressure statistics	140
8.4	Conclusion	153
9	Concluding remarks and recommendation for further research	155
9.1	Conclusions and recommendations for further research	155
9.1.1	Summary and conclusions of the research developed	155
9.1.2	Contributions of the dissertation	156
9.1.3	Proposed future research	157
	Bibliography	159
	Appendix A Software used	169
	Appendix B Validation of the software used	173

List of Figures

2.1	Venn diagram for sets A , A^c and Ω	10
2.2	Venn diagram for $A \cup B$	10
2.3	Venn diagram for $A \cap B$	11
2.4	Venn diagram for difference of A and B	11
2.5	Venn diagram for symmetric difference of A , B	11
2.6	Venn diagram for disjoint sets A , B	12
2.7	Probability density function for random variable $X \sim U(1, 3)$	17
2.8	Probability density function for random variable $X \sim N(0, 1)$	18
2.9	Probability density function for lognormal random variable X with $\mu_{\ln X} = 1$ and $\sigma_{\ln X} = 1$	19
3.1	Sample realizations of 1D random fields.	24
3.2	Sample realizations of 2D random fields.	25
3.3	Sample realizations of 3D random fields.	26
3.4	Plot of S_{f_0} with respect to wave number κ	31
3.5	Sample realizations of a 1D random field with $\sigma_f = 0.2$ and $b = 1.0 m$	32
3.6	Sample realizations of a 1D random field with $\sigma_f = 0.2$ and $b = 5.0 m$	33
3.7	Spectral density function in 2D for various correlation length parameters: (a) $b_1 = b_2 = 1.0 m$, (b) $b_1 = b_2 = 5.0 m$, (c) $b_1 = 1.0 m$, $b_2 = 5.0 m$ and (d) $b_1 = 5.0 m$, $b_2 = 1.0 m$	35
3.8	Sample realizations of a 2D random field for $b_1 = b_2 = 1.0 m$	36
3.9	Sample realizations of a 2D random field for $b_1 = b_2 = 5.0 m$	37
3.10	Sample realizations of a 2D random field for $b_1 = 1.0 m$ and $b_2 = 5.0 m$	38
6.1	Random field realizations for COV = 0.25 and correlation parameter $b_{\ln(k)} = b_{1\ln(k)} = b_{2\ln(k)}$: (a) 10 m, (b) 16 m, (c) 25 m and (d) 50 m.	69
6.2	Random field realizations for COV = 2.00 and correlation parameter $b_{\ln(k)} = b_{1\ln(k)} = b_{2\ln(k)}$: (a) 10 m, (b) 16 m, (c) 25 m and (d) 50 m.	69

List of Figures

6.3	Finite element mesh of the model.	71
6.4	Footing settlements.	71
6.5	Comparison of results between 4U4P and 8U8P quadrilateral element formulations, where: (a) Settlement of footing center and (b) Excess pore pressure at depth $B/2$	72
6.6	Comparison of the footing-soil response for different choices of the horizontal model dimension L , where: (a) Settlement of footing center and (b) Excess pore pressure at depth $B/2$	73
6.7	Mean differential settlement vs time for stochastic permeability k and COV values: (a) 0.25 and (b) 2.00.	75
6.8	Mean differential settlement vs time for stochastic elastic modulus E and COV values: (a) 0.25 and (b) 2.00.	75
6.9	Monte Carlo results of differential footing settlement for stochastic permeability with $b_{\ln(k)} = 10 m$ and COV values: (a) 0.25 and (b) 2.00.	76
6.10	Monte Carlo results of differential footing settlement for stochastic elastic modulus with $b_{\ln(E)} = 10 m$ and COV values: (a) 0.25 and (b) 2.00.	76
6.11	Mean of max differential settlement vs Monte Carlo simulations for stochastic permeability k and COV values: (a) 0.25 and (b) 2.00.	77
6.12	Mean of max differential settlement vs Monte Carlo simulations for stochastic elastic modulus E and COV values: (a) 0.25 and (b) 2.00.	77
6.13	STD of max differential settlement vs Monte Carlo simulations for stochastic permeability k and COV values: (a) 0.25 and (b) 2.00.	78
6.14	STD of max differential settlement vs Monte Carlo simulations for stochastic elastic modulus E and COV values: (a) 0.25 and (b) 2.00.	78
6.15	Monte Carlo results of footing center settlement for stochastic permeability with $b_{\ln(k)} = 10 m$ and COV values: (a) 0.25 and (b) 2.00.	79
6.16	Monte Carlo results of footing center settlement for stochastic elastic modulus with $b_{\ln(E)} = 10 m$ and COV values: (a) 0.25 and (b) 2.00.	79
6.17	Histogram of maximum footing differential settlement and fitted log-normal distribution for stochastic permeability with $b_{\ln(k)} = b1_{\ln(k)} = b2_{\ln(k)} = 10 m$ and COV values: (a) 0.25 and (b) 2.00.	80
6.18	Histogram of maximum footing differential settlement and fitted lognormal distribution for stochastic elastic modulus with $b_{\ln(E)} = b1_{\ln(E)} = b2_{\ln(E)} = 10 m$ and COV values: (a) 0.25 and (b) 2.00.	80

6.19	Histogram of maximum footing center settlement and fitted Gaussian distribution for stochastic permeability with $b_{\ln(k)} = b1_{\ln(k)} = b2_{\ln(k)} = 10 m$ and COV values: (a) 0.25 and (b) 2.00.	81
6.20	Histogram of maximum footing center settlement and fitted Gaussian distribution for stochastic elastic modulus with $b_{\ln(E)} = b1_{\ln(E)} = b2_{\ln(E)} = 10 m$ and COV values: (a) 0.25 and (b) 2.00.	81
6.21	a) Mean and b) STD of maximum differential settlement vs normalized correlation parameter $b_{\ln(k)}/B$ for stochastic permeability, where $b_{\ln(k)} = b1_{\ln(k)} = b2_{\ln(k)}$ and B the footing width.	82
6.22	a) Mean and b) STD of maximum differential settlement vs normalized correlation parameter $b_{\ln(E)}/B$ for stochastic elastic modulus, where $b_{\ln(E)} = b1_{\ln(E)} = b2_{\ln(E)}$ and B the footing width.	82
6.23	Mean excess pore pressure at depth $B/10$ vs time for stochastic permeability k and COV values: (a) 0.25 and (b) 2.00.	84
6.24	Mean excess pore pressure at depth $B/10$ vs time for stochastic Young's modulus E and COV values: (a) 0.25 and (b) 2.00.	84
6.25	Mean excess pore pressure at depth $B/2$ vs time for stochastic permeability k and COV values: (a) 0.25 and (b) 2.00.	85
6.26	Mean excess pore pressure at depth $B/2$ vs time for stochastic Young's modulus E and COV values: (a) 0.25 and (b) 2.00.	85
6.27	Excess pore pressure at depth $B/10$ vs time for stochastic permeability with $b_{\ln(k)} = 10 m$ and COV values: (a) 0.25 and (b) 2.00.	86
6.28	Excess pore pressure at depth $B/10$ vs time for stochastic elastic modulus with $b_{\ln(E)} = 10 m$ and COV values: (a) 0.25 and (b) 2.00.	86
6.29	Excess pore pressure at depth $B/2$ vs time for stochastic permeability with $b_{\ln(k)} = 10 m$ and COV values: (a) 0.25 and (b) 2.00.	87
6.30	Excess pore pressure at depth $B/2$ vs time for stochastic elastic modulus with $b_{\ln(E)} = 10 m$ and COV values: (a) 0.25 and (b) 2.00.	87
6.31	Mean of maximum excess pore pressure vs normalized correlation parameter $b_{\ln(k)}/B$ for stochastic permeability k and depth: (a) $B/10$, (b) $B/5$, (c) $B/2$ and (d) B	88
6.32	Mean of maximum excess pore pressure vs normalized correlation parameter $b_{\ln(E)}/B$ for stochastic elastic modulus E and depth: (a) $B/10$, (b) $B/5$, (c) $B/2$ and (d) B	89

List of Figures

6.33	STD of maximum excess pore pressure vs normalized correlation parameter b/B for stochastic permeability k and depth: (a) $B/10$, (b) $B/5$, (c) $B/2$ and (d) B	90
6.34	STD of maximum excess pore pressure vs normalized correlation parameter b/B for stochastic elastic modulus E and depth: (a) $B/10$, (b) $B/5$, (c) $B/2$ and (d) B	91
6.35	Histogram of max excess pore pressure at depth $B/10$ and fitted Gaussian distribution for stochastic permeability with $b_{ln(k)} = 10 m$ and COV values: (a) 0.25 and (b) 2.00.	92
6.36	Histogram of max excess pore pressure at depth $B/10$ and fitted Gaussian distribution for stochastic elastic modulus with $b_{ln(E)} = 10 m$ and COV values: (a) 0.25 and (b) 2.00.	92
6.37	Histogram of max excess pore pressure at depth $B/5$ and fitted lognormal distribution for stochastic permeability with $b_{ln(k)} = 10 m$ and COV values: (a) 0.25 and (b) 2.00.	93
6.38	Histogram of max excess pore pressure at depth $B/5$ and fitted lognormal distribution for stochastic elastic modulus with $b_{ln(E)} = 10 m$ and COV values: (a) 0.25 and (b) 2.00.	93
6.39	Histogram of max excess pore pressure at depth $B/2$ and fitted lognormal distribution for stochastic permeability with $b_{ln(k)} = 10 m$ and COV values: (a) 0.25 and (b) 2.00.	94
6.40	Histogram of max excess pore pressure at depth $B/2$ and fitted lognormal distribution for stochastic elastic modulus with $b_{ln(E)} = 10 m$ and COV values: (a) 0.25 and (b) 2.00.	94
6.41	Histogram of max excess pore pressure at depth B and fitted lognormal distribution for stochastic permeability with $b_{ln(k)} = 10 m$ and COV values: (a) 0.25 and (b) 2.00.	95
6.42	Histogram of max excess pore pressure at depth B and fitted lognormal distribution for stochastic elastic modulus with $b_{ln(E)} = 10 m$ and COV values: (a) 0.25 and (b) 2.00.	95
7.1	Numerical model used for the simulation of 1D shear wave propagation in soil	108
7.2	Numerical model used for the simulation of 2D shear wave propagation in soil	109

7.3	DMRF and DVRF of ground response for incoming Ricker wavelet with unit amplitude for $\sigma_{ff} = 0.2$: (a) displacement DMRF, (b) displacement DVRF, (c) velocity DMRF, (d) velocity DVRF, (e) acceleration DMRF and (f) acceleration DVRF.	115
7.4	DMRF and DVRF of ground response for incoming Mavroeidis & Papageorgiou wavelet with unit amplitude for $\sigma_{ff} = 0.2$: (a) displacement DMRF, (b) displacement DVRF, (c) velocity DMRF, (d) velocity DVRF, (e) acceleration DMRF and (f) acceleration DVRF.	116
7.5	DMRF and DVRF of ground response for incoming Gilroy earthquake motion record for $\sigma_{ff} = 0.2$: (a) displacement DMRF, (b) displacement DVRF, (c) velocity DMRF, (d) velocity DVRF, (e) acceleration DMRF and (f) acceleration DVRF.	117
7.6	Mean and variance of ground response for incoming Mavroeidis & Papageorgiou wavelet for a Gaussian field with $\sigma_{ff} = 0.2$ and correlation parameter $b = 40 m$: (a) displacement mean, (b) displacement variance, (c) velocity mean, (d) velocity variance, (e) acceleration mean and (f) acceleration variance.	118
7.7	Mean and variance of ground response for incoming Gilroy motion for a Gaussian field with $\sigma_{ff} = 0.2$ and correlation parameter $b = 40 m$: (a) displacement mean, (b) displacement variance, (c) velocity mean, (d) velocity variance, (e) acceleration mean and (f) acceleration variance.	119
7.8	Mean and variance of ground response for incoming Gilroy motion for a truncated Gaussian field with $\sigma_{ff} = 0.3$ and correlation parameter $b = 100 m$: (a) displacement mean, (b) displacement variance, (c) velocity mean, (d) velocity variance, (e) acceleration mean and (f) acceleration variance.	120
7.9	Mean and variance of ground response for incoming Ricker wavelet with unit amplitude for a lognormal field with $\sigma_{g_L g_L} = 0.3$ and correlation parameter $b = 20 m$: (a) displacement mean, (b) displacement variance, (c) velocity mean, (d) velocity variance, (e) acceleration mean and (f) acceleration variance.	121
7.10	Upper bounds of the mean and variance of ground response for incoming earthquake for $\sigma_{ff} = 0.2$: (a) displacement mean, (b) displacement variance, (c) velocity mean, (d) velocity variance, (e) acceleration mean and (f) acceleration variance.	122

List of Figures

7.11	DVRF of ground response for incoming Ricker wavelet for $\sigma_{ff} = 0.2$: (a) displacement DVRF for $\kappa_y = 0.0$ (rad/m), (b) displacement DVRF for $\kappa_x = 0.0$ (rad/m), (c) displacement DVRF for $\kappa_x = \kappa_y$, (d) velocity DVRF for $\kappa_y = 0.0$ (rad/m), (e) velocity DVRF for $\kappa_x = 0.0$ (rad/m), (f) velocity DVRF for $\kappa_x = \kappa_y$, (g) acceleration DVRF for $\kappa_y = 0.0$ (rad/m), (h) acceleration DVRF for $\kappa_x = 0.0$ (rad/m) and (i) acceleration DVRF for $\kappa_x = \kappa_y$	125
7.12	DVRF of ground response for incoming earthquake motion for $\sigma_{ff} = 0.2$: (a) displacement DVRF for $\kappa_y = 0.0$ (rad/m), (b) displacement DVRF for $\kappa_x = 0.0$ (rad/m), (c) displacement DVRF for $\kappa_x = \kappa_y$, (d) velocity DVRF for $\kappa_y = 0.0$ (rad/m), (e) velocity DVRF for $\kappa_x = 0.0$ (rad/m), (f) velocity DVRF for $\kappa_x = \kappa_y$, (g) acceleration DVRF for $\kappa_y = 0$ (rad/m), (h) acceleration DVRF for $\kappa_x = 0.0$ (rad/m) and (i) acceleration DVRF for $\kappa_x = \kappa_y$	126
7.13	Mean and variance of ground response for Ricker wavelet for a Gaussian field with $\sigma_{ff} = 0.2$ and correlation parameters $b_x = b_y = 100$ m : (a) displacement mean, (b) displacement variance, (c) velocity mean, (d) velocity variance, (e) acceleration mean and (f) acceleration variance. .	127
7.14	Mean and variance of ground response for Gilroy motion for a Gaussian field with $\sigma_{ff} = 0.2$ and correlation parameters $b_x = b_y = 100$ m : (a) displacement mean, (b) displacement variance, (c) velocity mean, (d) velocity variance, (e) acceleration mean and (f) acceleration variance. .	128
8.1	Mean and variance for various footing settlement for stochastic per- meability with $\sigma_k = 0.2$ and correlation length $b = 10$ m : (a) μ_{ν_C} , (b) $Var(\nu_C)$, (c) μ_{ν_A} , (d) $Var(\nu_A)$, (e) $\mu_{\nu_{AD}}$ and (f) $Var(\nu_{AD})$	134
8.2	Mean and variance for various footing settlement for stochastic Young's modulus with $\sigma_E = 0.2$ and correlation length $b = 10$ m : (a) μ_{ν_C} , (b) $Var(\nu_C)$, (c) μ_{ν_A} , (d) $Var(\nu_A)$, (e) $\mu_{\nu_{AD}}$ and (f) $Var(\nu_{AD})$	135
8.3	DVRF functions for settlement ν_{AD} of the footing for permeability with $\sigma_k = 0.2$ for: (a) $\kappa_y = 0.0$ (rad/m), (b) $\kappa_y = 0.0$ (rad/m) and (c) $\kappa_x = \kappa_y$.	136
8.4	DVRF functions for settlement ν_{AD} of the footing for stochastic Young's modulus with $\sigma_E = 0.2$ for: (a) $\kappa_y = 0.0$ (rad/m), (b) $\kappa_y = 0.0$ (rad/m) and (c) $\kappa_x = \kappa_y$	137

8.5	DMRF and DVRF functions for settlement ν_C of the footing center for permeability with $\sigma_k = 0.2$: (a) DMRF for $\kappa_y = 0.0$ (<i>rad/m</i>), (b) DVRF for $\kappa_y = 0.0$ (<i>rad/m</i>), (c) DMRF for $\kappa_x = 0.0$ (<i>rad/m</i>), (d) DVRF for $\kappa_x = 0.0$ (<i>rad/m</i>), (e) DMRF for $\kappa_x = \kappa_y$ and (f) DVRF for $\kappa_x = \kappa_y$. . .	138
8.6	DMRF and DVRF functions for settlement ν_C of the footing center for stochastic Young's modulus with $\sigma_E = 0.2$: (a) DMRF for $\kappa_y = 0.0$ (<i>rad/m</i>), (b) DVRF for $\kappa_y = 0.0$ (<i>rad/m</i>), (c) DMRF for $\kappa_x = 0.0$ (<i>rad/m</i>), (d) DVRF for $\kappa_x = 0.0$ (<i>rad/m</i>), (e) DMRF for $\kappa_x = \kappa_y$ and (f) DVRF for $\kappa_x = \kappa_y$	139
8.7	Mean and variance for excess pore pressure at depths $B/10$ and $B/5$ for stochastic permeability with $\sigma_k = 0.2$ and correlation length $b = 10$ m: (a) $\mu_{p_{B/10}}$, (b) $Var(p_{B/10})$, (c) $\mu_{p_{B/5}}$ and (d) $Var(p_{B/5})$	141
8.8	Mean and variance for excess pore pressure at depths $B/2$ and B for stochastic permeability with $\sigma_k = 0.2$ and correlation length $b = 10$ m: (a) $\mu_{p_{B/2}}$, (b) $Var(p_{B/2})$, (c) μ_{p_B} and (d) $Var(p_B)$	142
8.9	Mean and variance for excess pore pressure at depths $B/10$ and $B/5$ for stochastic Young's modulus with $\sigma_E = 0.2$ and correlation length $b = 10$ m: (a) $\mu_{p_{B/10}}$, (b) $Var(p_{B/10})$, (c) $\mu_{p_{B/5}}$ and (d) $Var(p_{B/5})$. . .	143
8.10	Mean and variance for excess pore pressure at depths $B/2$ and B for stochastic Young's modulus with $\sigma_E = 0.2$ and correlation length $b = 10$ m: (a) $\mu_{p_{B/2}}$, (b) $Var(p_{B/2})$, (c) μ_{p_B} and (d) $Var(p_B)$	144
8.11	DMRF and DVRF functions for pore pressure $p_{B/10}$ for stochastic permeability with $\sigma_E = 0.2$: (a) DMRF for $\kappa_y = 0.0$ (<i>rad/m</i>), (b) DVRF for $\kappa_y = 0.0$ (<i>rad/m</i>), (c) DMRF for $\kappa_x = 0.0$ (<i>rad/m</i>), (d) DVRF for $\kappa_x = 0.0$ (<i>rad/m</i>), (e) DMRF for $\kappa_x = \kappa_y$ and (f) DVRF for $\kappa_x = \kappa_y$. . .	145
8.12	DMRF and DVRF functions for pore pressure $p_{B/10}$ for stochastic Young's modulus with $\sigma_E = 0.2$: (a) DMRF for $\kappa_y = 0.0$ (<i>rad/m</i>), (b) DVRF for $\kappa_y = 0.0$ (<i>rad/m</i>), (c) DMRF for $\kappa_x = 0.0$ (<i>rad/m</i>), (d) DVRF for $\kappa_x = 0.0$ (<i>rad/m</i>), (e) DMRF for $\kappa_x = \kappa_y$ and (f) DVRF for $\kappa_x = \kappa_y$	146
8.13	DMRF and DVRF functions for pore pressure $p_{B/5}$ for stochastic permeability with $\sigma_k = 0.2$: (a) DMRF for $\kappa_y = 0.0$ (<i>rad/m</i>), (b) DVRF for $\kappa_y = 0.0$ (<i>rad/m</i>), (c) DMRF for $\kappa_x = 0.0$ (<i>rad/m</i>), (d) DVRF for $\kappa_x = 0.0$ (<i>rad/m</i>), (e) DMRF for $\kappa_x = \kappa_y$ and (f) DVRF for $\kappa_x = \kappa_y$. . .	147

List of Figures

8.14	DMRF and DVRF functions for pore pressure $p_{B/5}$ for stochastic Young's modulus with $\sigma_E = 0.2$: (a) DMRF for $\kappa_y = 0.0$ (rad/m), (b) DVRF for $\kappa_y = 0.0$ (rad/m), (c) DMRF for $\kappa_x = 0.0$ (rad/m), (d) DVRF for $\kappa_x = 0.0$ (rad/m), (e) DMRF for $\kappa_x = \kappa_y$ and (f) DVRF for $\kappa_x = \kappa_y$. . .	148
8.15	DMRF and DVRF functions for pore pressure $p_{B/2}$ for stochastic permeability with $\sigma_k = 0.2$: (a) DMRF for $\kappa_y = 0.0$ (rad/m), (b) DVRF for $\kappa_y = 0.0$ (rad/m), (c) DMRF for $\kappa_x = 0.0$ (rad/m), (d) DVRF for $\kappa_x = 0.0$ (rad/m), (e) DMRF for $\kappa_x = \kappa_y$ and (f) DVRF for $\kappa_x = \kappa_y$. . .	149
8.16	DMRF and DVRF functions for pore pressure $p_{B/2}$ for stochastic Young's modulus with $\sigma_E = 0.2$: (a) DMRF for $\kappa_y = 0.0$ (rad/m), (b) DVRF for $\kappa_y = 0.0$ (rad/m), (c) DMRF for $\kappa_x = 0.0$ (rad/m), (d) DVRF for $\kappa_x = 0.0$ (rad/m), (e) DMRF for $\kappa_x = \kappa_y$ and (f) DVRF for $\kappa_x = \kappa_y$. . .	150
8.17	DMRF and DVRF functions for pore pressure p_B for stochastic permeability with $\sigma_k = 0.2$: (a) DMRF for $\kappa_y = 0.0$ (rad/m), (b) DVRF for $\kappa_y = 0.0$ (rad/m), (c) DMRF for $\kappa_x = 0.0$ (rad/m), (d) DVRF for $\kappa_x = 0.0$ (rad/m), (e) DMRF for $\kappa_x = \kappa_y$ and (f) DVRF for $\kappa_x = \kappa_y$. . .	151
8.18	DMRF and DVRF functions for pore pressure p_B for stochastic Young's modulus with $\sigma_E = 0.2$: (a) DMRF for $\kappa_y = 0.0$ (rad/m), (b) DVRF for $\kappa_y = 0.0$ (rad/m), (c) DMRF for $\kappa_x = 0.0$ (rad/m), (d) DVRF for $\kappa_x = 0.0$ (rad/m), (e) DMRF for $\kappa_x = \kappa_y$ and (f) DVRF for $\kappa_x = \kappa_y$. . .	152
B.1	Finite element mesh of the model.	174
B.2	Comparison between the results obtained by Solverize and (Smith and Griffiths, 2004) for a benchmark 1D consolidation problem, where: (a) Vertical displacement of node 1 and (b) Excess pore pressure of node 21.	174

List of Tables

7.1 Table of Newmark constants 101

Chapter 1

Introduction

1.1 Motivation and Scope

Soils in their natural state are among the most variable materials, while spatial variability and uncertainty of their properties is present even in soil layers considered homogeneous in geotechnical engineering practice. Nevertheless, lack of sufficient data required for accurately estimating the properties of soil materials involved in geotechnical problems has led to the adoption of deterministic analysis methods, which rely on safety factors to take into consideration the uncertainty and variability of soil properties. Currently, computing power provided by modern parallel computers is opening new frontiers in the incorporation of uncertainty in engineering problems in general. To this purpose, an increasing amount of research is dedicated to solving stochastic problems in order to quantify the effect of the uncertainty in material and geometry properties, as well as load and boundary conditions.

In recent years, the influence of inherent soil variability on geotechnical engineering applications has attracted considerable attention. A number of researchers have studied the effect of spatial variability of various soil properties such as elasticity modulus, friction angle and permeability on different related applications. Investigations of footing bearing capacity (Al-Bittar and Soubra, 2013; Cho and Park, 2010; Griffiths et al., 2002, 2006; Simões et al., 2014) and settlements (Fenton and Griffiths, 2005; Maheshwari and Kumar, 2011; Paice et al., 1996), slope stability (Griffiths and Fenton, 2004; Griffiths et al., 2009), as well as seepage (Griffiths and Fenton, 1997), are some characteristic cases. Furthermore, the consolidation phenomenon in a probabilistic setting has been studied by various researchers. In (Badaoui et al., 2007; Houmadi et al., 2012), for example, the effect of the variability of k and E on the vertical direction for the 1-D consolidation problem was investigated. Additionally, in (Bong et al., 2014),

Introduction

the effect of the spatial variability of the consolidation coefficients in the vertical and horizontal directions on the degree of consolidation of the loaded soil was studied. What's more, in (Huang et al., 2010), the effect of the correlation between the stochastic soil permeability k and the coefficient of volume compressibility m_v on 1-D and 2-D coupled consolidation problem was investigated. Dynamic problems with stochastic soil parameters were also investigated in a number of research articles (Ho Lee et al., 2013; Johari and Khodaparast, 2015; Johari and Momeni, 2015; Wang and Sett, 2016). An in-depth coverage of probabilistic modeling in geotechnical engineering, along with a variety of case studies, are presented in (Fenton and Griffiths, 2008) too.

The most robust computational tool used to examine the effect of spatial variability of material properties on the response of various problems in general, is the stochastic finite element method (SFEM) (Stefanou, 2009). Concerning SFEM, the three most important alternative formulations are: the perturbation method, the spectral stochastic finite element method (SSFEM) and the Monte Carlo simulation (MCS). The perturbation method consists of the Taylor series expansion of the stochastic finite element matrix and of the resulting response vector of the physical system. In the SSFEM context, the stochastic finite element matrix consists of the sum of a deterministic and a stochastic part obtained through the Karhunen-Loève (K-L) expansion, whereas the response vector is expanded using random Hermite polynomials. In the analysis of complex problems, these two approaches may be quite difficult to implement and sometimes they are computationally expensive (Stavroulakis et al., 2014). Thus, the MCS, and in particular the direct MCS method, remains the only reliable and universal, albeit computationally intensive procedure for treating this kind of problems, particularly for large variation of the stochastic parameters (Stavroulakis et al., 2014).

One of the most important parts of Monte Carlo simulation is the generation of sample functions of the random fields (Vanmarcke, 2010) that accurately describe the variability of the studied property. Various methods are available for the generation of the required field realizations. The spectral representation method (Shinozuka and Deodatis, 1996) is one of the most widely used methodologies for generating homogeneous Gaussian random fields in 1D, 2D and 3D. Using the spectral representation method followed by a memoryless transformation in the form of translation fields (Grigoriu, 1995, 2002), non-Gaussian random field realizations can be easily generated.

In most studies, geotechnical problems have been analyzed in the context of the finite element method, incorporating in various ways the stochastic property of the soil. Specifically, a version of the globally applicable MCS method has been adopted

to quantify the response variability with respect to the stochastic property considered. The advantage of the MCS is its applicability to any probabilistic finite element model regardless of its complexity. Besides the well-known limitations of MCS due to its large computational cost, the main disadvantage of this approach is that the correlation structure of the underlying stochastic property of the soil materials has to be known in advance, which is rarely the case. As a result, the study of sensitivity of the required response with respect to different correlation characteristics makes the MCS almost prohibitive for the treatment of realistic examples.

In order to tackle the aforementioned limitations, the concept of variability response functions (VRF) was introduced in a number of articles (Bucher and Shinozuka, 1988; Kardara et al., 1989; Shinozuka, 1987). The VRF is a Green's function which relates the variance of a response quantity of a system to the spectral density function of its underlying uncertain parameters (Shinozuka, 1987). The VRF depends on deterministic system properties related to geometry, boundary and loading conditions, mean material properties as well as the standard deviation σ_{ff} of the considered stochastic parameter. The VRF function was initially expressed in closed form for statically determinate and indeterminate beam and truss structures under deterministic loading conditions; later the concept was extended to stochastic plate bending problems (Graham and Deodatis, 1998). As stated in (Papadopoulos et al., 2005), in most problems, a closed form expression of the VRF is extremely difficult, if not impossible to extract. However, the VRF can alternatively be estimated numerically using a so-called fast Monte Carlo finite element based procedure explained in (Papadopoulos et al., 2005, 2006). Other applications of the variability response function include the study of apparent material properties for heterogeneous random materials (Shinozuka, 1987), as well as robust design optimization taking into account the stochastic system parameters (Kokkinos and Papadopoulos, 2016). Keep in mind that the original VRF was formulated for static stochastic problems; an extension of the VRF for dynamic problems leading to the dynamic variability response function (DVRF) was recently introduced in (Papadopoulos and Kokkinos, 2012). It was also demonstrated that the DVRF and the closely related dynamic mean response function (DMRF) provide the same spectral-free advantages of the VRF for dynamic loadings, giving insight on the sensitivity of the response of dynamical systems with respect to the stochastic properties (Papadopoulos and Kokkinos, 2015).

1.2 Dissertation Objective

The objective of the research required for the completion of the dissertation is twofold; or, as one might arguably say, the amount of work demanded was double in size, since it involved both: a) the exploration, assessment and validation of novel computational methods to examine soil behavior with the use of uncertain parameters and b) the development of the software framework needed to support these applications. Please note that the second was the prerequisite, not the primary goal, nor the main subject of the thesis, something which may well explain why its importance is overlooked or overshadowed by the “achievements” of the latter. Taken into consideration though, this detail is staggering, revealing the difficulty and complexity of the overall attempt; however, there was a reason for this unconventionality. To the author’s knowledge, there are no commercial finite element software packages available up to now, which could support stochastic finite element computations. Therefore, the development of an in-house numerical package was the only way to achieve this goal. Once accomplished, this specially tuned software framework could then be used to quantify the uncertainty and variability of soil material properties on response quantities of interest in geotechnical problems. At this point, we have to stress this out: since soils in general are among the most uncertain materials, incorporating the variability of their properties in numerical simulations is of utmost importance.

1.2.1 Software Development

As mentioned above, a central objective throughout the dissertation was the development of the numerical methods necessary to successfully perform stochastic finite element analyses. To this purpose, the in-house, object-oriented finite element software suite *Solverize* had to be expanded in terms of new interfaces, classes and methods. Given this, the overall software development procedure can be furtherly divided in two phases:

- a) The first one, consisting of all the software developed in order to enable *Solverize* to tackle new problems for deterministic material properties, involved the following:
 - Enrichment with two-dimensional quadrilateral and triangular isoparametric elements with various choices of element nodes, supporting both plane strain and plane stress conditions. Additionally, three-dimensional hexahedral and tetrahedral finite elements were introduced, supporting various shape function orders.

- Addition of one-dimensional shear elements for simulation of 1D ground response analyses.
 - Development of quadrilateral and hexahedral elements of the u-p family for simulation of porous media. It has to be noted that, separate choice of shape functions for displacement and pore pressure dofs is supported, allowing for versatile interpolation schemes.
 - Introduction of implicit generalized Newmark (GN11) time integration scheme to enable the simulation of the consolidation phenomenon in soils.
 - Viscous damper elements of the Lysmer type to be used as absorbing boundary conditions in wave propagation analyses were also introduced.
 - Programming of implicit time integration algorithms for the equation of motion, namely the Newmark, HHT- α and Bathe schemes, to tackle dynamic problems.
 - Addition of a special class, handling the transformation of given earthquake motion records to equivalent nodal forces applied at the base of the finite element model.
- b) The second phase included the required numerical algorithms, which enabled *Solverize* to perform stochastic finite element simulations. To this purpose, the following software components were developed:
- Development of the multidimensional *spectral representation method* for generation of homogeneous Gaussian random field realizations in 1D, 2D and 3D. Various correlation structures were added, along with lognormal translation field transformations. Furthermore, emphasis was given, so that modern multicore processors were adequately supported in order to accelerate the generation of the fields.
 - Programming of the Monte Carlo stochastic finite element method with support for parallel multicore execution and efficient storage of results through Hdf5 files.
 - Development of the fast Monte Carlo simulation method in order to be able to calculate DMRF and DVRF functions for general finite element systems. Again, multicore support and storage efficiency were crucial.
 - Development of the software components needed to calculate response statistics via the DMRF and DVRF functions and the provided correlation structures.

- Development of scripts, written in Python, for the post-processing of the response statistics, along with their graphical representation.

1.2.2 Geotechnical Applications

After successfully incorporating the required software components, *Solverize* was used to perform a number of case studies of geotechnical nature, considering spatial variability of soil properties. The first application consists of the study of the settlement of a rigid footing resting on a consolidating soil layer. Stochastic finite element analyses were performed, incorporating the uncertainty of Young's modulus and soil permeability. A sensitivity study, with respect to the correlation structure of the underlying soil property, provided insight into the statistics of the differential footing settlements, as well as the excess pore pressures below the footing.

The following application deals with the problem of shear wave propagation in soils with uncertain shear modulus. In this case, the methodology of DVRF functions calculated through the fMCS method was employed. Both 1D and 2D wave propagation analyses were performed, demonstrating the validity of the DVRF, as well as its spectral-free nature. It is shown that the response statistics at the ground surface are sensitive to strongly correlated fields, i.e. the propagating wave is affected mainly by smooth random fields representing the shear modulus.

Finally, the problem of soil consolidation is revisited under the DVRF methodology, where the DVRF function concept is once again validated in terms of accuracy. Additionally, the value of the DVRF functions is further demonstrated, since they reveal the mechanisms controlling the response variability.

1.3 Thesis Outline

The present thesis consists of nine chapters outlined as follows:

- a) Chapter 2 introduces the basic concepts of probability theory. Specifically, sets and set operations are illustrated with the help of Venn diagrams. Furthermore, the probability axioms are established, accompanied with the concept of conditional probability, Bayes' rule and event independence. Definition of random variables, probability and cumulative distribution functions, as well as measures of central tendency and dispersion follow. The most common probability distributions and their properties are then presented, while the chapter concludes with

- the definition of jointly distributed random variables, together with the concepts of covariance, correlation and independence.
- b) Chapter 3 is dedicated to stochastic processes and fields. Definitions of the index set and state space are given for random processes and fields. Ensembles and ensemble averages are then introduced, while realizations of random fields in 1D, 2D and 3D are illustrated. Next, stationary random processes and their spatial equivalents, i.e. homogeneous random fields, are presented. The concept of ergodicity is stressed followed by the analysis of random fields in the frequency domain via the Wiener-Khinchine relations. The spectral representation is then thoroughly analyzed as the method of choice for computer generation of realizations of 1D, 2D and 3D homogeneous Gaussian random fields. What's more, the application of the method is demonstrated through illustrated examples showing the effect of different parameters of the correlation structure of the random fields on the generated realizations. Finally, the chapter concludes with a brief discussion on non-Gaussian random fields focusing on the concept of translation fields, which is used to present a methodology for generation of lognormal fields in a step-by-step manner.
 - c) In chapter 4, the most widely used methodologies comprising the stochastic finite element method are presented. In particular, main concepts of the perturbation method, the spectral stochastic finite element method and the globally applicable Monte Carlo method are introduced. Furthermore, the available spatial discretization methods regarding the random fields representing the stochastic parameter of interest, i.e. the nodal point method, the integration point method and the midpoint method adopted in this thesis are covered.
 - d) In chapter 5, the concept of variability and mean response functions is presented. The main advantage of MRF/VRF functions which lies in their independence of the correlation structure of the uncertain property considered, is emphasized. The extension of the MRF/VRF to time dependent problems through the concept of their dynamic equivalents, namely the dynamic mean and variability response functions, follows. In addition, the use of the DMRF/DVRF functions for calculation of upper bounds of response mean and variance in the time domain is presented. The fast Monte Carlo simulation method is then explained, which is the method of choice for numerically calculating the DMRF/DVRF functions for general stochastic finite element systems in 1D, 2D and 3D.

Introduction

- e) In chapter 6, the direct MCS method is applied to a classical geotechnical problem. Specifically, the problem of a rigid rough footing resting on a consolidating soil layer and loaded with a ramp loading is studied. The stochastic parameters incorporated in the analysis are the Young's modulus and permeability, which are simulated as lognormal random fields in 2D. Different correlation lengths and coefficients of variation are used in order to quantify the effect of the uncertain parameters on the variability of the response in terms of footing settlements, as well as excess soil pore pressures. Examination of the calculated response statistics provides insight into the different effect of the uncertainty in Young's modulus and permeability on the differential footing settlements. In the end, useful guidelines are provided regarding the design of footings on consolidating soil layers when spatial variability data of the soil properties is available.

- f) In chapter 7, the problem of shear wave propagation in soils exhibiting spatial variability of their shear modulus is studied. To this purpose, the DMRF/DVRF functions are employed in order to quantify the effect of the uncertain shear modulus on the response of the soil surface. The FMCS method is used to numerically evaluate the DMRF/DVRF functions. Test cases include simulation of propagation of synthetic wavelets, as well as a real recorded earthquake motion in both 1D and 2D soil domains. Comparison between the results obtained via the FMCS and the MCS is made, validating the accuracy and efficiency of the FMCS. Furthermore, the spectral and probability distribution free nature of the DMRF/DVRF is taken advantage of, in order to calculate upper bounds of the response mean and variance. Finally, inspection of the DMRF/DVRF functions illustrated offers insight into the mechanisms affecting the model sensitivity to uncertainty.

- g) In chapter 8, the stochastic consolidation problem studied in chapter 6 is revisited on the basis of the DMRF/DVRF methodology. The FMCS method is used in order to numerically calculate the DMRF/DVRF functions for footing settlements, as well as excess soil pore pressures. Results obtained via the FMCS-based DMRF/DVRF functions, regarding statistics of the response quantities, are then compared with the corresponding results from analogous MCS analyses. It is thus shown that the proposed method is accurate and computationally efficient, revealing the model sensitivity to the uncertain material parameters, i.e. the Young's modulus and permeability.

- h) Chapter 9 is the final one, summarizing the research conducted throughout the dissertation. To this purpose, the main contributions of the current work are outlined. A number of topics is finally proposed for future research, which could extend the scope of the methodologies discussed and promote the use of the SFEM for solving additional geotechnical engineering problems.

Chapter 2

Basic probability theory

In this chapter, the basic concepts of sets, probability theory and random variables are introduced. Together, they constitute the fundamental components needed in order to understand and use stochastic processes and random fields. For further understanding of the concepts presented, the reader may refer to (Bertsekas and Tsitsiklis, 2008; Papoulis and Pillai, 2002), which explain the probability theory in much greater depth.

2.1 Sets

In this section we introduce the basic components of the set theory needed in order to use sets and set relations; operations, which are widely used in probability theory. Venn diagrams are used in order to help understand the basic concepts.

2.1.1 Terminology

A *set* is a collection of items which are called the *members* of the set. Let A denote a set and x a member of the set. We say that x belongs to the set A which can be written in mathematical form as $x \in A$. If x does not belong to set A , we write $x \notin A$. A set which does not contain any elements is called *null set* or *empty set* and is denoted as \emptyset .

If every element x of set A is also an element of set B , set A is called a *subset* of B and we write $A \subseteq B$. Two sets A and B are *equal*, if and only if, $A \subseteq B$ and $B \subseteq A$, and we write $A = B$. A set C is called a *proper subset* of a set D denoted by $C \subset D$, if it is a subset that is strictly contained in D thus excluding at least one element of D . Finally, a set Ω is defined, which contains all the items of interest and is called the *universal set*, while every other set is considered a subset of Ω .

2.1.2 Set operations

We introduce the *complement* of a set A , A^c , so that if $x \in A$, then $x \notin A^c$. The complement of the universal set Ω is the empty set \emptyset . In general, relations and operations involving sets are best understood through the use of *Venn diagrams* like the one illustrated in fig. 2.1, where the white area indicates set A , the gray area set A^c and the rectangle area corresponds to the universal set Ω .

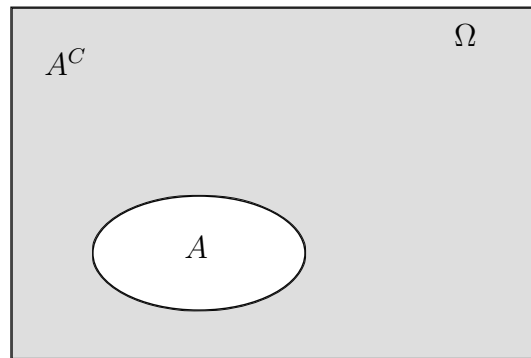


Figure 2.1. Venn diagram for sets A , A^c and Ω

The *union* of two sets A , B , written as $A \cup B$, is the set for which if $x \in A \cup B$ then $x \in A$ or $x \in B$. In fig. 2.2, the gray area indicates the set $A \cup B$.

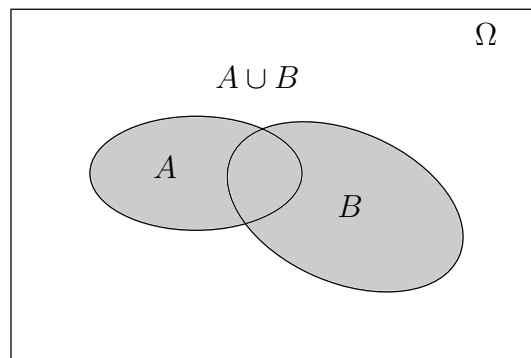
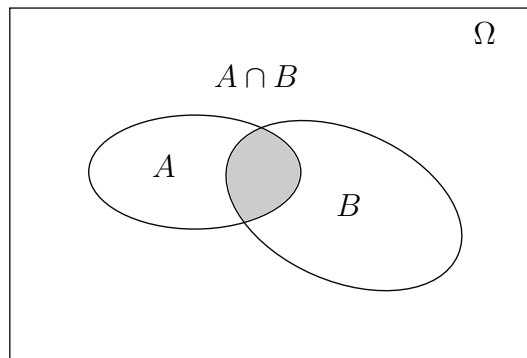
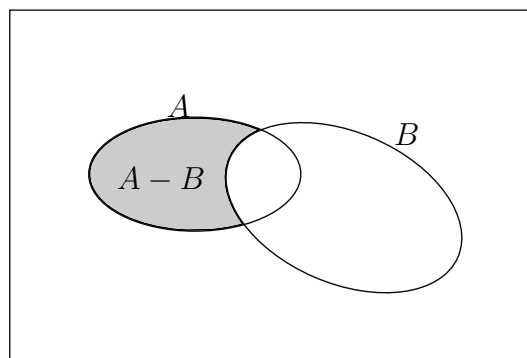


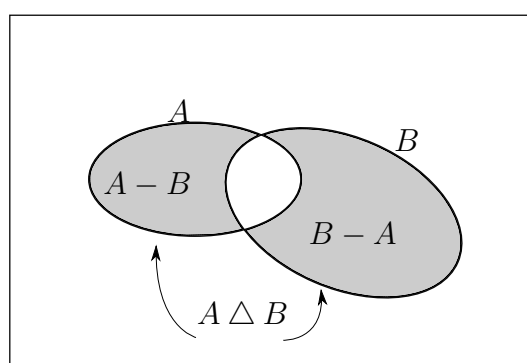
Figure 2.2. Venn diagram for $A \cup B$

The *intersection* of two sets A , B , written as $A \cap B$ is the set for which if $x \in A \cap B$, then $x \in A$ and $x \in B$. In fig. 2.3, the gray area indicates the set $A \cap B$. Alternative symbols denoting the intersection of A and B are AB and $A + B$.

The *difference* of two sets A , B , written as $A - B$ is the set for which $x \in A$ and $x \notin B$. In fig. 2.4, the gray area indicates the set $A - B$.

Figure 2.3. Venn diagram for $A \cap B$ Figure 2.4. Venn diagram for difference of A and B

The *symmetric difference* of two sets A, B , written as $A \Delta B$ is the set for which $x \in A$ or $x \in B$, but $x \notin A \cap B$; that is, $A \Delta B = (A - B) \cup (B - A)$. In fig. 2.5, the gray area indicates the set $A \Delta B$.

Figure 2.5. Venn diagram for symmetric difference of A, B

Two sets A, B are called *mutually exclusive* or *disjoint*, if they do not have any element in common, which in set terminology is written as $A \cap B = \emptyset$. For example, in fig. 2.6, sets A, B are disjoint.

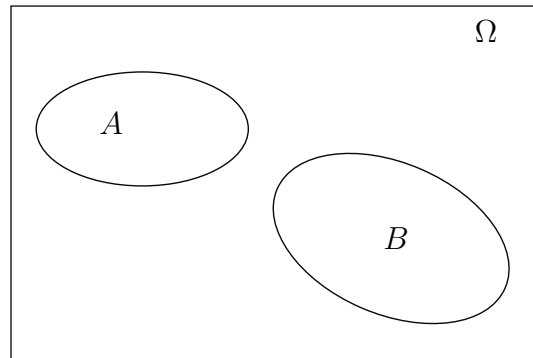


Figure 2.6. Venn diagram for disjoint sets A, B

2.2 Probability law

The basic components of probability theory are the notions of an *experiment* and its possible *outcomes* while, the set of all possible outcomes is called the sample space Ω . A subset of Ω , which is a collection of possible outcomes is called an *event*. The *probability law* assigns a number to an event E called the probability of event E , denoted as $P(E)$, satisfies $0 \leq P(E) \leq 1$ and expresses how likely this event takes place. There are two ways of describing the meaning of $P(E)$. First, assume that we devise an experiment related to a roll of a fair six-sided die. Let event A denote the case when the roll of the die results in number six. For a fair die, it is natural to say that $P(A) = 1/6$, which is the same for all possible results of the roll. Suppose that we repeat the experiment n times and let n_A denote the number of times that the die roll results in six. Then $P(A)$ can be interpreted as the ratio n_A/n i.e., the relative frequency of the roll of the die resulting in number six when the number n of repetitions is sufficiently large. Nevertheless, there are cases where the experiment cannot be repeated and the frequency concept is not valid. For example, let event G denote the collapse of a building due to a strong earthquake motion in the next 50 years; then the probability $P(G)$ is used to express our beliefs of how likely event G is going to take place.

2.2.1 Probability axioms

The theory of probability is founded on the following three *probability axioms*:

1. For every event A , $P(A) \geq 0$.
2. If events A and B are disjoint, i.e. $A \cap B = \emptyset$, then $P(A \cup B) = P(A) + P(B)$.
3. The probability of the sample space Ω is $P(\Omega) = 1$.

2.2.2 Conditional probability

Conditional probability provides a mechanism for incorporating additional information in calculations regarding the outcome of an experiment. Practically, while studying an experiment with given sample space Ω and probability law, we want to take advantage of the extra information that the outcome lies into an event B . This changes our beliefs regarding the outcome of the studied experiment, and it is desired to quantify the probability of an event A , given that it lies into B . In probability terms, a new probability law is established and the term *conditional probability* is used for the probability of event A given B , denoted as $P(A|B)$. The conditional probability of A given B is defined as:

$$P(A|B) = \frac{P(A \cap B)}{P(B)} \quad (2.1)$$

Equation (2.1) is defined only for events B with nonzero probability, i.e. $P(B) > 0$.

2.2.3 Total probability theorem and Bayes' rule

Let events A_1, A_2, \dots, A_n be some disjoint sets that form a partition of the sample space Ω , with positive probabilities i.e. $P(A_i) > 0, \forall i \in 1, 2, \dots, n$; let B be any event, then the *total probability theorem* states that:

$$\begin{aligned} P(B) &= P(A_1 \cap B) + P(A_2 \cap B) + \dots + P(A_n \cap B) \\ &= \sum_{i=1}^n P(A_i \cap B) \\ &= P(A_1) \cdot P(B|A_1) + P(A_2) \cdot P(B|A_2) + \dots + P(A_n) \cdot P(B|A_n) \\ &= \sum_{i=1}^n P(A_i) \cdot P(B|A_i) \end{aligned} \quad (2.2)$$

Bayes' theorem or Bayes' rule relates conditional probability $P(A|B)$ to conditional probability $P(B|A)$ for two events A, B . Let again events A_1, A_2, \dots, A_n be some disjoint sets that form a partition of the sample space Ω , with positive probabilities i.e. $P(A_i) > 0, \forall i \in 1, 2, \dots, n$. Then, by making use of the total probability theorem stated in eq. (2.2) Bayes' theorem is defined as follows:

$$\begin{aligned} P(A_i|B) &= \frac{P(A_i) \cdot P(B|A_i)}{P(B)} \\ \implies P(A_i|B) &= \frac{P(A_i) \cdot P(B|A_i)}{\sum_{i=1}^n P(A_i) \cdot P(B|A_i)} \end{aligned} \quad (2.3)$$

Basic probability theory

Bayes's theorem is the foundation of *Bayesian inference*, which is a method of statistical inference in which Bayes' theorem is used to update the probability for an hypothesis, as more evidence or information becomes available.

2.2.4 Independence of events

Two events A and B are called *independent* if the following relation holds:

$$P(A \cap B) = P(A) \cdot P(B) \quad (2.4)$$

Practically, independence of events A and B means that knowledge of occurrence of event B does not give any extra information regarding event A . Applying conditional probabilities, the following relation holds:

$$P(A|B) = P(A) \quad (2.5)$$

i.e. the conditional probability of A given B is equal to the unconditional one. The notion of independence can be extended to more than two events. We say that events A_1, A_2, \dots, A_n , are *mutually independent* if the following is true:

$$P(A_1 \cap A_2 \cap \dots \cap A_n) = P(A_1) \cdot P(A_2) \cdot \dots \cdot P(A_n) \quad (2.6)$$

2.3 Random variables

If the outcome of an experiment is a numerical value, this value is called a *random variable*. In mathematical terms, a random variable is a function which maps events of the sample space to numerical values. Distinction is made based on the nature of the numerical values a random variable can take. Therefore, random variables that take only distinct arithmetic values, are called *discrete random variables*. The term *continuous random variable* applies to random variables that can take range of values on the real line. In this dissertation only continuous random variables are used and are analyzed in this chapter.

2.3.1 Probability density and cumulative distribution functions

In order to fully describe a continuous random variable X , one only needs its *probability density function (pdf)*, which is designated $f_X(x)$. Using the pdf, the probability that the random variable X lies between two values a, b is calculated by:

$$P(a \leq X \leq b) = \int_a^b f_X(x) dx \quad (2.7)$$

In order to satisfy the probability axioms, the pdf satisfies the following relations:

$$f_X(x) \geq 0 \quad (2.8)$$

$$\int_{-\infty}^{\infty} f_X(x) dx = 1 \quad (2.9)$$

The *cumulative distribution function (cdf)* of a random variable X designated $F_X(x)$ is related to the pdf by the following relation:

$$F_X(x) = \int_{-\infty}^x f_X(u) du \quad (2.10)$$

expressing the probability that the random variable X is less than or equal to a specific value x :

$$F_X(x) = P(X \leq x) \quad (2.11)$$

The pdf of a random variable can be obtained from the cdf by differentiation:

$$f_X(x) = \frac{dF_X(x)}{dx} \quad (2.12)$$

2.3.2 Measures of central tendency and dispersion

The pdf and cdf give too much information regarding a random variable X . Sometimes, it is critical to compress all this information to representative quantities characterizing a random variable. The *expectation* $E[X]$ or *mean value* μ_X of a random variable X is the average of all the possible values of X ; it is given by the following relation:

$$E[X] = \mu_X = \int_{-\infty}^{+\infty} x f_X(x) dx \quad (2.13)$$

$E[X]$, expresses the representative value of the random variable X .

Basic probability theory

Other important quantities which offer information on a random variable X are its *moments*. In particular, the n -*moment* of X is the expectation of the random variable X^n and is given by:

$$E[X^n] = \mu_X = \int_{-\infty}^{+\infty} x^n f_X(x) dx \quad (2.14)$$

One very important quantity of the random variable X is its *variance* given by:

$$\text{Var}(X) = E[(X - E[X])^2] \quad (2.15)$$

which is a measure of the variation of X around its mean value μ_X . The square root of the variance is called the *standard deviation* σ_X :

$$\sigma_X = \sqrt{\text{Var}(X)} \quad (2.16)$$

and is a more natural measure of the variation of X , because it shares the same units with it. The variance and the standard deviation are always non-negative.

Finally, an alternative measure of spread of the random variable X is the *coefficient of variation* (*COV*); it describes the amount of variability relative to the mean and is defined as follows:

$$\text{COV}_X = \frac{\sigma_X}{\mu_X} \quad (2.17)$$

2.4 Common probability distributions

Although there is a large collection of distribution families, the most common ones which are also used in later chapters when considering applications, are the uniform, the normal and the lognormal distributions.

2.4.1 Uniform distribution

The simplest case of a random variable is the one that has the same probability of taking values in a closed interval $[a, b]$ and is called the *uniform* or *uniformly distributed* random variable. Specifically, we use the symbol $X \sim U(a, b)$ in order to denote that the random variable X follows the uniform distribution, while the probability density function of a uniform random variable is given by:

$$f_X(x) = \begin{cases} \frac{1}{b-a}, & \text{if } a \leq x \leq b \\ 0, & \text{otherwise} \end{cases} \quad (2.18)$$

2.4 Common probability distributions

Figure 2.7 illustrates the probability density function of $X \sim U(1, 3)$.

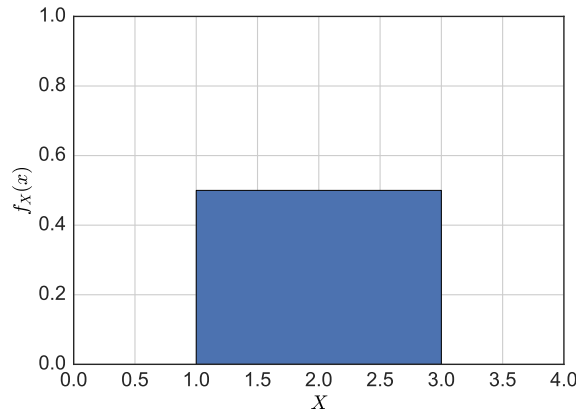


Figure 2.7. Probability density function for random variable $X \sim U(1, 3)$.

The mean and variance of a uniformly distributed random variable X are:

$$E[X] = \frac{b - a}{2}$$
$$Var(X) = \frac{(b - a)^2}{12}$$

2.4.2 Normal distribution

The *normal* or *Gaussian distribution* is the most important continuous probability distribution. This is true mainly because of the central limit theorem according to which the sum of independent identically distributed (iid) random variables follows the normal distribution. The probability density function of a normally distributed random variable is given by:

$$f_X(x) = \frac{1}{\sqrt{2\pi}\sigma} \exp\left(-\frac{(x - \mu)^2}{2\sigma^2}\right) \quad (2.19)$$

where μ is the mean value of X , σ the standard deviation and we write $X \sim N(\mu, \sigma^2)$. For the special case where $\mu = 0$ and $\sigma = 1$, the normal is called *standard normal*. The probability density function of the standard normal is illustrated in fig. 2.8.

2.4.3 Lognormal distribution

The last distribution presented in this chapter is the *lognormal distribution*. It represents a random variable, whose natural logarithm is normally distributed and is commonly

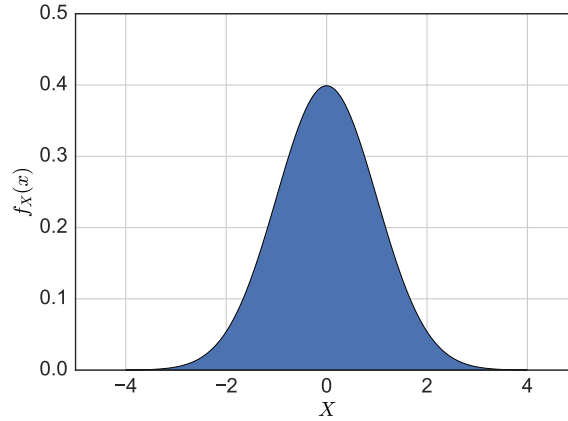


Figure 2.8. Probability density function for random variable $X \sim N(0, 1)$.

used because it takes strictly positive values. Given these, the probability density function of a lognormally distributed random variable X is given by:

$$f_X(x) = \frac{1}{\sqrt{2\pi}\sigma_{\ln X}} \exp\left(-\frac{(\ln x - \mu_{\ln X})^2}{2\sigma_{\ln X}^2}\right) \quad (2.20)$$

where $\mu_{\ln X}$ and $\sigma_{\ln X}^2$ are the mean and variance of the natural logarithm of X respectively. The mean and variance of X are given by the following relations:

$$\begin{aligned} \mu_X &= \exp\left(\mu_{\ln X} + \frac{1}{2}\sigma_{\ln X}^2\right) \\ \sigma_X^2 &= \mu_X^2 \left(\exp(\sigma_{\ln X}^2) - 1\right) \end{aligned} \quad (2.21)$$

Alternatively, it is possible to compute $\mu_{\ln X}$ and $\sigma_{\ln X}^2$ from the corresponding mean and variance μ_X and σ_X^2 by making use of the following relations:

$$\begin{aligned} \sigma_{\ln X}^2 &= \ln\left(1 + \frac{\sigma_X^2}{\mu_X^2}\right) \\ \mu_{\ln X} &= \ln(\mu_X) - \frac{1}{2}\sigma_{\ln X}^2 \end{aligned} \quad (2.22)$$

Figure 2.9 illustrates the probability density function of a lognormally distributed random variable.

2.5 Jointly distributed continuous random variables

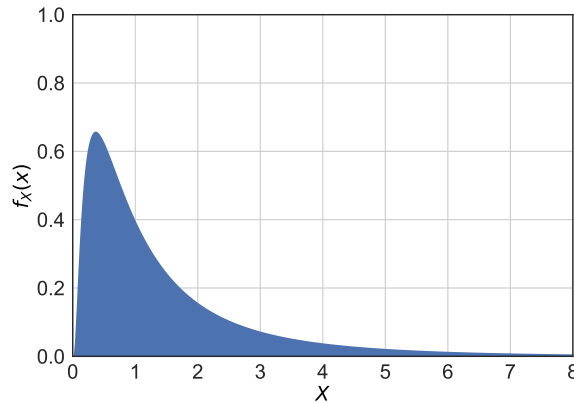


Figure 2.9. Probability density function for lognormal random variable X with $\mu_{\ln X} = 1$ and $\sigma_{\ln X} = 1$.

2.5 Jointly distributed continuous random variables

In many cases, we are interested in two or more continuous random variables belonging to the same sample space and the relations between them. Thus, the study of *jointly distributed random variables* is of utter importance and considered in this section.

2.5.1 Joint and marginal distributions

In analogy to the single random variable space, we are interested in the probability of two random variables X and Y acquiring particular values. Similar to the cumulative distribution function, in case of two or more random variables, the *joint cumulative distribution function* is defined as:

$$F_{XY}(x, y) = P[(X \leq x) \cap (Y \leq y)] \quad (2.23)$$

The joint probability density function is defined as:

$$f_{XY}(x, y) = \frac{\partial^2 F_{XY}}{\partial x \partial y}(x, y) \quad (2.24)$$

and satisfies:

$$\int_{-\infty}^{+\infty} \int_{-\infty}^{+\infty} f_{XY}(x, y) dx dy = 1 \quad (2.25)$$

Given the joint probability density function, we can calculate the so-called *marginal probability density functions* of X and Y , which correspond to the probability densities

of X, Y , treated as separate random variables:

$$f_X(x) = \int_{-\infty}^{+\infty} f_{XY}(x, y) dy \quad (2.26)$$

$$f_Y(y) = \int_{-\infty}^{+\infty} f_{XY}(x, y) dx \quad (2.27)$$

2.5.2 Covariance and correlation coefficient

The joint moment of two random variables X and Y is defined as $E[X^n \cdot Y^m]$ where the sum of n and m is called the total order of the moment. Particularly, the second moment of X, Y around their centroid is known as *covariance*, and is denoted as σ_{XY} . The covariance can be calculated by the following relation:

$$\sigma_{XY} = E[(X - \mu_X)(Y - \mu_Y)] = \int_{-\infty}^{+\infty} \int_{-\infty}^{+\infty} (x - \mu_x)(y - \mu_y) f_{XY}(x, y) dx dy \quad (2.28)$$

By expanding the product of eq. (2.28), an alternative more useful relation can also be derived:

$$\sigma_{XY} = E[XY] - \mu_X \mu_Y \quad (2.29)$$

If $\sigma_{XY} = 0$, the random variables X, Y are *uncorrelated*. Two independent random variables are uncorrelated, while the inverse is not always the case. In order to get a better notion of the degree of correlation of two random variables X, Y , the covariance can be normalized by the product of the standard deviations of X, Y , and the resulting ratio is known as the *correlation coefficient*:

$$\rho_{XY} = \frac{\sigma_{XY}}{\sigma_X \sigma_Y} \quad (2.30)$$

The correlation coefficient can be defined only if $\sigma_X \neq 0$ and $\sigma_Y \neq 0$; furthermore, the correlation coefficient satisfies $-1 \leq \rho_{XY} \leq +1$.

2.5.3 Independent random variables

Two random variables X, Y are independent if their joint probability density function equals the product of their corresponding marginal probability density functions i.e:

$$f_{XY}(x, y) = f_X(x) f_Y(y) \quad (2.31)$$

Independence of random variables can be generalized to more than two random variables. For example, if random variable X, Y and Z are independent, then eq. (2.31) can be

2.5 Jointly distributed continuous random variables

generalized as:

$$f_{XYZ}(x, y, z) = f_X(x)f_Y(y)f_Z(z) \quad (2.32)$$

Similarly to eqs. (2.31) and (2.32), the joint CDF of independent random variables equals the product of their marginal CDFs:

$$F_{XY}(x, y) = F_X(x)F_Y(y) \quad (2.33)$$

When two random variables X, Y are independent, some useful relations hold. First, the expectation of the product of X, Y equals the product of the expectations:

$$E[XY] = E[X]E[Y] \quad (2.34)$$

In addition, the variance of their sum equals to the sum of the variances:

$$\text{Var}(X + Y) = \text{Var}(X) + \text{Var}(Y) \quad (2.35)$$

To conclude, a special case of independent random variables is presented, namely the case of two independent normal random variables. In this particular case, the joint probability density function of X, Y is given by:

$$f_{XY}(x, y) = f_X(x)f_Y(y) = \frac{1}{2\pi\sigma_X\sigma_Y} \exp\left(-\frac{(x - \mu_X)^2}{2\sigma_X^2} - \frac{(y - \mu_Y)^2}{2\sigma_Y^2}\right) \quad (2.36)$$

where μ_X and μ_Y are the mean values of X, Y and σ_X, σ_Y are the standard deviations of X and Y respectively.

Chapter 3

Random processes and random fields

3.1 Basic definitions

Stochastic or *random processes* generate sequences of random variables. Generally speaking, the term stochastic process refers to the process itself or to the generated sequence. Let $Y(t)$ denote a stochastic process. The set of all possible values of the random variable Ω constitutes the *state space* of the process, while the set consisting of the values of index t is the *index set* of the process. In scientific literature, the term stochastic or random process is used whenever the index refers to some point in time, while the term *random field* is used when the index space consists of points in a spatial domain. It should be noted that in this dissertation the two terms are used interchangeably. For a thorough coverage of random processes and fields, the reader may refer to (Grigoriu, 2002; Papoulis and Pillai, 2002; Vanmarcke, 2010; Wirsching et al., 2006).

In particular, we are considering real scalar, continuous index random fields i.e. fields where the random variables are real numbers and the index is a point in space in either 1D, 2D or 3D. Samples of the random field are called *realizations* of the field and are assumed to be independent and identically distributed. Figure 3.1, for example, illustrates sample realizations of a random field in 1D space, while in fig. 3.2 realizations of a random field in 2D are presented. Finally, in fig. 3.3, realizations for a 3D random field are plotted in isocontour form. As for random fields of more than 3 spatial dimensions, they cannot be visualized for all spatial axes simultaneously.

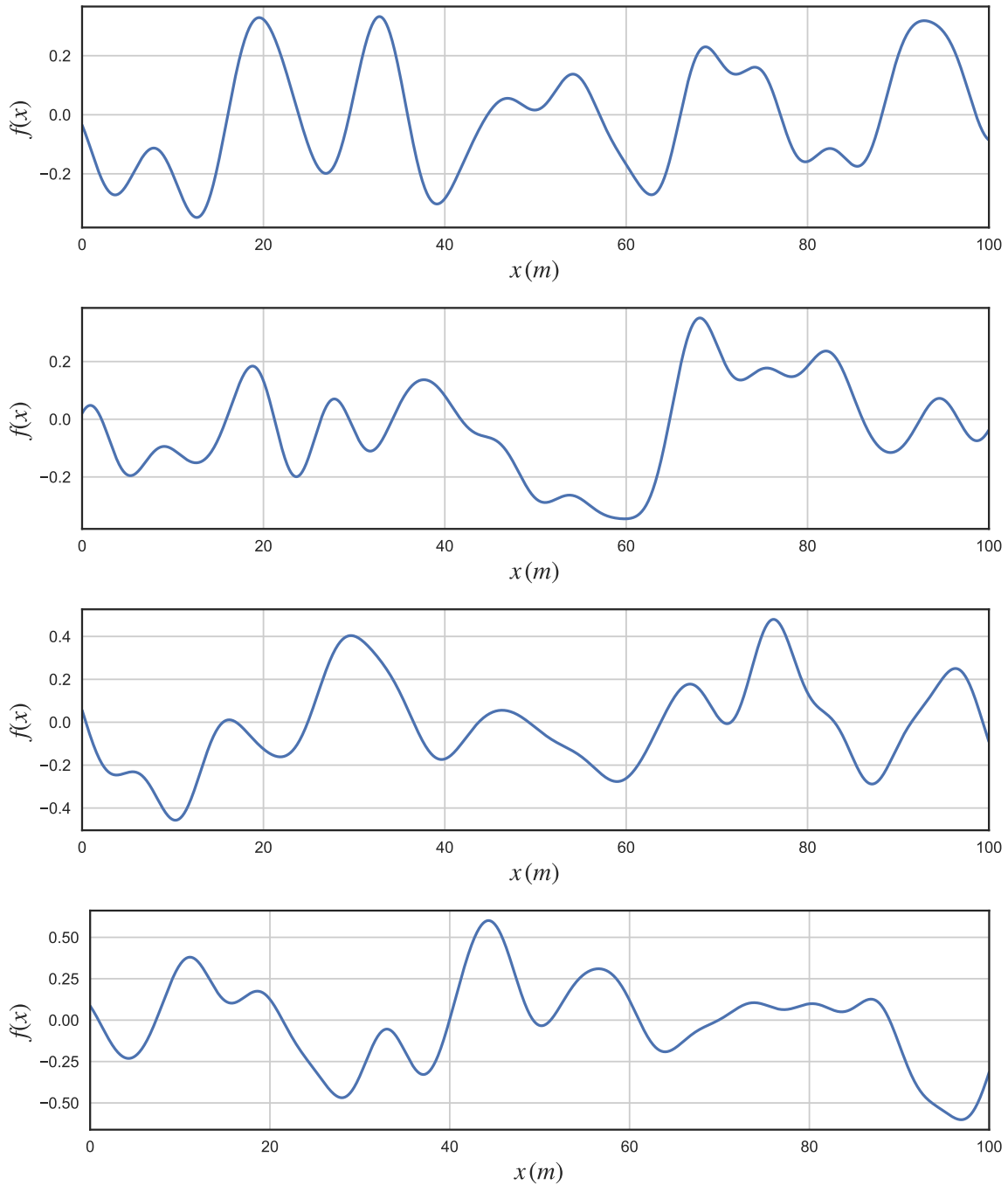


Figure 3.1. Sample realizations of 1D random fields.

3.1.1 Ensembles and ensemble averages

The set of all possible realizations of a random field is called the *ensemble*. Specifically, we use the symbol $Y(\mathbf{x})$ to refer to a random field Y with respect to spatial position \mathbf{x} . At each spatial point \mathbf{x} , the distribution of the corresponding random variable $f(\mathbf{x})$

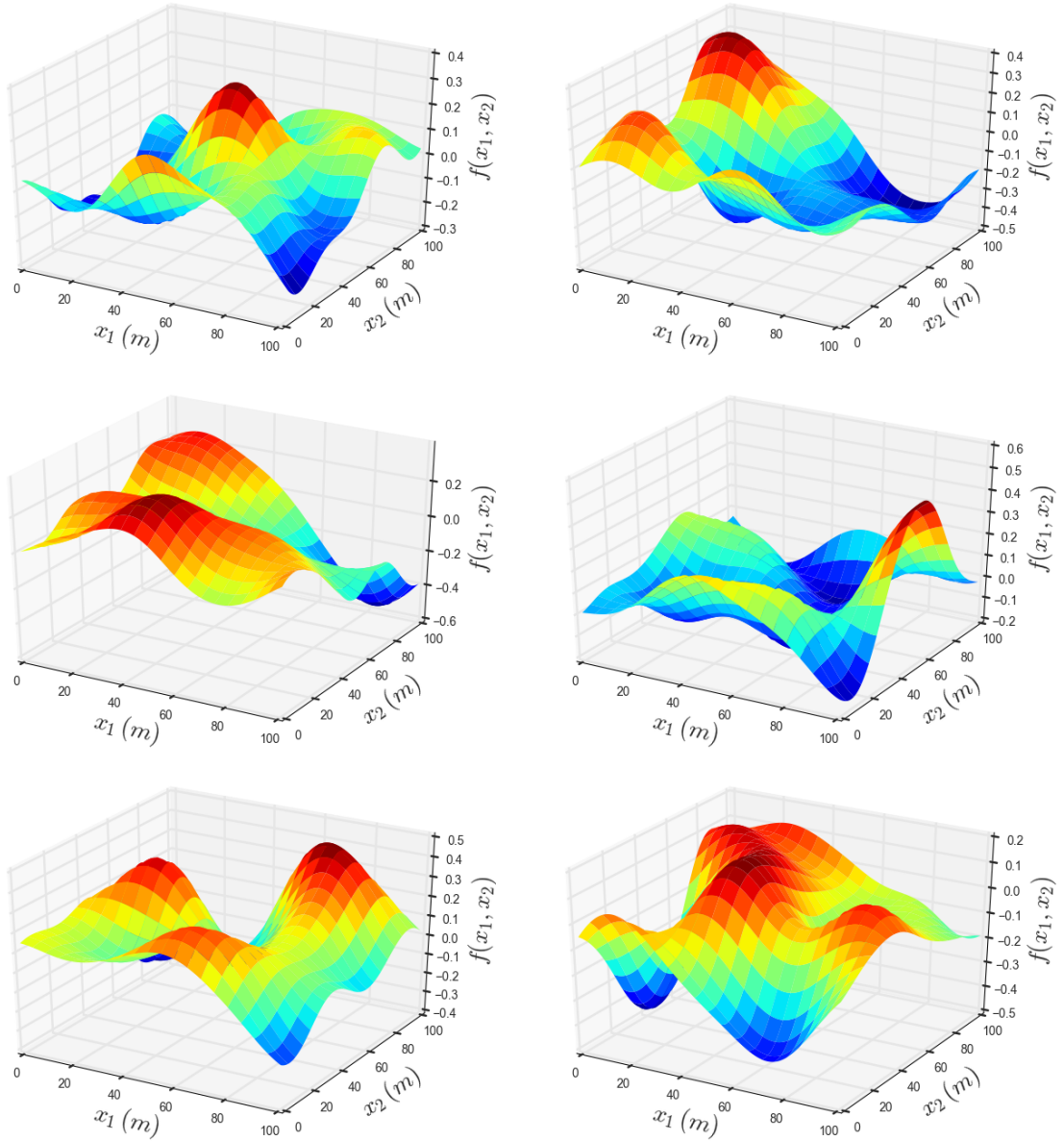


Figure 3.2. Sample realizations of 2D random fields.

is the marginal distribution of the process $f_{Y(\mathbf{x})}(y)$. Thus, for each point \mathbf{x} the mean and variance can be calculated using the following relations:

$$\mu_Y(\mathbf{x}) = E[Y(\mathbf{x})] = \int_{-\infty}^{+\infty} y f_{Y(\mathbf{x})}(y) dy \quad (3.1)$$

$$\sigma_{Y(\mathbf{x})}^2 = E[(Y(\mathbf{x}) - \mu_Y(\mathbf{x}))^2] = \int_{-\infty}^{+\infty} (y - \mu_Y(\mathbf{x}))^2 f_{Y(\mathbf{x})}(y) dy \quad (3.2)$$

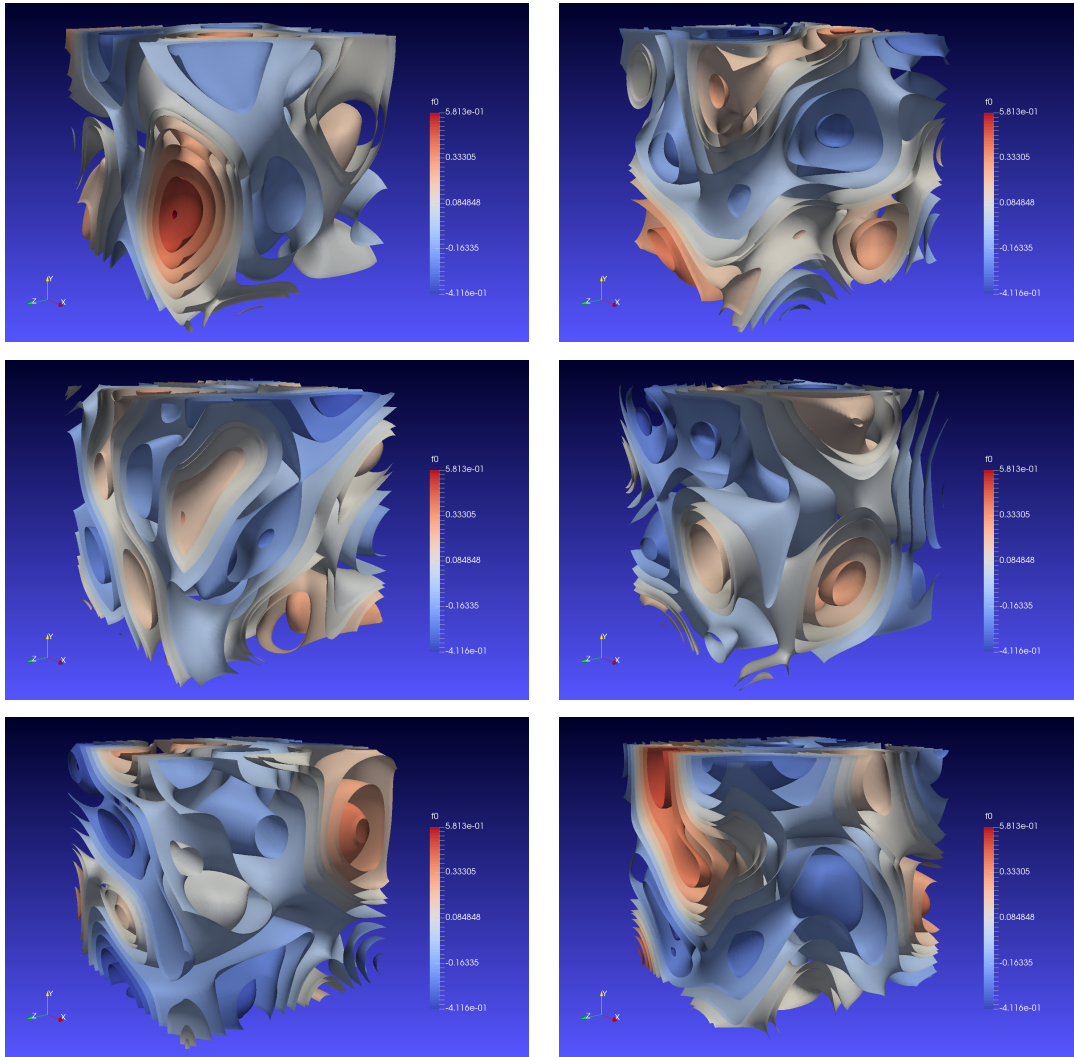


Figure 3.3. Sample realizations of 3D random fields.

The quantities calculated via eqs. (3.1) and (3.2) are called the ensemble average and ensemble variance.

3.1.2 Stationary random processes and homogeneous random fields

In general, the distribution describing a temporal stochastic process changes in time; this means that the mean, variance and autocorrelation function depend on time t . Random processes for which the probability distribution stays constant in time are called *stationary processes* (Yaglom and Silverman, 1973).

A random process is *strictly stationary* if its joint probability distribution stays constant through time. In practice, this requirement is not easy to prove and a relaxed stationarity condition is used. A stochastic process is called *stationary in the wide sense* (or *stationary in Khinchin's sense*) if its mean is constant and the correlation function depends only on the relative time distance of two different time points. Thus, the correlation function between two time points t_1 and t_2 depends only on $\tau = t_1 - t_2$, which is called the *time lag*.

When considering random processes or fields in space, the term *homogeneous* is used to characterize a random process or field for which the probability distribution is constant in space. In this case, the autocorrelation function between two spatial points, with coordinate vectors \mathbf{x} and \mathbf{y} , depends only on the vectorial difference $\boldsymbol{\tau} = \mathbf{x} - \mathbf{y}$ which is called the *lag vector*. Alternatively, the term *separation distance* is used to denote the lag vector $\boldsymbol{\tau}$.

An additional property closely related to homogeneity of random fields of two and more spatial dimensions is *isotropy*. A random field is isotropic if its joint pdf is invariant under rotations. Isotropy implies statistical homogeneity, while the inverse is not always true. The correlation between two spatial points of an isotropic random field, therefore depends only on their separation distance and not on the orientation relative to one another.

3.1.3 Ergodic random processes and fields

Let $X(t)$ be a temporal random process and $X_m(t)$ a sample realization of it. $X(t)$ is called *ergodic in the mean* if the temporal mean of any realization $X_m(t)$ is equal to the ensemble average $\mu_X(t)$. It is clear that for a process to be ergodic, it must be stationary, although the inverse doesn't always hold. Similarly, we can define ergodicity in the variance, the autocorrelation function, as well as higher order moments. The process is called *strongly ergodic*, if all the corresponding temporal averages are equal to the corresponding ensemble quantities. It's called *weakly ergodic*, if it is ergodic in the mean, variance and autocorrelation function.

For random fields $f(\mathbf{x})$ where the index \mathbf{x} is a point in a spatial domain ergodicity in the mean refers to the case when the spatial average of a realization of f equals to the ensemble average. Ergodicity can be defined in the variance, autocorrelation equivalently to the random process case.

3.1.4 Random processes and fields in the frequency domain

In this subsection, an alternative description of the second order characteristics of a statistically homogeneous random field, namely its *spectral representation*, is presented. The autocorrelation function can be represented equivalently in the frequency domain in the form of the *spectral density function*. To begin the derivation of the spectral density function, we define the Fourier transform pair $g(x)$ and $G(\kappa)$ as:

$$G(\kappa) = \frac{1}{2\pi} \int_{-\infty}^{+\infty} g(x) e^{-i\kappa x} dx \quad (3.3)$$

$$g(x) = \int_{-\infty}^{+\infty} G(\kappa) e^{i\kappa x} d\kappa \quad (3.4)$$

where the function $G(\kappa)$ is called the Fourier transform of function $g(x)$. Equation (3.3) is the *forward Fourier transform* and eq. (3.4) the *inverse Fourier transform*.

3.1.4.1 Wiener-Khinchine relations

We now present the Wiener-Khinchine relations for homogeneous random fields in 1d defined as:

$$S_X(\kappa) = \frac{1}{2\pi} \int_{-\infty}^{+\infty} R_X(\tau) e^{-i\kappa\tau} d\tau \quad (3.5)$$

$$R_X(\tau) = \int_{-\infty}^{+\infty} S_X(\kappa) e^{i\kappa\tau} d\kappa \quad (3.6)$$

where $S_X(\kappa)$ is the *spectral density function*, κ the *wave number* and $R_X(\tau)$ is the autocorrelation function defined in terms of the separation distance τ .

For homogenous real valued random fields, the spectral density function is real and symmetric; eqs. (3.5) and (3.6) can thus be used without including the imaginary i as:

$$S_X(\kappa) = \frac{1}{2\pi} \int_{-\infty}^{+\infty} R_X(\tau) \cos(\kappa\tau) d\tau \quad (3.7)$$

$$R_X(\tau) = \int_{-\infty}^{+\infty} S_X(\kappa) \cos(\kappa\tau) d\kappa \quad (3.8)$$

The Wiener-Khinchine relations can be written for 2D random fields as:

$$S_X(\kappa_1, \kappa_2) = \frac{1}{4\pi^2} \int_{-\infty}^{+\infty} \int_{-\infty}^{+\infty} R_X(\tau_1, \tau_2) \cos(\kappa_1\tau_1 + \kappa_2\tau_2) d\tau_1 d\tau_2 \quad (3.9)$$

$$R_X(\tau_1, \tau_2) = \int_{-\infty}^{+\infty} \int_{-\infty}^{+\infty} S_X(\kappa_1, \kappa_2) \cos(\kappa_1\tau_1 + \kappa_2\tau_2) d\kappa_1 d\kappa_2 \quad (3.10)$$

3.2 Simulation of Gaussian random fields by the spectral representation method

Finally, for 3d random fields the Wiener-Khichine relations are the following:

$$S_X(\kappa_1, \kappa_2, \kappa_3) = \frac{1}{8\pi^3} \int_{-\infty}^{+\infty} \int_{-\infty}^{+\infty} \int_{-\infty}^{+\infty} R_X(\tau_1, \tau_2, \tau_3) \cos(\kappa_1\tau_1 + \kappa_2\tau_2 + \kappa_3\tau_3) d\tau_1 d\tau_2 d\tau_3 \quad (3.11)$$

$$R_X(\tau_1, \tau_2, \tau_3) = \int_{-\infty}^{+\infty} \int_{-\infty}^{+\infty} \int_{-\infty}^{+\infty} S_X(\kappa_1, \kappa_2, \kappa_3) \cos(\kappa_1\tau_1 + \kappa_2\tau_2 + \kappa_3\tau_3) d\kappa_1 d\kappa_2 d\kappa_3 \quad (3.12)$$

3.2 Simulation of Gaussian random fields by the spectral representation method

In this section, the spectral representation method is introduced for simulating Gaussian random fields in one, two and three spatial dimensions (Giovanis and Papadopoulos, 2015; Shinozuka and Deodatis, 1996; Stefanou and Papadrakakis, 2007). It should be noted that the advantage of the spectral representation method lies on its general applicability, as well as the implementation simplicity. According to the spectral representation method, the stochastic field $f(\mathbf{x})$ is expanded as a sum of trigonometric functions with random phase angles and amplitudes. In this work, the version which uses random phase angles and deterministic amplitudes is adopted, as it leads to sample functions which are ergodic in the mean value and autocorrelation.

3.2.1 Spectral representation method for simulation of 1D fields

The simulation formula for a truncated after N_1 terms one-dimensional homogeneous random field $\hat{f}(\mathbf{x}_1)$ is the following:

$$\hat{f}(\mathbf{x}_1) = \sqrt{2} \sum_{i=1}^{N_1} A_i \cos(\kappa_{1i}\mathbf{x}_1 + \phi_i) \quad (3.13)$$

where $\phi_i (i = 1, \dots, N_1)$ are independent random phase angles uniformly distributed in the range $[0, 2\pi]$. The frequencies κ_{1i} correspond to the first spatial axis and are given by:

$$\kappa_{1i} = i\Delta\kappa_1 = i \frac{\kappa_{1u}}{N_1} \quad \text{for } i = 1, \dots, N_1 \quad (3.14)$$

Random processes and random fields

where κ_{1u} is the upper cut-off wave number. The deterministic coefficients A_i are defined as follows:

$$A_0 = 0 \quad A_i = \sqrt{2S_{f_0}(\kappa_{1i})\Delta\kappa_1} \quad \text{for } i = 1, \dots, N_1 \quad (3.15)$$

where S_{f_0} is the power spectral density function, which is a real non-negative function of the wave number κ_{1i} . The coefficient A_0 is chosen zero in order to ensure that the mean value averaged over the whole simulation domain $T_0 = 2\pi/\Delta\kappa_1$ of the generated random field $\hat{f}(\mathbf{x}_1)$ remains zero. Due to the central limit theorem, the simulated random field is asymptotically Gaussian as $N_1 \rightarrow \infty$; the mean value and the autocorrelation function of the simulated field are identical to the corresponding targets as $N_1 \rightarrow \infty$; in addition $\hat{f}(\mathbf{x}_1)$, is periodic with period T_0 .

An additional constraint must be applied to the space increment Δx_1 , when generating sample function of the simulated stochastic field according to eq. (3.13):

$$\Delta x_1 \leq \frac{2\pi}{2\kappa_{1u}} \quad (3.16)$$

The condition of eq. (3.16) is necessary in order to avoid aliasing according to the sampling theorem.

An application of the spectral representation method for 1D Gaussian random fields is presented below. The power spectral density function used is of the following type:

$$S_{f_0}(\kappa) = \frac{\sigma_f^2 b^3 \kappa^2 e^{-b|\kappa|}}{4} \quad (3.17)$$

where σ_f is the standard deviation, b a correlation length parameter and κ the wave number. Figure 3.4 illustrates the spectral density function for $\sigma_f = 0.2$ and correlation length parameters $b = 1.0 m$ and $b = 5.0 m$.

The spectral representation method is applied in order to generate random field realizations with underlying spectral density function given by eq. (3.17). The standard deviation is chosen as $\sigma_f = 0.2$; the spatial domain has a total length of $10.0 m$ and is subdivided in 1000 intervals so that $\Delta x = 0.01 m$. Two different values of the correlation length parameter b are chosen in order to illustrate its effect on the generated fields:

- (a) For $b = 1.0 m$, the upper cut-off wave number is chosen $\kappa_u = 12.0 rad/m$. The wave number axis is subdivided to 100 intervals so that, according to eq. (3.14), $N_1 = 100$ and $\Delta\kappa_1 = 0.12 rad/m$. Note that the values of the parameters chosen ensure that the condition of eq. (3.16) is satisfied. while sample realizations of the random field $f(x)$ for $b = 1.0 m$ are illustrated in fig. 3.5,

3.2 Simulation of Gaussian random fields by the spectral representation method

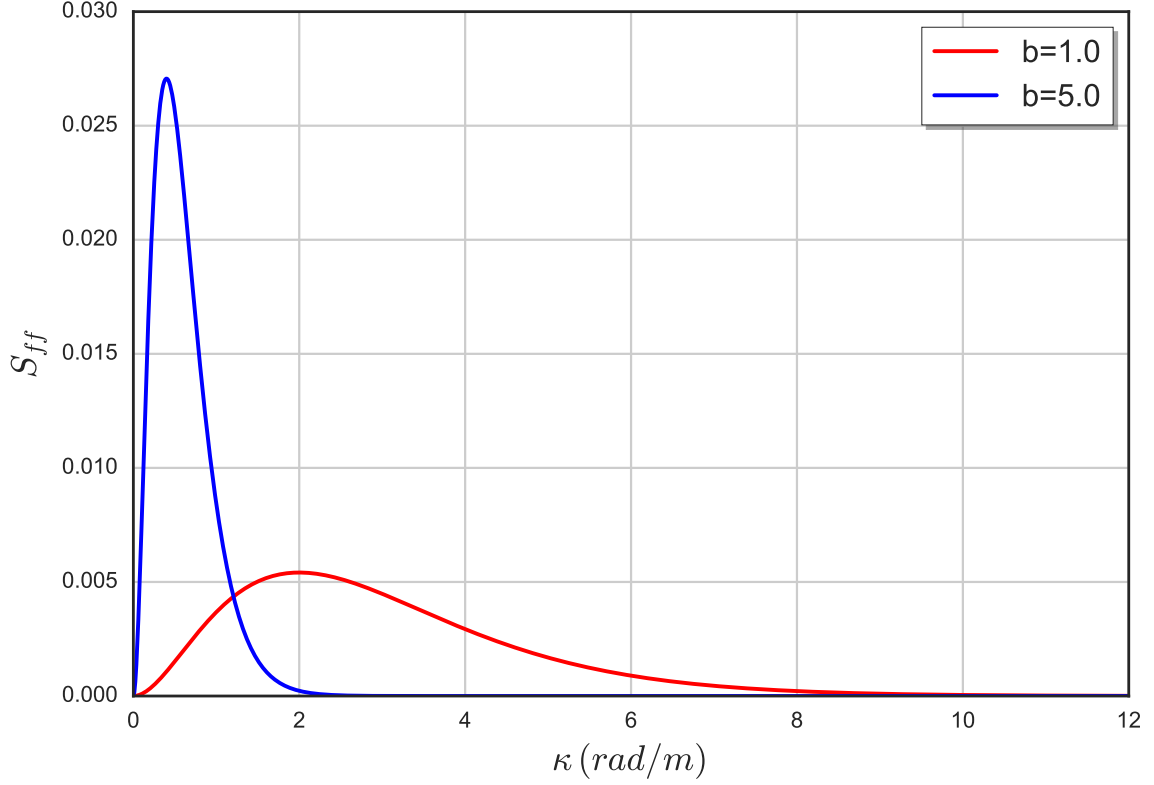


Figure 3.4. Plot of S_{f_0} with respect to wave number κ

- (b) For $b = 5.0 m$, the upper cut-off wave number is chosen as $\kappa_u = 2.5 rad/m$, the wave number axis is again subdivided to 100 intervals so that, according to eq. (3.14), $N_1 = 100$ and $\Delta\kappa_1 = 0.025 rad/m$. The selection of the above parameters therefore satisfies eq. (3.16), while sample realizations of the random field $f(x)$ for $b = 5.0 m$ are illustrated in fig. 3.6

3.2.2 Spectral representation method for simulation of 2D fields

The corresponding spectral representation formula for 2D homogeneous Gaussian random fields $\hat{f}(\mathbf{x}_1, \mathbf{x}_2)$ is the following:

Random processes and random fields

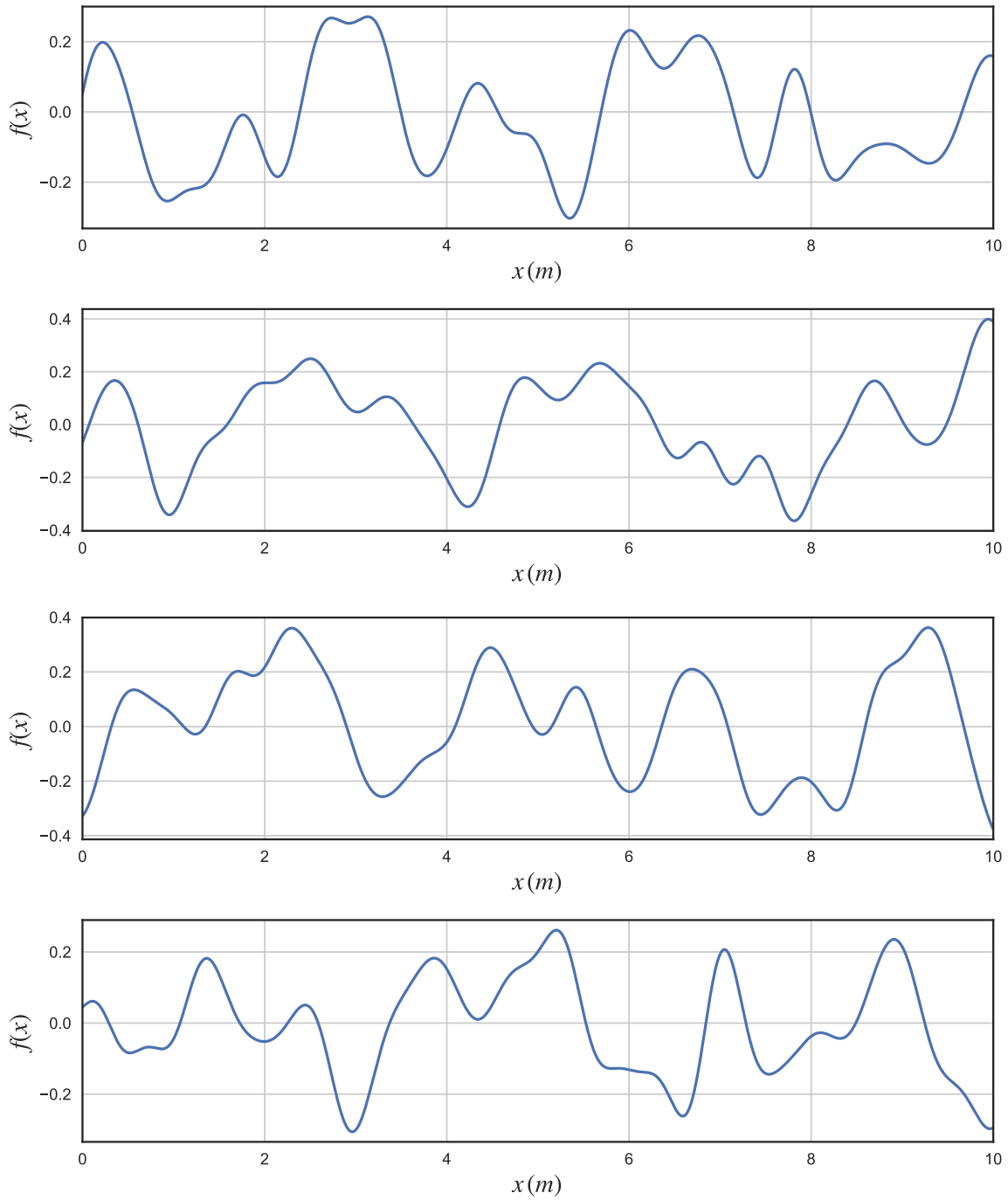


Figure 3.5. Sample realizations of a 1D random field with $\sigma_f = 0.2$ and $b = 1.0 m$.

$$\begin{aligned}
 \hat{f}(\mathbf{x}_1, \mathbf{x}_2) = \sqrt{2} \sum_{i=1}^{N_1} \sum_{j=1}^{N_2} & \left[A_{ij}^{(1)} \cos(\kappa_{1i} \mathbf{x}_1 + \kappa_{2j} \mathbf{x}_2 + \phi_{ij}^{(1)}) \right. \\
 & \left. + A_{ij}^{(2)} \cos(\kappa_{1i} \mathbf{x}_1 - \kappa_{2j} \mathbf{x}_2 + \phi_{ij}^{(2)}) \right] \quad (3.18)
 \end{aligned}$$

3.2 Simulation of Gaussian random fields by the spectral representation method

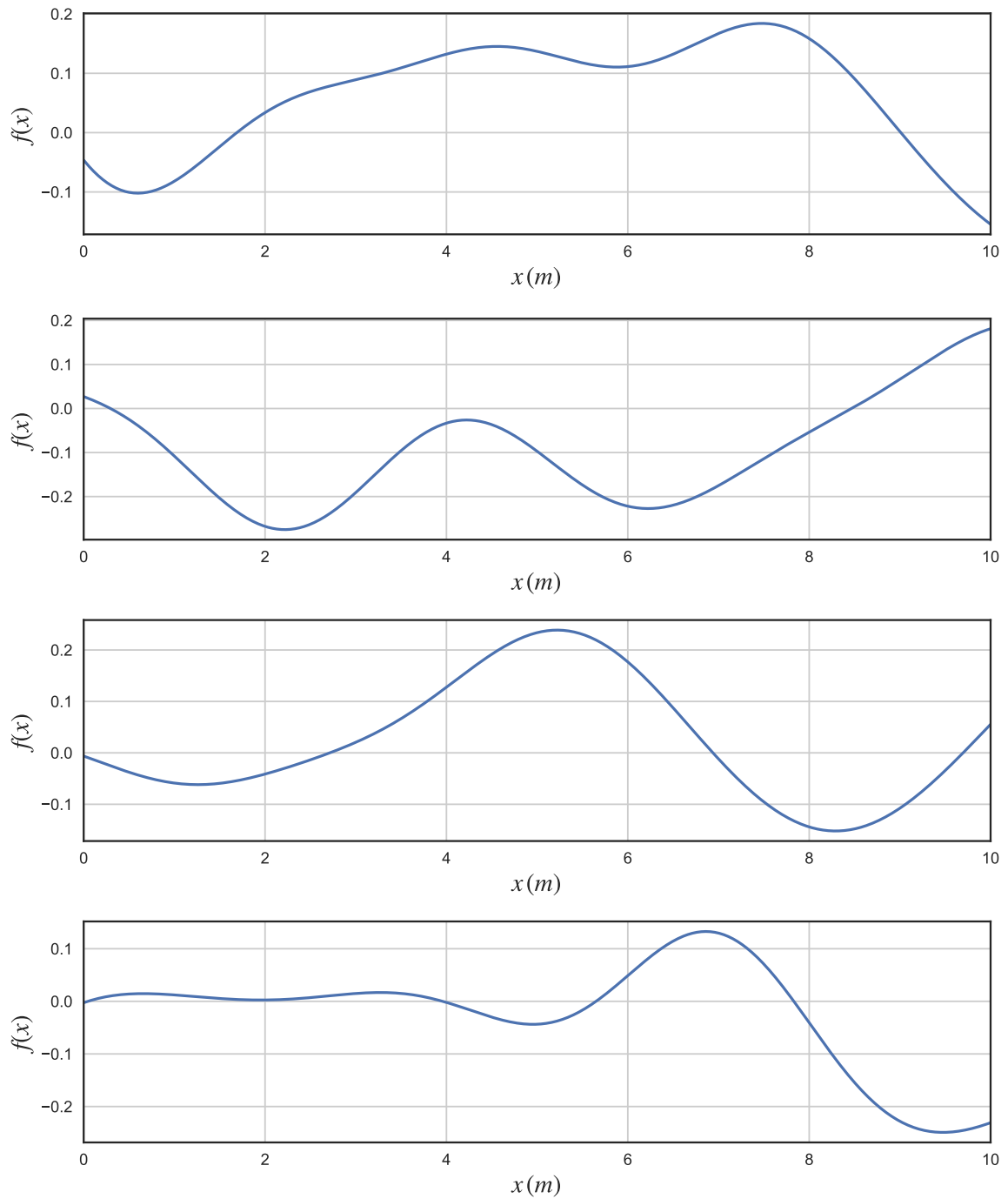


Figure 3.6. Sample realizations of a 1D random field with $\sigma_f = 0.2$ and $b = 5.0 m$.

where the sums are truncated to N_1 and N_2 for the first and second wave number axes respectively. The wave numbers are given by:

Random processes and random fields

$$\kappa_{1i} = i\Delta\kappa_1 \quad \text{and} \quad \Delta\kappa_1 = \frac{\kappa_{1u}}{N_1} \quad (3.19)$$

$$\kappa_{2j} = j\Delta\kappa_2 \quad \text{and} \quad \Delta\kappa_2 = \frac{\kappa_{2u}}{N_2} \quad (3.20)$$

In eqs. (3.19) and (3.20), κ_{1u} and κ_{2u} indicate the upper cut-off wave numbers for axis 1 and axis 2 respectively, while in eq. (3.18), $\phi^{(1)}$, $\phi^{(2)}$ are two sets of independent random uniformly distributed phase angles in the range $[0, 2\pi]$. Finally, the deterministic amplitudes are given by:

$$A_{ij}^{(1)} = \sqrt{2S_{f_0f_0}(\kappa_{1i}, \kappa_{2j})\Delta\kappa_1\Delta\kappa_2} \quad (3.21)$$

$$A_{ij}^{(2)} = \sqrt{2S_{f_0f_0}(\kappa_{1i}, -\kappa_{2j})\Delta\kappa_1\Delta\kappa_2} \quad (3.22)$$

where $S_{f_0f_0}$ is the 2D power spectral density function and $\Delta\kappa_1$, $\Delta\kappa_2$ are the increments of the wave number axes given by eqs. (3.19) and (3.20). The simulated random fields are periodic with respect to the two spatial axes and the corresponding periods are $T_{01} = 2\pi/\Delta\kappa_1$ and $T_{02} = 2\pi/\Delta\kappa_2$. In order to avoid aliasing, the space increments along the x_1 and x_2 must obey:

$$\Delta x_1 \leq \frac{2\pi}{2\kappa_{1u}} \quad , \quad \Delta x_2 \leq \frac{2\pi}{2\kappa_{2u}} \quad (3.23)$$

The 2D version of the spectral representation method is applied in order to generate random field realizations with an underlying spectral density function of exponential type given by eq. (3.24). The standard deviation is chosen as $\sigma_f = 0.2$. The 2D spatial domain has lengths of $L_1 = L_2 = 10.0 m$ on axes 1, 2 respectively and is subdivided in 200 intervals so that $\Delta x_1 = \Delta x_2 = 0.05 m$. Various combinations of the correlation length parameters b_1 , b_2 are chosen in order to illustrate their effect on the generated fields:

- (a) For $b_1 = b_2 = 1.0 m$, the upper cut-off wave number is chosen $\kappa_{u_1} = \kappa_{u_2} = 5.0 rad/m$; the wave number axis is subdivided to 500 intervals so that, according to eq. (3.20), $N_1 = N_2 = 500$ and $\Delta\kappa_1 = \Delta\kappa_2 = 0.01 rad/m$. The values of the parameters chosen ensure that the condition of eq. (3.23) is satisfied. Sample realizations of the random field $f(x)$ for $b_1 = b_2 = 1.0 m$ are illustrated in fig. 3.8.
- (b) For $b_1 = b_2 = 5.0 m$, the upper cut-off wave number is chosen as $\kappa_{u_1} = \kappa_{u_2} = 1.0 rad/m$. The wave number axis is again subdivided to 500 intervals so that, according to eq. (3.20), $N_1 = N_2 = 500$ and $\Delta\kappa_1 = 0.002 rad/m$. The selection

3.2 Simulation of Gaussian random fields by the spectral representation method

of the aforementioned parameters satisfies eq. (3.23). Sample realizations of the random field $f(x_1, x_2)$ for $b_1 = b_2 = 5.0 m$ are illustrated in fig. 3.9.

- (c) Furthermore, realizations of the 2D random field for $b_1 = 1.0 m$ and $b_2 = 5.0 m$ are illustrated in fig. 3.10 where the effect of the correlation length parameter on each axis is demonstrated.

$$S_{ff}(\kappa_1, \kappa_2) = \frac{\sigma_{ff}^2 b_1 b_2}{4\pi} \exp\left(-\left(\frac{b_1 \kappa_1}{2}\right)^2 - \left(\frac{b_2 \kappa_2}{2}\right)^2\right) \quad (3.24)$$

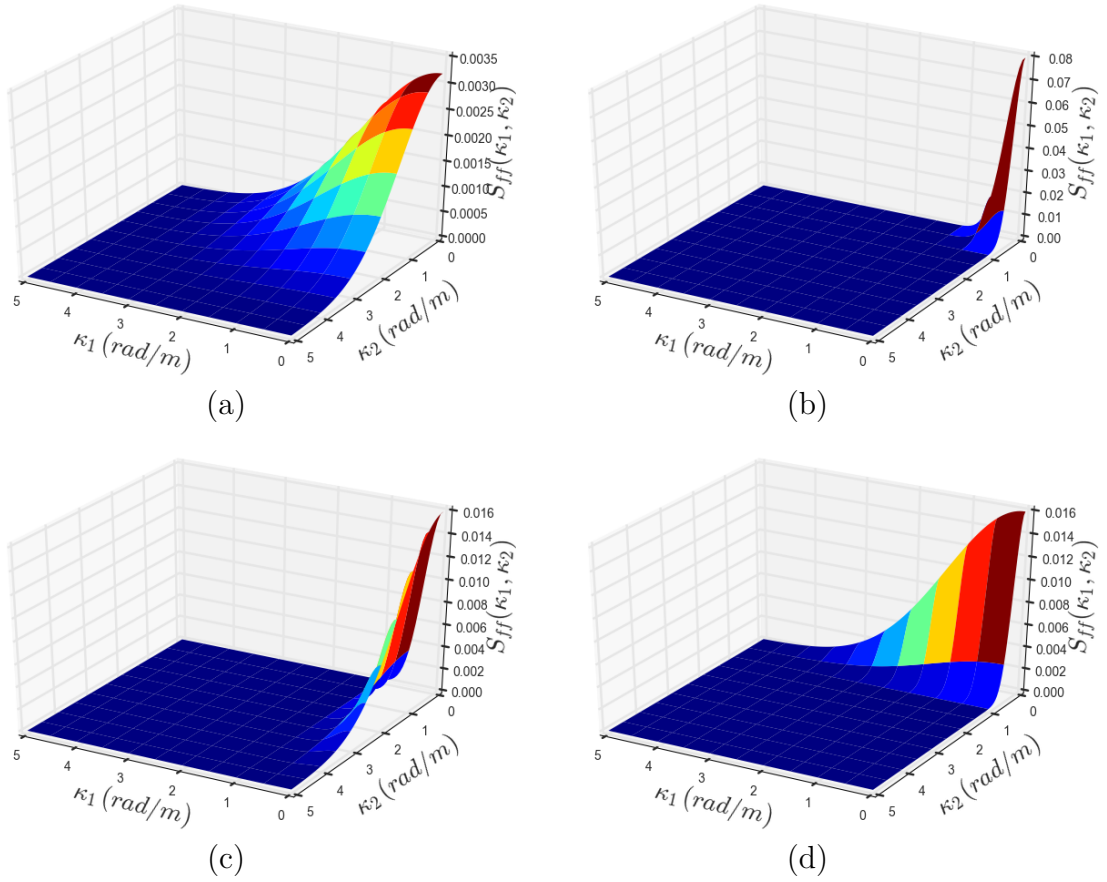


Figure 3.7. Spectral density function in 2D for various correlation length parameters: (a) $b_1 = b_2 = 1.0 m$, (b) $b_1 = b_2 = 5.0 m$, (c) $b_1 = 1.0 m$, $b_2 = 5.0 m$ and (d) $b_1 = 5.0 m$, $b_2 = 1.0 m$.

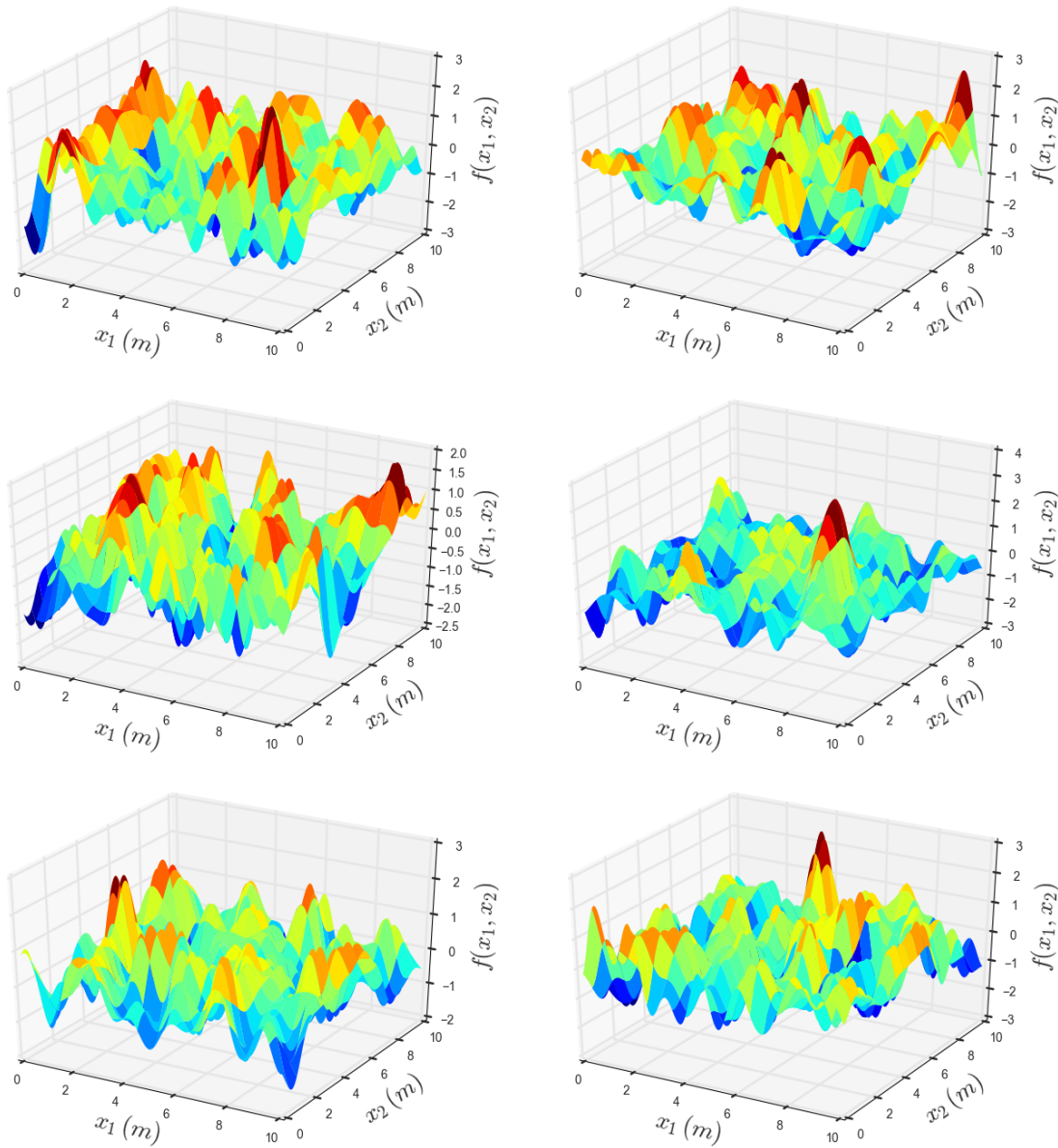


Figure 3.8. Sample realizations of a 2D random field for $b_1 = b_2 = 1.0$ m.

3.2.3 Spectral representation method for simulation of 3D fields

Although applications in this dissertation do not include 3D random fields, the spectral representation method for simulation of 3D homogeneous Gaussian random fields is presented. Due to the inherent difficulty in visualizing random fields in 3D, only the basic simulation methodology is outlined. The spectral representation formula for 3D

3.2 Simulation of Gaussian random fields by the spectral representation method

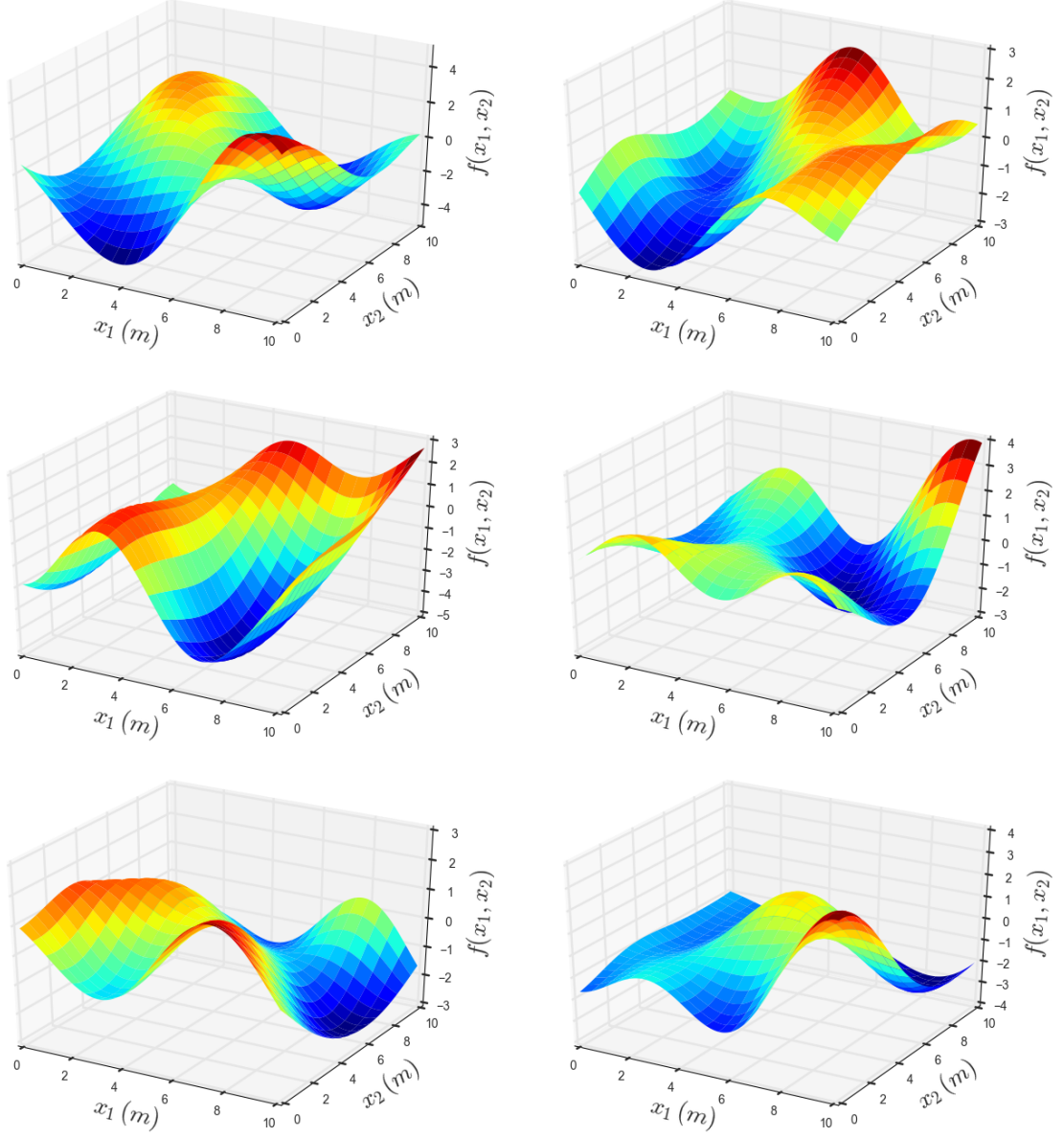


Figure 3.9. Sample realizations of a 2D random field for $b_1 = b_2 = 5.0 m$.

homogeneous Gaussian random fields $\hat{f}(\mathbf{x}_1, \mathbf{x}_2, \mathbf{x}_3)$ is the following:

$$\begin{aligned}
 \hat{f}(\mathbf{x}_1, \mathbf{x}_2, \mathbf{x}_3) = & \sqrt{2} \sum_{i=1}^{N_1} \sum_{j=1}^{N_2} \sum_{k=1}^{N_3} \left[A_{ijk}^{(1)} \cos(\kappa_{1i}\mathbf{x}_1 + \kappa_{2j}\mathbf{x}_2 + \kappa_{3k}\mathbf{x}_3 + \phi_{ijk}^{(1)}) \right. \\
 & + A_{ijk}^{(2)} \cos(\kappa_{1i}\mathbf{x}_1 + \kappa_{2j}\mathbf{x}_2 - \kappa_{3k}\mathbf{x}_3 + \phi_{ijk}^{(2)}) \\
 & + A_{ijk}^{(3)} \cos(\kappa_{1i}\mathbf{x}_1 - \kappa_{2j}\mathbf{x}_2 + \kappa_{3k}\mathbf{x}_3 + \phi_{ijk}^{(3)}) \\
 & \left. + A_{ijk}^{(4)} \cos(\kappa_{1i}\mathbf{x}_1 - \kappa_{2j}\mathbf{x}_2 - \kappa_{3k}\mathbf{x}_3 + \phi_{ijk}^{(4)}) \right]
 \end{aligned} \tag{3.25}$$

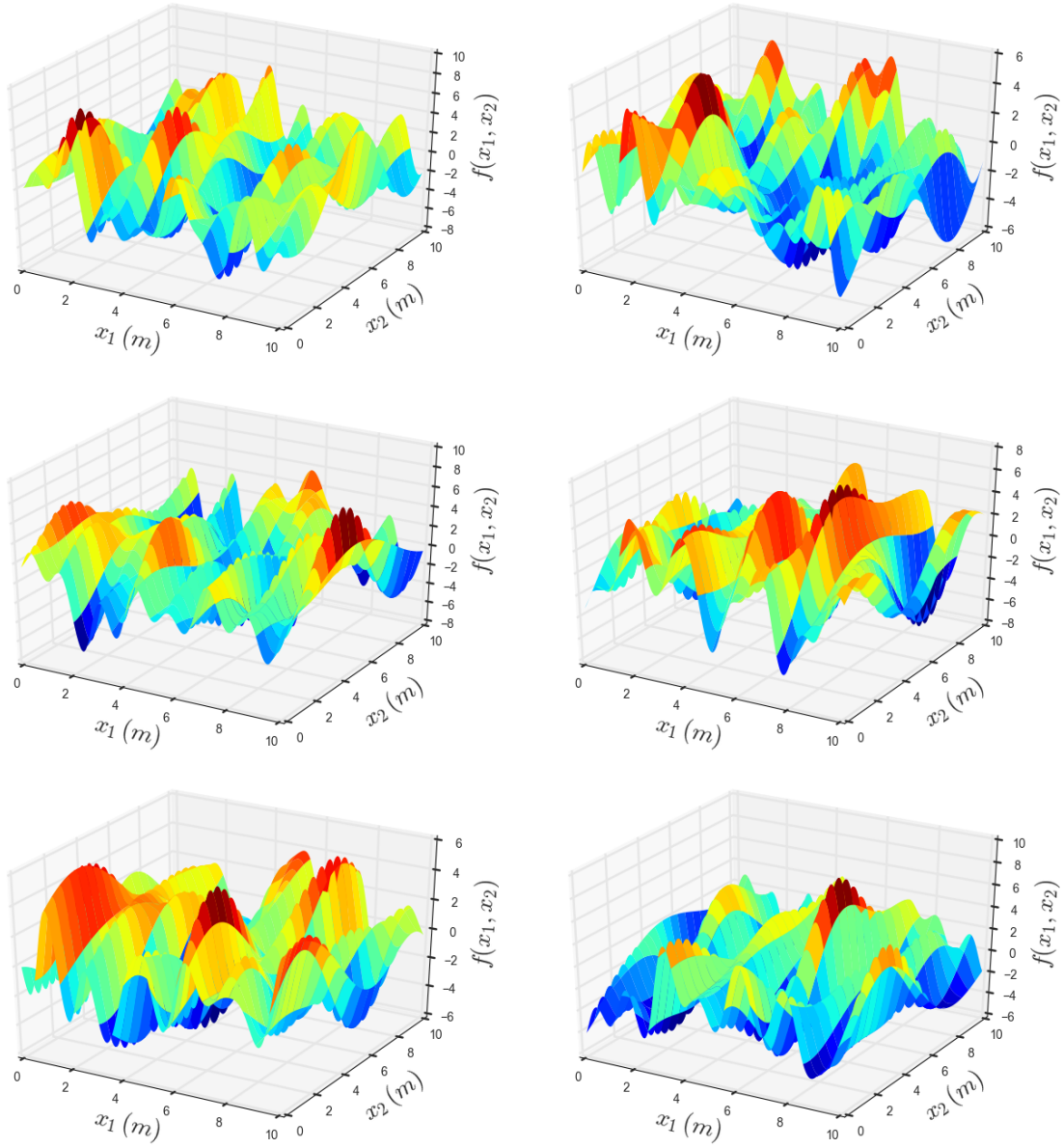


Figure 3.10. Sample realizations of a 2D random field for $b_1 = 1.0\text{ m}$ and $b_2 = 5.0\text{ m}$.

where the sums are truncated to N_1 , N_2 and N_3 for the first, second and third wave number axes respectively. The corresponding wave numbers are given by:

$$\kappa_{1i} = i\Delta\kappa_1 \quad \text{and} \quad \Delta\kappa_1 = \frac{\kappa_{1u}}{N_1} \quad (3.26)$$

$$\kappa_{2j} = j\Delta\kappa_2 \quad \text{and} \quad \Delta\kappa_2 = \frac{\kappa_{2u}}{N_2} \quad (3.27)$$

$$\kappa_{3k} = k\Delta\kappa_3 \quad \text{and} \quad \Delta\kappa_3 = \frac{\kappa_{3u}}{N_3} \quad (3.28)$$

3.3 Non-Gaussian random processes and fields

In eqs. (3.26) to (3.28), κ_{1u} , κ_{2u} and κ_{3u} indicate the upper cut-off wave numbers for axis 1, axis 2 and axis 3 respectively, while in eq. (3.25), $\phi^{(1)}$, $\phi^{(2)}$, $\phi^{(3)}$ and $\phi^{(4)}$, represent four sets of independent random uniformly distributed phase angles in the range $[0, 2\pi]$. Finally, the deterministic amplitudes are given by:

$$A_{ijk}^{(1)} = \sqrt{2S_{f_0f_0f_0}(\kappa_{1i}, \kappa_{2j}, \kappa_{3k})\Delta\kappa_1\Delta\kappa_2\Delta\kappa_3} \quad (3.29)$$

$$A_{ijk}^{(2)} = \sqrt{2S_{f_0f_0f_0}(\kappa_{1i}, \kappa_{2j}, -\kappa_{3k})\Delta\kappa_1\Delta\kappa_2\Delta\kappa_3} \quad (3.30)$$

$$A_{ijk}^{(3)} = \sqrt{2S_{f_0f_0f_0}(\kappa_{1i}, -\kappa_{2j}, \kappa_{3k})\Delta\kappa_1\Delta\kappa_2\Delta\kappa_3} \quad (3.31)$$

$$A_{ijk}^{(4)} = \sqrt{2S_{f_0f_0f_0}(\kappa_{1i}, -\kappa_{2j}, -\kappa_{3k})\Delta\kappa_1\Delta\kappa_2\Delta\kappa_3} \quad (3.32)$$

where $S_{f_0f_0f_0}$ indicates the 3D power spectral density function and $\Delta\kappa_1$, $\Delta\kappa_2$, $\Delta\kappa_3$ the increments of the wave number axes given by eqs. (3.26) to (3.28). The simulated random fields are periodic with respect to the three spatial axes with corresponding periods $T_{01} = 2\pi/\Delta\kappa_1$, $T_{02} = 2\pi/\Delta\kappa_2$ and $T_{03} = 2\pi/\Delta\kappa_3$. In order to avoid aliasing, the space increments along x_1 , x_2 and x_3 must obey:

$$\Delta x_1 \leq \frac{2\pi}{2\kappa_{1u}}, \quad \Delta x_2 \leq \frac{2\pi}{2\kappa_{2u}}, \quad , \quad \Delta x_3 \leq \frac{2\pi}{2\kappa_{3u}} \quad (3.33)$$

3.3 Non-Gaussian random processes and fields

In general, most material properties represented as random processes or fields are non-Gaussian in nature. Therefore, the study of non-Gaussian stochastic processes and fields is essential in order to correctly simulate the spatial variability of material properties of interest (Grigoriu, 1995). In this section, a special class of processes (and fields), namely translation processes (and fields), are presented, which offer a simple methodology for deriving non-Gaussian processes (and fields) from Gaussian ones.

3.3.1 Memoryless transformations

Let $\mathbf{Y}(t)$ represent a m -dimensional Gaussian vector process and let \mathbf{g} be a measurable mapping from \mathbb{R}^m to \mathbb{R}^n . The n -dimensional process $\mathbf{X}(t)$ resulting from the following transformation:

$$\mathbf{X}(t) = \mathbf{g}(\mathbf{Y}(t)) \quad (3.34)$$

is Gaussian only if \mathbf{g} is a linear function. The mapping defined in eq. (3.34) is called a *memoryless transformation* since $\mathbf{X}(t)$ depends only on the values of $\mathbf{Y}(t)$ at the time instant t . Through the memoryless transformation, the process $\mathbf{X}(t)$ is then defined

Random processes and random fields

from the mean and covariance functions of $\mathbf{Y}(t)$. In addition, if $\mathbf{Y}(t)$ is stationary, the resulting process $\mathbf{X}(t)$ is also stationary in the strict sense.

3.3.1.1 Translation processes and fields

In this subsection, we consider the case where $m = n = 1$, i.e. $X(t)$ and $Y(t)$ are univariate real valued stochastic processes. Let g be a monotonic function and $Y(t)$ a zero-mean stationary Gaussian stochastic process with unit variance and correlation function $\rho(\tau) = E[Y(t + \tau)Y(t)]$. Then the process resulting from the following memoryless transformation:

$$X(t) = g(Y(t)) \quad (3.35)$$

is called a *translation process*.

In an analogous manner, if $Y(\mathbf{t})$ with $\mathbf{t} \in \mathbb{R}^d$ is a univariate zero mean, homogenous Gaussian random field with unit variance and correlation function $\rho(\boldsymbol{\tau}) = E[Y(\mathbf{t} + \boldsymbol{\tau})Y(\mathbf{t})]$, the random field resulting from the following transformation:

$$X(\mathbf{t}) = g(Y(\mathbf{t})) \quad (3.36)$$

is called a *translation field*.

Translation processes and fields are a very attractive class of processes (and fields), since the available methods for generating realizations of Gaussian processes (and fields), such as the spectral representation method analyzed in section 3.2, are used with suitable nonlinear functions g to generate via eqs. (3.35) and (3.36) the corresponding realizations of various families of non-Gaussian processes (or fields).

3.3.1.2 Lognormal random processes and fields

Lognormal random processes and fields are a very attractive option when simulating material properties. In particular, soil properties such as Young's modulus, permeability etc. which are strictly positive can be represented by underlying lognormal random fields, which are by nature strictly positive. Realizations of lognormal random fields can be easily obtained as translations fields from zero mean homogeneous Gaussian random fields. The key relation which enables the mapping from a zero mean homogeneous Gaussian random field with unit variance $G(\mathbf{x})$, to a lognormal field $Y(\mathbf{x})$ is the following:

$$Y(\mathbf{x}) = \exp(\mu_{\ln Y} + \sigma_{\ln Y} \cdot G(\mathbf{x})) \quad (3.37)$$

3.3 Non-Gaussian random processes and fields

where $\mu_{\ln Y}$ and $\sigma_{\ln Y}$ are the mean and standard deviation of the natural logarithm of field Y . They are calculated from the target mean and standard deviation of the random field Y from the following set of relations:

$$COV_Y = \frac{\sigma_Y}{\mu_Y} \quad (3.38)$$

$$\sigma_{\ln Y}^2 = \ln(1 + COV_Y^2) \quad (3.39)$$

$$\mu_{\ln Y} = \ln(\mu_Y) - \frac{1}{2}\sigma_{\ln Y}^2 \quad (3.40)$$

To conclude, the process of generating realizations of lognormal random fields can be summarized in the following steps:

- (a) Generate realizations $G^{(i)}(\mathbf{x})$ where $i = 1, 2, \dots, n$ of homogeneous zero mean unit variance Gaussian fields using one of the available methods such as the spectral representation method section 3.2 (here i indicates the i^{th} realization of a total of n).
- (b) Use eqs. (3.38) to (3.40) to calculate $\sigma_{\ln Y}$ and $\mu_{\ln Y}$ from the corresponding σ_Y and μ_Y of the target lognormal field Y .
- (c) Use eq. (3.37) to transform the components of each Gaussian realization $G^{(i)}(x_j)$ to the corresponding $Y^{(i)}(x_j)$, where x_j is the spatial position of the j^{th} point.

Chapter 4

The Stochastic Finite Element Method

In the last two decades, the stochastic finite element method (SFEM) has emerged as the most powerful method used to solve problems in computational stochastic mechanics. This fact is the result of extensive scientific research, accompanied by advances in computer technology that provide the computational power required to tackle stochastic problems. The classical FEM has been the predominant method applied up to now for deterministic problems, but cannot be directly used to take into account uncertainty. On the contrary, the SFEM, which is an extension of the deterministic FEM, can incorporate uncertainties in loading and boundary conditions, as well as model geometry and material properties.

4.1 Main variants of the Stochastic Finite Element Method

The two main variants of the SFEM are the perturbation method and the Spectral Stochastic finite element method (SSFEM). An additional method is the Monte Carlo simulation method (MCS), which is the method of choice in this dissertation.

4.1.1 The Perturbation method

The *perturbation method* is one of the most widely used methods in computational stochastic mechanics. Its analytical tractability together with the ability to estimate response statistics for general linear and nonlinear stochastic systems makes it thus

The Stochastic Finite Element Method

very effective and computationally efficient. The main aspects of the perturbation method are covered in this section.

4.1.1.1 Main aspects of the Perturbation method

Let a general differential equation with a given right-hand side q :

$$G(u) = q \quad (4.1)$$

where G is a differential operator and u the solution of eq. (4.1). Making the assumption that a solution exists, a linear operator L is introduced and the following auxiliary equation is used:

$$\begin{aligned} L(u) &= q \\ \rightarrow u &= L^{-1}q \end{aligned} \quad (4.2)$$

The initial differential equation 4.1, enriched with the auxiliary equation 4.2, can now be written as:

$$L(u) + G(u) - L(u) = q \quad (4.3)$$

By defining the new differential operator N :

$$N(u) = G(u) - L(u) \quad (4.4)$$

eq. (4.3) is rewritten as:

$$L(u) + N(u) = q \quad (4.5)$$

Now a parameter ϵ is defined and finally eq. (4.5) is reformulated as:

$$L(u) + N(u)\epsilon = q \quad (4.6)$$

The solution u of eq. (4.6) can be expressed as a series expansion with respect to parameter ϵ as:

$$u = u_0 + u_1\epsilon + u_2\epsilon^2 + \dots \quad (4.7)$$

Substituting eq. (4.7) in eq. (4.5) and moving terms related to operator N to the right-hand side, the following relation is produced:

$$L(u_0 + u_1\epsilon + u_2\epsilon^2 + \dots) = q - N(u_0 + u_1\epsilon + u_2\epsilon^2 + \dots)\epsilon \quad (4.8)$$

4.1 Main variants of the Stochastic Finite Element Method

and, by taking into account that L is a linear operator by definition, the left-hand side of eq. (4.8) is rewritten as:

$$L(u_0 + u_1\epsilon + u_2\epsilon^2 + \dots) = L(u_0) + L(u_1)\epsilon + L(u_2)\epsilon^2 + \dots \quad (4.9)$$

The right-hand side part of eq. (4.8) related to operator N is reformulated as:

$$N(u_0 + u_1\epsilon + u_2\epsilon^2 + \dots) = N(u_0) + N_1(u_0, u_1)\epsilon + N_2(u_0, u_1, u_2)\epsilon^2 + \dots \quad (4.10)$$

The final step consists of equating terms with ϵ powers of eqs. (4.9) and (4.10) through eq. (4.8) to obtain the following set of equations:

$$\begin{aligned} L(u_0) &= q \\ L(u_1) &= -N(u_0) \\ L(u_2) &= -N_1(u_0, u_1) \\ &\vdots \\ L(u_{k+1}) &= -N_k(u_0, u_1, \dots, u_k) \end{aligned} \quad (4.11)$$

and using the inverse of the linear operator L , the set of solutions of eq. (4.11) is calculated by:

$$\begin{aligned} u_0 &= L^{-1}q \\ u_1 &= L^{-1}(-N(u_0)) \\ u_2 &= L^{-1}(-N_1(u_0, u_1)) \\ &\vdots \\ u_{k+1} &= L^{-1}(-N_k(u_0, u_1, \dots, u_k)) \end{aligned} \quad (4.12)$$

By setting $\epsilon = 1$, the solution of the initial eq. (4.1) can be calculated.

Now, the disadvantage of the perturbation approach lies on the fact that, in order for the method to be valid, the fluctuation of the stochastic parameters considered cannot be large. The solution of the stochastic problems can be approximated by the set of equations given in eq. (4.12), by making the almost valid assumption that the random variables involved do not deviate much from their respective mean values, so that the term $N(u)\epsilon$ introduced in eq. (4.6) is small enough.

4.1.1.2 The Perturbation-based stochastic finite element method

In this section, the perturbation method is described in the SFEM context. The perturbation-based SFEM has been successfully applied to a variety of stochastic problems including linear elastic static and dynamic systems, as well as nonlinear and eigenvalue problems. In order to demonstrate the application of the method, a linear elastic structural problem under static loading conditions with stochastic material properties is used.

The fundamental equations of equilibrium for a structural system discretized with finite elements can be written in the following compact matrix form:

$$\mathbf{K}\mathbf{U} = \mathbf{P} \quad (4.13)$$

where \mathbf{K} is the total assembled stiffness matrix, \mathbf{U} the nodal displacement vector and \mathbf{P} the external force vector, which is considered deterministic and is constant over time. System parameters such as Young's modulus, Poisson's ratio, as well as additional structural properties like the cross section area, moment of inertia and torsional stiffness can be treated as stochastic or uncertain properties of the studied structure. Note that a discretization method to produce the underlying random fields of the corresponding stochastic parameters has to be chosen to incorporate the uncertain properties in the analysis.

Let $\boldsymbol{\epsilon}$ denote a random vector involved in the calculation of the total stiffness matrix \mathbf{K} . Vector $\boldsymbol{\epsilon}$ is assumed to have zero mean value and known covariance matrix. The purpose of the stochastic analysis is the calculation of the first and second moments of the response quantities of interest such as nodal displacements and stresses, strains at certain points of the structure.

The total stiffness matrix is expanded with respect to powers of the random vector $\boldsymbol{\epsilon}$ at its mean values as:

$$\mathbf{K} = \mathbf{K}^{(0)} + \sum_{i=1}^n \mathbf{K}_i^{(1)} \boldsymbol{\epsilon}_i + \sum_{i=1}^n \sum_{j=1}^n \mathbf{K}_{ij}^{(2)} \boldsymbol{\epsilon}_i \boldsymbol{\epsilon}_j + \dots \quad (4.14)$$

where $\mathbf{K}^{(0)}$, $\mathbf{K}_i^{(1)}$ and $\mathbf{K}_{ij}^{(2)}$ are the zeroth, first and second mean-centered second rates of change of the stiffness matrix with respect to $\boldsymbol{\epsilon}_i$ and $\boldsymbol{\epsilon}_j$, and n is the total number of random variables considered.

4.1 Main variants of the Stochastic Finite Element Method

The nodal displacement vector \mathbf{U} is also expanded as:

$$\mathbf{U} = \mathbf{U}^{(0)} + \sum_{i=1}^n \mathbf{U}_i^{(1)} \boldsymbol{\epsilon}_i + \sum_{i=1}^n \sum_{j=1}^n \mathbf{U}_{ij}^{(2)} \boldsymbol{\epsilon}_i \boldsymbol{\epsilon}_j + \dots \quad (4.15)$$

Equation (4.15) is the system response expressed in terms of the lower-order polynomial function with respect to the random vector $\boldsymbol{\epsilon}$. To specify, this is an approximation of the response surface, while the solution accuracy depends on how accurate the response surface is. Substituting eqs. (4.14) and (4.15) to the equilibrium equation i.e. eq. (4.13), and equating the corresponding terms, results in the following set of equations:

$$\begin{aligned} \mathbf{K}^{(0)} \mathbf{U}^{(0)} &= \mathbf{P} \\ \mathbf{K}^{(0)} \mathbf{U}_i^{(1)} &= -\mathbf{K}_i^{(1)} \mathbf{U}^{(0)} \\ \mathbf{K}^{(0)} \mathbf{U}_{ij}^{(2)} &= -\left(\mathbf{K}_i^{(1)} \mathbf{U}_j^{(1)} + \mathbf{K}_j^{(1)} \mathbf{U}_i^{(1)} \right) \\ &\vdots \end{aligned} \quad (4.16)$$

Truncating the expanded series given by eqs. (4.14) and (4.15) so that only terms up to second order are included, the expected value of the nodal displacement vector is obtained:

$$E[\mathbf{U}] = \mathbf{U}^{(0)} + \sum_{i=1}^n \sum_{j=1}^n \mathbf{U}_{ij}^{(2)} E[\boldsymbol{\epsilon}_i \boldsymbol{\epsilon}_j] \quad (4.17)$$

where the expectation operator is denoted as $E[\cdot]$, and $E[\boldsymbol{\epsilon}_i \boldsymbol{\epsilon}_j]$ is the covariance matrix of the random vector $\boldsymbol{\epsilon}$. Furthermore, the covariance matrix of the nodal displacement vector can be calculated by:

$$\begin{aligned} E[(\mathbf{U} - E[\mathbf{U}])(\mathbf{U} - E[\mathbf{U}])^T] &= \sum_{i=1}^n \sum_{j=1}^n (\mathbf{U}_i^{(1)}) (\mathbf{U}_j^{(1)})^T E[\boldsymbol{\epsilon}_i \boldsymbol{\epsilon}_j] \\ &\quad + \sum_{i=1}^n \sum_{j=1}^n \sum_{k=1}^n (\mathbf{U}_i^{(1)}) (\mathbf{U}_{jk}^{(2)})^T E[\boldsymbol{\epsilon}_i \boldsymbol{\epsilon}_{jk}] \\ &\quad + \sum_{i=1}^n \sum_{j=1}^n \sum_{k=1}^n (\mathbf{U}_{ij}^{(2)}) (\mathbf{U}_k^{(1)})^T E[\boldsymbol{\epsilon}_{ij} \boldsymbol{\epsilon}_k] \\ &\quad + \sum_{i=1}^n \sum_{j=1}^n \sum_{k=1}^n \sum_{l=1}^n (\mathbf{U}_{ij}^{(2)}) (\mathbf{U}_{kl}^{(2)})^T E[\boldsymbol{\epsilon}_{ij} \boldsymbol{\epsilon}_{kl}] \end{aligned} \quad (4.18)$$

where $\boldsymbol{\epsilon}_{ij} = \boldsymbol{\epsilon}_i \boldsymbol{\epsilon}_j - E[\boldsymbol{\epsilon}_i \boldsymbol{\epsilon}_j]$. Statistics of any other response quantities such as stresses and strains can be calculated according to eqs. (4.17) and (4.18).

4.1.2 The Spectral Stochastic Finite Element Method

The spectral stochastic finite element method (SSFEM) was introduced by Ghanem and Spanos (Ghanem and Spanos, 2003). It is an extension of the classical deterministic finite element method, which is used to solve boundary value problems considering spatial variability of the material properties. The random material property is described by an underlying Gaussian stochastic field, represented according to the Karhunen-Loève (K-L) expansion. According to the (K-L) expansion, the random field $f(\mathbf{x}, \theta)$ representing the studied material property can be written as:

$$f(\mathbf{x}, \theta) = \mu(\mathbf{x}) \sum_{i=1}^{\infty} \sqrt{\lambda_i} \phi_i(\mathbf{x}) \xi_i(\theta) \quad (4.19)$$

where $\mu(\mathbf{x})$ is the mean value of the field at the spatial point with coordinates \mathbf{x} , ξ_i a set of uncorrelated random variables and λ_i , $\phi_i(\mathbf{x})$ the eigenvalues and eigenfunctions of the autocorrelation function $C_{ff}(\mathbf{x}_1, \mathbf{x}_2)$ of f , calculated from the solution of the following Fredholm integral equation of the second kind:

$$\int_D C_{ff}(\mathbf{x}_1, \mathbf{x}_2) \phi_i(\mathbf{x}_1) d\mathbf{x}_1 = \lambda_i \phi_i(\mathbf{x}_2) \quad (4.20)$$

The stochastic stiffness matrix of element (e) can then be written according to:

$$\mathbf{K}^{(e)}(\theta) = \mathbf{K}_0^{(e)} + \sum_{i=1}^{\infty} \mathbf{K}_i^{(e)} \xi_i(\theta) \quad (4.21)$$

where $\mathbf{K}_0^{(e)}$ is the mean value of $\mathbf{K}^{(e)}(\theta)$ and $\mathbf{K}_i^{(e)}$ are deterministic and given by:

$$\mathbf{K}_i^{(e)} = \sqrt{\lambda_i} \int_{\Omega_e} \phi_i(\mathbf{x}) \mathbf{B}^T \mathbf{D}_0 \mathbf{B} d\Omega_e \quad (4.22)$$

where \mathbf{B} is the classical strain-displacement matrix and \mathbf{D}_0 corresponds to the mean value of the constitutive matrix. If we assume deterministic loading conditions, the final equilibrium finite element equation can be written as follows:

$$\left[\mathbf{K}_0 + \sum_{i=1}^{\infty} \mathbf{K}_i \xi_i(\theta) \right] \mathbf{U}(\theta) = \mathbf{F} \quad (4.23)$$

where $\mathbf{U}(\theta)$ is the unknown vector of random nodal displacements and \mathbf{F} the deterministic loading vector. The next step in the SSFEM is the expansion of the random nodal displacement vector $\mathbf{U}(\theta)$ in a series of random Hermite polynomials $\{\Psi_j(\theta)\}_{j=0}^{\infty}$, a process known as *polynomial chaos expansion (PCE)*. According to the PCE, the

4.1 Main variants of the Stochastic Finite Element Method

displacement vector is expressed as the following sum:

$$\mathbf{U}(\theta) = \sum_{j=0}^{\infty} \mathbf{U}_j \Psi_j(\theta) \quad (4.24)$$

while the final form of the equilibrium equation is:

$$\left(\sum_{i=0}^{\infty} \mathbf{K}_i(\theta) \right) \cdot \left(\sum_{j=0}^{\infty} \mathbf{U}_j \psi_j(\theta) \right) - \mathbf{F} = 0 \quad (4.25)$$

When considering the application of the SSFEM, the K-L and PCE expansions are truncated to a finite number of terms. Let $M+1$ denote the number of terms retained in the K-L expansion and P the corresponding number for the PCE. After some algebraic manipulations, the following linear system with NP unknowns has to be solved:

$$\begin{bmatrix} \mathbf{K}_{00} & \cdots & \mathbf{K}_{0,P-1} \\ \mathbf{K}_{10} & \cdots & \mathbf{K}_{1,P-1} \\ \vdots & & \vdots \\ \mathbf{K}_{P-1,0} & \cdots & \mathbf{K}_{P-1,P-1} \end{bmatrix} \cdot \begin{bmatrix} \mathbf{U}_0 \\ \mathbf{U}_1 \\ \vdots \\ \mathbf{U}_{P-1} \end{bmatrix} = \begin{bmatrix} \mathbf{F}_0 \\ \mathbf{F}_1 \\ \vdots \\ \mathbf{F}_{P-1} \end{bmatrix} \quad (4.26)$$

which is written in compact form as:

$$\mathcal{K}\mathbf{U} = \mathcal{F} \quad (4.27)$$

The dimension of the resulting system of eq. (4.27) depends on the number of terms P retained in the PCE and the number of degrees of freedom N of the corresponding finite element problem. Thus, the computational cost required for the solution of the stochastic problem is much larger compared to the deterministic one. In most cases, the size of \mathcal{K} makes direct solution methods prohibitive and iterative solution schemes, such as the preconditioned conjugate gradient, have to be used.

4.1.3 The Monte Carlo Simulation Method

The class of Monte Carlo methods is a classical computational tool used in many fields of science and engineering to simulate natural phenomena based on probabilities (Greenbaum and Chartier, 2012). The MCS method in the context of stochastic finite elements is but an adaptation of the classical technique to incorporate uncertain model parameters in a finite element model. The main methodology consists of the following steps:

The Stochastic Finite Element Method

1. Generate a number of random field or random process realizations representing the desired stochastic property or properties to be incorporated in the analysis.
2. Run a separate deterministic finite element simulation using each of the above realizations as input and keep track of the response quantities of choice.
3. Analyze the resulting data of the analyses and calculate the required statistical quantities such as mean values, variances and probability distributions. At this stage, probabilities of failure according to a predefined criterion may also be determined.

The MCS finite element method is globally applicable regardless of the number of uncertain parameters considered, the model nonlinearity, time dependence etc. In addition, it is effective even in cases where the magnitude of the variations of the system properties is large, which might make the other available methods unsuitable. Furthermore, the MCS is used to check the validity of the alternative methods used.

The main disadvantage of the MCS is the substantial computational cost, which results from the extensive number of realizations that have to be considered to correctly calculate the statistical quantities of interest. Nevertheless, since each finite element simulation is independent of the others, this method is embarrassingly parallel, a property that makes it a successful candidate for taking advantage of today's multicore and multi-cpu computer architectures.

4.2 Discretization methods

4.2.1 The nodal point method

The nodal point method dictates that the values of the chosen random field representing the uncertain property have to be calculated at each finite element node of the model mesh. Thus, the spatially continuous random field f is transformed to a discrete vector of size N_{nodes}^{mesh} , which is the total number of mesh nodes with values:

$$f_j = f(\mathbf{x}_j) \quad (4.28)$$

where \mathbf{x}_j is the vector of coordinates of the j^{th} node and f_j the value of the random field at this node.

4.2.2 The integration point method

According to the integration point method, the random field representing the stochastic property of interest must be calculated at the integration points of each finite element of the given mesh. This particular method is used for finite elements which employ numerical integration, such as Gauss quadrature for calculation of the corresponding matrices. The problem of this approach simply lies on the increased computational cost in large scale problems, especially when high-order elements are used.

4.2.3 The Midpoint method

The midpoint method is one of the most widely used methodologies related to SFEM analysis. According to the midpoint method, the random field is discretized at the middle point of each finite element of the model mesh considered. The coordinate vector of the central point of each element is then calculated according to:

$$\mathbf{x}_c^e = \frac{1}{N^e} \sum_{j=1}^{N^e} \mathbf{x}_j^e \quad (4.29)$$

where \mathbf{x}_j^e are the nodal coordinates of the j^{th} node and N^e the number of nodes of the element. The midpoint method makes the assumption that the random field property is uniform on each element and that the value of the random field at the central point is representative for the whole element. This is the method of choice in this dissertation, mainly due to its implementation simplicity and low computational cost.

Chapter 5

Variability response functions

The concept of variability response functions (VRF) was first introduced by Shinozuka in the late 1980s, in a series of seminal papers: (Bucher and Shinozuka, 1988; Kardara et al., 1989; Shinozuka, 1987). The main advantage demonstrated by the VRF is the variance information related to a response quantity expressed independently of the correlation structure of the underlying uncertain system property considered. As a result, the VRF is a deterministic function which depends on the structure to be analyzed, its boundary conditions and the loading applied.

Initially, the VRF methodology was applied to simple statically determinate truss and frame structures with linear material properties under static loading conditions. The method has since then been extended to treat dynamic problems leading to the concept of dynamic variability response functions (DVRF), as described in (Papadopoulos and Kokkinos, 2012, 2015).

Finally, an explicit formula for the VRF can be derived only for very simple models. In order to address this limitation, a fast Monte Carlo simulation (FMCS) methodology was devised, which generalized the applicability of the VRF in general finite element models.

5.1 Definition of VRF and MRF

The VRF concept is defined through the following integral expression for the variance of a response quantity u of a finite element model in 1D:

$$Var[u] = \int_{-\infty}^{+\infty} VRF(\kappa) S_f(\kappa) d\kappa \quad (5.1)$$

Variability response functions

where $S_f(\kappa)$ is the power spectral density of the underlying random field representing the random property of the system. Equivalently, a mean response function (MRF) is defined, expressing the corresponding information for the mean value of a response quantity u :

$$\mu_u = \int_{-\infty}^{+\infty} MRF(\kappa)S_f(\kappa)d\kappa \quad (5.2)$$

Furthermore, the VRF and MRF can be defined for 2D and 3D problems, where the corresponding definitions for 2D are:

$$Var[u] = \int_{-\infty}^{+\infty} \int_{-\infty}^{+\infty} VRF(\kappa_1, \kappa_2)S_f(\kappa_1, \kappa_2)d\kappa_1d\kappa_2 \quad (5.3)$$

$$E[u] = \int_{-\infty}^{+\infty} \int_{-\infty}^{+\infty} MRF(\kappa_1, \kappa_2)S_f(\kappa_1, \kappa_2)d\kappa_1d\kappa_2 \quad (5.4)$$

and for 3D:

$$Var[u] = \int_{-\infty}^{+\infty} \int_{-\infty}^{+\infty} \int_{-\infty}^{+\infty} VRF(\kappa_1, \kappa_2, \kappa_3)S_f(\kappa_1, \kappa_2, \kappa_3)d\kappa_1d\kappa_2d\kappa_3 \quad (5.5)$$

$$E[u] = \int_{-\infty}^{+\infty} \int_{-\infty}^{+\infty} \int_{-\infty}^{+\infty} MRF(\kappa_1, \kappa_2, \kappa_3)S_f(\kappa_1, \kappa_2, \kappa_3)d\kappa_1d\kappa_2d\kappa_3 \quad (5.6)$$

5.2 Definition of DVRF and DMRF

The concept of dynamic variability response functions (DVRF) and dynamic mean response functions (DMRF) was initially proposed in (Papadopoulos and Kokkinos, 2012, 2015). They are but a straightforward generalization of the classical VRF and MRF defined in section 5.1; the DVRF/DMRF pair is used to treat the limitations of VRF/MRF which treat stochastic problems under static loading conditions. Thus, the DVRF and DMRF can tackle stochastic analyses where the studied responses are transient. The DVRF is defined as:

$$Var[u(t)] = \int_{-\infty}^{+\infty} DVRF(t, \kappa, \sigma_{ff})S_{ff}(\kappa)d\kappa \quad (5.7)$$

where $u(t)$ is the studied response, which is a function of time, and S_{ff} the 1D spectral density function of the underlying random field. The definition of the DMRF is analogous:

$$E[u(t)] = \int_{-\infty}^{+\infty} DMRF(t, \kappa, \sigma_{ff})S_{ff}(\kappa)d\kappa \quad (5.8)$$

where $E[u(t)]$ is the mean value of the response quantity u , which is a function of time.

5.3 Upper bounds of the response variance and mean value

To complete, the equivalent relations for 2D stochastic problems are given:

$$Var[u(t)] = \int_{-\infty}^{+\infty} \int_{-\infty}^{+\infty} DVRF(t, \kappa_1, \kappa_2, \sigma_{ff}) S_{ff}(\kappa_1, \kappa_2) d\kappa_1 d\kappa_2 \quad (5.9)$$

for the DVRF, and furthermore the DMRF:

$$E[u(t)] = \int_{-\infty}^{+\infty} \int_{-\infty}^{+\infty} DMRF(t, \kappa_1, \kappa_2, \sigma_{ff}) S_{ff}(\kappa_1, \kappa_2) d\kappa_1 d\kappa_2 \quad (5.10)$$

which are both functions of time t , the standard deviation σ_{ff} of the underlying random field and wave numbers corresponding to the two spatial axes, namely κ_1 and κ_2 .

To conclude, the corresponding DVRF and DMRF definitions for 3D stochastic transient problems are:

$$Var[u(t)] = \int_{-\infty}^{+\infty} \int_{-\infty}^{+\infty} \int_{-\infty}^{+\infty} DVRF(t, \kappa_1, \kappa_2, \kappa_3, \sigma_{ff}) S_{ff}(\kappa_1, \kappa_2, \kappa_3) d\kappa_1 d\kappa_2 d\kappa_3 \quad (5.11)$$

for the DVRF and:

$$E[u(t)] = \int_{-\infty}^{+\infty} \int_{-\infty}^{+\infty} \int_{-\infty}^{+\infty} DMRF(t, \kappa_1, \kappa_2, \kappa_3, \sigma_{ff}) S_{ff}(\kappa_1, \kappa_2, \kappa_3) d\kappa_1 d\kappa_2 d\kappa_3 \quad (5.12)$$

for the DMRF. They again are function of time t , the standard deviation (std) σ_{ff} of the underlying random field and wave number axes corresponding to the three spatial axes κ_1 , κ_2 and κ_3 .

5.3 Upper bounds of the response variance and mean value

One of the main advantages of the VRF/MRF methodology and their transient equivalents DVRF/DMRF is the establishment of spectral- and distribution-free upper bounds of the response variance and mean value. In this section, the methods for calculating these upper bounds based on the VRF/MRF, as well as DVRF/DMRF, are described.

5.3.1 Time independent response

For static loading cases with constant loading conditions, the classical VRF and MRF functions are used in order to calculate the upper bounds of the response variance and mean. Regarding the variance of the studied response quantity u , the following

Variability response functions

relation is satisfied:

$$Var[u] = \int_{-\infty}^{+\infty} VRF(\kappa, \sigma_{ff}) S_{ff}(\kappa) d\kappa \leq VRF(\kappa^{max}, \sigma_{ff}) \sigma_{ff}^2 \quad (5.13)$$

where κ^{max} is the wave number for which the VRF function is maximum. The analogous expression, regarding the mean value of u is written with respect to the MRF function, is thus as follows:

$$E[u] = \int_{-\infty}^{+\infty} MRF(\kappa, \sigma_{ff}) S_{ff}(\kappa) d\kappa \leq MRF(\kappa^{max}, \sigma_{ff}) \sigma_{ff}^2 \quad (5.14)$$

where κ^{max} now denotes the wave number at which the MRF function is maximized. Equations (5.13) and (5.14) are used to calculate the upper bounds of the variance and mean of the response quantity u respectively for stochastic finite element models in 1D, while the extension to 2D and 3D problems follows.

For 2D problems, the upper bound of the variance is calculated from the following relation:

$$Var[u] = \int_{-\infty}^{+\infty} \int_{-\infty}^{+\infty} VRF(\kappa_x, \kappa_y, \sigma_{ff}) S_{ff}(\kappa_x, \kappa_y) d\kappa \leq VRF(\kappa_x^{max}, \kappa_y^{max}, \sigma_{ff}) \sigma_{ff}^2 \quad (5.15)$$

where $(\kappa_x^{max}, \kappa_y^{max})$ indicate the pair of wave numbers maximizing the 2D VRF function. The upper bound for the mean of the response is calculated by:

$$E[u] = \int_{-\infty}^{+\infty} \int_{-\infty}^{+\infty} MRF(\kappa_x, \kappa_y, \sigma_{ff}) S_{ff}(\kappa_x, \kappa_y) d\kappa \leq MRF(\kappa_x^{max}, \kappa_y^{max}, \sigma_{ff}) \sigma_{ff}^2 \quad (5.16)$$

where $(\kappa_x^{max}, \kappa_y^{max})$ now denotes the pair of wave numbers maximizing the 2D MRF function.

Finally, for 3D problems, the upper bound of the response variance is established through the following relation:

$$\begin{aligned} Var[u] &= \int_{-\infty}^{+\infty} \int_{-\infty}^{+\infty} \int_{-\infty}^{+\infty} VRF(\kappa_x, \kappa_y, \kappa_z, \sigma_{ff}) S_{ff}(\kappa_x, \kappa_y, \kappa_z) d\kappa \\ &\leq VRF(\kappa_x^{max}, \kappa_y^{max}, \kappa_z^{max}, \sigma_{ff}) \sigma_{ff}^2 \end{aligned} \quad (5.17)$$

where $(\kappa_x^{max}, \kappa_y^{max}, \kappa_z^{max})$ is the triplet of wave numbers maximizing the 3D VRF function. The corresponding upper bound for the mean of the response quantity d is

5.3 Upper bounds of the response variance and mean value

calculated by:

$$\begin{aligned}
 E[u] &= \int_{-\infty}^{+\infty} \int_{-\infty}^{+\infty} \int_{-\infty}^{+\infty} MRF(\kappa_x, \kappa_y, \kappa_z, \sigma_{ff}) S_{ff}(\kappa_x, \kappa_y, \kappa_z) d\kappa \\
 &\leq MRF(\kappa_x^{max}, \kappa_y^{max}, \kappa_z^{max}, \sigma_{ff}) \sigma_{ff}^2
 \end{aligned} \tag{5.18}$$

where $(\kappa_x^{max}, \kappa_y^{max}, \kappa_z^{max})$ denotes the triplet of wave numbers maximizing the 3D MRF function.

5.3.2 Transient response

When considering stochastic systems with transient response, i.e. the response is a function of time, the upper bounds of the response variability and mean value are calculated through the use of the DVRF and DMRF functions respectively. It has to be noted though that in the transient case, unlike section 5.3, the upper bounds of the corresponding response quantity of interest d are functions of time t . For the 1D stochastic systems, the upper bound of the response variance is therefore specifically established through the following relation:

$$Var[d(t)] = \int_{-\infty}^{+\infty} DVRF(t, \kappa, \sigma_{ff}, t) S_{ff}(\kappa) d\kappa \leq DVRF(t, \kappa^{max}(t), \sigma_{ff}) \sigma_{ff}^2 \tag{5.19}$$

where $\kappa^{max}(t)$ is the wave number that maximizes the DVRF function at time instance t . The analogous expressions for the mean value of the response quantity d is:

$$E[d(t)] = \int_{-\infty}^{+\infty} DMRF(t, \kappa, \sigma_{ff}, t) S_{ff}(\kappa) d\kappa \leq DMRF(t, \kappa^{max}(t), \sigma_{ff}) \sigma_{ff}^2 \tag{5.20}$$

where $\kappa^{max}(t)$ is the wave number maximizing the DMRF function at time t .

For 2D stochastic systems, the corresponding upper bound of the response variance can be derived from the following relation:

$$\begin{aligned}
 Var[d(t)] &= \int_{-\infty}^{+\infty} \int_{-\infty}^{+\infty} DVRF(t, \kappa_x, \kappa_y, \sigma_{ff}) S_{ff}(\kappa_x, \kappa_y) d\kappa_x d\kappa_y \\
 &\leq DVRF(t, \kappa_x^{max}(t), \kappa_y^{max}(t), \sigma_{ff}) \sigma_{ff}^2
 \end{aligned} \tag{5.21}$$

where $(\kappa_x^{max}(t), \kappa_y^{max}(t))$, denotes the pair of wave numbers in axes κ_x and κ_y which maximize the DVRF function at time t . The corresponding relation for the time-

Variability response functions

dependent upper bound of the response mean is:

$$\begin{aligned} E[d(t)] &= \int_{-\infty}^{+\infty} \int_{-\infty}^{+\infty} DMRF(t, \kappa_x, \kappa_y, \sigma_{ff}) S_{ff}(\kappa_x, \kappa_y) d\kappa_x d\kappa_y \\ &\leq DMRF(t, \kappa_x^{max}(t), \kappa_y^{max}(t), \sigma_{ff}) \sigma_{ff}^2 \end{aligned} \quad (5.22)$$

where $(\kappa_x^{max}(t), \kappa_y^{max}(t))$ is now the wave number pair maximizing the DMRF function at time t .

Finally, for 3D stochastic systems, the corresponding relations used to calculate the upper bounds of the response variability and mean are given right below, the relation for the upper bound of the variance being:

$$\begin{aligned} Var[d(t)] &= \int_{-\infty}^{+\infty} \int_{-\infty}^{+\infty} \int_{-\infty}^{+\infty} DVRF(t, \kappa_x, \kappa_y, \kappa_z, \sigma_{ff}) S_{ff}(\kappa_x, \kappa_y, \kappa_z) d\kappa_x d\kappa_y d\kappa_z \\ &\leq DVRF(t, \kappa_x^{max}(t), \kappa_y^{max}(t), \kappa_z^{max}(t), \sigma_{ff}) \sigma_{ff}^2 \end{aligned} \quad (5.23)$$

where $(\kappa_x^{max}(t), \kappa_y^{max}(t), \kappa_z^{max}(t))$ is the triplet of the wave number values that maximizes the DVRF function at time t . The analogous relation for the upper bound of the mean of response quantity d is:

$$\begin{aligned} E[d(t)] &= \int_{-\infty}^{+\infty} \int_{-\infty}^{+\infty} \int_{-\infty}^{+\infty} DMRF(t, \kappa_x, \kappa_y, \kappa_z, \sigma_{ff}) S_{ff}(\kappa_x, \kappa_y, \kappa_z) d\kappa_x d\kappa_y d\kappa_z \\ &\leq DMRF(t, \kappa_x^{max}(t), \kappa_y^{max}(t), \kappa_z^{max}(t), \sigma_{ff}) \sigma_{ff}^2 \end{aligned} \quad (5.24)$$

where $(\kappa_x^{max}(t), \kappa_y^{max}(t), \kappa_z^{max}(t))$ is the triplet of the wave number values that maximizes the DMRF function at time t .

5.4 The fast Monte Carlo simulation method

An explicit formula for the DVRF and DMRF functions can be only obtained for very simple models. As a result, the calculation of discrete versions of DVRF and DMRF is possible only when using numerical techniques. In this thesis, the FMCS method is used. The concept behind the FMCS is the generation of random fields $f(x)$ for 1D problems, $f(x, y)$ for 2D and $f(x, y, z)$ for 3D, corresponding to random sinusoids, with monochromatic spectral densities. By computing the variance and mean of the response quantity for these sinusoids, the DVRF and DMRF are then calculated separately for each wave number.

5.4.1 Problems in 1D

For 1D problems, the FMCS method is reduced to the following steps:

1. For the standard deviation σ_{ff} of the studied quantity generate $N(5-10)$, sample functions of sinusoids for each corresponding wave number κ given by:

$$f_j(x) = \sqrt{2}\sigma_{ff} \cos(\kappa \cdot x + \phi_j) \quad (5.25)$$

where ϕ_j is the center of intervals $\left(\frac{2\pi j}{N}, \frac{2\pi(j+1)}{N}\right)$ for $j = 0, 1, \dots, N-1$. In general, due to the symmetry of the DMRF/DVRF functions for stochastic systems in 1D, only positive wave numbers are used. An upper cut-off wave number κ_u is each time chosen and the wave number axis is subdivided in M intervals. Given this, the discretized version of eq. 5.25 is:

$$f_{ij}(x) = \sqrt{2}\sigma_{ff} \cos(\kappa_i \cdot x + \phi_j) \quad (5.26)$$

where $\kappa_i = i\Delta\kappa$ for $i = 0, 1, \dots, M$ and $\Delta\kappa = \kappa_u/M$ indicates the wave number spacing.

2. For each discrete wave number κ_i , calculate the variance and mean of the response from the N corresponding f_{ij} $j = 1, 2, \dots, N$ realizations of the random sinusoid.
3. Calculate the values of the DMRF and DVRF at the wave number κ_i using the following relations:

$$DMRF(t, \kappa_i, \sigma_{ff}) = \frac{E[d(t)]_{\kappa_i}}{\sigma_{ff}^2} \quad (5.27)$$

$$DVRF(t, \kappa_i, \sigma_{ff}) = \frac{Var[d(t)]_{\kappa_i}}{\sigma_{ff}^2} \quad (5.28)$$

4. Gather all the required DMRF and DVRF values for each wave number κ_i and each time step for the standard deviation σ_{ff} ; the overall procedure may be repeated for alternative values of σ_{ff} .

5.4.2 Problems in 2D

For 2D problems, the method is adjusted in order to take into account the two wave number axes:

Variability response functions

1. For the standard deviation σ_{ff} of the studied quantity generate $N(5-10)$, sample functions of sinusoids for each pair of wave numbers κ_x and κ_y given by:

$$f_k(x, y) = \sqrt{2}\sigma_{ff} \cos(\kappa_x \cdot x + \kappa_y \cdot y + \phi_k) \quad (5.29)$$

where ϕ_k is the center of intervals $\left(\frac{2\pi k}{N}, \frac{2\pi(k+1)}{N}\right)$ for $k = 0, 1, \dots, N-1$. Unlike the 1D case, the DMRF/DVRF functions in 2D are not fully symmetric, prompting us to consider positive, as well as negative wave numbers for the two wave number axes. Lower and upper cut-off wave numbers are selected for each axis, namely $(\kappa_{xl}, \kappa_{xu})$ and $(\kappa_{yl}, \kappa_{yu})$, whereas the two wave number axes are discretized in M_1 and M_2 intervals respectively. However, in most cases, the lower and cut-off wave numbers are selected to be symmetric with respect to the axis origin, so that half of the selected intervals are used to discretize the negative portion of the axis and the other half for the positive one. Given these, the discretized version of eq. 5.29 is:

$$f_{ijk}(x, y) = \sqrt{2}\sigma_{ff} \cos(\kappa_{xi} \cdot x + \kappa_{yj} \cdot y + \phi_k) \quad (5.30)$$

where $\kappa_{xi} = \kappa_{xl} + i\Delta\kappa_x$ for $i = 0, 1, \dots, M_1$, $\Delta\kappa_x = (\kappa_{xu} - \kappa_{xl})/M_1$ indicates the wave number spacing in the first wave number axis, and $\kappa_{yj} = \kappa_{yl} + j\Delta\kappa_y$ for $j = 0, 1, \dots, M_2$ and $\Delta\kappa_y = (\kappa_{yu} - \kappa_{yl})/M_2$, the wave number spacing in the second wave number axis.

2. For each discrete wave number pair $(\kappa_{xi}, \kappa_{yj})$, calculate the variance and mean of the response from the N corresponding f_{ijk} $k = 1, 2, \dots, N$ realizations of the random sinusoid.
3. Calculate the values of the DMRF and DVRF at the wave number pair κ_{xi}, κ_{yj} using the following relations:

$$DMRF(t, \kappa_{xi}, \kappa_{yj}, \sigma_{ff}) = \frac{E[d(t)]_{\kappa_{xi}\kappa_{yj}}}{\sigma_{ff}^2} \quad (5.31)$$

$$DVRF(t, \kappa_{xi}, \kappa_{yj}, \sigma_{ff}) = \frac{Var[d(t)]_{\kappa_{xi}\kappa_{yj}}}{\sigma_{ff}^2} \quad (5.32)$$

4. Gather all the required DMRF/DVRF values for each wave number pair $(\kappa_{xi}, \kappa_{yj})$ and each time step for the standard deviation σ_{ff} ; the overall procedure may then be repeated for alternative values of σ_{ff} .

5.4.3 Problems in 3D

For 3D problems, the FMCS method is adjusted in order to incorporate the three wave number axes and is summarized in the following steps:

1. For the standard deviation σ_{ff} of the studied quantity generate $N(5-10)$, sample functions of sinusoids for each tuple of wave numbers κ_x , κ_y and κ_z given by:

$$f_l(x, y, z) = \sqrt{2}\sigma_{ff} \cos(\kappa_x \cdot x + \kappa_y \cdot y + \kappa_z \cdot z + \phi_l) \quad (5.33)$$

where ϕ_l is the midpoint of intervals $\left(\frac{2\pi l}{N}, \frac{2\pi(l+1)}{N}\right)$ for $l = 0, 1, \dots, N - 1$. Again, unlike the 1D case, the DMRF/DVRF functions in 3D are not fully symmetric, so positive, as well as negative wave numbers have to be considered for the three wave number axes. Lower and upper cut-off wave numbers are selected for each axis, namely $(\kappa_{xl}, \kappa_{xu})$, $(\kappa_{yl}, \kappa_{yu})$ and $(\kappa_{zl}, \kappa_{zu})$, while the three wave number axes are subdivided in M_1 , M_2 and M_3 intervals respectively. In most cases, the lower and upper cut-off wave numbers are selected to be symmetric with respect to the axis origin, resulting in half of the selected intervals being used to discretize the negative portion of the axis and the other half for the positive one. This time, the discretized version of eq. 5.33 is:

$$f_{ijkl}(x, y, z) = \sqrt{2}\sigma_{ff} \cos(\kappa_{xi} \cdot x + \kappa_{yj} \cdot y + \kappa_{zk} \cdot z + \phi_k) \quad (5.34)$$

where $\kappa_{xi} = \kappa_{xl} + i\Delta\kappa_x$ for $i = 0, 1, \dots, M_1$, $\Delta\kappa_x = (\kappa_{xu} - \kappa_{xl})/M_1$ indicates the wave number spacing for the κ_x axis, $\kappa_{yj} = \kappa_{yl} + j\Delta\kappa_y$ for $j = 0, 1, \dots, M_2$ with $\Delta\kappa_y = (\kappa_{yu} - \kappa_{yl})/M_2$ the spacing for the κ_y axis and $\kappa_{zk} = \kappa_{zl} + k\Delta\kappa_z$ for $k = 0, 1, \dots, M_3$ with $\Delta\kappa_z = (\kappa_{zu} - \kappa_{zl})/M_3$ the corresponding spacing for the κ_z axis.

2. For each discrete wave number tuple $(\kappa_{xi}, \kappa_{yj}, \kappa_{zk})$, calculate the variance and mean of the response from the N corresponding f_{ijkl} $l = 1, 2, \dots, N$ realizations of the random sinusoid.
3. Calculate the values of the DMRF and DVRF at the wave number tuple $(\kappa_{xi}, \kappa_{yj}, \kappa_{zk})$ using the following relations:

$$DMRF(t, \kappa_{xi}, \kappa_{yj}, \kappa_{zk}, \sigma_{ff}) = \frac{E[d(t)]_{\kappa_{xi}\kappa_{yj}\kappa_{zk}}}{\sigma_{ff}^2} \quad (5.35)$$

$$DVRF(t, \kappa_{xi}, \kappa_{yj}, \kappa_{zk}, \sigma_{ff}) = \frac{Var[d(t)]_{\kappa_{xi}\kappa_{yj}\kappa_{zk}}}{\sigma_{ff}^2} \quad (5.36)$$

4. Gather all the required DMRF and DVRF values for each wave number tuple $(\kappa_{xi}, \kappa_{yj}, \kappa_{zk})$ and each time step for the standard deviation σ_{ff} ; the overall procedure may well be repeated for alternative values of σ_{ff} .

5.5 Symmetries of the DMRF and DVRF functions

5.5.1 Symmetry in the 1D case

In this subsection, the complete symmetry of the DMRF and DVRF functions are proven for the 1D case. Consider a certain wave number denoted κ^* and the corresponding negative wave number $-\kappa^*$. Let one of the angles chosen for the random sinusoid in eq. (5.25) be denoted ϕ^* . Then, the corresponding random sinusoid $f^*(x)$ is given by:

$$f^*(x) = \cos(\kappa^* \cdot x + \phi^*) \quad (5.37)$$

Taking into account that \cos is an even function, the following relation holds:

$$f^*(x) = \cos(\kappa^* \cdot x + \phi^*) = \cos(-\kappa^* \cdot x - \phi^*) = \cos(-\kappa^* \cdot x + (2\pi - \phi^*)) \quad (5.38)$$

The DMRF and DVRF for the wave number κ^* are calculated from N random sinusoids which are uniformly distributed in $[0, 2\pi]$. Let us take for example that $N = 5$; then, $\phi \in \{\pi/5, 3\pi/5, \pi, 7\pi/5, 9\pi/5\}$, whereas for each value of ϕ , the corresponding value of $2\pi - \phi$ is also used in the calculation. Given these, the N random sinusoids used to generate the DMRF/DVRF functions for the wave number κ^* and $-\kappa^*$ are the same according to eq. (5.38). This proves that the DMRF/DVRF functions are even with respect to κ i.e. $DMRF(\kappa, t) = DMRF(-\kappa, t)$, while the same holds for the DVRF. Taking advantage of the symmetry of the DVRF and DMRF in 1D, only positive wave numbers have to be considered and the computational cost is reduced by half. Thus, relations eqs. (7.40) and (7.42) can be written as:

$$E[d(t)] = 2 \int_0^{+\infty} DMRF(t, \kappa, \sigma_{ff}) \cdot S_{ff}(\kappa) d\kappa \quad (5.39)$$

$$Var[d(t)] = 2 \int_0^{+\infty} DVRF(t, \kappa, \sigma_{ff}) \cdot S_{ff}(\kappa) d\kappa \quad (5.40)$$

5.5.2 Symmetry in the 2D case

In this subsection, the partial symmetry of the DMRF and DVRF functions are proven for the 2D case. Consider a certain wave number pair denoted (κ_x^*, κ_y^*) and the

5.5 Symmetries of the DMRF and DVRF functions

corresponding negative wave number pair $(-\kappa_x^*, -\kappa_y^*)$. Let one of the angles chosen for the random sinusoid in eq. (5.29) be denoted ϕ^* . Then, the corresponding random sinusoid $f^*(x, y)$ is given by:

$$f^*(x, y) = \cos(\kappa_x^* \cdot x + \kappa_y^* \cdot y + \phi^*) \quad (5.41)$$

Taking into account that \cos is an even function, the following relation holds:

$$\begin{aligned} f^*(x) &= \cos(\kappa_x^* \cdot x + \kappa_y^* \cdot y + \phi^*) = \cos(-\kappa_x^* \cdot x - \kappa_y^* \cdot y - \phi^*) \\ &= \cos(-\kappa_x^* \cdot x - \kappa_y^* \cdot y + (2\pi - \phi^*)) \end{aligned} \quad (5.42)$$

The DMRF and DVRF for the wave number pair (κ_x^*, κ_y^*) are calculated from N random sinusoids which are uniformly distributed in $[0, 2\pi]$. As already explained for the 1D case, for each value of ϕ , the corresponding value of $2\pi - \phi$ is also used in the calculation. Therefore, the N random sinusoids used to calculate the DMRF and DVRF functions for the wave number pair (κ_x^*, κ_y^*) and $(-\kappa_x^*, -\kappa_y^*)$ are the same according to eq. (5.42). In the same way, it can be proved that the N random sinusoids used to calculate the DMRF and DVRF functions are the same considering the wave number pairs $(\kappa_x^*, -\kappa_y^*)$ and $(-\kappa_x^*, \kappa_y^*)$. Thus, the DMRF and DVRF functions in 2D are symmetric in quadrants 1, 3 and 2, 4 of the κ_x - κ_y plane i.e. $DMRF(\kappa_x, \kappa_y, t) = DMRF(-\kappa_x, -\kappa_y, t)$, $DMRF(\kappa_x, -\kappa_y, t) = DMRF(-\kappa_x, \kappa_y, t)$, while the same is true regarding the DVRF. This fact alone can indeed help reduce computational cost by considering either only non-negative κ_x values or only non-negative κ_y values. In case of non-negative κ_x , eqs. (7.41) and (7.43) may be written as follows:

$$E[d(t)] = 2 \int_{-\infty}^{+\infty} \int_0^{\infty} DMRF(t, \kappa_x, \kappa_y, \sigma_{ff}) \cdot S_{ff}(\kappa_x, \kappa_y) d\kappa_x d\kappa_y \quad (5.43)$$

$$Var[d(t)] = 2 \int_{-\infty}^{+\infty} \int_0^{\infty} DVRF(t, \kappa_x, \kappa_y, \sigma_{ff}) \cdot S_{ff}(\kappa_x, \kappa_y) d\kappa_x d\kappa_y \quad (5.44)$$

Chapter 6

Consolidation of a soil layer with stochastic material properties

In this chapter, the consolidation phenomenon of a saturated soil layer with stochastic permeability k and Young's modulus E is studied. The direct Monte Carlo stochastic finite element method is employed in order to numerically solve the consolidation equations and incorporate the spatial variability of k and E . In particular, the case study consists of the loading of a rigid rough strip footing resting on a consolidating soil layer, where the effect of the variability of k and E on the footing settlements, as well as the generated excess pore pressures of the underlying soil is investigated.

6.1 The Consolidation Equation and its Numerical Solution

Soil consolidation is the phenomenon involving the gradual dissipation of porous fluid pressure accompanied by deformation of the soil skeleton. When a load is applied on a saturated soil layer, it is initially undertaken by the fluid contained in the soil pores in the form of excess pore pressures, and is gradually transferred to the soil skeleton. The one-dimensional theory of soil consolidation introduced by Terzaghi was later extended to three dimensions by Biot (Maurice A. Biot, 1941). The key to understanding the consolidation phenomenon is the notion of effective soil stress, which refers to the portion of the total stress undertaken by the soil skeleton and causes its actual deformation. The equations of equilibrium and balance of mass are combined with Darcy's law governing the flow of water through a soil medium, leading to the coupled set of consolidation equations.

Consolidation of a soil layer with stochastic material properties

The consolidation equations are discretized in space using the finite element u-p formulation, according to which the following matrix equation is derived (ignoring water sources and sinks):

$$\mathbf{K}_m \mathbf{u} + \mathbf{C} \mathbf{u}_w = \mathbf{f} \quad (6.1)$$

$$\mathbf{C}^T \frac{d\mathbf{u}}{dt} - \mathbf{K}_c \mathbf{u}_w = \mathbf{0} \quad (6.2)$$

where \mathbf{K}_m denotes the stiffness matrix of the soil elements, \mathbf{C} the coupling matrix and \mathbf{K}_c the fluid conductivity matrix, whereas \mathbf{u} and \mathbf{u}_w are the displacement and excess pore pressure nodal degrees of freedom. The matrices used in eqs. (6.1) and (6.2) are formulated according to the shape functions used to interpolate the displacement and pore pressure degrees of freedom. Derivation of the consolidation equations, their discretized form in terms of finite elements and the numerical solution schemes used are analytically explained in (Lewis et al., 1998; O. C. Zienkiewicz et al., 1999; Smith and Griffiths, 2004). In this study, the permeability coefficient k is used with dimensions of $[length]^3[time]/[mass]$ or equivalently $[length]^4[force]^{-1}/[time]$, which is different from the usual soil mechanics convention where it is defined in velocity terms. The two different permeability measures, are related through $k = k'/\gamma_w$, where k' is the permeability coefficient in velocity terms and γ_w the specific weight of water (O. C. Zienkiewicz et al., 1999). Furthermore, isotropic soil permeability is considered and thus, the permeability tensor \mathbf{k} is given by $\mathbf{k} = k\mathbf{I}$, where \mathbf{I} is the second order identity tensor. The fully implicit form of the generalized Newmark first order scheme (GN11) is used for time integration of the coupled set of consolidation equations according to:

$$\frac{\mathbf{u}^{(n+1)} - \mathbf{u}^{(n)}}{\Delta t} = \frac{d\mathbf{u}^{(n+1)}}{dt} \quad (6.3)$$

where $n+1$ refers to time $t+\Delta t$, n to time t and Δt is the time step used. Equations (6.1) and (6.2) are written for time $t + \Delta t$ as follows:

$$\mathbf{K}_m \mathbf{u}^{(n+1)} + \mathbf{C} \mathbf{u}_w^{(n+1)} = \mathbf{f}^{(n+1)} \quad (6.4)$$

$$\mathbf{C}^T \frac{d\mathbf{u}^{(n+1)}}{dt} - \mathbf{K}_c \mathbf{u}_w^{(n+1)} = \mathbf{0} \quad (6.5)$$

Substituting eq. (6.3) in eq. (6.5), we get:

$$\mathbf{C}^T \frac{\mathbf{u}^{(n+1)} - \mathbf{u}^{(n)}}{\Delta t} - \mathbf{K}_c \mathbf{u}_w^{(n+1)} = \mathbf{0} \quad (6.6)$$

6.2 Representation of uncertain soil properties

while, by multiplying both sides of eq. (6.6) with the timestep Δt , the following expression is derived:

$$\mathbf{C}^T \mathbf{u}^{(n+1)} - \Delta t \mathbf{K}_c \mathbf{u}_w^{(n+1)} = \mathbf{C}^T \mathbf{u}^{(n)} \quad (6.7)$$

Combining all the above equations the combined set of consolidation equations is expressed in the compact matrix form:

$$\begin{bmatrix} \mathbf{K}_m & \mathbf{C} \\ \mathbf{C}^T & -\Delta t \mathbf{K}_c \end{bmatrix} \begin{Bmatrix} \mathbf{u}^{(n+1)} \\ \mathbf{u}_w^{(n+1)} \end{Bmatrix} = \begin{Bmatrix} \mathbf{f}^{(n+1)} \\ \mathbf{C}^T \mathbf{u}^{(n+1)} \end{Bmatrix} \quad (6.8)$$

The extensive magnitude difference between the permeability coefficient k and Young's modulus E may lead to an ill-conditioned coefficient matrix on the left-hand side of the linear equation system of eq. (6.8). Ill-conditioning is even worse in stochastic finite elements analyses with large variations of k . To overcome this, a technique proposed in (Reed, 1984), which improves the condition number of the coefficient matrix, is used; the coupled set of equations is written as:

$$\begin{bmatrix} \mathbf{K}_m & s\mathbf{C} \\ s\mathbf{C}^T & -s^2\Delta t \mathbf{K}_c \end{bmatrix} \begin{Bmatrix} \mathbf{u}^{(n+1)} \\ \frac{1}{s}\mathbf{u}_w^{(n+1)} \end{Bmatrix} = \begin{Bmatrix} \mathbf{f}^{(n+1)} \\ s\mathbf{C}^T \mathbf{u}^{(n+1)} \end{Bmatrix} \quad (6.9)$$

where s is a scalar constant which renders \mathbf{K}_m and $-s^2\Delta t \mathbf{K}_c$ matrix entries of the same order of magnitude. This leads to increased stability in direct linear system solvers, as well as improved rate of convergence of iterative schemes.

6.2 Representation of uncertain soil properties

In general, Gaussian and non-Gaussian random fields have been used to represent uncertain material properties. Nevertheless, the Gaussian assumption is not valid for soil material properties which are strictly positive, such as the permeability coefficient k and the elastic modulus E , making the study of non-Gaussian stochastic fields essential for treating this limitation.

In this study, soil permeability coefficient k , as well as elastic modulus E are simulated as lognormal random fields in two dimensions. Thus, a robust and efficient procedure to generate the required random field realizations is needed. In general, various methods exist for simulation of random fields. The multi-dimensional spectral representation method (Shinozuka and Deodatis, 1996) and specifically the sum of

cosines version is considered here for its implementation simplicity, as well as its applicability in nonuniform finite element meshes.

6.2.1 Stochastic finite element analysis

It is assumed that the permeability coefficient k and the elastic modulus E are represented by two-dimensional uni-variate (2D-1V) homogeneous stochastic fields. The effect of k and E is examined separately in different Monte Carlo simulations. The midpoint method (Der Kiureghian and Ke, 1988) is used in order to derive the stochastic fluid conductivity matrix \mathbf{K}_c and the stochastic soil stiffness matrix \mathbf{K}_m . According to this, the spatially continuous soil property, such as k , is approximated by a single random variable $\hat{k}(x)$ defined as the value of the field at the centroid x_c of each finite element domain Ω_e :

$$\hat{k}(x) = k(x_c) \quad \forall x \in \Omega_e \quad (6.10)$$

As a result, each realization of the random property is piecewise constant and the discontinuities are localized at element boundaries. First, the spectral representation method described in section 3.2 is used to generate unit-variance zero mean homogeneous Gaussian fields at each finite element centroid and then, the following relations are used to calculate the lognormal parameters (Fenton and Griffiths, 2008):

$$v_k = \frac{\sigma_k}{\mu_k} \quad (6.11)$$

$$\sigma_{\ln(k)}^2 = \ln(1 + v_k^2) \quad (6.12)$$

$$\mu_{\ln(k)} = \ln(\mu_k) - \frac{1}{2}\sigma_{\ln(k)}^2 \quad (6.13)$$

Finally, the corresponding permeability k_i (equivalently for E_i) is calculated from the Gaussian G_i through the lognormal transformation by the following relation:

$$k_i = \exp(\mu_{\ln(k)} + \sigma_{\ln(k)}G_i) \quad (6.14)$$

Characteristic random field realizations of permeability coefficient k , indicating the influence of correlation length $b_{\ln(k)}$ and the COV on the simulated lognormal fields, are shown in figs. 6.1 and 6.2. As illustrated in both cases, smaller values of the correlation length parameter $b_{\ln(k)}$ lead to weakly correlated random field values compared to larger values, which result in strongly correlated fields. On the other hand, the COV value dictates the expected distance of the permeability values from

6.2 Representation of uncertain soil properties

the corresponding mean. As a result, random fields with $COV = 2.00$, illustrated in fig. 6.2 contain permeability values which in some cases are much larger or much smaller than the mean value, visualized with more vibrant color compared to the case of $COV = 0.25$ in fig. 6.1.

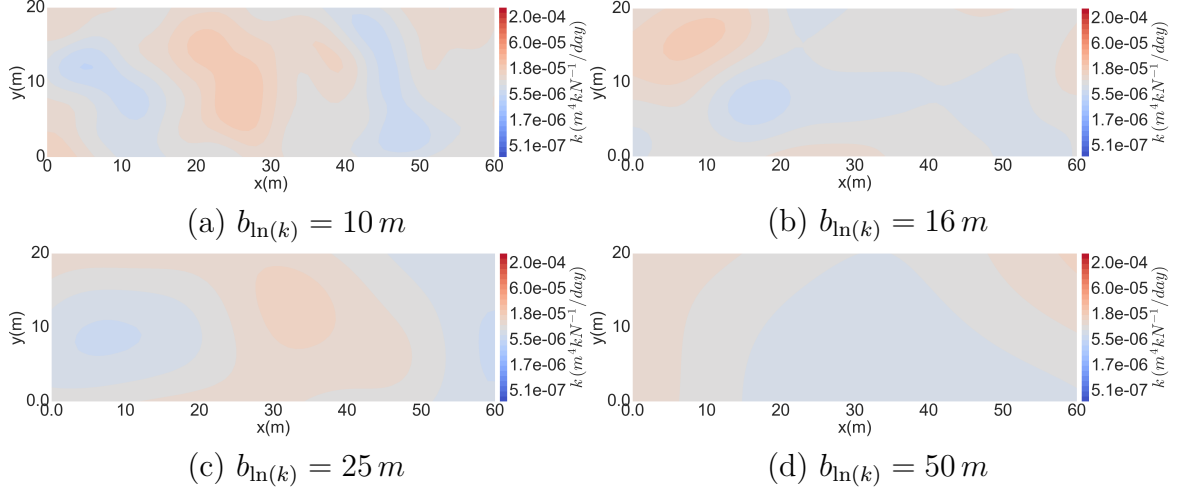


Figure 6.1. Random field realizations for $COV = 0.25$ and correlation parameter $b_{\ln(k)} = b1_{\ln(k)} = b2_{\ln(k)}$: (a) $10\ m$, (b) $16\ m$, (c) $25\ m$ and (d) $50\ m$.

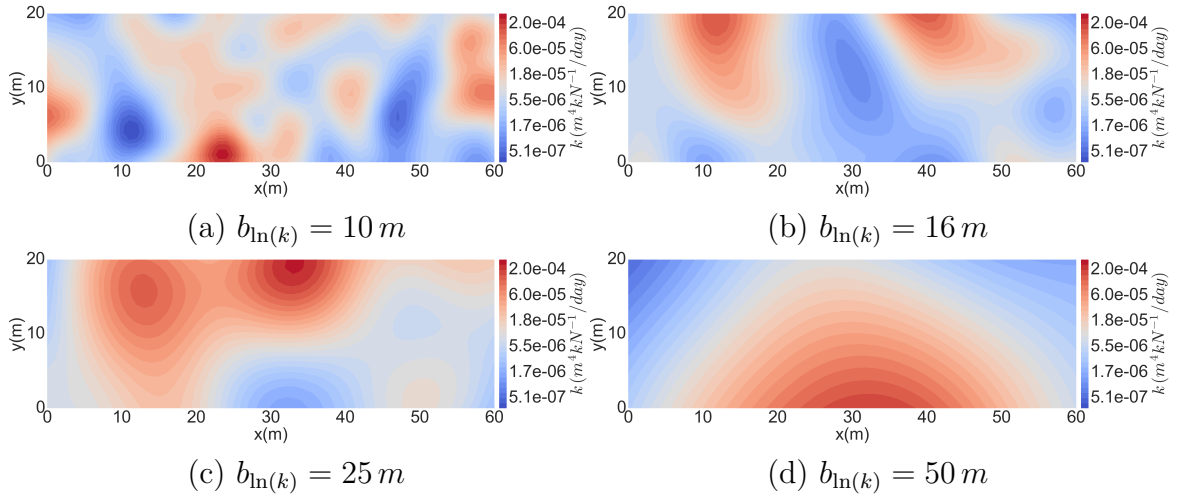


Figure 6.2. Random field realizations for $COV = 2.00$ and correlation parameter $b_{\ln(k)} = b1_{\ln(k)} = b2_{\ln(k)}$: (a) $10\ m$, (b) $16\ m$, (c) $25\ m$ and (d) $50\ m$.

In this study, a Gaussian type correlation structure is considered for the underlying Gaussian fields and its power spectral density function is given by:

$$S_{gg}(\kappa_1, \kappa_2) = \sigma_g^2 \frac{b_1 b_2}{4\pi^2} \exp\left(-\frac{1}{4\pi} \left((\kappa_1 b_1)^2 + (\kappa_2 b_2)^2\right)\right) \quad (6.15)$$

where σ_g denotes the standard deviation of the stochastic field and b_1, b_2 the correlation lengths the x and y axes, respectively.

6.3 Case Study

6.3.1 Description of the numerical example

The case study considered consists of a rigid, rough strip footing resting on a saturated soil layer. A uniform area load, which follows a ramp pattern over time, is applied on the footing. The finite element mesh used is depicted in fig. 6.3, the soil layer thickness is $H = 20\text{ m}$ and the footing width $B = 10\text{ m}$. In order to represent the horizontal extent of the soil layer, a total length of $L = 60\text{ m}$ is considered. Isoparametric 4-node quadrilateral elements are used for the discretization of soil and footing. Elements corresponding to soil have both displacement and pore pressure degrees of freedom (dofs) and make use of bilinear shape functions, while footing elements contain only displacement dofs. The problem is analyzed assuming plain strain conditions and a uniform mesh with all element edges equal to 1 m . The applied displacement boundary conditions consist of fixed displacements in x and y directions for the soil layer base and fixed x displacements for the vertical sides. The hydraulic boundary conditions consist of impervious conditions at the soil base and side nodes, while free drainage is allowed at the soil surface. The uniform area load p applied on the footing increases linearly from time 0 to time $t_0 = 25$ days and then remains constant at value $p_{max} = 1.0\text{ kN/m}^2$. Since the problem is linear elastic, the choice of a unit load allows generalization to different load magnitudes. Soil permeability coefficient k and elasticity modulus E are the stochastic parameters considered in the simulation, whereas the other soil and footing mechanical properties are constant throughout the analysis. The Poisson's ratio of the soil is $\nu = 0.3$ and footing material properties are $E = 20\text{ GPa}$ and $\nu = 0.4$. The permeability coefficient k is simulated as a lognormal random field with mean value $\mu_k = 1.22 \cdot 10^{-5}\text{ m}^4 \cdot \text{kN}^{-1}/\text{day}$. The elastic modulus E is also simulated as a lognormal random field with mean value $\mu_E = 622.7\text{ kPa}$. Different coefficients of variation are considered, $\text{COV} = \{0.25, 0.5, 1.0, 2.0, 5.0\}$ for both random soil properties. In addition, the correlation length parameters $b1_{\ln(k)} = b2_{\ln(k)} = b_{\ln(k)}$ for k and $b1_{\ln(E)} = b2_{\ln(E)} = b_{\ln(E)}$ for E , which dictate the autocorrelation distance of the simulated random fields, range from 4.0 m to 100.0 m . A variable time step is implemented to accelerate the time integration process, in order to simulate the consolidation phenomenon for a large time period and retain a reasonable computational

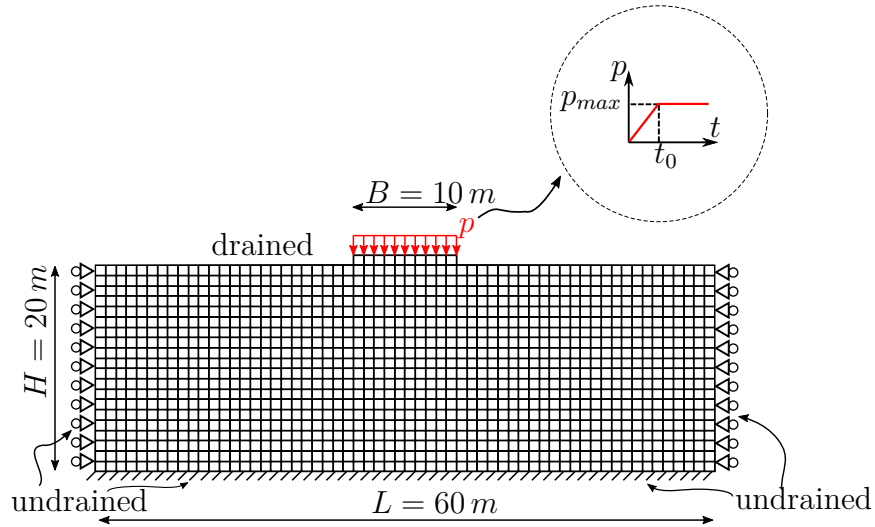


Figure 6.3. Finite element mesh of the model.

cost. Finally, a number of 1000 Monte Carlo analyses are executed for each COV-correlation length parameter pair.

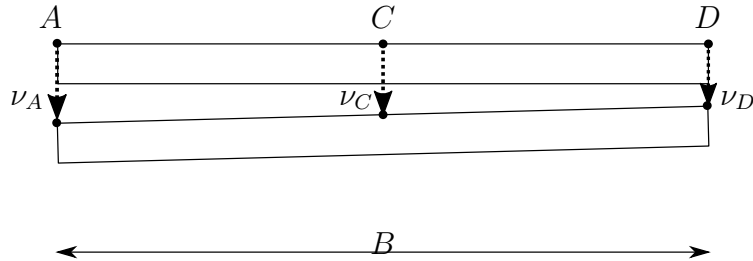


Figure 6.4. Footing settlements.

In fig. 6.4, points A and D correspond to the top left and top right footing points, while point C is the center of the top of the footing. The vertical displacements of A , C and D are denoted as ν_A , ν_B and ν_C respectively. Throughout this study, the term *differential footing settlement* is used corresponding to the absolute value of the vertical displacement difference of points A and D , i.e. $\Delta\nu = |\nu_A - \nu_D|$. Furthermore, the term *absolute settlement* is used to denote the vertical displacement of point C , i.e. ν_C .

Nodal displacements on top of the footing, as well as excess pore pressures along all the nodes below its center, are obtained from each Monte Carlo simulation analysis. Statistical processing of the response quantities leads to quantification of the influence of spatial variability of permeability k and elastic modulus E on the overall footing-soil system response.

6.3.2 On the choice of finite elements and model dimensions

In many consolidation applications throughout the scientific literature, researchers use quadrilateral 8-node isoparametric finite elements, where each node has displacement degrees of freedom, while only the 4 vertices have both displacement and pore pressure degrees of freedom. In this case study, quadrilateral 4-node isoparametric elements are used instead, in order to reduce the computational cost. To verify the accuracy obtained by the elements used, a comparison between the results obtained with 4-node and 8-node elements is made, where the two different formulations are denoted as **4U4P** and **8U4P**. To this purpose, the problem described in section 6.3 is simulated for the deterministic case with both formulations. The corresponding results are illustrated in fig. 6.5, a closer look at which reveals that the choice of the **4U4P** quadrilateral elements provides sufficient accuracy, while retaining a relatively low computational cost.

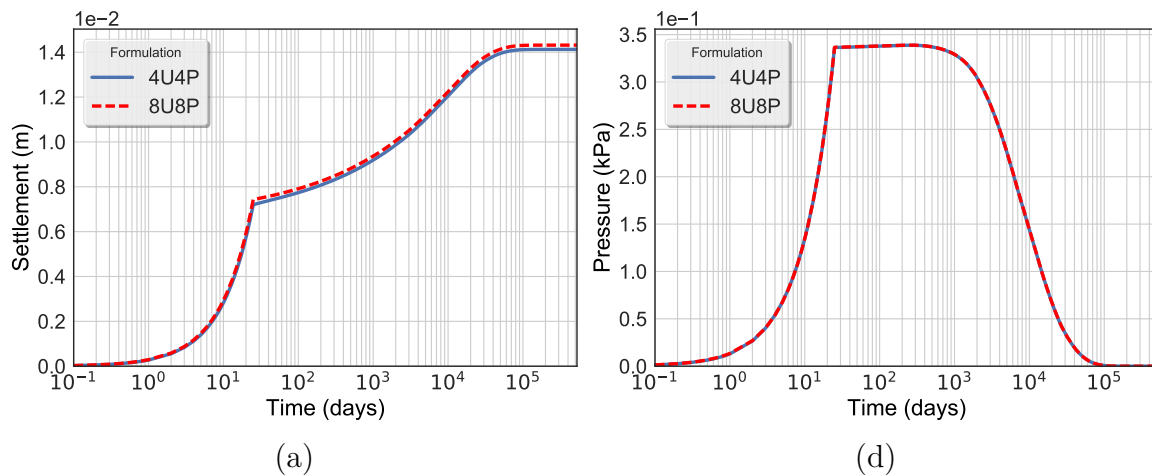


Figure 6.5. Comparison of results between **4U4P** and **8U8P** quadrilateral element formulations, where: (a) Settlement of footing center and (b) Excess pore pressure at depth $B/2$.

An additional modeling assumption requiring validation is the horizontal dimension of the model L shown in fig. 6.3, which has to be large enough so that its effect on the footing-soil response is diminished. To this purpose, a parametric study has been performed, where different choices of L are made and the resulting footing-soil responses are compared. By inspecting fig. 6.6, it is clear that the choice of $L = 60 m$ gives satisfying results, and is therefore used to reduce the computational cost.

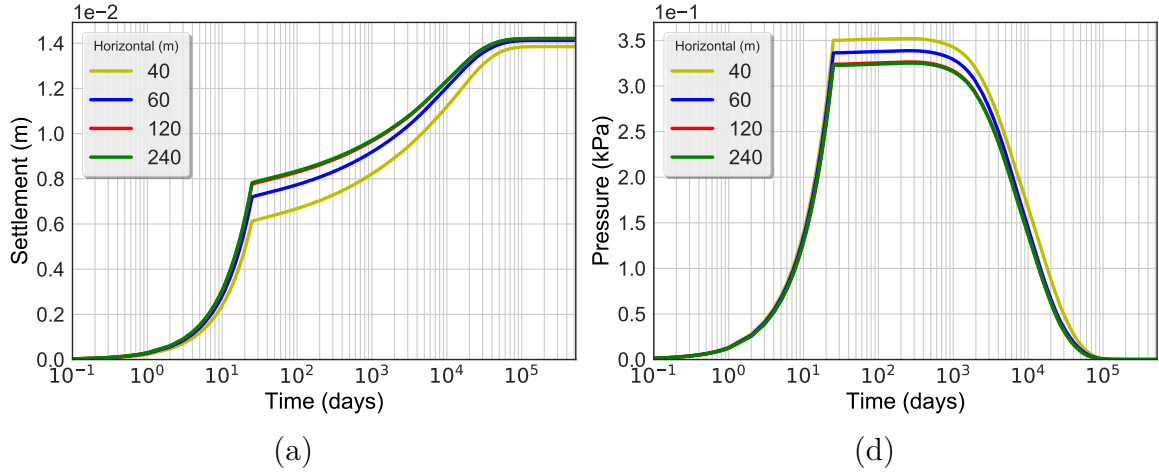


Figure 6.6. Comparison of the footing-soil response for different choices of the horizontal model dimension L , where: (a) Settlement of footing center and (b) Excess pore pressure at depth $B/2$.

6.3.3 Discussion of results

6.3.3.1 Footing settlement

In this section, footing settlements resulting from the Monte Carlo analyses are discussed.

The influence of the correlation length parameter $b_{\ln(k)} = b_{1\ln(k)} = b_{2\ln(k)}$, considered equal in both dimensions, as well as of the COV on the mean differential footing settlement, is illustrated in fig. 6.7. It is clear that larger COV values lead to greater differential settlements overall. By comparing the results to the corresponding case of variable E shown in fig. 6.8, it is also evident that the magnitude of the differential settlement is much larger in the stochastic E case. As a result, the footing-soil system is much more sensitive to the variability of the elastic modulus E . In addition, the pattern of the time evolution of the differential settlement is completely different in the case of spatially variable elastic modulus. When considering a random permeability k , the differential settlement first reaches a peak value and then gradually tends to zero as excess pore pressures dissipate, a fact amply illustrated in fig. 6.7. In the stochastic E case though, the differential settlements remain throughout the consolidation phenomenon and increase monotonically over time as shown in fig. 6.8.

What's more, as b increases, the magnitude of differential settlement increases up to $b_{\ln(k)} = 10 m$ for k and $b_{\ln(E)} = 16 m$ for E , and then gradually decreases. This is verified by inspection of figs. 6.11 and 6.12, where the convergence of maximum differential settlements with increasing number of Monte Carlo simulations is demonstrated. Larger

COV values correspond to greater standard deviation of the maximum differential settlements, as shown in figs. 6.13 and 6.14. It is important to emphasize that, the differential settlement for the deterministic case of the same problem is zero throughout the consolidation process, since the problem examined is symmetric in geometry and loading.

In order to demonstrate the validity of the Monte Carlo method in terms of differential settlements, figs. 6.11 to 6.14 illustrate the convergence of both mean and standard deviation of the maximum differential settlement with respect to the number of MCS analyses performed. It is thus obvious that the 1000 simulations performed give satisfactory convergence.

Next, we examine the influence of spatial variability of permeability k and elastic modulus E in terms of settlements of the footing center. Time evolution of the settlements of footing center is illustrated in figs. 6.15 and 6.16. Direct comparison between the mean value μ_{ν_C} , the median $\tilde{\nu}_C$ and the values corresponding to $\mu_{\nu_C} \pm \sigma_{\nu_C}$ follow. Observing these, it is evident that the deviation from the mean response becomes greater as COV increases. In addition, the median value of the absolute settlement $\tilde{\nu}_C$ is identical to the mean for small COV values, while it starts to deviate for larger COV values. The corresponding results for the footing edge points are identical and are therefore not illustrated. In any case, the influence of spatial variability of k , as well as E is less dramatic compared to the differential settlements.

Additionally, the distributions of maximum value of differential footing settlements are plotted in figs. 6.17 and 6.18, whereas maximum settlements of the footing center are shown in figs. 6.19 and 6.20. In the differential settlements case, the histogram is skewed and thus, a lognormal distribution is fitted and presented with red color. Regarding the settlements of the footing center though, the values corresponding to the stochastic permeability case are concentrated around a particular value for each COV case as illustrated in fig. 6.19, indicating that the maximum settlement of the footing center is not affected by the variation of the permeability. The situation is different when considering the maximum settlement of the footing center for the stochastic elastic modulus as shown in fig. 6.20, where the distribution resembles a Gaussian one and the resulting fit is marked with red color.

Examination of the sensitivity of the mean and STD of the max differential footing settlements to the normalized correlation parameter b/B (where B is the footing width) leads to the most important finding of the analysis. Observing fig. 6.21, it is clear that a peak of the mean value of the max differential settlement coincides with values of $b_{\ln(k)}/B$ close to unity for the case of variable k , regardless of the COV value; the same

6.3 Case Study

is true for the STD of the max differential settlement. Regarding the spatial variability of E , the maximum mean and STD values of the max differential settlement are obtained for values of $b_{ln(E)}/B$ ranging from 1.5 to 2.5 as shown in fig. 6.22. This leads to the conclusion that, the footing response with respect to the differential settlement is worse for a critical value of correlation parameter $b_{ln(k)}$ equal to the footing width B when the variability of k is considered, and for a larger value close to $b_{ln(E)} = 1.5B$ when considering variability of E .

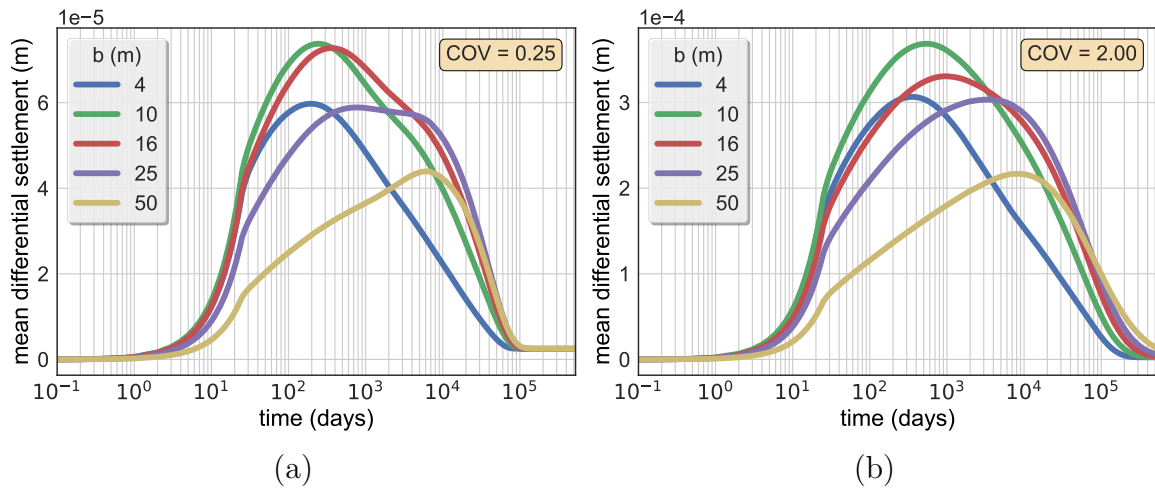


Figure 6.7. Mean differential settlement vs time for stochastic permeability k and COV values: (a) 0.25 and (b) 2.00.

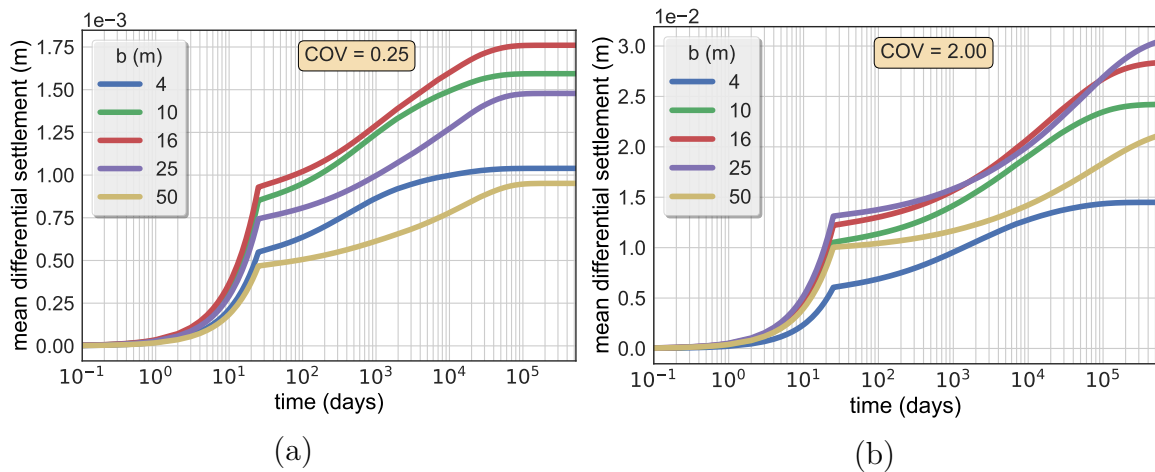


Figure 6.8. Mean differential settlement vs time for stochastic elastic modulus E and COV values: (a) 0.25 and (b) 2.00.

Consolidation of a soil layer with stochastic material properties

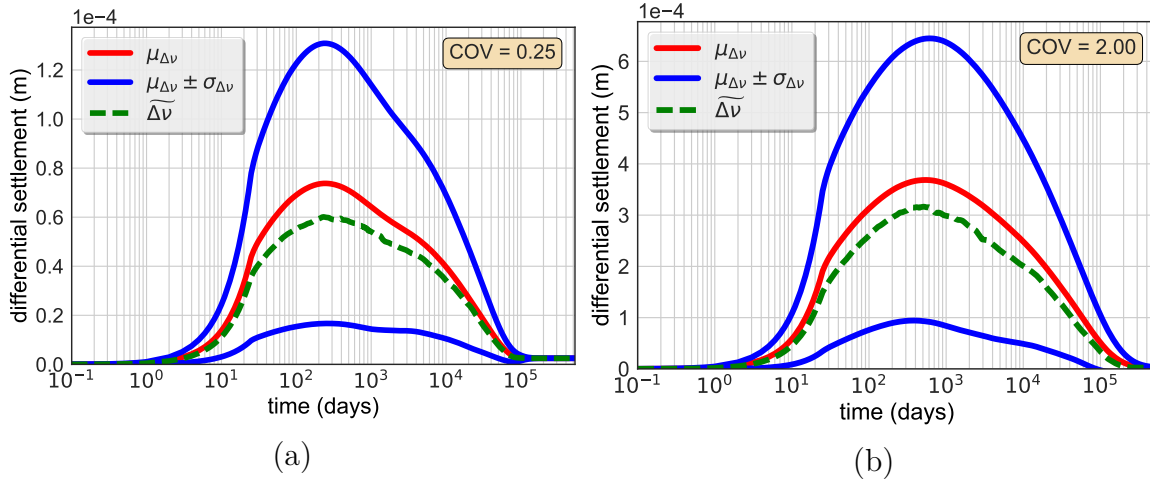


Figure 6.9. Monte Carlo results of differential footing settlement for stochastic permeability with $b_{ln(k)} = 10\text{ m}$ and COV values: (a) 0.25 and (b) 2.00.

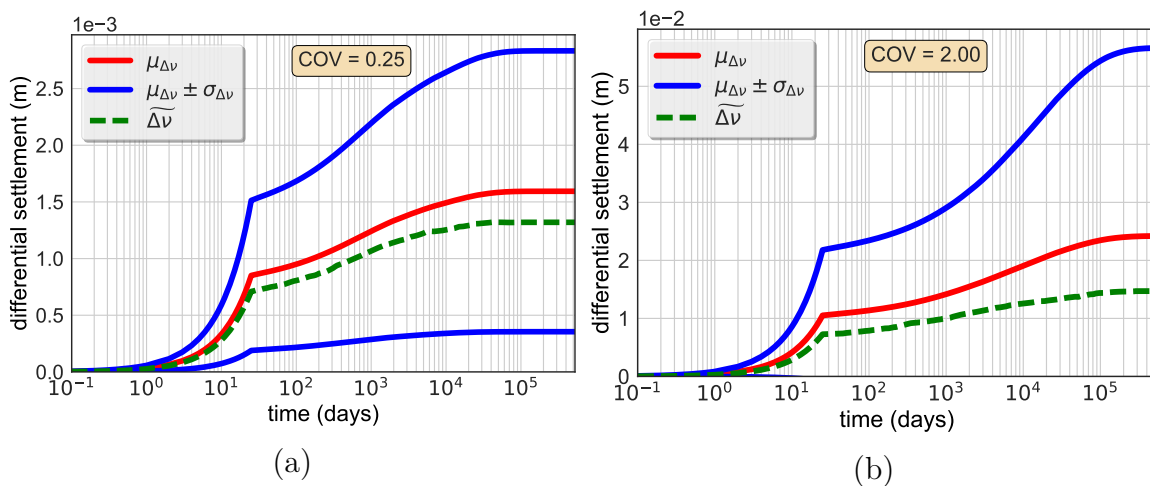


Figure 6.10. Monte Carlo results of differential footing settlement for stochastic elastic modulus with $b_{ln(E)} = 10\text{ m}$ and COV values: (a) 0.25 and (b) 2.00.

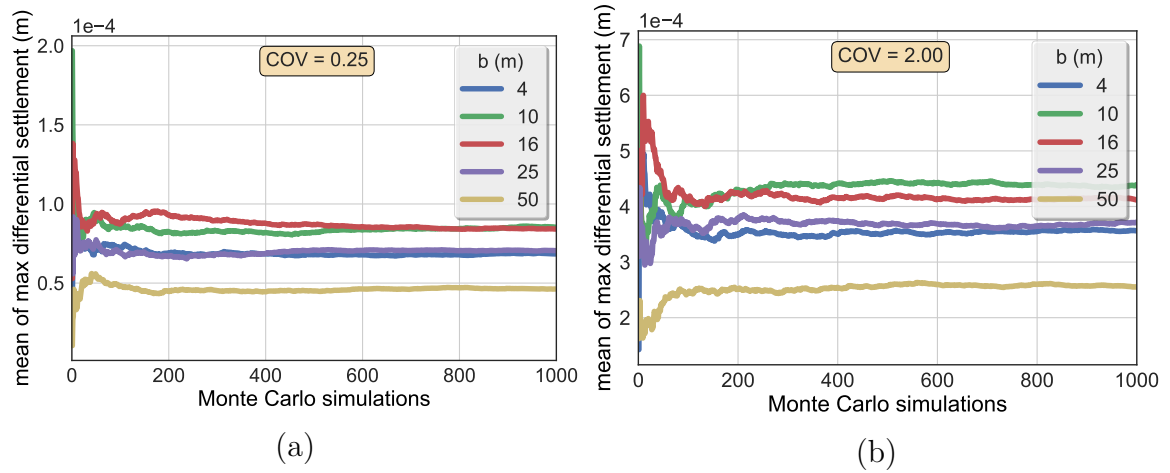


Figure 6.11. Mean of max differential settlement vs Monte Carlo simulations for stochastic permeability k and COV values: (a) 0.25 and (b) 2.00.

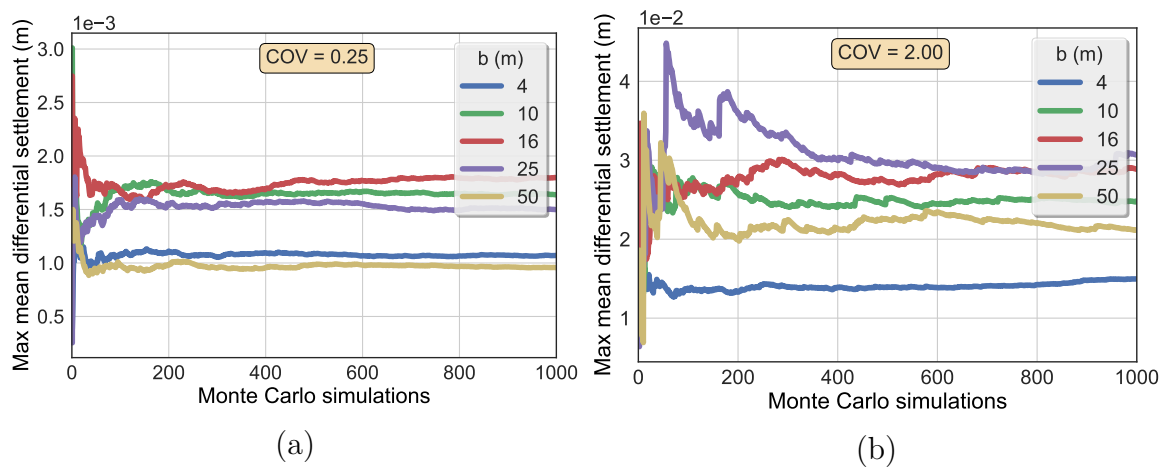


Figure 6.12. Mean of max differential settlement vs Monte Carlo simulations for stochastic elastic modulus E and COV values: (a) 0.25 and (b) 2.00.

Consolidation of a soil layer with stochastic material properties

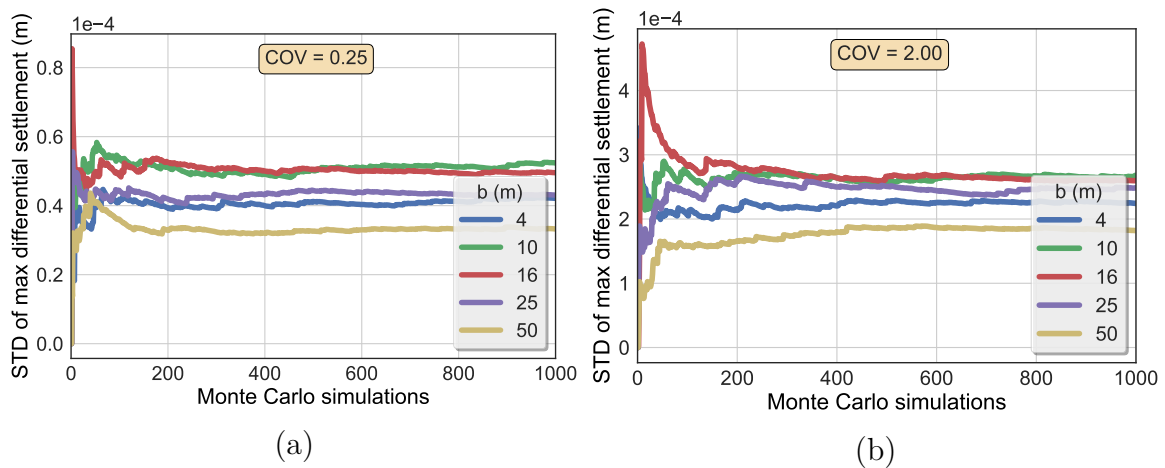


Figure 6.13. STD of max differential settlement vs Monte Carlo simulations for stochastic permeability k and COV values: (a) 0.25 and (b) 2.00.

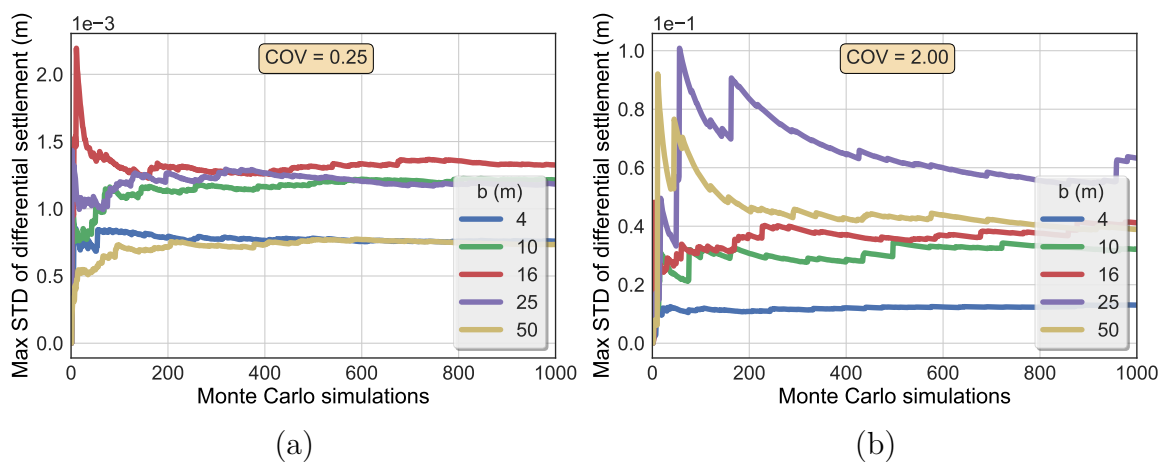


Figure 6.14. STD of max differential settlement vs Monte Carlo simulations for stochastic elastic modulus E and COV values: (a) 0.25 and (b) 2.00.

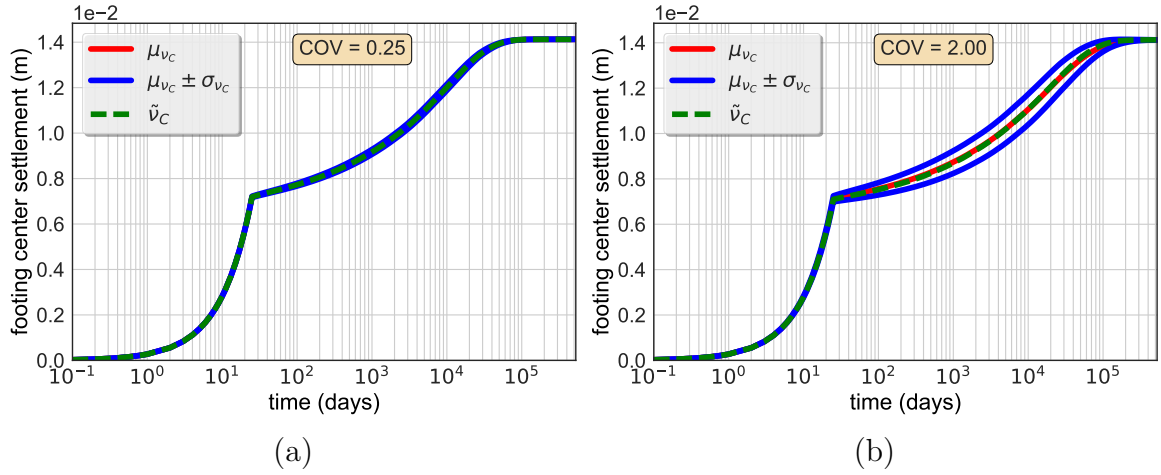


Figure 6.15. Monte Carlo results of footing center settlement for stochastic permeability with $b_{\ln(k)} = 10\text{ m}$ and COV values: (a) 0.25 and (b) 2.00.

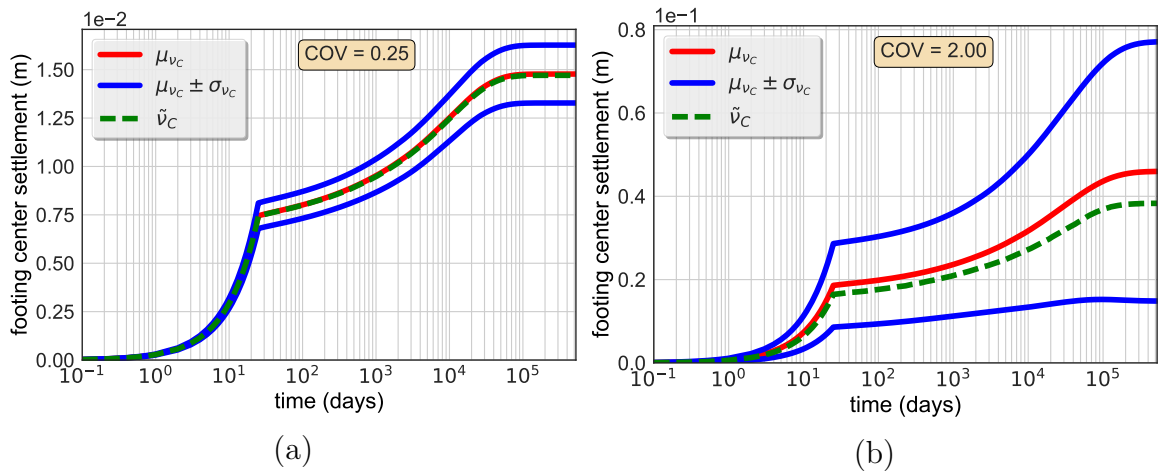


Figure 6.16. Monte Carlo results of footing center settlement for stochastic elastic modulus with $b_{\ln(E)} = 10\text{ m}$ and COV values: (a) 0.25 and (b) 2.00.

Consolidation of a soil layer with stochastic material properties

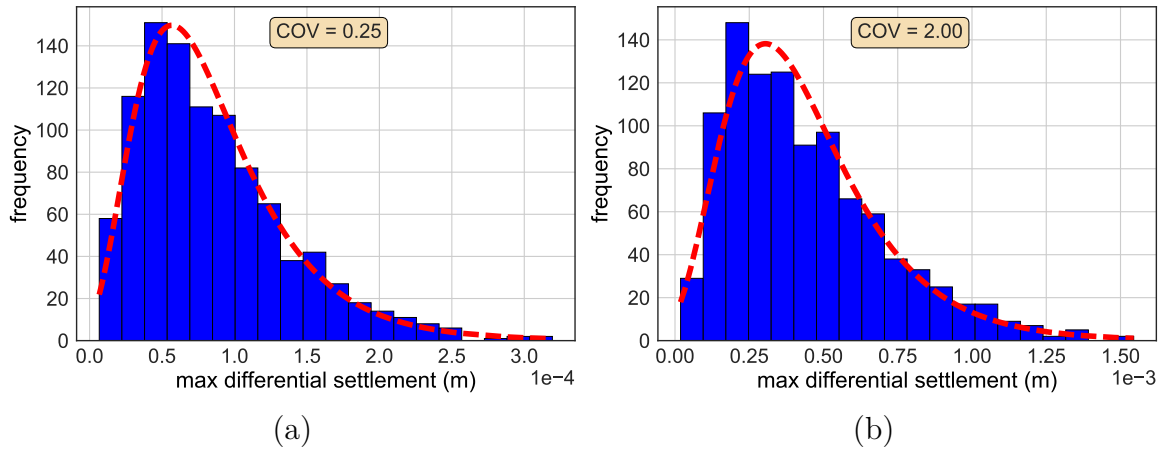


Figure 6.17. Histogram of maximum footing differential settlement and fitted lognormal distribution for stochastic permeability with $b_{\ln(k)} = b_{1\ln(k)} = b_{2\ln(k)} = 10 m$ and COV values: (a) 0.25 and (b) 2.00.

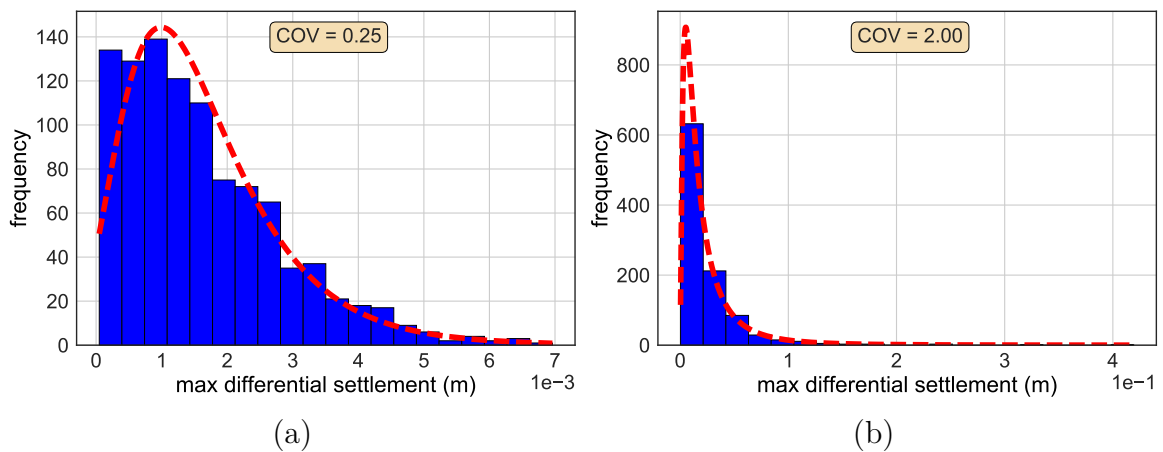


Figure 6.18. Histogram of maximum footing differential settlement and fitted lognormal distribution for stochastic elastic modulus with $b_{\ln(E)} = b_{1\ln(E)} = b_{2\ln(E)} = 10 m$ and COV values: (a) 0.25 and (b) 2.00.

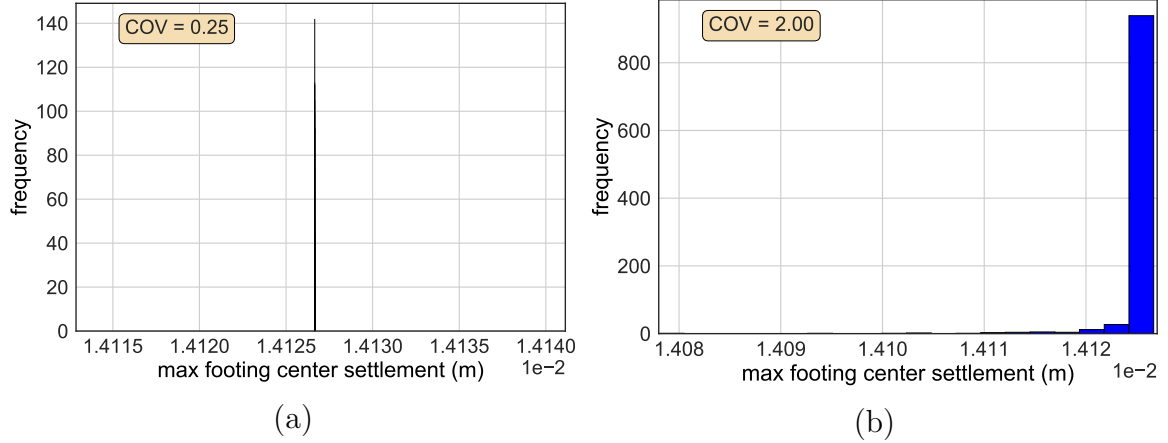


Figure 6.19. Histogram of maximum footing center settlement and fitted Gaussian distribution for stochastic permeability with $b_{\ln(k)} = b_{1_{\ln(k)}} = b_{2_{\ln(k)}} = 10\text{ m}$ and COV values: (a) 0.25 and (b) 2.00.

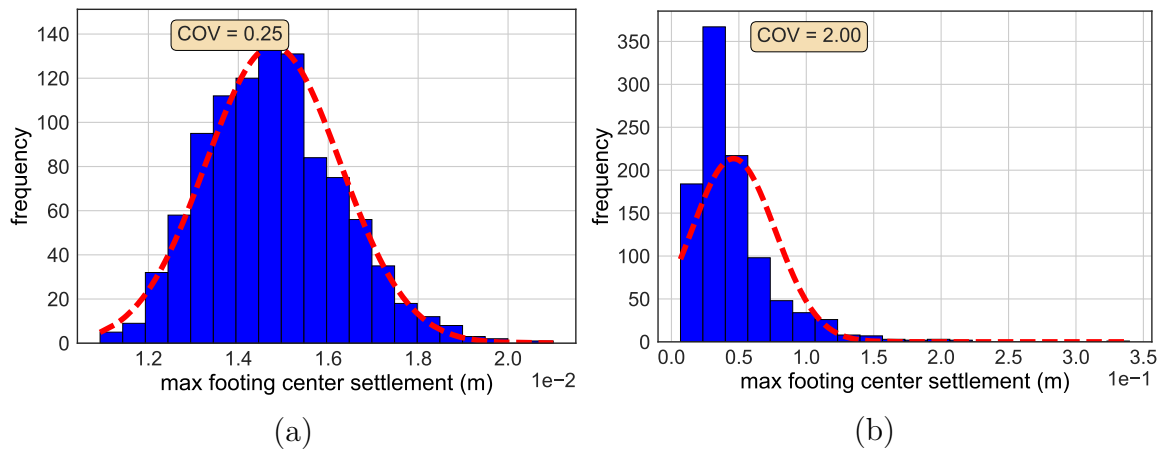


Figure 6.20. Histogram of maximum footing center settlement and fitted Gaussian distribution for stochastic elastic modulus with $b_{\ln(E)} = b_{1_{\ln(E)}} = b_{2_{\ln(E)}} = 10\text{ m}$ and COV values: (a) 0.25 and (b) 2.00.

Consolidation of a soil layer with stochastic material properties

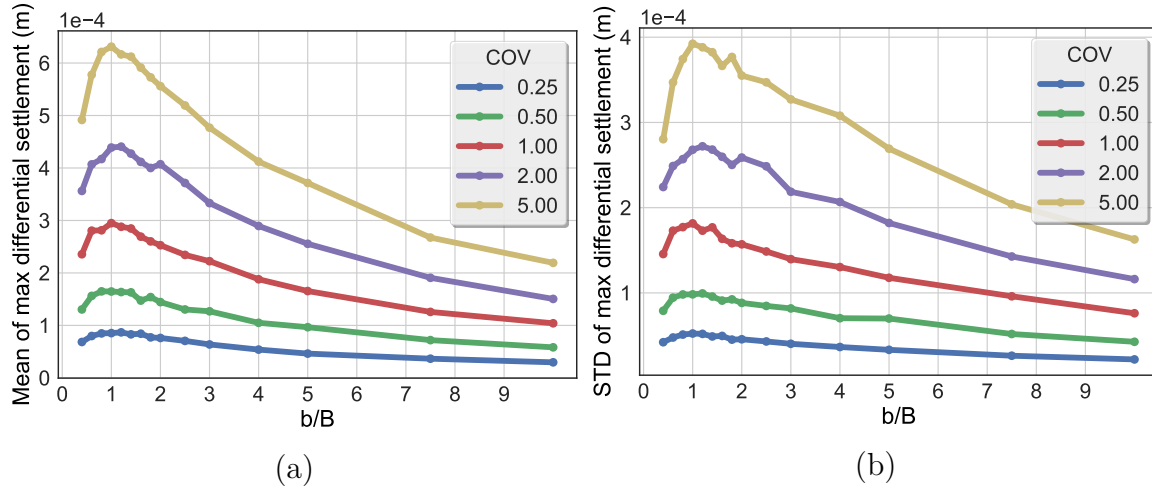


Figure 6.21. a) Mean and b) STD of maximum differential settlement vs normalized correlation parameter $b_{\ln(k)}/B$ for stochastic permeability, where $b_{\ln(k)} = b1_{\ln(k)} = b2_{\ln(k)}$ and B the footing width.

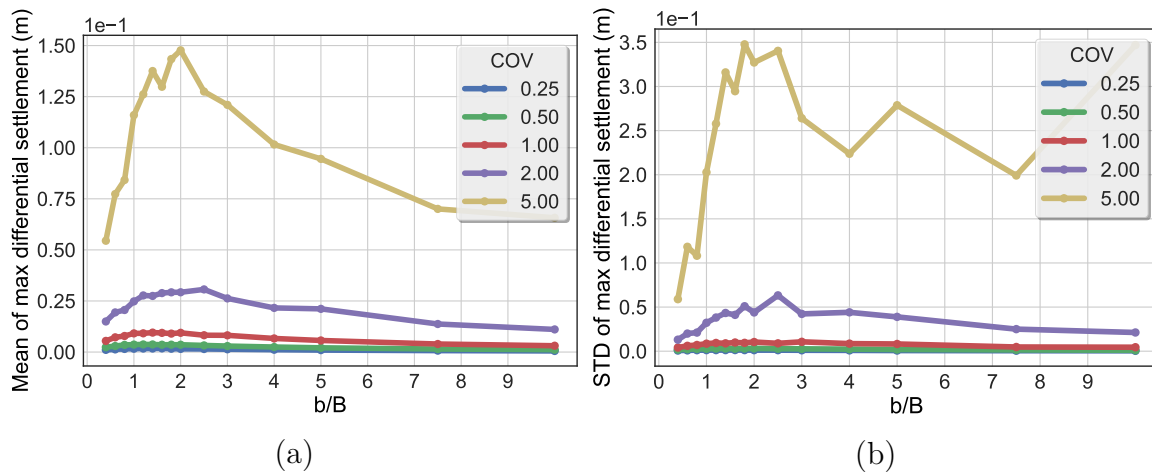


Figure 6.22. a) Mean and b) STD of maximum differential settlement vs normalized correlation parameter $b_{\ln(E)}/B$ for stochastic elastic modulus, where $b_{\ln(E)} = b1_{\ln(E)} = b2_{\ln(E)}$ and B the footing width.

6.3.3.2 Pore pressures

In this subsection, the response of the loaded soil in terms of excess pore pressure generation is analyzed. All nodes below the footing center are monitored in every Monte Carlo analysis. Four characteristic points in depths $B/10$, $B/5$, $B/2$ and B from the soil surface are examined, where B is the footing width.

First, by inspecting figs. 6.23 and 6.25, it can be seen that the mean of the excess pore pressure is largely insensitive to correlation length parameter b , as well as to the COV value of the permeability k . This is also true when considering spatial variability of the elastic modulus E illustrated in figs. 6.23 and 6.25; the situation is similar for points in depth $B/5$ and B which are not shown.

Only a very slight deviation from the mean is evident for small COV values regardless of the depth from the soil surface. The median of the pore pressure for $b_{\ln(k)} = 10\text{ m}$, shown in figs. 6.27 and 6.29, starts to deviate from the mean curve for large COV values of k . The deviation, also evident in the case of spatially variable elastic modulus, is depicted in figs. 6.28 and 6.30. However, it is important to notice that for large coefficients of variation, the max excess pore pressure generated at depth $B/10$ exceeds in many cases the value of the maximum applied load $p_{max} = 1.0\text{ kPa}$ for variable both k and E .

Unlike the response of the differential settlements of fig. 6.21, the mean and STD of the maximum pressure, depicted in figs. 6.31 to 6.34, follow no general pattern regarding the influence of the correlation length parameter $b_{\ln(k)}$. On the contrary, when considering random E , it becomes clear that the mean and STD of the maximum pore pressure at the various studied depths are maximized for small correlation lengths, while tending to stabilize for large $b_{\ln(E)}$ as shown in figs. 6.32 and 6.34.

Finally, histograms of the maximum values of the resulting pressures are presented in figs. 6.35, 6.37, 6.39 and 6.41 for stochastic permeability k and figs. 6.36, 6.38, 6.40 and 6.42 for stochastic Young's modulus E . For depth $B/10$ a Gaussian distribution is fitted, while for depths $B/5$, $B/5$ and B , a lognormal distribution gives a better fit for both k and E .

Consolidation of a soil layer with stochastic material properties

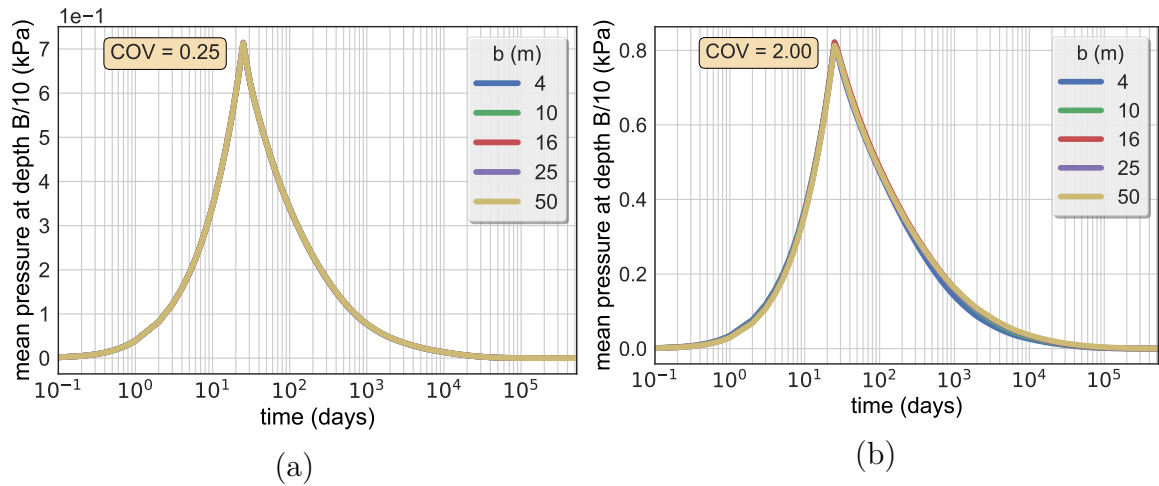


Figure 6.23. Mean excess pore pressure at depth $B/10$ vs time for stochastic permeability k and COV values: (a) 0.25 and (b) 2.00.

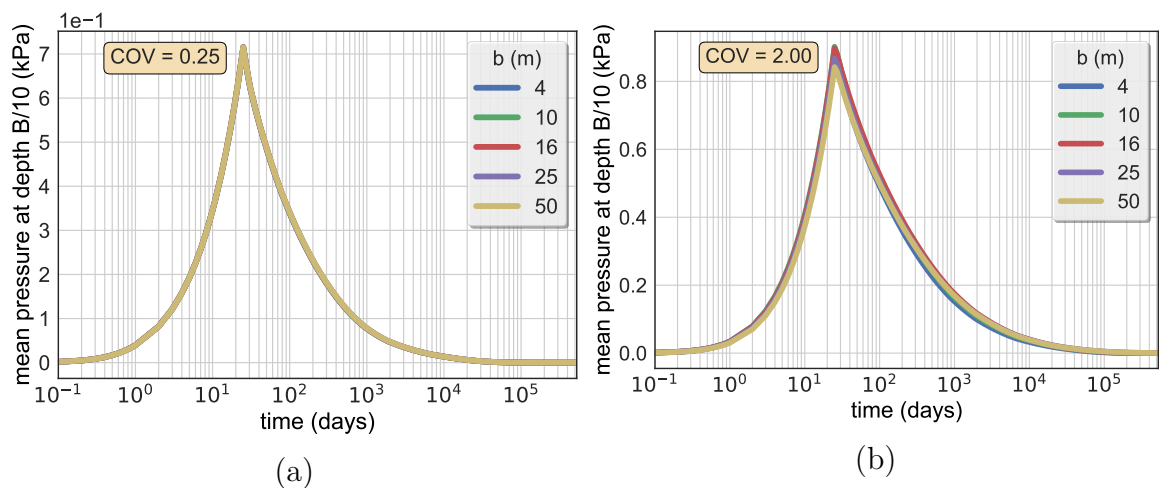


Figure 6.24. Mean excess pore pressure at depth $B/10$ vs time for stochastic Young's modulus E and COV values: (a) 0.25 and (b) 2.00.

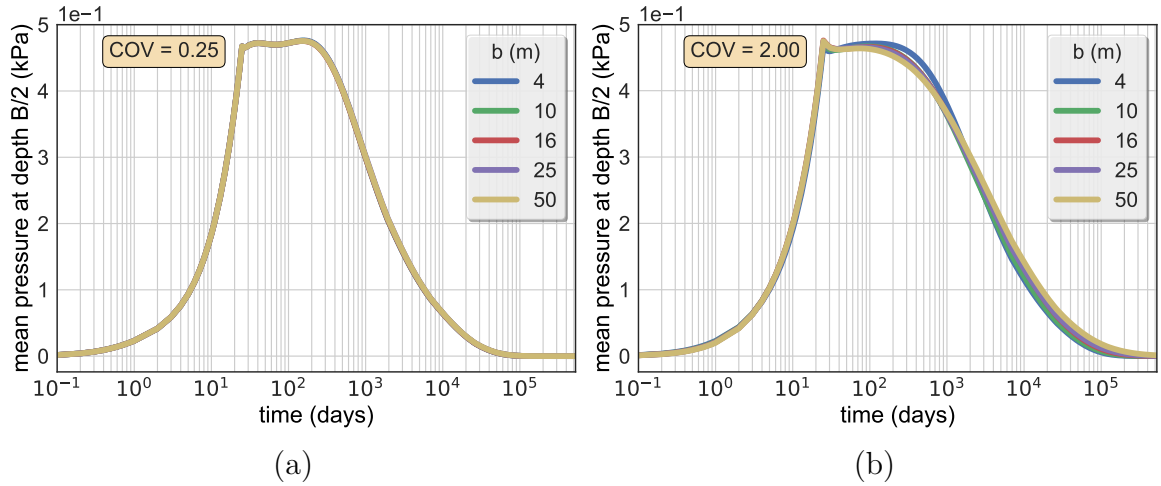


Figure 6.25. Mean excess pore pressure at depth $B/2$ vs time for stochastic permeability k and COV values: (a) 0.25 and (b) 2.00.

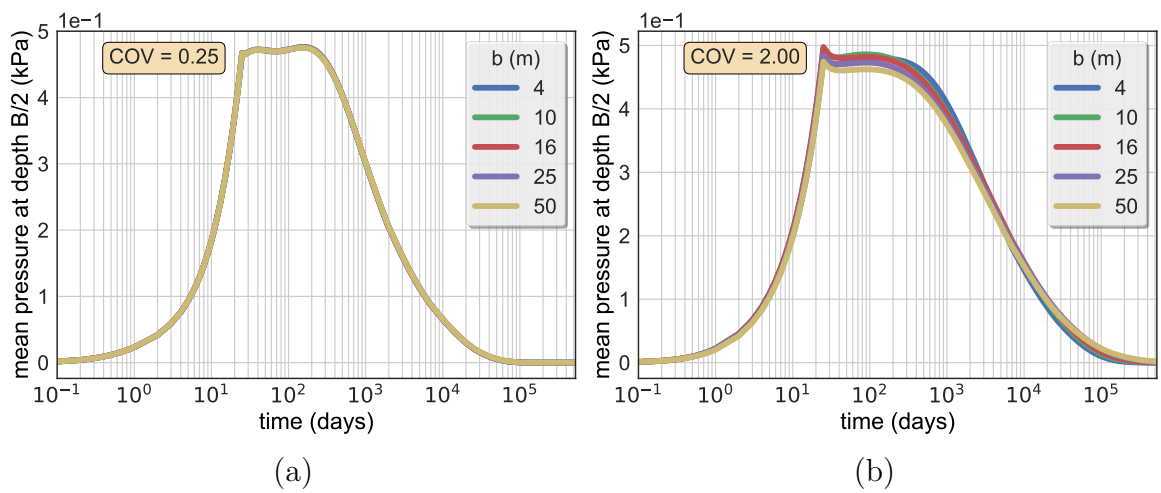


Figure 6.26. Mean excess pore pressure at depth $B/2$ vs time for stochastic Young's modulus E and COV values: (a) 0.25 and (b) 2.00.

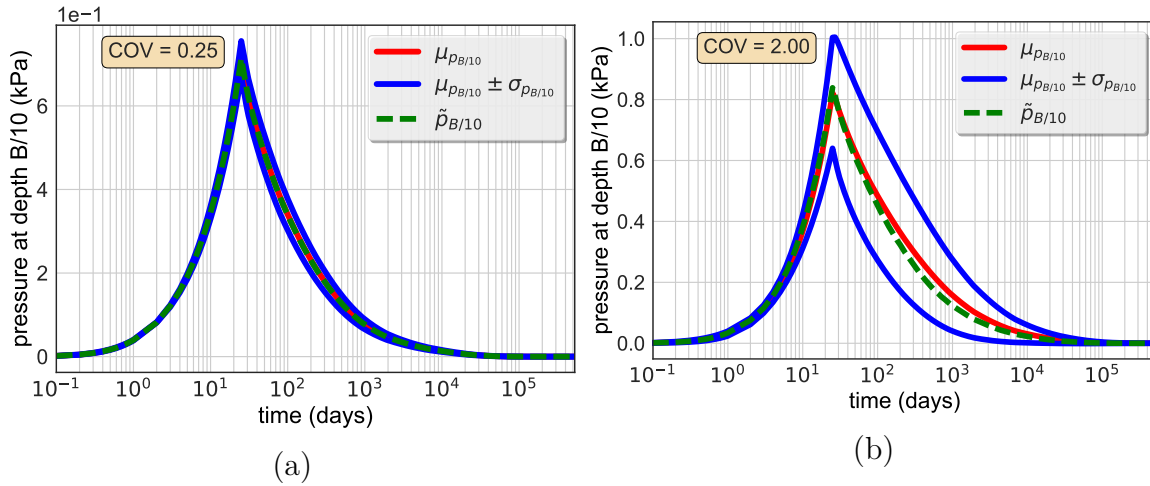


Figure 6.27. Excess pore pressure at depth $B/10$ vs time for stochastic permeability with $b_{\ln(k)} = 10$ m and COV values: (a) 0.25 and (b) 2.00.

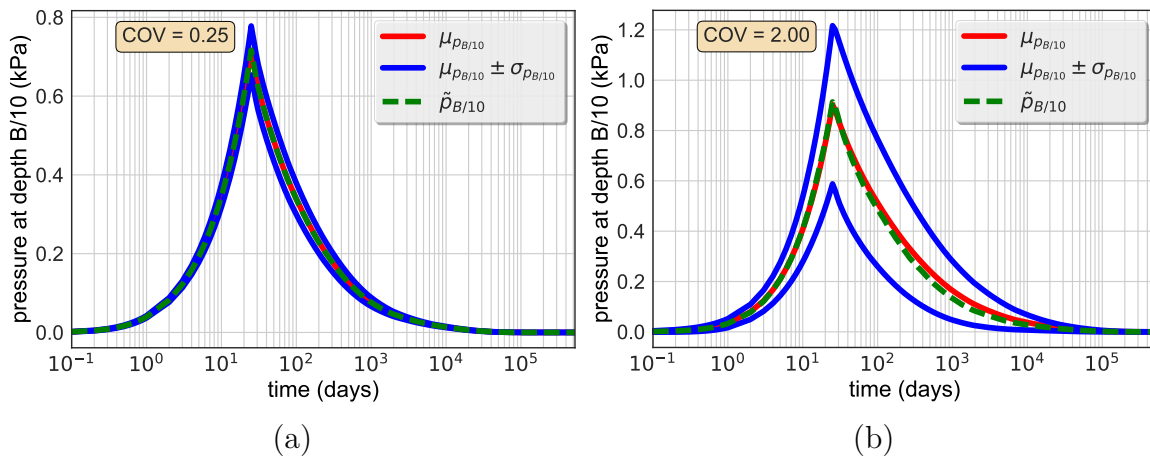


Figure 6.28. Excess pore pressure at depth $B/10$ vs time for stochastic elastic modulus with $b_{\ln(E)} = 10$ m and COV values: (a) 0.25 and (b) 2.00.

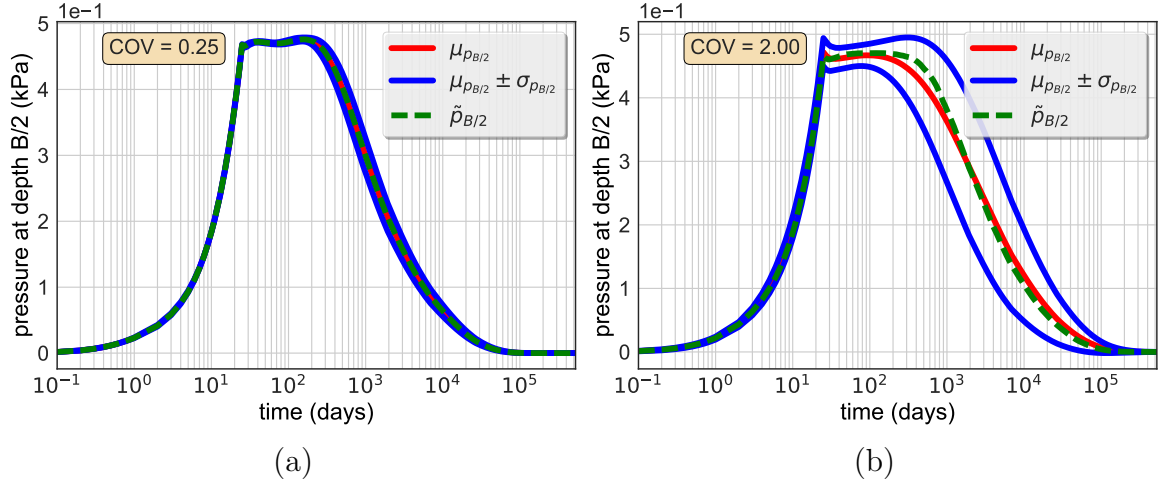


Figure 6.29. Excess pore pressure at depth $B/2$ vs time for stochastic permeability with $b_{\ln(k)} = 10\text{ m}$ and COV values: (a) 0.25 and (b) 2.00.

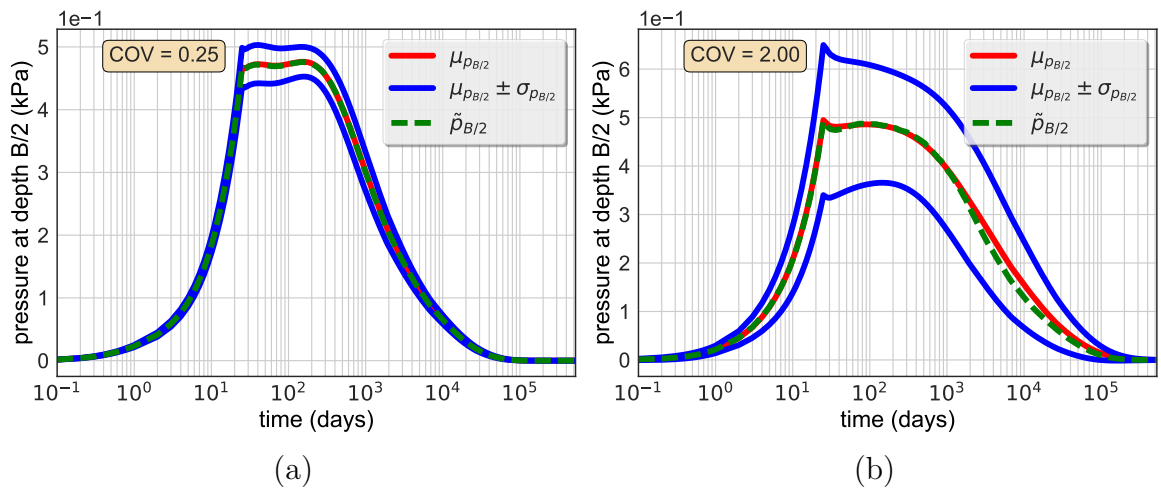


Figure 6.30. Excess pore pressure at depth $B/2$ vs time for stochastic elastic modulus with $b_{\ln(E)} = 10\text{ m}$ and COV values: (a) 0.25 and (b) 2.00.

Consolidation of a soil layer with stochastic material properties

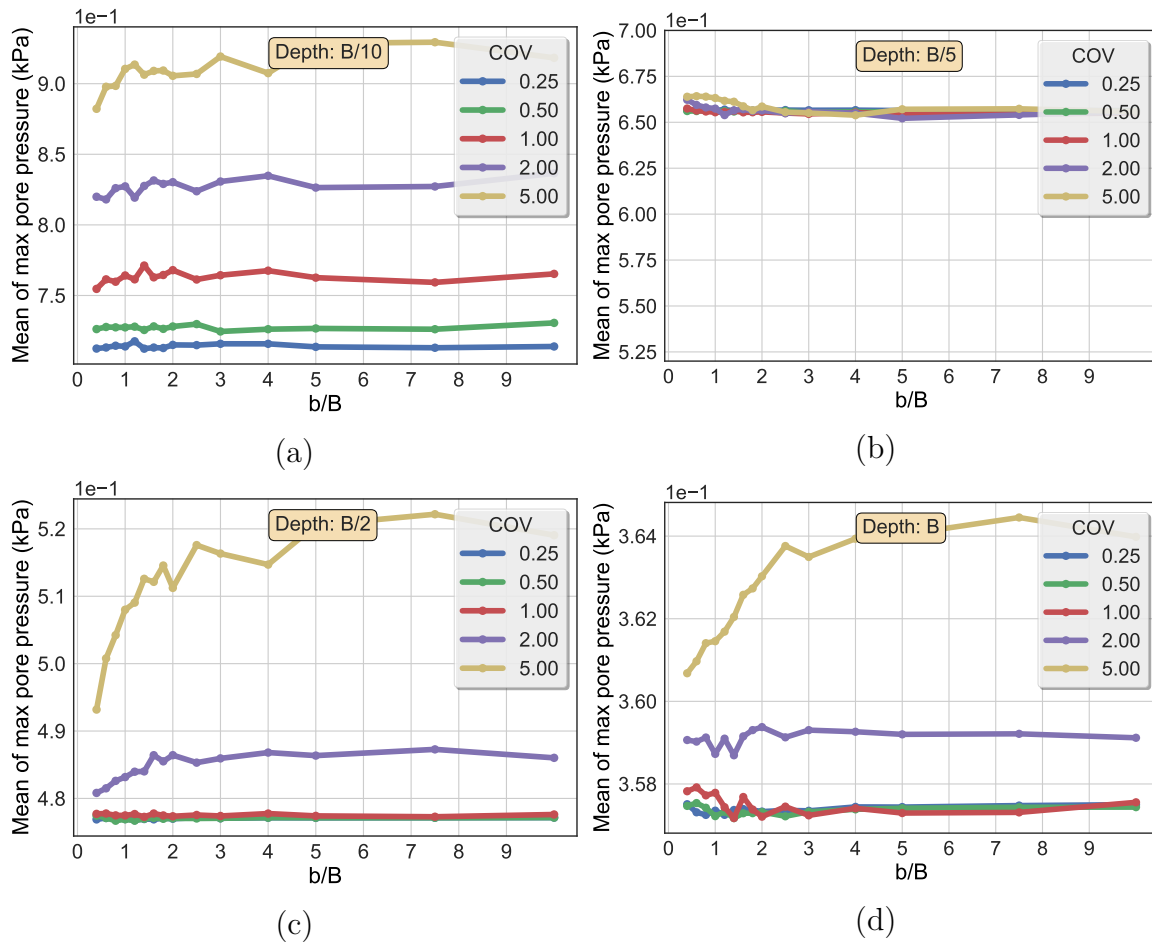


Figure 6.31. Mean of maximum excess pore pressure vs normalized correlation parameter $b_{\ln(k)}/B$ for stochastic permeability k and depth: (a) $B/10$, (b) $B/5$, (c) $B/2$ and (d) B .

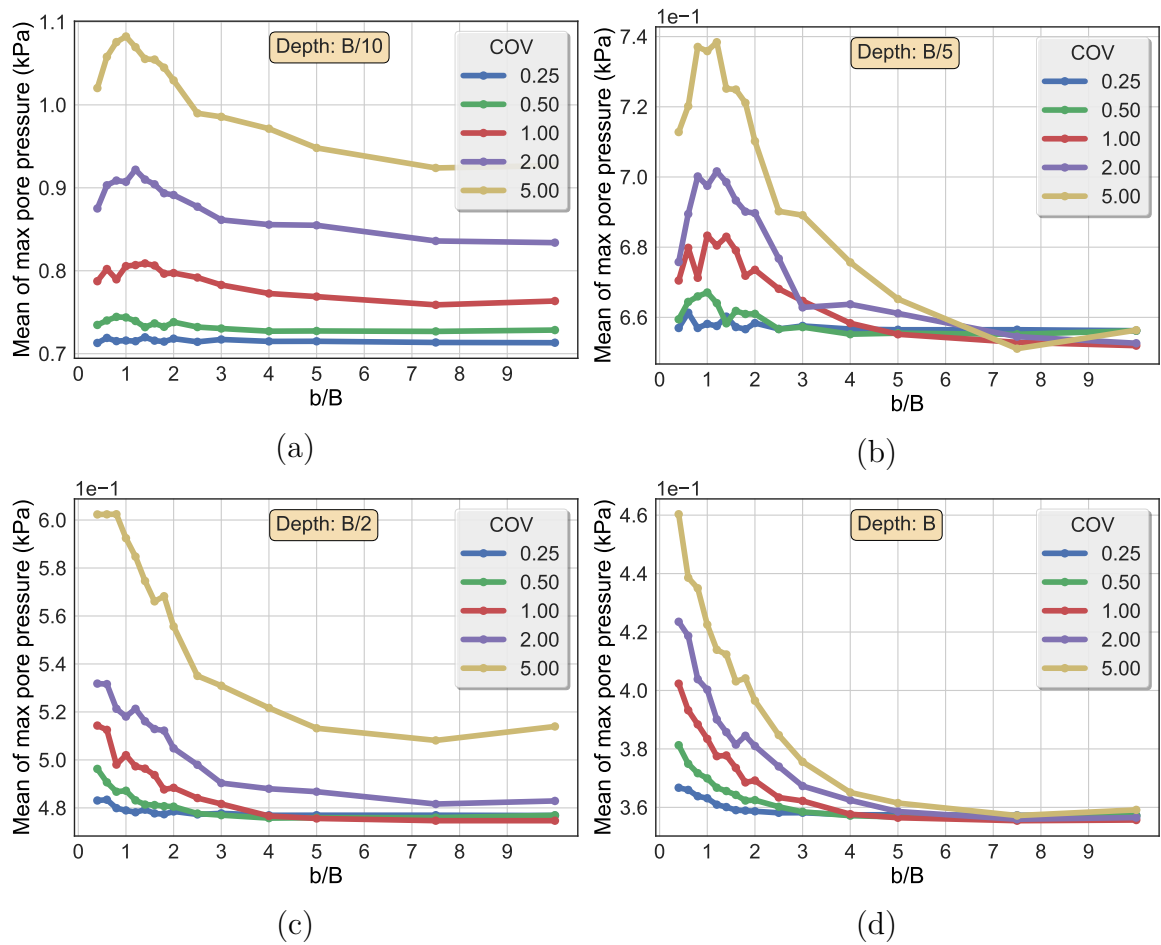


Figure 6.32. Mean of maximum excess pore pressure vs normalized correlation parameter $b_{\ln(E)}/B$ for stochastic elastic modulus E and depth: (a) $B/10$, (b) $B/5$, (c) $B/2$ and (d) B .

Consolidation of a soil layer with stochastic material properties

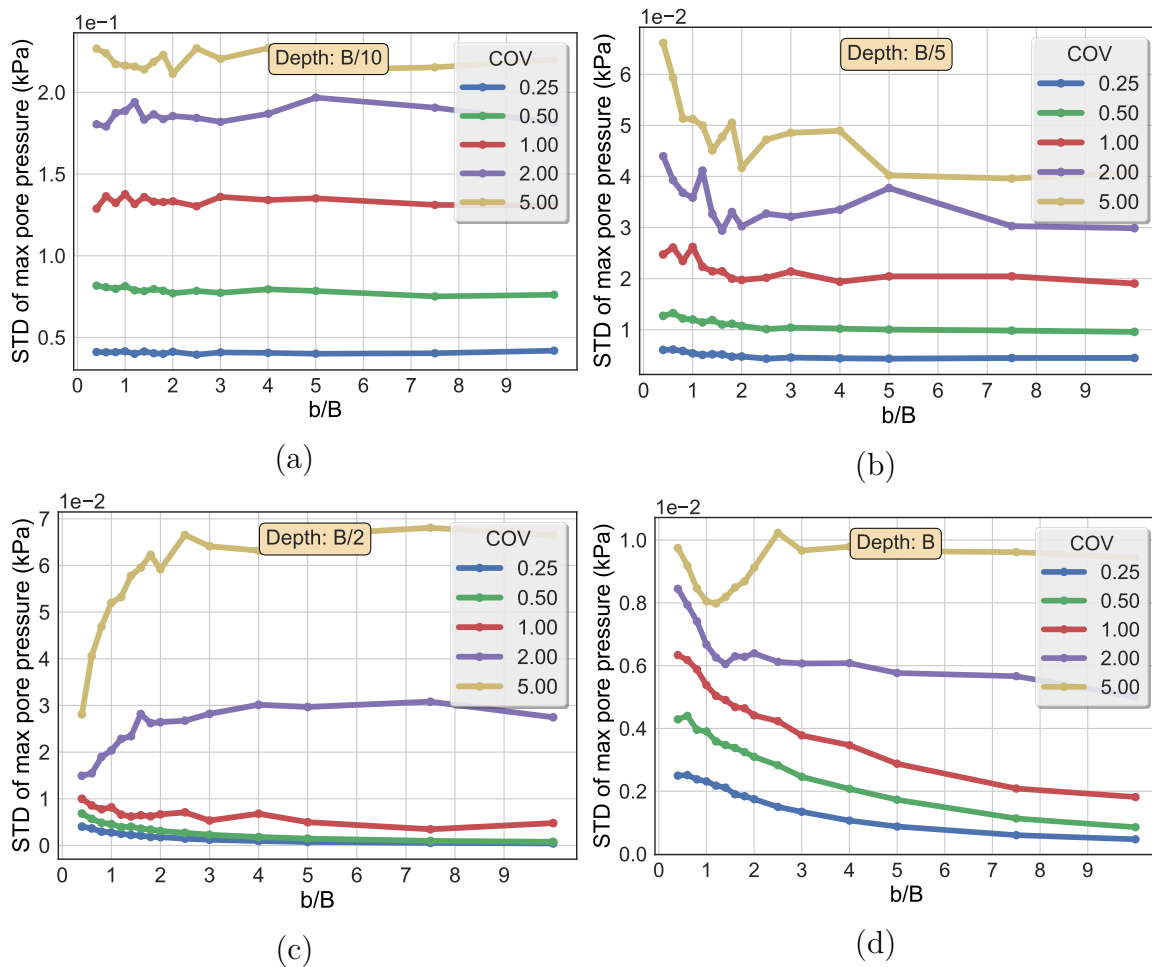


Figure 6.33. STD of maximum excess pore pressure vs normalized correlation parameter b/B for stochastic permeability k and depth: (a) $B/10$, (b) $B/5$, (c) $B/2$ and (d) B .

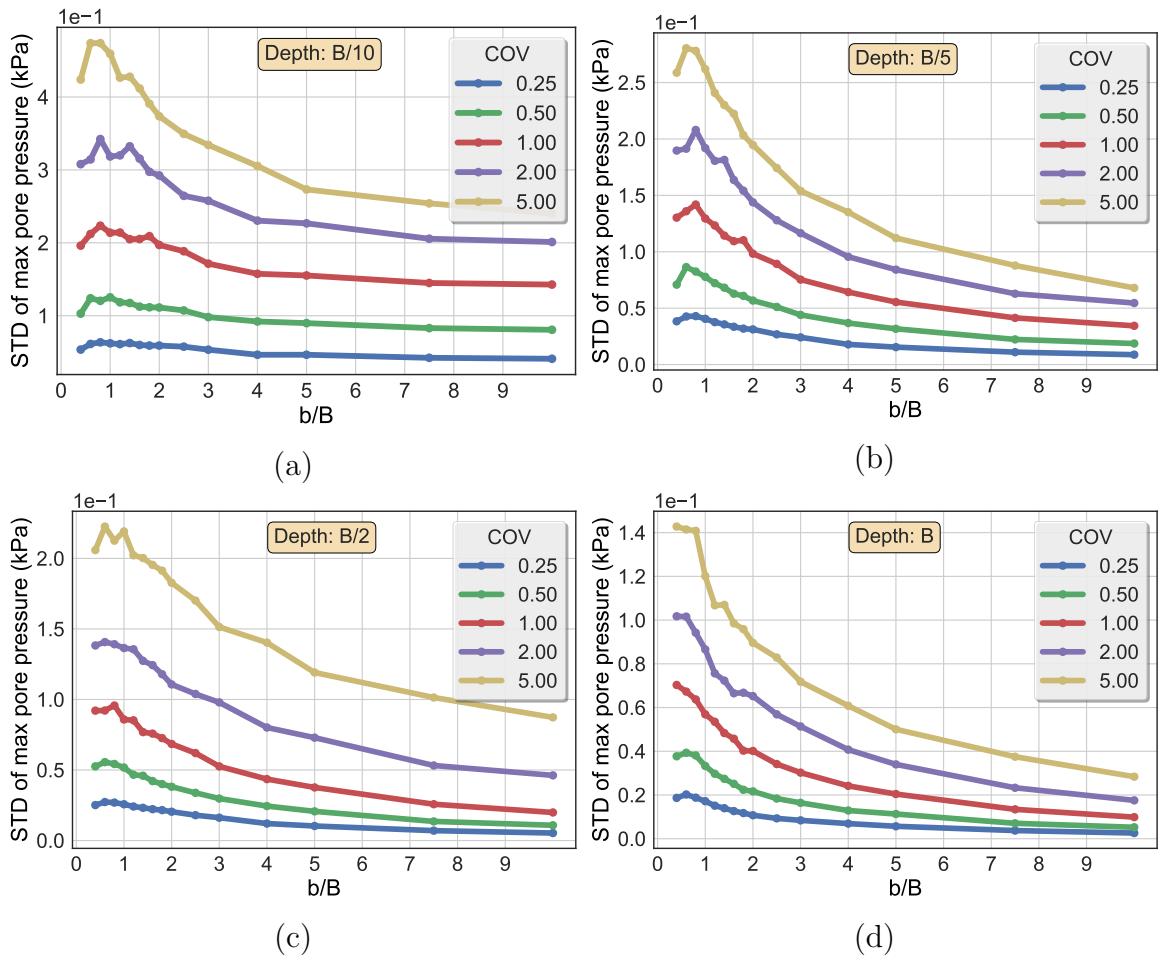


Figure 6.34. STD of maximum excess pore pressure vs normalized correlation parameter b/B for stochastic elastic modulus E and depth: (a) $B/10$, (b) $B/5$, (c) $B/2$ and (d) B .

Consolidation of a soil layer with stochastic material properties

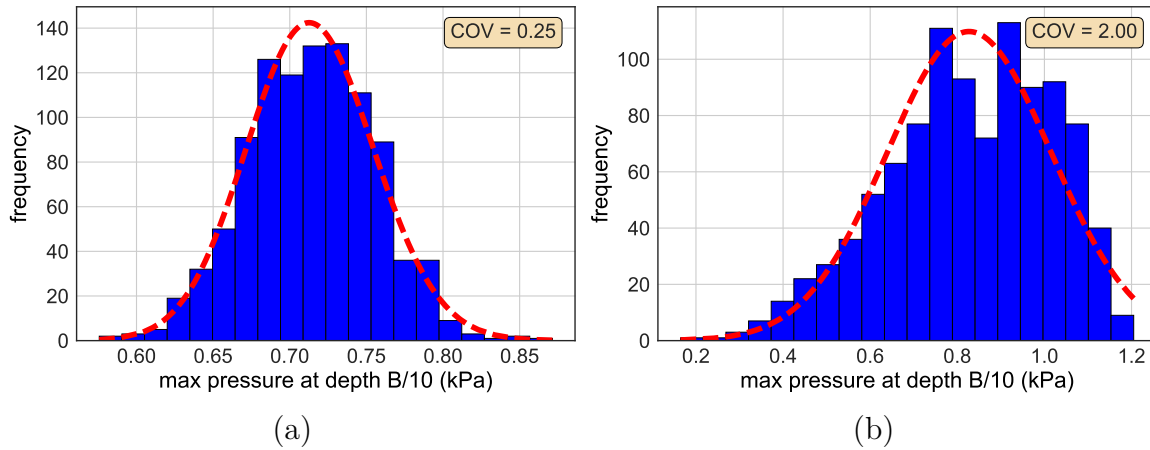


Figure 6.35. Histogram of max excess pore pressure at depth $B/10$ and fitted Gaussian distribution for stochastic permeability with $b_{ln(k)} = 10 m$ and COV values: (a) 0.25 and (b) 2.00.

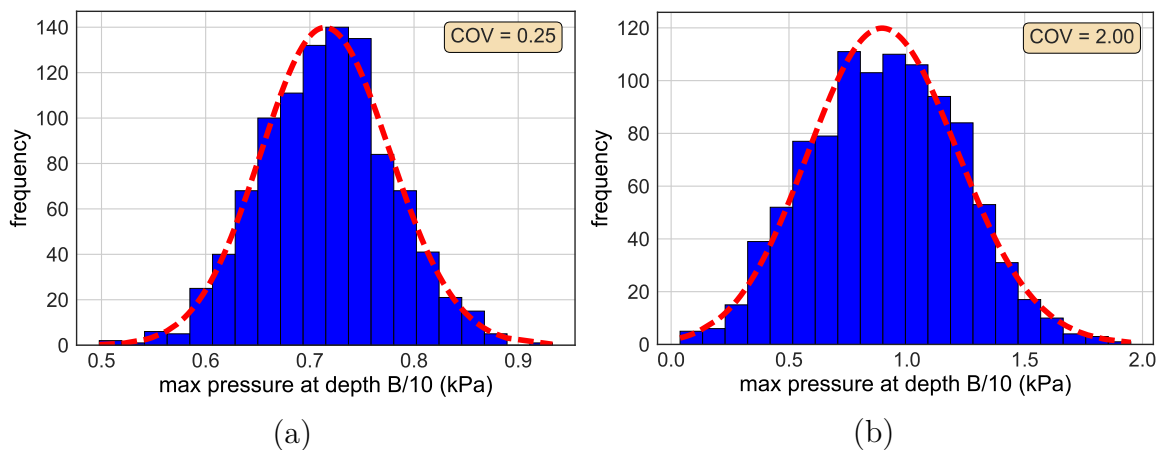


Figure 6.36. Histogram of max excess pore pressure at depth $B/10$ and fitted Gaussian distribution for stochastic elastic modulus with $b_{ln(E)} = 10 m$ and COV values: (a) 0.25 and (b) 2.00.

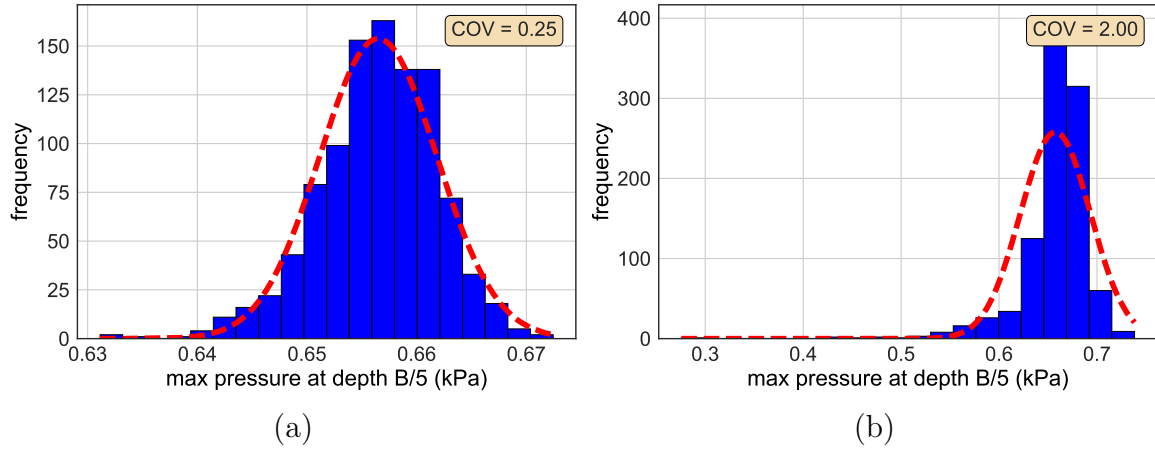


Figure 6.37. Histogram of max excess pore pressure at depth B/5 and fitted lognormal distribution for stochastic permeability with $b_{ln(k)} = 10 m$ and COV values: (a) 0.25 and (b) 2.00.

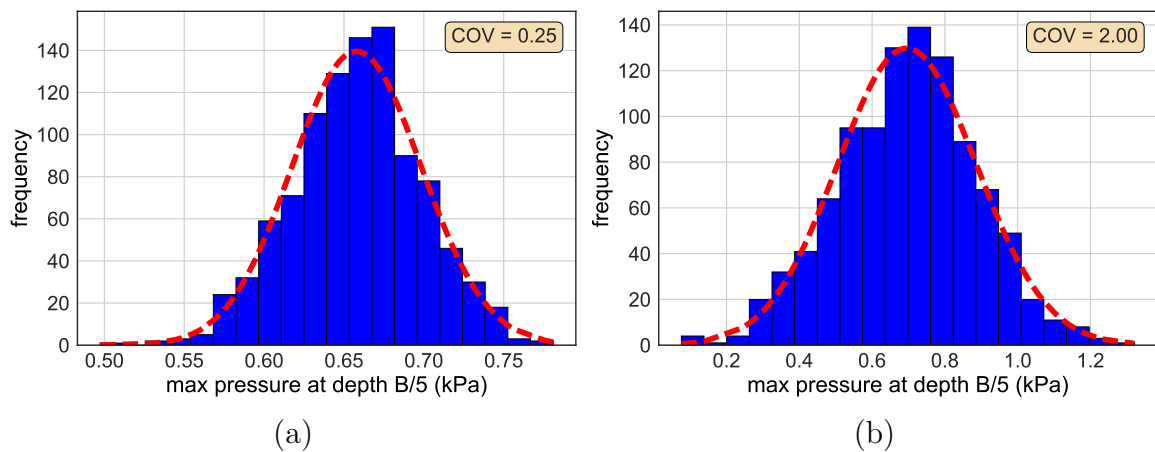


Figure 6.38. Histogram of max excess pore pressure at depth B/5 and fitted lognormal distribution for stochastic elastic modulus with $b_{ln(E)} = 10 m$ and COV values: (a) 0.25 and (b) 2.00.

Consolidation of a soil layer with stochastic material properties

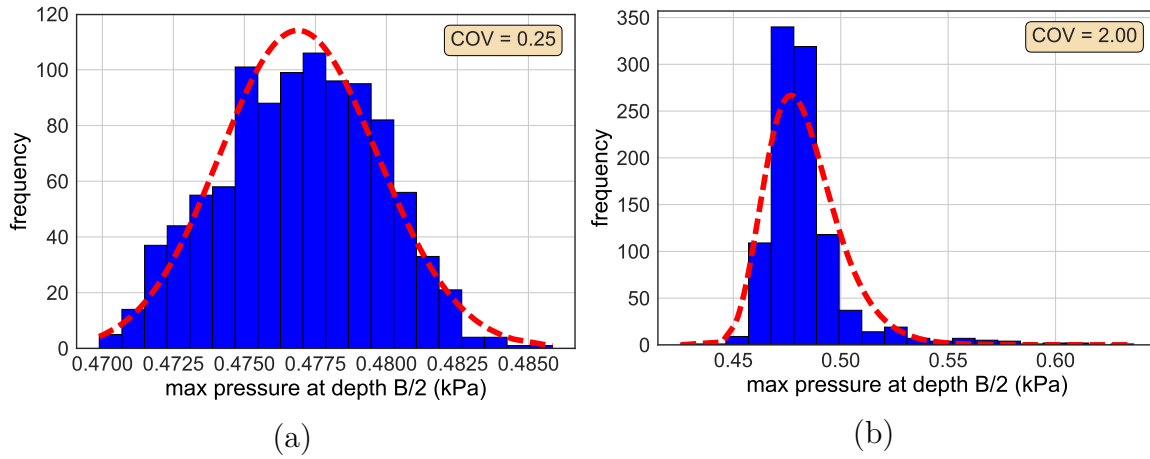


Figure 6.39. Histogram of max excess pore pressure at depth $B/2$ and fitted lognormal distribution for stochastic permeability with $b_{ln(k)} = 10 m$ and COV values: (a) 0.25 and (b) 2.00.

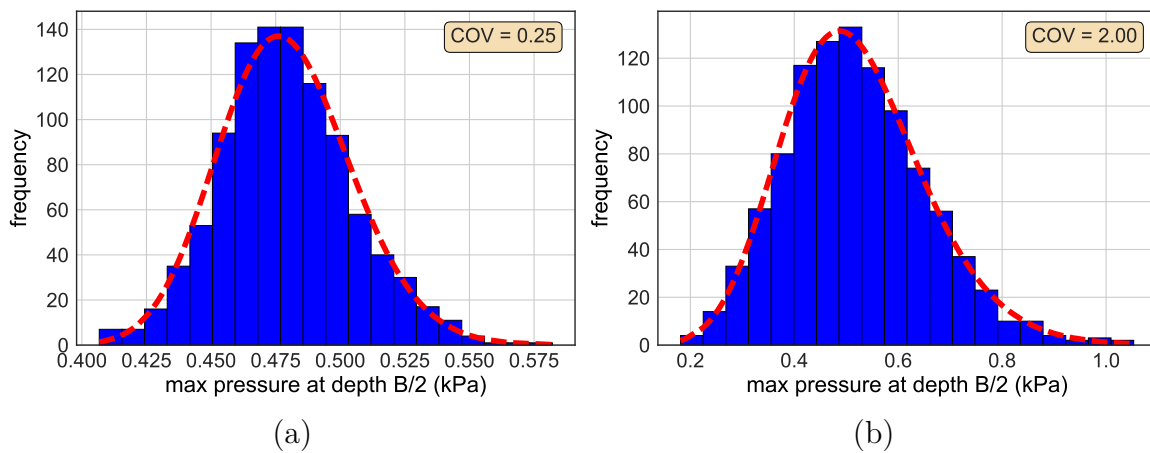


Figure 6.40. Histogram of max excess pore pressure at depth $B/2$ and fitted lognormal distribution for stochastic elastic modulus with $b_{ln(E)} = 10 m$ and COV values: (a) 0.25 and (b) 2.00.

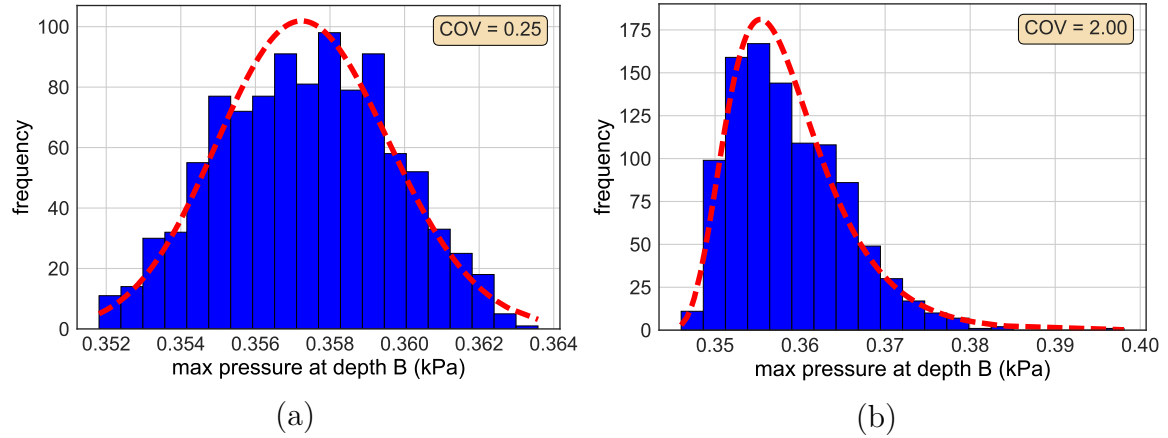


Figure 6.41. Histogram of max excess pore pressure at depth B and fitted lognormal distribution for stochastic permeability with $b_{ln(k)} = 10 m$ and COV values: (a) 0.25 and (b) 2.00.

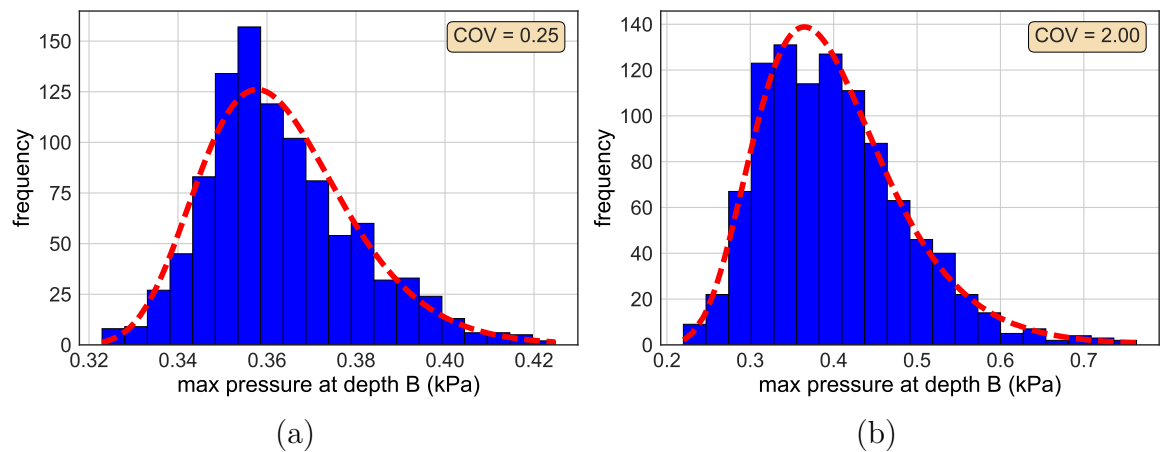


Figure 6.42. Histogram of max excess pore pressure at depth B and fitted lognormal distribution for stochastic elastic modulus with $b_{ln(E)} = 10 m$ and COV values: (a) 0.25 and (b) 2.00.

6.3.4 Foundation design guidelines

Regarding the design of foundations resting on saturated consolidating soil layers the findings of the previous parametric study may lead to notable recommendations. First, when considering superstructures sensitive to differential settlement, a safety threshold for the maximum differential settlement should be set. The probability of failure can then be easily calculated from the area of the corresponding differential settlement histograms corresponding to values higher than the allowed threshold. Furthermore, if data of the soil variability and autocorrelation is available, Monte Carlo analyses can be carried out to find the critical footing widths resulting to the greater differential settlement. In case of square or more complicated footing shapes, full 3-D probabilistic analyses might have to be considered. It is also important to take into account the spatial soil variability whenever considering the settlements corresponding to the footing center, despite the fact that the sensitivity of the system is lower with respect to them. Nevertheless, it is possible to calculate probabilities of exceeding an allowable absolute settlement. To conclude, it may be the case that the generated water pore pressures, which in many cases exceed the magnitude of the applied load, reduce the strength of the underlying soil. If this is the case, bearing capacity analyses which take into account the consolidation process and the variability of the soil parameters have to be taken into consideration at the design stage. In this scenario, the footing design might have to change; otherwise, techniques such as installation of prefabricated vertical drains (PVDs), in combination with soil pre-loading that accelerate the consolidation of the soil layer, might be considered as proposed in (Bari et al., 2016).

6.4 Concluding remarks

In this work, the influence of spatial variability of the soil permeability k and elastic modulus E on the consolidation phenomenon is investigated. A coupled u-p finite element formulation is considered to discretize the underlying governing equations. Permeability and elastic modulus were simulated as lognormal random fields using the spectral representation method. A case study of a classical geotechnical engineering footing settlement problem is presented. The direct Monte Carlo simulation method was used to carry out the stochastic finite element analysis. A number of different parametric studies were performed to study the response of the footing-soil system. It was shown that the spatial variability of the soil permeability and elastic modulus has a direct effect on the footing-soil system response. Differential footing settlements, absent in deterministic analysis for the case study examined, are observed even for

slight variations of k or E . They have to be taken into account, especially in cases of structures sensitive to differential movement. It was also found that the soil-footing system is much more sensitive to variation of E compared to k . Furthermore, in the case of spatially variable E , a different pattern of differential settlement is observed. Specifically, the differential footing settlement increases continuously, while for the spatially variable k , it obtains a maximum value and then gradually decreases to zero. In addition, different values of b maximize the variability of the system response when k and E are considered, namely $1.0B$ for k and about $1.5B$ for E where B is the footing width. The generated excess pore pressures of the underlying consolidating soil layer are also affected by the variation of soil properties. The variation of E is crucial once more, although variations of both k and E can lead to pore pressures with larger magnitudes than the applied footing load. This alone might affect the strength of the underlying soil and play a negative role in the footing bearing capacity. To conclude, it was demonstrated that probabilistic analyses can provide an insight into the influence of uncertain soil parameters in various geotechnical applications. Under these circumstances, the stochastic finite element method proves to be a valuable tool for analysis and design in geotechnical engineering.

Chapter 7

Dynamic variability response functions for shear wave propagation in soils

In this chapter, the problem of shear wave propagation in soils with spatially varying shear modulus G is studied on the basis of the DMRF/DVRF concept. The independence assumption of DMRF/DVRF functions to the spectral density function of the underlying material property renders the methodology ideal for problems involving soil materials, where lack of sufficient data is the common case. It is shown that through the DMRF/DVRF functions, the time history of mean and variance of the response quantity of interest can be accurately and efficiently calculated for stochastic shear wave propagation problems in 1D and 2D soil domains. Specifically, the FMCS method is used to numerically evaluate the DMRF/DVRF functions for displacement, velocity and acceleration of the soil layer surface. Application of finite element analyses of propagation of synthetic Ricker and (Mavroeidis and Papageorgiou, 2003) wavelets, as well as a real recorded earthquake motion are then used as test-cases to demonstrate the potential and validity of the method. Furthermore, upper bounds of the mean and variance of the response quantities of interest are established through the use of the calculated DMRF and DVRF functions. The accuracy of the proposed approach is verified by direct comparison of the results obtained via the MCS method. Useful conclusions regarding the sensitivity of the statistical characteristics of the soil response on the underlying nature of the material correlation properties are finally drawn.

7.1 Time integration of equations of motion

In wave propagation analyses in the time domain, the general dynamic equilibrium system of equations must be solved:

$$\mathbf{M}\ddot{\mathbf{u}}(t) + \mathbf{C}\dot{\mathbf{u}}(t) + \mathbf{K}\mathbf{u}(t) = \mathbf{P}(t) \quad (7.1)$$

where \mathbf{M} , \mathbf{C} and \mathbf{K} are the mass, damping and stiffness matrices, $\ddot{\mathbf{u}}(t)$, $\dot{\mathbf{u}}(t)$ and $\mathbf{u}(t)$ the acceleration, velocity and displacement vectors and $\mathbf{P}(t)$ the external force vector. The equation of motion which is alternatively called *equation of dynamical equilibrium* has to be satisfied throughout time t . In order to numerically solve eq. (7.1), various time integrations schemes are used. To this purpose, three alternative numerical time integrations schemes are presented, namely the Newmark algorithm, the Hilber-Hughes-Taylor and the latest Bathe method.

7.1.1 The Newmark algorithm

In this section the classical Newmark time integration scheme is presented. According to the Newmark scheme, the following assumptions are used to relate the response quantities between two successive timesteps, namely t and $t + \Delta t$, where Δt is the chosen timestep:

$$\dot{\mathbf{u}}_{t+\Delta t} = \dot{\mathbf{u}}_t + [(1 - \delta) + \delta\ddot{\mathbf{u}}_{t+\Delta t}] \Delta t \quad (7.2)$$

$$\mathbf{u}_{t+\Delta t} = \mathbf{u}_t + \dot{\mathbf{u}}_t \Delta t + \left[\left(\frac{1}{2} - \alpha \right) \ddot{\mathbf{u}}_t + \alpha \ddot{\mathbf{u}}_{t+\Delta t} \right] \Delta t^2 \quad (7.3)$$

while parameters α and δ are determined for integration accuracy and stability. The originally proposed values $\alpha = 1/4$ and $\delta = 1/2$ lead to the unconditionally stable scheme known as the constant-average acceleration method or trapezoidal rule. In order to determine the final form of the Newmark integration scheme, the aforementioned equilibrium according to eq. (7.1) is considered at timestep $t + \Delta t$:

$$\mathbf{M}\ddot{\mathbf{u}}_{t+\Delta t} + \mathbf{C}\dot{\mathbf{u}}_{t+\Delta t} + \mathbf{K}\mathbf{u}_{t+\Delta t} = \mathbf{P}_{t+\Delta t} \quad (7.4)$$

Combining eqs. (7.2) and (7.5) an analogous relation for the nodal acceleration vector at time $t + \Delta t$ can be derived:

$$\ddot{\mathbf{u}}_{t+\Delta t} = \left(1 - \frac{1}{2\alpha} \right) \ddot{\mathbf{u}}_t - \frac{1}{\alpha \Delta t} \dot{\mathbf{u}}_t + \frac{1}{\alpha \Delta t^2} (\mathbf{u}_{t+\Delta t} - \mathbf{u}_t) \quad (7.5)$$

7.1 Time integration of equations of motion

The following table introduces the eight effective constants $\alpha_0, \dots, \alpha_7$ used in the following derivations for the Newmark algorithm.

Equations (7.2), (7.3) and (7.5) are now rewritten using constants of section 7.1.1 as:

Newmark constants	
Constant	Value
α_0	$\frac{1}{\alpha\Delta t^2}$
α_1	$\frac{\delta}{\alpha\Delta t}$
α_2	$\frac{1}{\alpha\Delta t}$
α_3	$\frac{1}{2\alpha} - 1$
α_4	$\frac{\delta}{\alpha} - 1$
α_5	$\frac{\Delta t}{2} \left(\frac{\delta}{\alpha} - 2 \right)$
α_6	$\Delta t (1 - \delta)$
α_7	$\delta\Delta t$

Table 7.1. Table of Newmark constants

$$\ddot{\mathbf{u}}_{t+\Delta t} = \alpha_0 (\mathbf{u}_{t+\Delta t} - \mathbf{u}_t) - \alpha_2 \dot{\mathbf{u}}_t - \alpha_3 \ddot{\mathbf{u}}_t \quad (7.6)$$

$$\dot{\mathbf{u}}_{t+\Delta t} = \dot{\mathbf{u}}_t + \alpha_6 \ddot{\mathbf{u}}_t + \alpha_7 \ddot{\mathbf{u}}_{t+\Delta t} \quad (7.7)$$

$$\mathbf{u}_{t+\Delta t} = \mathbf{u}_t + \Delta t \dot{\mathbf{u}} + \frac{\alpha_3}{\alpha_0} \ddot{\mathbf{u}}_t + \frac{1}{\alpha_0} \ddot{\mathbf{u}}_{t+\Delta t} \quad (7.8)$$

Substituting eqs. (7.6) and (7.7) in eq. (7.4) the following relation is obtained:

$$\begin{aligned} & \mathbf{M} [\alpha_0 (\mathbf{u}_{t+\Delta t} - \mathbf{u}_t) - \alpha_2 \dot{\mathbf{u}}_t - \alpha_3 \ddot{\mathbf{u}}_t] \\ & + \mathbf{C} [\dot{\mathbf{u}}_t + \alpha_6 \ddot{\mathbf{u}}_t + \alpha_7 \ddot{\mathbf{u}}_{t+\Delta t}] + \mathbf{K} \mathbf{u}_{t+\Delta t} = \mathbf{P}_{t+\Delta t} \end{aligned} \quad (7.9)$$

By keeping all terms related to $\mathbf{u}_{t+\Delta t}$ at the left-hand side of eq. (7.9) and rearranging the right-hand side, another relation is obtained:

$$(\mathbf{K} + \alpha_0 \mathbf{M} + \alpha_1 \mathbf{C}) \mathbf{u}_{t+\Delta t} = \mathbf{P}_{t+\Delta t} + \mathbf{M} (\alpha_0 \mathbf{u}_t + \alpha_2 \dot{\mathbf{u}}_t + \alpha_3 \ddot{\mathbf{u}}_t) + \mathbf{C} (\alpha_1 \mathbf{u}_t + \alpha_4 \dot{\mathbf{u}}_t + \alpha_3 \ddot{\mathbf{u}}_t) \quad (7.10)$$

which may be written in the compact form:

$$\mathbf{K}^{eff} \mathbf{u}_{t+\Delta t} = \mathbf{P}_{t+\Delta t}^{eff} \quad (7.11)$$

To conclude, the Newmark time integration scheme for linear problems is summarized in the following simple steps:

Dynamic variability response functions for shear wave propagation in soils

1. Assemble the total mass matrix \mathbf{M} , the stiffness matrix \mathbf{K} and the damping matrix \mathbf{C} .
2. Use the initial conditions \mathbf{u}_0 , $\dot{\mathbf{u}}_0$ and $\ddot{\mathbf{u}}_0$; the initial vector of accelerations can be calculated by solving the equation of motion eq. (7.1) at the zeroth timestep.
3. Select the timestep Δt and the Newmark integration parameters α , δ which have to satisfy the following conditions:

$$\delta \geq 0.50 \quad (7.12)$$

$$\alpha \geq 0.25(0.5 + \delta)^2 \quad (7.13)$$

4. Calculate the Newmark constants from section 7.1.1.
5. Form the effective stiffness matrix from the left-hand side of eq. (7.10).
6. For each timestep repeat the following steps:
 - 6.1. Calculate the effective external force vector from the right-hand side of eq. (7.10).
 - 6.2. Solve eq. (7.11).
 - 6.3. Calculate the accelerations and velocities at timestep $t + \Delta t$ from eqs. (7.6) and (7.7).

7.1.2 Bathe algorithm

The algorithm of Bathe was first introduced in (Bathe, 2007) and further analyzed in (Bathe and Noh, 2012); it has been successfully applied to wave propagation problems (Noh et al., 2013). The Bathe method is a composite implicit direct time integrations scheme for solving the equation of motion with respect to time. The main idea behind the algorithm is the division of each timestep Δt into two equal sub-steps and the subsequent use of two different integration rules for each of the sub-steps. This composite integration scheme has three advantages; it offers numerical damping of high frequency modes, is second order accurate and unconditionally stable. It is effective for linear and nonlinear finite element analyses even in the presence of large deformations of the analyzed model.

The classical equation of dynamical equilibrium given by eq. (7.1) has to be solved at each timestep. Initially the equation of motion is written at the half of the interval

7.1 Time integration of equations of motion

between time points t and $t + \Delta t$ as follows:

$$\mathbf{M}\ddot{\mathbf{u}}_{t+\Delta t/2} + \mathbf{C}\dot{\mathbf{u}}_{t+\Delta t/2} + \mathbf{K}\mathbf{u}_{t+\Delta t/2} = \mathbf{P}_{t+\Delta t/2} \quad (7.14)$$

In order to integrate the equation of motion of eq. (7.14), the trapezoidal rule is used. Velocity and displacement at timestep $t + \Delta t/2$ are calculated via:

$$\dot{\mathbf{u}}_{t+\Delta t/2} = \mathbf{u}_t + \frac{\Delta t}{4} (\ddot{\mathbf{u}}_t + \ddot{\mathbf{u}}_{t+\Delta t/2}) \quad (7.15)$$

$$\mathbf{u}_{t+\Delta t/2} = \mathbf{u}_t + \frac{\Delta t}{4} (\dot{\mathbf{u}}_t + \dot{\mathbf{u}}_{t+\Delta t/2}) \quad (7.16)$$

Substituting eq. (7.15) in eq. (7.16) and solving with respect to $\dot{\mathbf{u}}_{t+\Delta t/2}$ results into the following relation:

$$\dot{\mathbf{u}}_{t+\Delta t/2} = \frac{4}{\Delta t} (\mathbf{u}_{t+\Delta t/2} - \mathbf{u}_t) - \dot{\mathbf{u}}_t \quad (7.17)$$

Combining eqs. (7.16) and (7.17) and solving with respect to $\ddot{\mathbf{u}}_{t+\Delta t/2}$, the following relation is derived:

$$\ddot{\mathbf{u}}_{t+\Delta t/2} = \frac{16}{\Delta t^2} (\mathbf{u}_{t+\Delta t/2} - \mathbf{u}_t) - \frac{8}{\Delta t} \dot{\mathbf{u}}_t - \ddot{\mathbf{u}}_t \quad (7.18)$$

Now, eqs. (7.17) and (7.18) can be used directly in eq. (7.14):

$$\begin{aligned} & \mathbf{M} \left(\frac{16}{\Delta t^2} \mathbf{u}_{t+\Delta t/2} - \frac{16}{\Delta t^2} \mathbf{u}_t - \frac{8}{\Delta t} \dot{\mathbf{u}}_t - \ddot{\mathbf{u}}_t \right) \\ & + \mathbf{C} \left(\frac{4}{\Delta t} \mathbf{u}_{t+\Delta t/2} - \frac{4}{\Delta t} \mathbf{u}_t - \dot{\mathbf{u}}_t \right) + \mathbf{K} \mathbf{u}_{t+\Delta t/2} = \mathbf{P}_{t+\Delta t/2} \end{aligned} \quad (7.19)$$

Rearranging terms in eq. (7.19) and keeping all vectors related to time $t + \Delta t/2$ at the left-hand side, the following equation is obtained:

$$\begin{aligned} \left(\mathbf{K} + \frac{4}{\Delta t} \mathbf{C} + \frac{16}{\Delta t^2} \mathbf{M} \right) \mathbf{u}_{t+\Delta t/2} &= \mathbf{P}_{t+\Delta t/2} + \mathbf{M} \left(\frac{16}{\Delta t^2} \mathbf{u}_t + \frac{8}{\Delta t} \dot{\mathbf{u}}_t + \ddot{\mathbf{u}}_t \right) \\ &+ \mathbf{C} \left(\frac{4}{\Delta t} \mathbf{u}_t + \dot{\mathbf{u}}_t \right) \end{aligned} \quad (7.20)$$

which can be written in the more compact form:

$$\mathbf{K}^{eff1} \mathbf{u}_{t+\Delta t/2} = \mathbf{P}_{t+\Delta t/2}^{eff1} \quad (7.21)$$

Dynamic variability response functions for shear wave propagation in soils

The linear equation system of eq. (7.21) can now be solved with any available method in order to calculate the displacement nodal vector $\mathbf{u}_{t+\Delta t/2}$.

For the second sub-step, i.e. for time integration between time points $t + \Delta t/2$ and $t + \Delta t$, the three-point backward Euler is used, where velocity and acceleration are now calculated via the following relations:

$$\dot{\mathbf{u}}_{t+\Delta t} = \frac{1}{\Delta t}\mathbf{u}_t - \frac{4}{\Delta t}\mathbf{u}_{t+\Delta t/2} + \frac{3}{\Delta t}\mathbf{u}_{t+\Delta t} \quad (7.22)$$

$$\ddot{\mathbf{u}}_{t+\Delta t} = \frac{1}{\Delta t}\dot{\mathbf{u}}_t - \frac{4}{\Delta t}\dot{\mathbf{u}}_{t+\Delta t/2} + \frac{3}{\Delta t^2}\mathbf{u}_t - \frac{12}{\Delta t^2}\mathbf{u}_{t+\Delta t/2} + \frac{9}{\Delta t^2}\mathbf{u}_{t+\Delta t} \quad (7.23)$$

Substituting eqs. (7.22) and (7.23) in the equation of motion at time $t + \Delta t$, the following relation is derived:

$$\begin{aligned} \mathbf{M} \left(\frac{9}{\Delta t^2}\mathbf{u}_{t+\Delta t} - \frac{12}{\Delta t^2}\mathbf{u}_{t+\Delta t/2} + \frac{3}{\Delta t^2}\mathbf{u}_t - \frac{4}{\Delta t}\dot{\mathbf{u}}_{t+\Delta t/2} + \frac{1}{\Delta t}\dot{\mathbf{u}}_t \right) \\ + \mathbf{C} \left(\frac{3}{\Delta t}\mathbf{u}_{t+\Delta t} - \frac{4}{\Delta t}\mathbf{u}_{t+\Delta t/2} + \frac{1}{\Delta t}\mathbf{u}_t \right) + \mathbf{K}\mathbf{u}_{t+\Delta t} = \mathbf{P}_{t+\Delta t} \end{aligned} \quad (7.24)$$

Keeping only the vectors related to time point $t + \Delta t$ on the left-hand side of eq. (7.24), we get:

$$\begin{aligned} \left(\mathbf{K} + \frac{3}{\Delta t}\mathbf{C} + \frac{9}{\Delta t^2}\mathbf{M} \right) \mathbf{u}_{t+\Delta t} = \mathbf{P}_{t+\Delta t} \\ + \mathbf{M} \left(\frac{3}{\Delta t^2} (4\mathbf{u}_{t+\Delta t/2} - \mathbf{u}_t) + \frac{1}{\Delta t} (4\dot{\mathbf{u}}_{t+\Delta t/2} - \dot{\mathbf{u}}_t) \right) + \mathbf{C} \left(\frac{1}{\Delta t} (4\mathbf{u}_{t+\Delta t/2} - \mathbf{u}_t) \right) \end{aligned} \quad (7.25)$$

which is written in the more compact form:

$$\mathbf{K}^{eff2}\mathbf{u}_{t+\Delta t} = \mathbf{P}_{t+\Delta t}^{eff2} \quad (7.26)$$

This time, the only unknown is the nodal displacement vector at time point $t + \Delta t$ and eq. (7.26) can be solved by standard methods for linear systems.

To conclude, the Bathe time integration scheme for linear problems is summarized in the following simple steps:

1. Assemble the total mass matrix \mathbf{M} , the stiffness matrix \mathbf{K} and the damping matrix \mathbf{C} .
2. Use the initial conditions \mathbf{u}_0 , $\dot{\mathbf{u}}_0$ and $\ddot{\mathbf{u}}_0$. The initial vector of accelerations may be calculated by solving the equation of motion eq. (7.1) at the zeroth timestep.

3. Select the timestep Δt for the time integration.
4. Form the effective stiffness matrices \mathbf{K}^{eff1} and \mathbf{K}^{eff2} used in eqs. (7.20) and (7.25) respectively.
5. For each timestep repeat the following steps:
 - 5.1. Calculate the effective external force vector $\mathbf{P}_{t+\Delta t/2}^{eff1}$ of eq. (7.21).
 - 5.2. Solve eq. (7.21).
 - 5.3. Calculate the accelerations and velocities at timestep $t+\Delta t/2$ from eqs. (7.17) and (7.18).
 - 5.4. Calculate the effective external force vector $\mathbf{P}_{t+\Delta t}^{eff2}$ of eq. (7.26).
 - 5.5. Solve eq. (7.26).
 - 5.6. Calculate the accelerations and velocities at timestep $t + \Delta t$ from eqs. (7.22) and (7.23).

7.1.3 Hilber-Hughes-Taylor α method

In order to integrate the equation of motion 7.1 in this chapter, the implicit unconditionally stable α -method (Hilber-Hughes-Taylor) Hughes (2000) is used. The basic parameters are the timestep Δt and parameter α , which lies in the interval $[-1/3, 0]$ and controls the numerical damping. The two other parameters β and γ are calculated as a function of α by the following relations:

$$\beta = \frac{1}{4}(1 - \alpha)^2 \quad (7.27)$$

$$\gamma = \frac{1}{2}(1 - 2\alpha) \quad (7.28)$$

According to this time integration scheme, the following relations are used:

$$\dot{\mathbf{u}}_{n+1} = \dot{\mathbf{u}}_n + [(1 - \gamma)\ddot{\mathbf{u}}_n + \gamma\ddot{\mathbf{u}}_{n+1}] \Delta t = \dot{\mathbf{u}}_n + \ddot{\mathbf{u}}_n \Delta t + (\ddot{\mathbf{u}}_{n+1} - \ddot{\mathbf{u}}_n) \gamma \Delta t \quad (7.29)$$

$$\begin{aligned} \mathbf{u}_{n+1} &= \mathbf{u}_n + \dot{\mathbf{u}}_n \Delta t + [(1 - 2\beta)\ddot{\mathbf{u}}_n + 2\beta\ddot{\mathbf{u}}_{n+1}] \frac{1}{2} \Delta t^2 \\ &= \mathbf{u}_n + \dot{\mathbf{u}}_n \Delta t + \ddot{\mathbf{u}}_n \frac{1}{2} \Delta t^2 + (\ddot{\mathbf{u}}_{n+1} - \ddot{\mathbf{u}}_n) \beta \Delta t^2 \end{aligned} \quad (7.30)$$

Note that, in eqs. (7.29) and (7.30), the quantities with subscript n refer to time t , whereas $n + 1$ refers to time $t + \Delta t$ for a chosen timestep Δt . Combining eqs. (7.29)

Dynamic variability response functions for shear wave propagation in soils

and (7.30) so that the basic unknown is \mathbf{u}_{n+1} , the following relations hold:

$$\ddot{\mathbf{u}}_{n+1} = \left(1 - \frac{1}{2\beta}\right) \ddot{\mathbf{u}}_n - \frac{1}{\beta\Delta t} \dot{\mathbf{u}}_n + \frac{1}{\beta\Delta t^2} (\mathbf{u}_{n+1} - \mathbf{u}_n) \quad (7.31)$$

$$\dot{\mathbf{u}}_{n+1} = \left(1 - \frac{\gamma}{2\beta}\right) \Delta t \ddot{\mathbf{u}}_n + \left(1 - \frac{\gamma}{\beta}\right) \dot{\mathbf{u}}_n + \frac{\gamma}{\beta\Delta t} (\mathbf{u}_{n+1} - \mathbf{u}_n) \quad (7.32)$$

The equation of motion 7.1 is written at a time instance between timesteps t and $t + \Delta t$:

$$\mathbf{M}\ddot{\mathbf{u}}_{n+1} + (1 + \alpha) \mathbf{C}\dot{\mathbf{u}}_{n+1} - \alpha \mathbf{C}\dot{\mathbf{u}}_n + (1 + \alpha) \mathbf{K}\mathbf{u}_{n+1} - \alpha \mathbf{K}\mathbf{u}_n = (1 + \alpha) \mathbf{P}_{n+1} - \alpha \mathbf{P}_n \quad (7.33)$$

Substituting eqs. (7.31) and (7.32) in eq. (7.33) and moving the $t + \Delta t$ terms at the left-hand side and the t terms at the right-hand side, the final form of the linear system of equations is obtained:

$$\begin{aligned} \left(\frac{1}{\beta\Delta t^2} \mathbf{M} + \frac{(1 + \alpha)\gamma}{\beta\Delta t} \mathbf{C} + (1 + \alpha) \mathbf{K} \right) \mathbf{u}_{n+1} &= (1 + \alpha) \mathbf{P}_{n+1} - \alpha \mathbf{P}_n + \alpha \mathbf{K}\mathbf{u}_n \\ + \mathbf{C} \left(\frac{(1 + \alpha)\gamma}{\beta\Delta t} \mathbf{u}_n + \left(\frac{\alpha\gamma}{\beta} + \frac{\gamma}{\beta} - 1 \right) \dot{\mathbf{u}}_n + (1 + \alpha) \left(\frac{\gamma}{2\beta} - 1 \right) \Delta t \ddot{\mathbf{u}}_n \right) & \quad (7.34) \\ + \mathbf{M} \left(\frac{1}{\beta\Delta t^2} \mathbf{u}_n + \frac{1}{\beta\Delta t} \dot{\mathbf{u}}_n + \left(\frac{1}{2\beta} - 1 \right) \ddot{\mathbf{u}}_n \right) & \end{aligned}$$

which may be written in the more compact form:

$$\mathbf{K}^{eff} \mathbf{u}_{n+1} = \mathbf{P}_{n+1}^{eff} \quad (7.35)$$

This particular equation can now be solved for the unknown displacement vector \mathbf{u}_{n+1} at time $t + \Delta t$.

To conclude, the HHT- α time integration scheme for linear problems is summarized in the following simple steps:

1. Assemble the total mass matrix \mathbf{M} , the stiffness matrix \mathbf{K} and the damping matrix \mathbf{C} .
2. Use the initial conditions \mathbf{u}_0 , $\dot{\mathbf{u}}_0$ and $\ddot{\mathbf{u}}_0$; the initial vector of accelerations can be calculated by solving the equation of motion eq. (7.1) at the zeroth timestep.
3. Select the timestep Δt and the integration parameter α , which has to lie in the interval $[-1/3, 0]$. Furthermore, calculate the additional parameters β and γ from eqs. (7.27) and (7.28).

4. Form the effective stiffness matrix from the left-hand side of eq. (7.35).
5. For each timestep repeat the following steps:
 - 5.1. Calculate the effective external force vector from the right-hand side of eq. (7.35).
 - 5.2. Solve eq. (7.35).
 - 5.3. Calculate the accelerations and velocities at timestep $t + \Delta t$ from eqs. (7.31) and (7.32).

7.2 Simulation of stochastic shear wave propagation in soils

The stochastic soil parameter considered is the inverse of the soil shear modulus $1/G$, which varies randomly along the vertical axis y in 1D models and in the horizontal and vertical axes x, y for plane strain models. In the general 2D case, the following relation holds:

$$\frac{1}{G(x, y)} = F_0 \cdot (1 + f(x, y)) \quad (7.36)$$

where $G(x, y)$ denotes the soil shear modulus at the spatial point with coordinates (x, y) and $f(x, y)$ is a zero-mean homogeneous stochastic field which models the spatial variation of $1/G$ around its mean value $F_0 = 1/G_0$.

The shear wave propagates through an underlying bedrock layer which is considered homogeneous to the soil layer above. What's more, the compliance of the underlying bedrock layer is taken into account by attaching viscous dampers to the base nodes of the soil model, according to the methodology proposed in (Lysmer and Kuhlemeyer). Both 1D and 2D shear wave propagation is considered and the corresponding models used are illustrated in figs. 7.1 and 7.2 respectively.

When considering shear wave propagation in 1D, the shear stress is given by:

$$\tau_{xy} = G \frac{\partial u}{\partial y} \quad (7.37)$$

where u is the displacement along the horizontal axis x . The nodal forces of a unit area 1D element of height h_{el} , illustrated in fig. 7.1, are then calculated as follows:

$$\begin{Bmatrix} F_i \\ F_j \end{Bmatrix} = \frac{1}{h_{el}} \begin{bmatrix} G & -G \\ -G & G \end{bmatrix} \begin{Bmatrix} u_i \\ u_j \end{Bmatrix} \quad (7.38)$$

Dynamic variability response functions for shear wave propagation in soils

where the matrix on the right-hand side of eq. 7.38 corresponds to the stiffness matrix for the 1D case. For the simulation of shear wave propagation in the 2D case, standard isoparametric plane strain 4-node quadrilateral elements are used.

It is very important to note that, when simulating the propagation of a recorded wave motion in either 1D or 2D domains, the incoming motion from the underlying bedrock layer has to be transformed to equivalent nodal forces, which are applied at the base of the model. To this purpose, the following relation is used according to (Joyner and Chen, 1975):

$$F_{wave}(t) = 2\rho_b \cdot V_{sb} \cdot V_I(t) \cdot A \quad (7.39)$$

where ρ_b is the density of the underlying bedrock, V_{sb} the shear wave propagation velocity of the bedrock, V_I the velocity history of the incoming shear wave and A the area corresponding to the node where the force is applied. The resulting nodal forces correspond to the external force vector $\mathbf{P}(t)$, which constitutes the right-hand side of eq. (7.1), and are applied to the base nodes of the 1D or 2D model as shown in figs. 7.1 and 7.2.

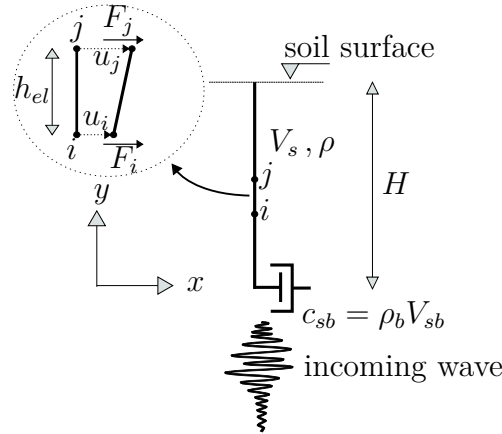


Figure 7.1. Numerical model used for the simulation of 1D shear wave propagation in soil

7.3 Dynamic Variability Response Function

The dynamic mean response function (DMRF) Papadopoulos and Kokkinos (2012) can be used to calculate the mean of the studied response quantity $d(t)$, i.e. $u(t)$, velocity

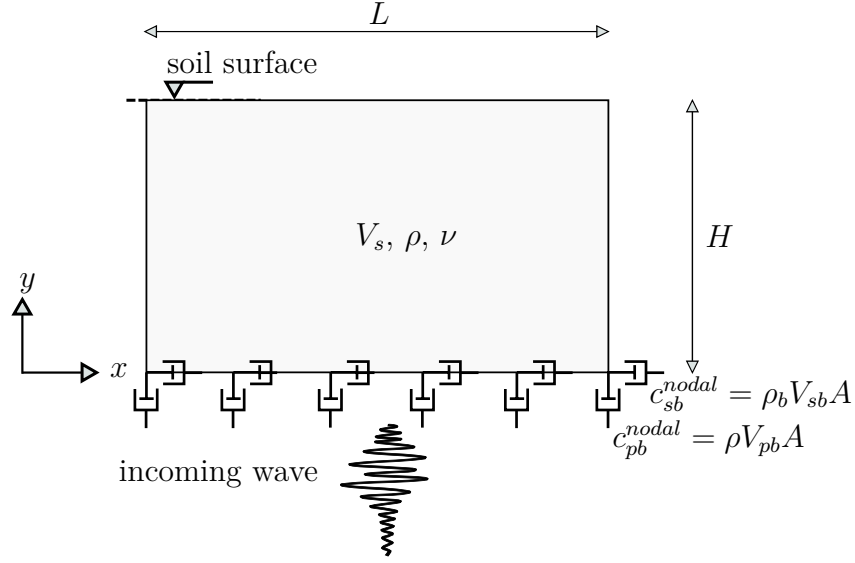


Figure 7.2. Numerical model used for the simulation of 2D shear wave propagation in soil

$\dot{u}(t)$ or acceleration $\ddot{u}(t)$, by the following expressions:

$$\text{for 1D : } E[d(t)] = \int_{-\infty}^{+\infty} DMRF(t, \kappa, \sigma_{ff}) \cdot S_{ff}(\kappa) d\kappa \quad (7.40)$$

$$\text{for 2D : } E[d(t)] = \int_{-\infty}^{+\infty} \int_{-\infty}^{\infty} DMRF(t, \kappa_x, \kappa_y, \sigma_{ff}) \cdot S_{ff}(\kappa_x, \kappa_y) d\kappa_x d\kappa_y \quad (7.41)$$

The same holds true for the variance of the response quantity where the dynamic variability response function (DVRF) is used instead:

$$\text{for 1D: } Var[d(t)] = \int_{-\infty}^{+\infty} DVRF(t, \kappa, \sigma_{ff}) \cdot S_{ff}(\kappa) d\kappa \quad (7.42)$$

$$\text{for 2D: } Var[d(t)] = \int_{-\infty}^{+\infty} \int_{-\infty}^{+\infty} DVRF(t, \kappa_x, \kappa_y, \sigma_{ff}) \cdot S_{ff}(\kappa_x, \kappa_y) d\kappa_x d\kappa_y \quad (7.43)$$

Explicit expressions for the DMRF/DVRF are rarely available; they have to be instead calculated numerically. To this purpose, the FMCS method analyzed in section 5.4 is adopted.

7.4 Numerical application

In this section, the DMRF/DVRF methodology is applied in the simulation of shear wave propagation in 1D and 2D soil domains; in both cases, the soil material properties considered are the same. The inverse of the shear modulus G is the uncertain soil

Dynamic variability response functions for shear wave propagation in soils

material parameter which has to be incorporated in the analysis. Both models consist of a soil layer which is loaded with an incoming stress wave from the bedrock layer below, considered homogeneous. The deterministic soil layer parameters assumed are: density $\rho = 1.8 \text{ Mg/m}^3$, Poisson's ratio $\nu = 0.3$, whereas the corresponding bedrock properties are: $V_{sb} = 760 \text{ m/s}$, $\rho_b = 2.4 \text{ Mg/m}^3$, $\nu_b = 0.3$. The parameter $\alpha = -0.02$ is chosen for the time integration method of eqs. (7.33) and (7.34) analyzed in section 7.2. The mean value of the shear wave velocity is $V_{s0} = 240 \text{ m/s}$ corresponding to a mean shear modulus of the soil $G_0 = \rho \cdot V_{s0}^2 = 103.68 \text{ MPa}$. The shear modulus of the bedrock is calculated by $G_b = \rho_b \cdot V_{sb}^2 = 1386.24 \text{ MPa}$. As explained in section 7.2, the inverse of the soil shear modulus is modeled as the random field with spatial value:

$$\frac{1}{G(x, y)} = \frac{1}{G_0} \cdot (1 + f(x, y)) \quad (7.44)$$

with $f(x, y)$ denoting a zero-mean homogeneous random field. For 1D fields, the horizontal coordinate x is omitted and eq. (7.44) is reduced to one dimension. It is important to emphasize that, in the FMCS case, f corresponds to the random sinusoid defined in eqs. (5.25) and (5.29), while in the direct MCS method, f corresponds to a zero-mean random field. In this study, the spectral representation method is used to generate realizations of the random field f in the MCS case.

7.4.1 Synthetic wavelets used

In this section, explicit relations for the Ricker and Mavroeidis & Papageorgiou synthetic wavelets are given; they are used as test loading cases in the numerical application (Semblat, 2009).

The Ricker wavelet is defined as the derivative of the Gaussian at various orders; the 0th, 1st and 2nd order cases are presented:

- The Ricker wavelet of order 0 is given by:

$$R_0(t) = \frac{A}{2} \exp \left[-\pi^2 \frac{(t - t_s)^2}{t_p^2} \right] \quad (7.45)$$

- The Ricker wavelet of order 1 is given by:

$$R_1(t) = -A\pi \frac{t - t_s}{t_p} \exp \left[-\pi^2 \frac{(t - t_s)^2}{t_p^2} \right] \quad (7.46)$$

- Finally, the Ricker wavelet of order 2 is defined as:

$$R_2(t) = A \left(2\pi^2 \frac{(t - t_s)^2}{t_p^2} - 1 \right) \exp \left[-\pi^2 \frac{(t - t_s)^2}{t_p^2} \right] \quad (7.47)$$

In eqs. (7.45) to (7.47), t_s denotes the time corresponding to the maximum amplitude of the 0th and 2nd order Ricker wavelets, while t_p is the fundamental period of the 2nd order wavelet.

The wavelet proposed by Mavroeidis & Papageorgiou is given by the following relation:

$$f(t) = \frac{A}{2} \left[1 + \cos \left(\frac{2\pi f_p t}{\gamma} \right) \right] \cos(2\pi f_p t + \nu) \quad (7.48)$$

In eq. (7.48), A is the amplitude, f_p the fundamental frequency, ν the phase angle and γ controls the oscillatory character of the wavelet.

7.4.2 Wave propagation in 1D

For the 1D simulation of shear wave propagation, the finite element model, which is illustrated in fig. 7.1, consists of 100 1D elements with height $h_{el} = 1.0 \text{ m}$ for a total soil layer height $H = 100 \text{ m}$. Unit area $A = 1.0 \text{ m}^2$ is used for each element, while Rayleigh damping is considered with damping ratios $\xi_1 = \xi_2 = 0.05$ corresponding to the first two vibrational modes of the model at $\omega_1 = (\pi V_{s0})/(2H)$ and $\omega_2 = (3\pi V_{s0})/(2H)$. A viscous damper is then added at the base node of the model to simulate the compliance of the bedrock layer with damping value $c_{sb}^{nodal} = \rho_b \cdot V_{sb} A = 1824.0 \text{ kN} \cdot \text{s/m}$. Loading cases consist of a propagating Ricker synthetic wavelet with amplitude 1 kN , as well as a real recorded earthquake motion, namely the Gilroy No1 EW recorded during the 1989 Loma Prieta earthquake (Kramer, 1996). The underlying correlation structure of the random field $f(y)$ is assumed to correspond to an exponential spectral density of the following type:

$$S_{ff}(\kappa) = \frac{1}{4} \sigma_{ff}^2 b^3 \kappa^2 \exp(-b|\kappa|) \quad (7.49)$$

The inverse of shear modulus of the soil $1/G$ is evaluated at the middle point of each element (midpoint approach) by:

$$\frac{1}{G} = \frac{1}{G_0} (1 + f(y)) \quad (7.50)$$

where $f(y)$ is a one dimensional zero-mean homogeneous random field.

Dynamic variability response functions for shear wave propagation in soils

As stated above, the FMCS is used to numerically evaluate the DMRF/DVRF functions. Figures 7.3 to 7.5 depict the DMRF and DVRF functions estimated via FMCS for a Ricker wavelet, a Mavroeidis & Papageorgiou wavelet and the Gilroy earthquake motion record for $\sigma_{ff} = 0.2$. It is clear that the DMRF of the response quantities is constant with respect to the wave number of the underlying random field. In contrast, the DVRF is affected by a range of small values of wave number κ , indicating that the response variance of the 1D shear wave propagation phenomenon is sensitive to strongly correlated values of $1/G$.

Figures 7.6 and 7.7 present plots of the mean and variance of the displacement, velocity and acceleration of the soil surface for Mavroeidis & Papageorgiou wavelet and the Gilroy motion respectively, calculated with MCS and FMCS for a Gaussian field with $\sigma_{ff} = 0.2$ and correlation parameter $b = 40 m$. In the case of the Gilroy motion, only the first 10 s of the time histories of the ground response quantities are illustrated, since their values for $t \geq 10 s$ are very small. From the comparison of mean of displacement, velocity and acceleration, it is also evident that the results calculated with the FMCS methodology coincide with those calculated with the MCS. In case of variance, the FMCS methodology differs slightly from the MCS only in the peak values of the response, with a maximum error of less than 15%.

The FMCS methodology is applied next for a truncated-Gaussian field. The truncated field values are obtained through simple truncation of the underlying Gaussian field values $f(y)$, in order to lie in the $[-0.95, 0.95]$ range. The truncated-Gaussian field $g(y)$ has a different spectral density, which can be estimated by the following formula:

$$S_{gg}(\kappa) = \frac{1}{2\pi L_y} \left| \int_0^{L_y} f(y) \exp(-i\kappa y) dy \right|^2 \quad (7.51)$$

where L_y is the length of the sample functions of the non-Gaussian field modelling the inverse shear modulus. It is therefore important to note that the variance of the truncated field needs also to be calculated by the following relation:

$$\sigma_{gg}^2 = 2 \int_0^{+\infty} S_{gg}(\kappa) d\kappa \quad (7.52)$$

where the standard deviation of the truncated field is $\sigma_{gg} = 0.29$, while the correlation length parameter of the underlying Gaussian field is $b = 100 m$. It is exactly this corrected value that must be used in the FMCS procedure of eqs. (5.39) and (5.40). Figure 7.8 presents a comparison of the mean and variance of the displacement, velocity and acceleration between the FMCS and MCS. From this figure, it is also clear that the mean of the response quantities is accurately calculated with the FMCS. Small

variance errors are again observed for steep changes of the variance time-history as in the previous case, with error level less than 20%.

Finally, the FMCS methodology is applied for a lognormal field $g_L(y)$ obtained as a translation field from the following transformation:

$$f_L(y) = F_L^{-1} \{F[f(y)]\} \quad (7.53)$$

where $f(y)$ is a zero-mean Gaussian field, whereas the lognormal field can be simulated as:

$$g_L(y) = \exp(m + sf(y)) + a_l \quad (7.54)$$

where $f(y)$ is a zero-mean unit-variance, underlying Gaussian field generated with the spectral representation method (Shinozuka and Deodatis, 1996). In this particular case, the values $m = -0.0431$, $s = 0.2936$ and $a_l = -1.0$ were selected, leading to a standard deviation of the lognormal field $\sigma_{g_L g_L} = 0.3$. The spectral density of the underlying Gaussian S_{ff} is then again chosen from eq. (7.49) with correlation parameter $b = 20m$, while the new spectral density function $S_{g_L}(y)$ is recalculated using eq. (7.51). Comparison of response statistics calculate via the DMRF/DVRF methodology and the standard direct MCS for the Ricker wavelet case are illustrated in fig. 7.9. From this, it is obvious that the results obtained with the FMCS coincide with those obtained with the MCS for both the mean and variance.

For all the above case studies, the parameters chosen for the FMCS method are invariably the same. Specifically, the number of sinusoids for each wave number is $N = 5$, the upper wave number $\kappa_u = 1.0 \text{ rad/m}$, while the wave number axis is discretized in $M = 200$ intervals, i.e. 201 discrete wave numbers were used; this results to a total cost of $5 \cdot 201 = 1005$ finite element analyses. The corresponding number of direct MCS used for comparison is 2000, a number in which the MCS is considered to exhibit a fair accuracy. It is thus clear that the computational cost of the FMCS is considerably lower compared to the cost of the MCS in terms of required finite element analyses. The real advantage in terms of efficiency though, comes from the fact that once the FMCS for the given σ_{ff} is complete, all information regarding the variance and mean of the specified response quantity $d(t)$ can be obtained for any other correlation structure without having to perform any additional finite element analysis. This alone allows for efficient sensitivity analysis of the studied system. On the contrary, in the direct MCS case, all available data from the analyses correspond to the specific correlation structure used when generating the underlying random fields of the stochastic material property. Therefore, statistical quantities of the studied

Dynamic variability response functions for shear wave propagation in soils

response $d(t)$ for a different correlation structure require the generation of new random fields, followed by another series of finite element analyses.

Subsequently, the upper bounds of the response statistics are calculated. For this calculation, the maximum values $\text{DMRF}(t, k_{max}, \sigma_{ff})$, $\text{DVRF}(t, k_{max}, \sigma_{ff})$ are selected at each time. Figure 7.10 illustrates the upper bounds of the mean and variance of the soil surface response calculated for $\sigma_{ff} = 0.2$ for the Gilroy earthquake record. There is ample evidence that the larger values of the variance for displacement, velocity and acceleration of the ground surface correspond to the timesteps where the maximum values of the corresponding mean quantities occur. It is however very important to note that, for the value of $\sigma_{ff} = 0.2$ considered, the upper bounds of the variance of the ground response quantities are significantly larger. For instance, at time $t = 4.67$ s, the upper bound of the acceleration mean is 4.0 m/s^2 and the corresponding upper bound of the variance $3.5 \text{ m}^2/\text{s}^4$, leading to a coefficient of variation $COV = \sqrt{3.5}/4.0 = 0.48$.

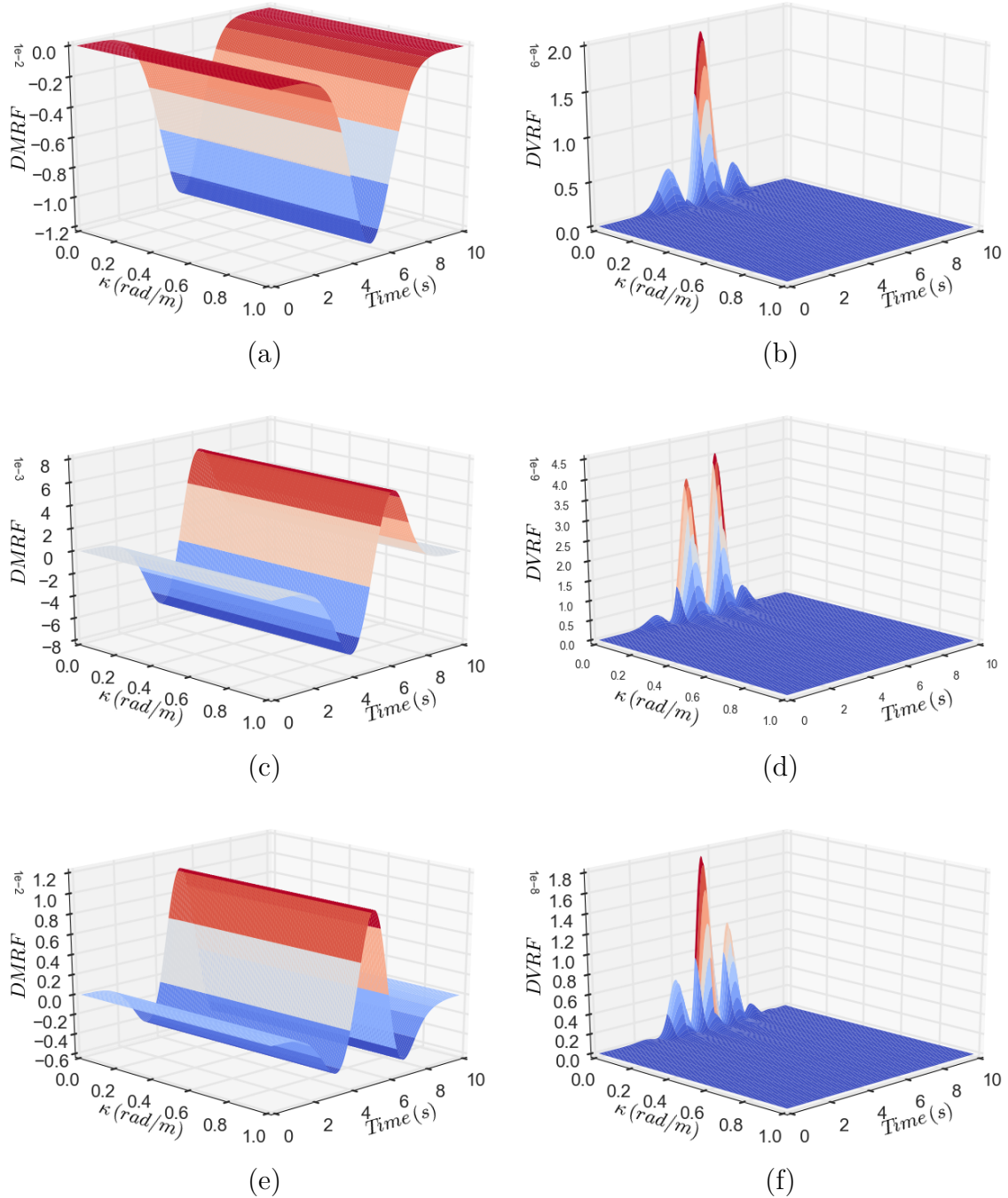


Figure 7.3. DMRF and DVRF of ground response for incoming Ricker wavelet with unit amplitude for $\sigma_{ff} = 0.2$: (a) displacement DMRF, (b) displacement DVRF, (c) velocity DMRF, (d) velocity DVRF, (e) acceleration DMRF and (f) acceleration DVRF.

Dynamic variability response functions for shear wave propagation in soils

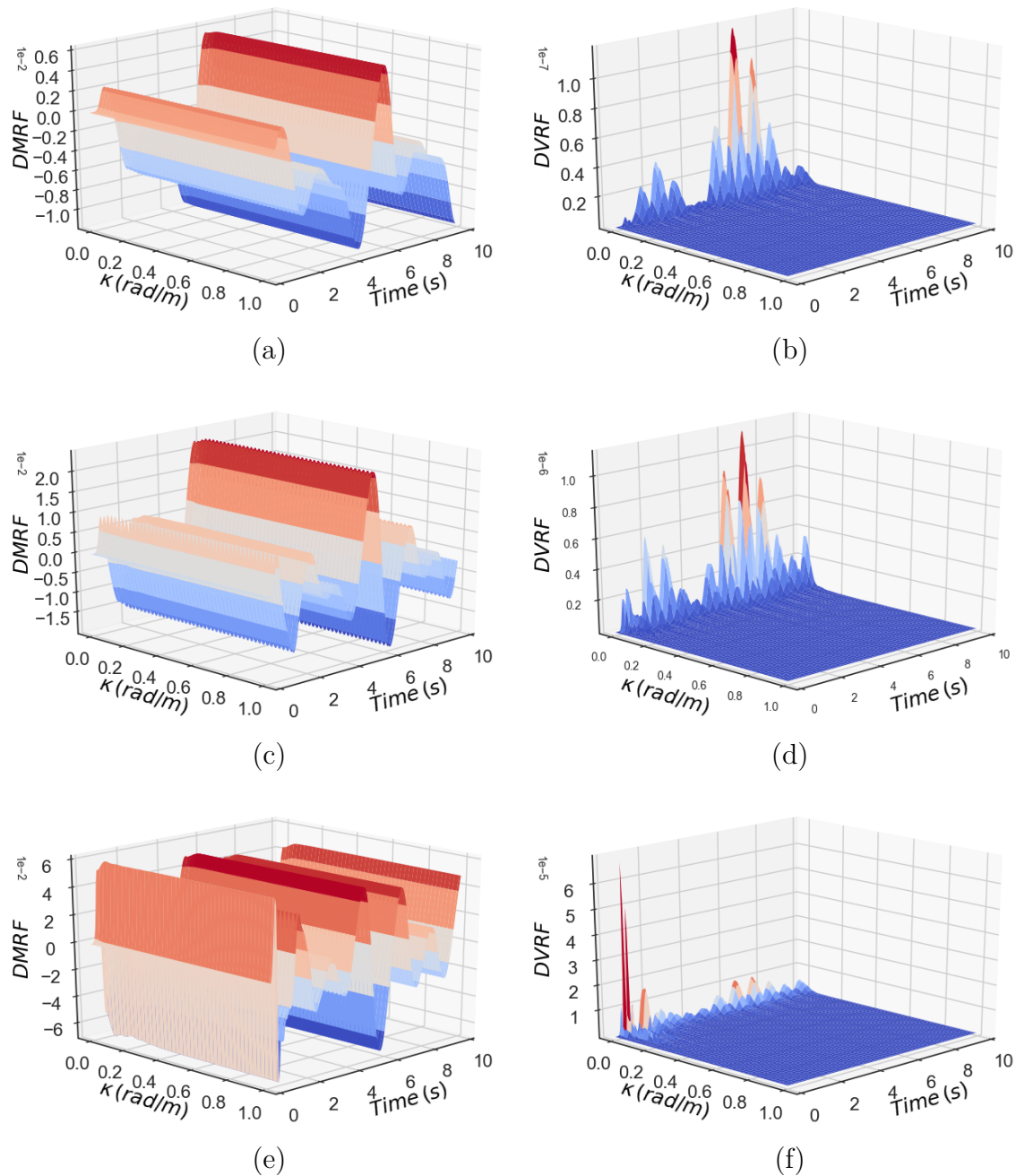


Figure 7.4. DMRF and DVRF of ground response for incoming Mavroeidis & Papageorgiou wavelet with unit amplitude for $\sigma_{ff} = 0.2$: (a) displacement DMRF, (b) displacement DVRF, (c) velocity DMRF, (d) velocity DVRF, (e) acceleration DMRF and (f) acceleration DVRF.

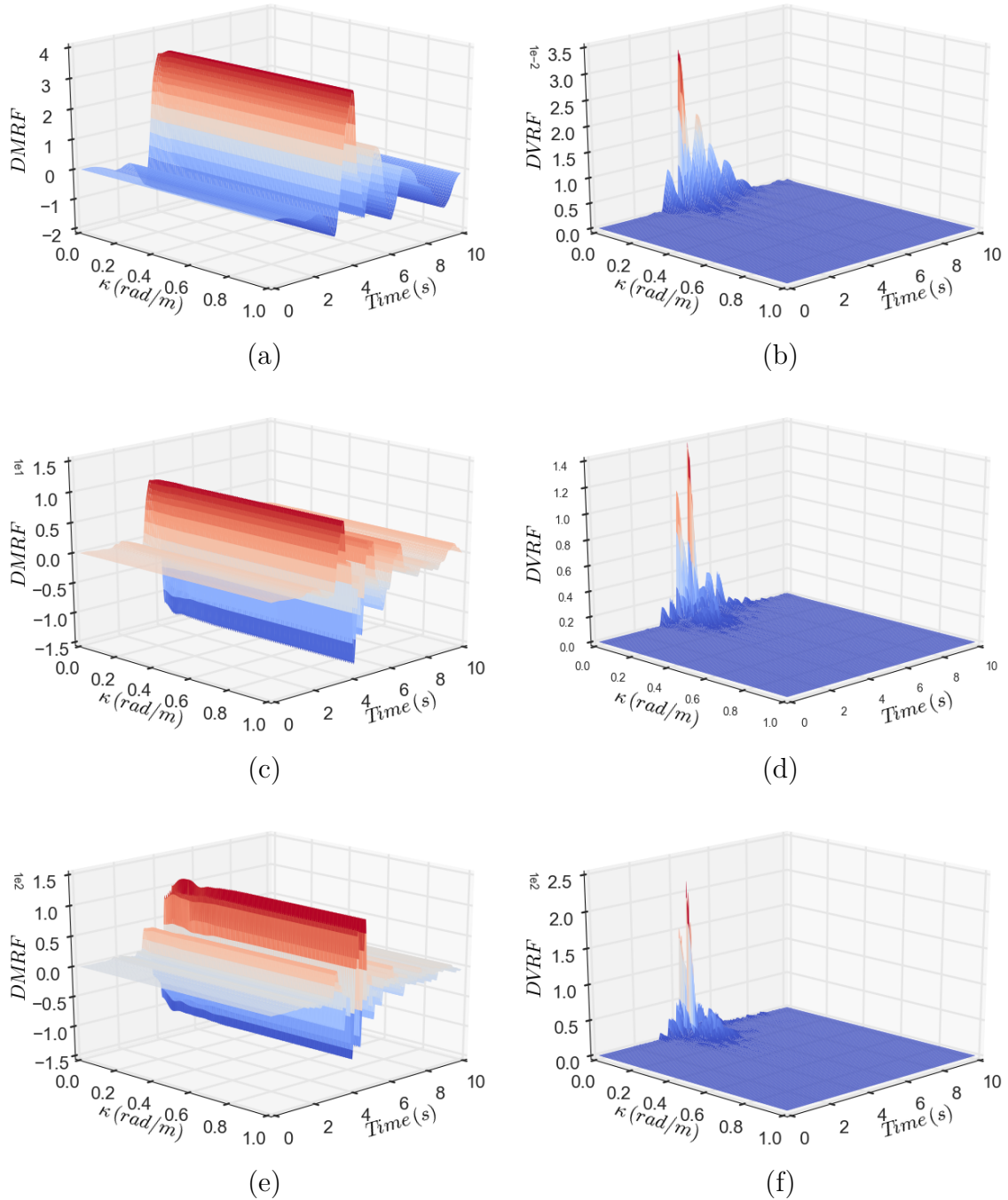


Figure 7.5. DMRF and DVRF of ground response for incoming Gilroy earthquake motion record for $\sigma_{ff} = 0.2$: (a) displacement DMRF, (b) displacement DVRF, (c) velocity DMRF, (d) velocity DVRF, (e) acceleration DMRF and (f) acceleration DVRF.

Dynamic variability response functions for shear wave propagation in soils

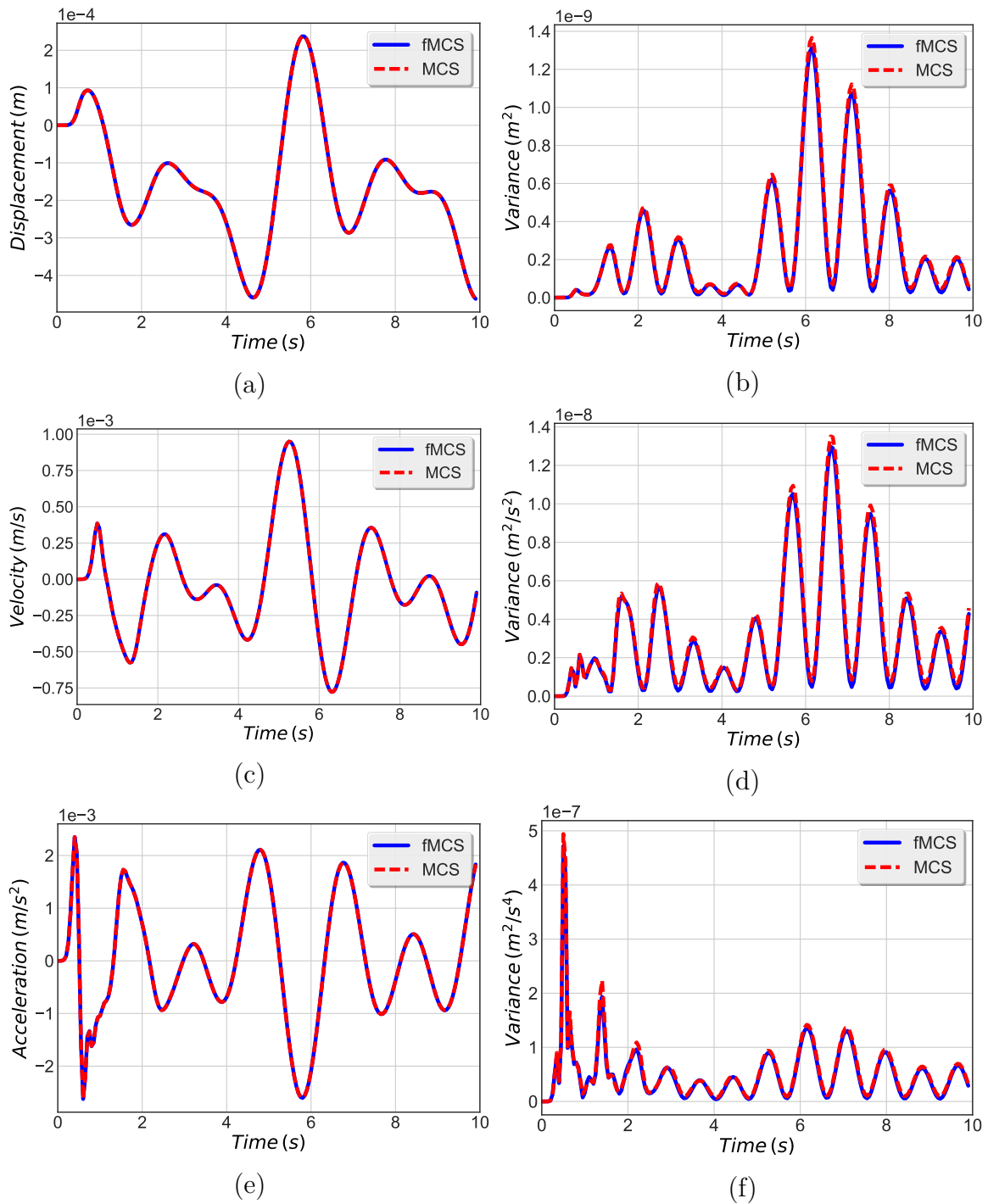


Figure 7.6. Mean and variance of ground response for incoming Mavroeidis & Papageorgiou wavelet for a Gaussian field with $\sigma_{ff} = 0.2$ and correlation parameter $b = 40 \text{ m}$: (a) displacement mean, (b) displacement variance, (c) velocity mean, (d) velocity variance, (e) acceleration mean and (f) acceleration variance.

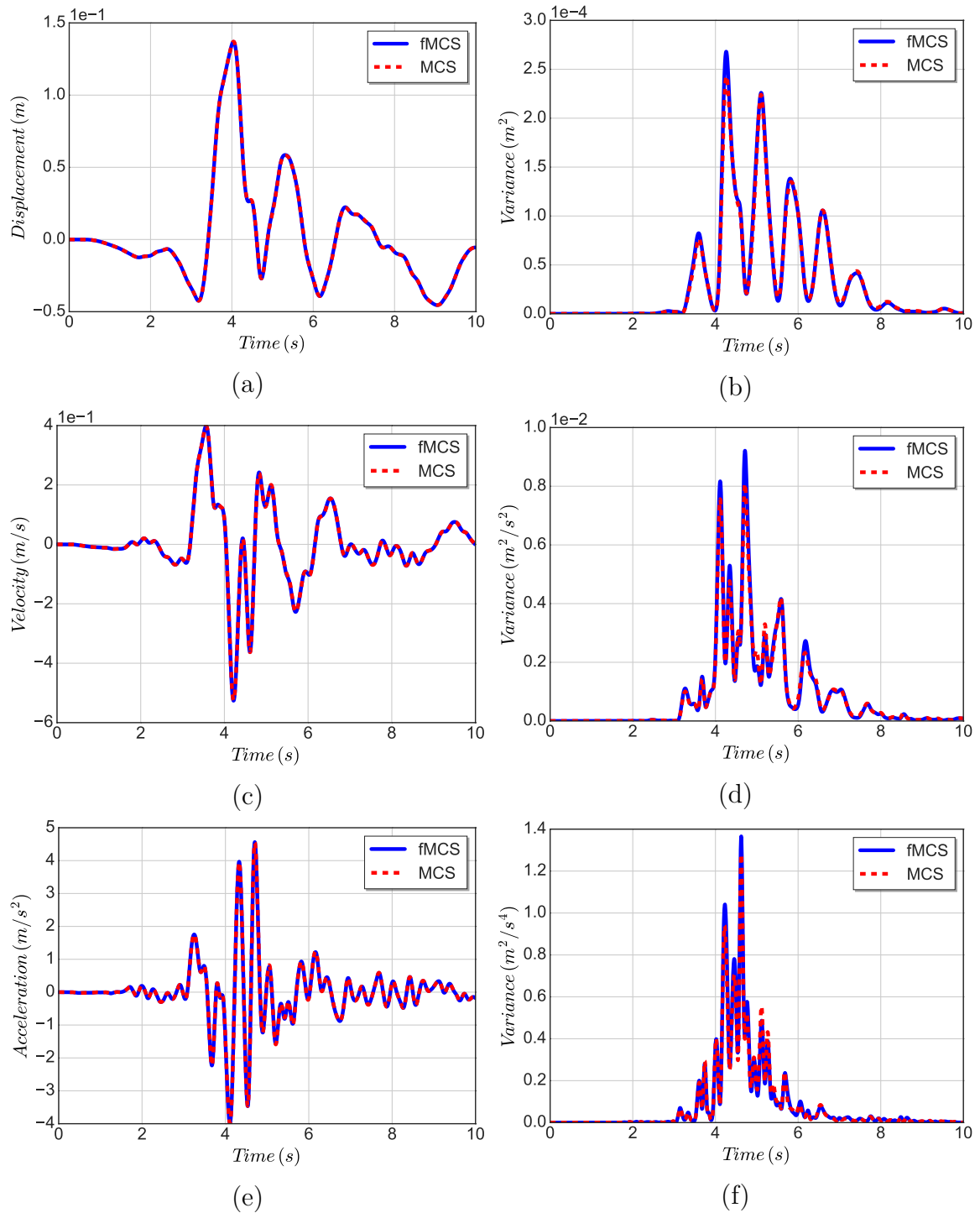


Figure 7.7. Mean and variance of ground response for incoming Gilroy motion for a Gaussian field with $\sigma_{ff} = 0.2$ and correlation parameter $b = 40 m$: (a) displacement mean, (b) displacement variance, (c) velocity mean, (d) velocity variance, (e) acceleration mean and (f) acceleration variance.

Dynamic variability response functions for shear wave propagation in soils

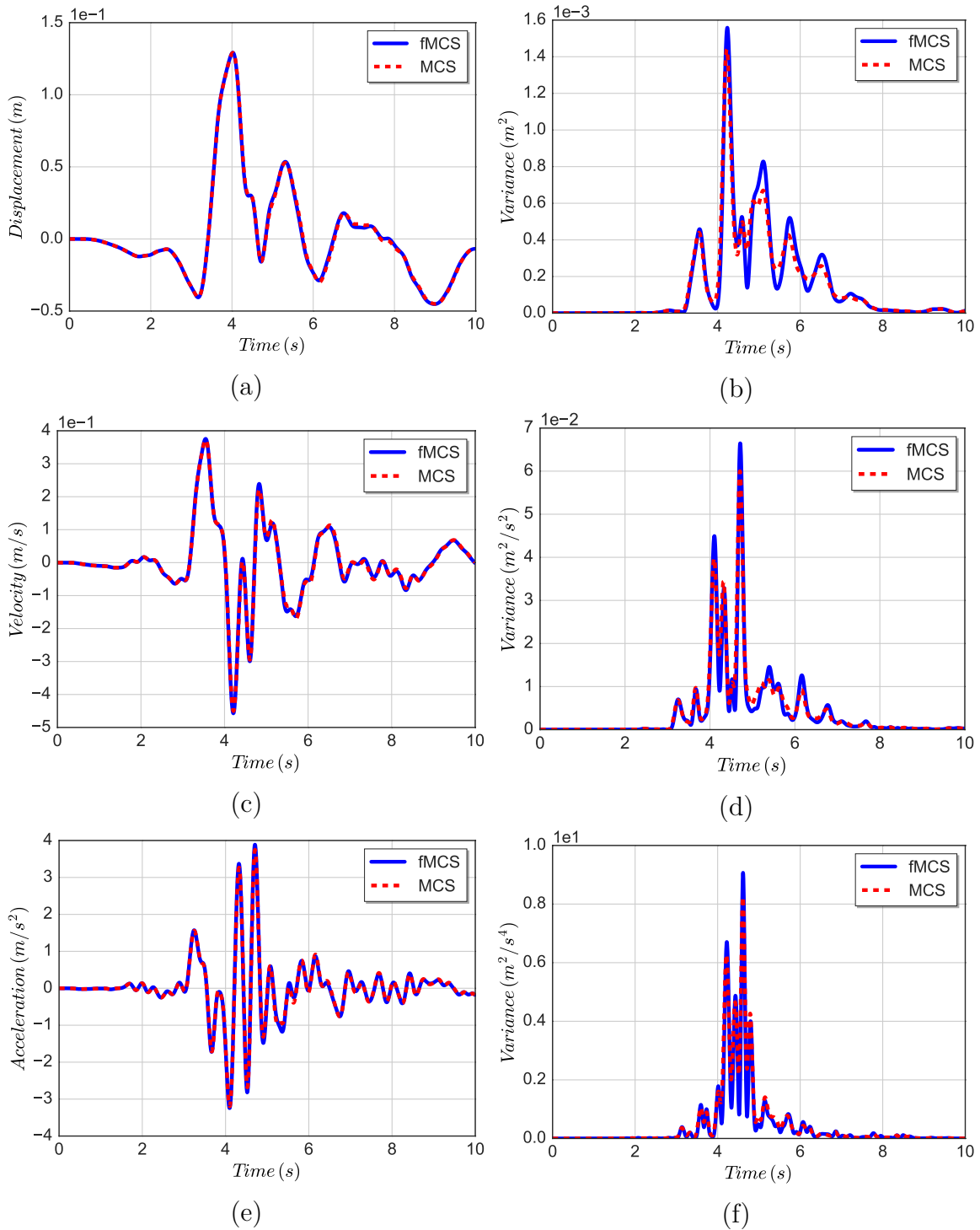


Figure 7.8. Mean and variance of ground response for incoming Gilroy motion for a truncated Gaussian field with $\sigma_{ff} = 0.3$ and correlation parameter $b = 100 m$: (a) displacement mean, (b) displacement variance, (c) velocity mean, (d) velocity variance, (e) acceleration mean and (f) acceleration variance.

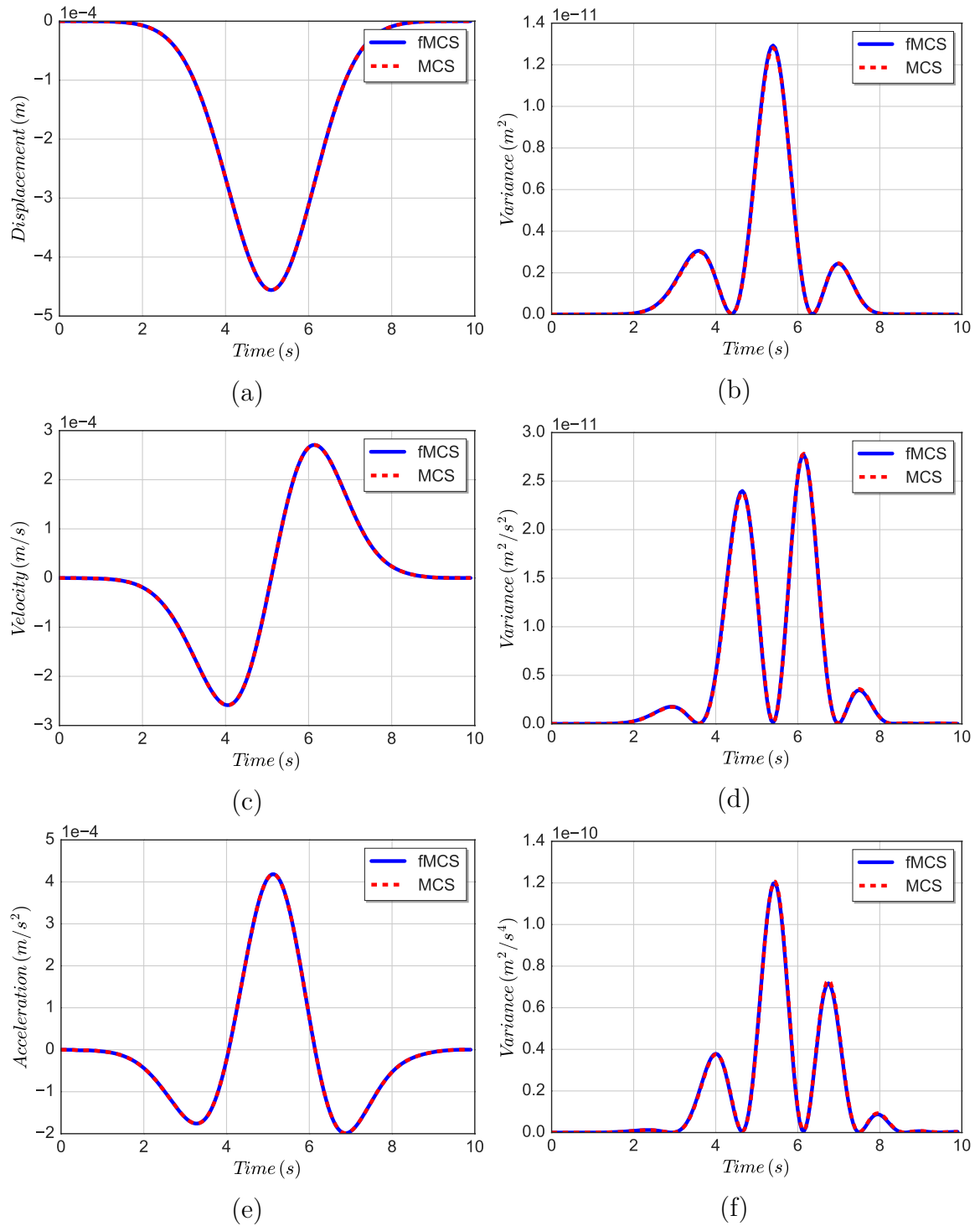


Figure 7.9. Mean and variance of ground response for incoming Ricker wavelet with unit amplitude for a lognormal field with $\sigma_{g_{Lg_L}} = 0.3$ and correlation parameter $b = 20 m$: (a) displacement mean, (b) displacement variance, (c) velocity mean, (d) velocity variance, (e) acceleration mean and (f) acceleration variance.

Dynamic variability response functions for shear wave propagation in soils

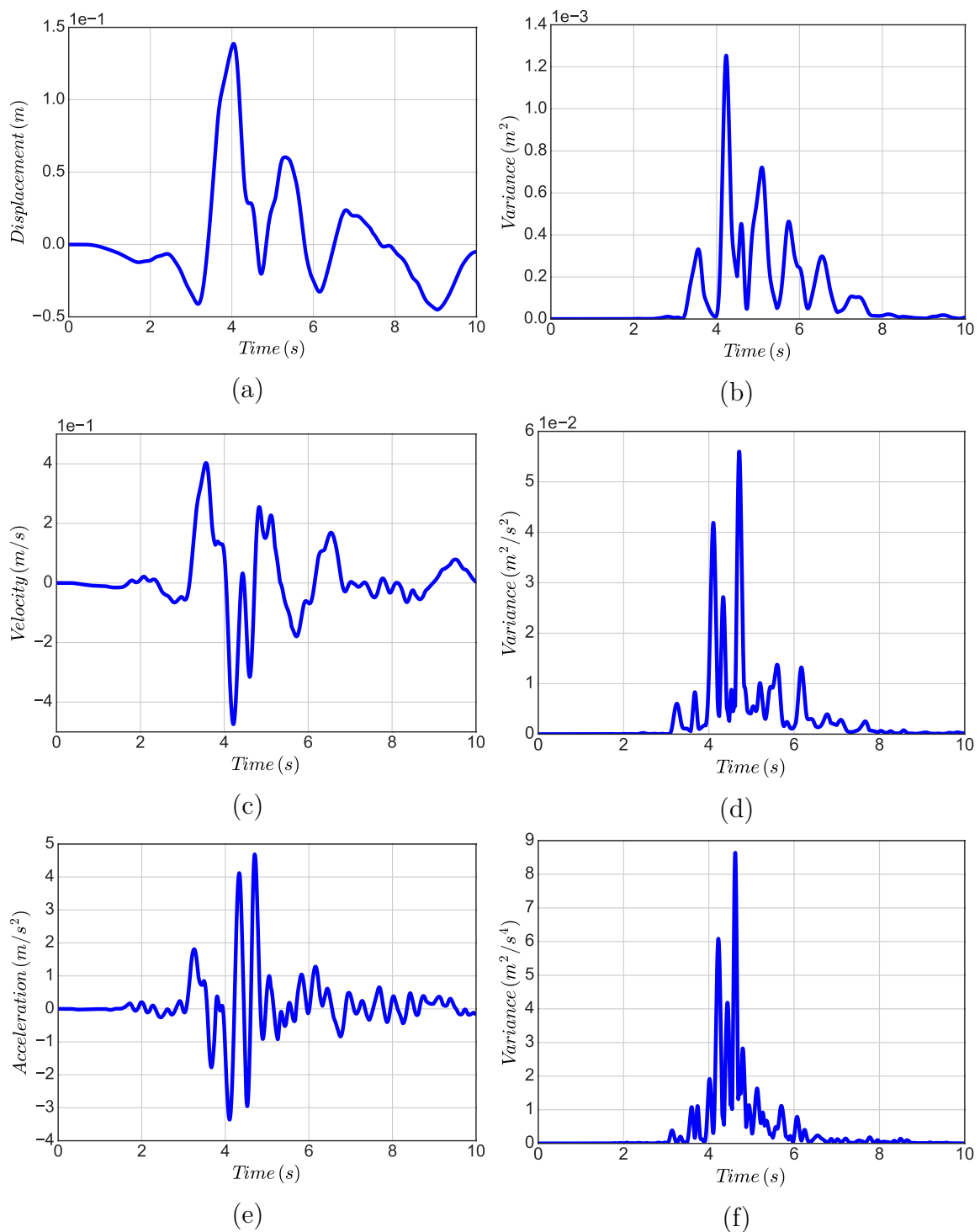


Figure 7.10. Upper bounds of the mean and variance of ground response for incoming earthquake for $\sigma_{ff} = 0.2$: (a) displacement mean, (b) displacement variance, (c) velocity mean, (d) velocity variance, (e) acceleration mean and (f) acceleration variance.

7.4.3 Wave propagation in 2D

For the 2D simulation of shear wave propagation, the corresponding model consists of a soil layer with horizontal dimension $L = 200\text{ m}$ and vertical dimension $H = 40\text{ m}$. Viscous dampers are added to the base nodes in both the horizontal and vertical directions, simulating the compliance of the bedrock layer; the numerical model is illustrated in fig. 7.2. The shear modulus of the bedrock is $G_b = 1386.24\text{ MPa}$ and its Poisson ratio $\nu = 0.3$, the damping values $c_{sb} = \rho_b \cdot V_{sb} = 1824.0\text{ kN} \cdot \text{s}/\text{m}^3$ for the horizontal and $c_{pb} = \rho_b \cdot V_{pb} = 3412.39\text{ kN} \cdot \text{s}/\text{m}^3$ for the vertical, where $V_{pb} = 1421.83\text{ m}/\text{s}$ is the P-wave velocity in the bedrock layer. In order to obtain the actual nodal damping values used in the finite element model, damping values c_{pb} and c_{sb} have to be multiplied with the corresponding nodal area A , i.e. $c_{sb}^{nodal} = c_{sb}A$ and $c_{pb}^{nodal} = c_{pb}A$. In general, given the shear modulus G , Poisson's ratio ν and density ρ of a material, the P-wave velocity can be calculated by $V_p = \sqrt{\left(\frac{G(2-2\nu)}{\rho(1-2\nu)}\right)}$. In addition, quadrilateral plane strain 4-node isoparametric elements (Bathe, 2006) with sides of 1 m have been used for a total number of 8000 elements. Analogous to the 1D cases, the test loads consist of a propagating unit Ricker synthetic wavelet, as well as a real recorded earthquake motion. A 2D correlation structure of exponential type is used with the spectral density function, given by:

$$S_{ff}(\kappa_x, \kappa_y) = \sigma_{ff}^2 \frac{b_x b_y}{4\pi} \exp\left(-\left(\frac{b_x \kappa_x}{2}\right)^2 - \left(\frac{b_y \kappa_y}{2}\right)^2\right) \quad (7.55)$$

The mean and variance of the response quantity $d(t)$ are calculated via eqs. (5.3) and (5.4) using numerical integration, since the FMCS methodology provides discrete values of the DMRF/DVRF functions. In the meanwhile, the horizontal response of the top middle node is monitored. Figures 7.11 and 7.12 depict the DMRF/DVRF functions estimated for the unit Ricker wavelet and Gilroy motion with underlying $\sigma_{ff} = 0.2$ for both cases. From these figures, it can be seen that the most interesting response variability characteristic lies on the observation that the DVRF values are high only for minute wave numbers on the κ_x axis, while a larger range of wave numbers on the κ_y axis contributes to the response variance. Thus, in 2D, the shear wave propagation variance is much more sensitive with respect to correlation characteristics of the vertical direction. In figs. 7.13 and 7.14, a comparison between the response mean and variance obtained via application of the FMCS and MCS is made for the Ricker wavelet and the Gilroy motion respectively. Note that the underlying random fields for both loading cases have standard deviation $\sigma_{ff} = 0.2$ and correlation parameters $b_x = b_y = 100\text{ m}$;

Dynamic variability response functions for shear wave propagation in soils

as anyone can see, the mean is accurately captured by the FMCS methodology. In terms of variance, similarly to the 1D case, errors exist only in cases of steep response changes, but stay within reasonable bounds with error less than 25%. Nevertheless, the actual shape of the variance is accurately captured.

For the FMCS in the 2D wave propagation analyses, the number of sinusoids for each wave number is $N = 5$, while wave number bounds are $\kappa_{xl} = 0.0 \text{ rad/m}$, $\kappa_{xu} = 0.1 \text{ rad/m}$ and $\kappa_{yl} = -0.5 \text{ rad/m}$, $\kappa_{yu} = 0.5 \text{ rad/m}$. The wave number axis κ_x is discretized in $M_1 = 10$ intervals, i.e. 11 discrete wave numbers, and the κ_y axis in $M_2 = 50$ intervals, i.e. 51 discrete wave numbers. This results to a total cost of $5 \cdot 11 \cdot 51 = 2805$ finite element analyses offering a good balance of computational cost and accuracy. The corresponding number of direct MCS analyses used for comparison is 2000; it is therefore obvious that, in terms of computational cost, the FMCS for the 2D case is comparable to the MCS in terms of required finite element analyses. As already stated in the 1D case, the true power of the DMRF/DVRF, lies the fact that all required data is available to calculate the statistics of the response quantities for alternative correlation structures without having to resort to further finite element analyses, which is the case for the direct MCS method.

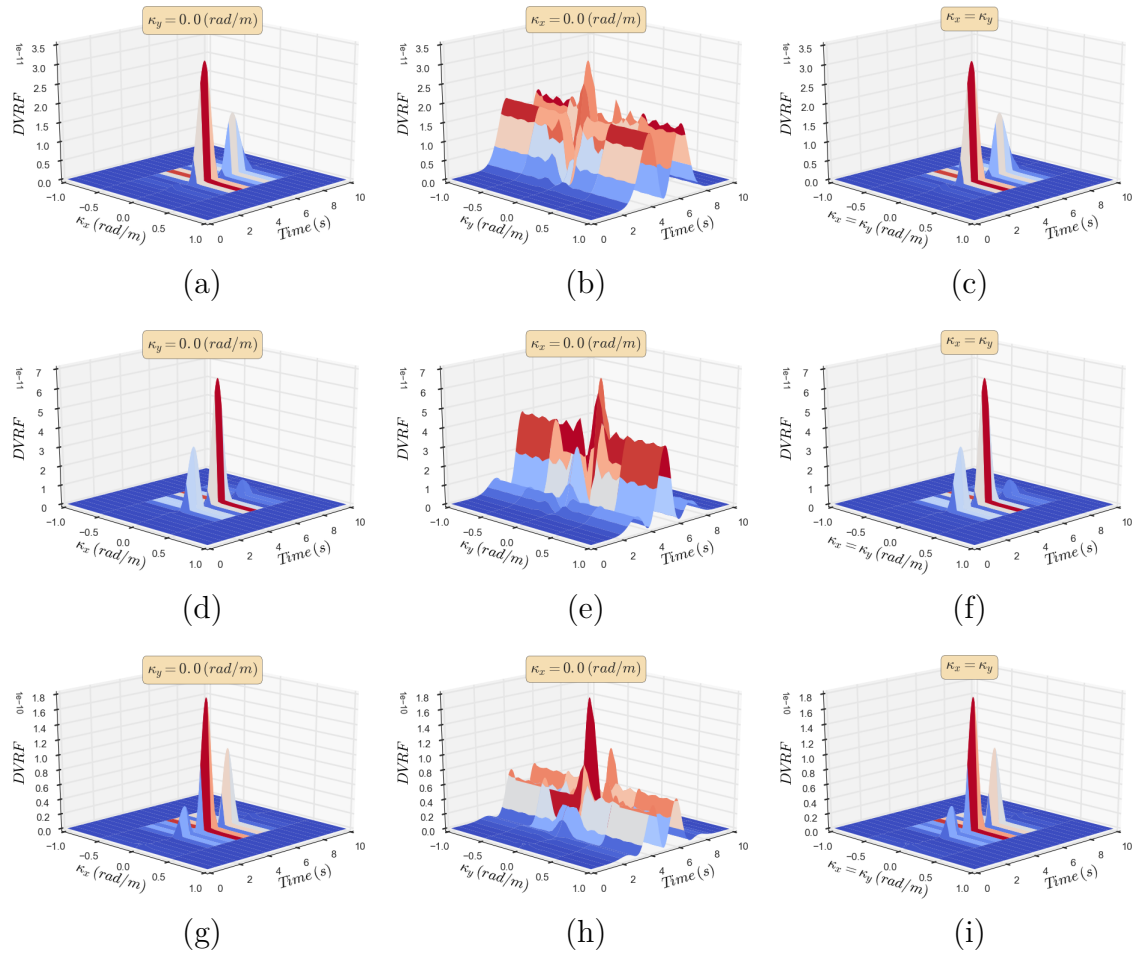


Figure 7.11. DVRF of ground response for incoming Ricker wavelet for $\sigma_{ff} = 0.2$: (a) displacement DVRF for $\kappa_y = 0.0$ (rad/m), (b) displacement DVRF for $\kappa_x = 0.0$ (rad/m), (c) displacement DVRF for $\kappa_x = \kappa_y$, (d) velocity DVRF for $\kappa_y = 0.0$ (rad/m), (e) velocity DVRF for $\kappa_x = 0.0$ (rad/m), (f) velocity DVRF for $\kappa_x = \kappa_y$, (g) acceleration DVRF for $\kappa_y = 0.0$ (rad/m), (h) acceleration DVRF for $\kappa_x = 0.0$ (rad/m) and (i) acceleration DVRF for $\kappa_x = \kappa_y$.

Dynamic variability response functions for shear wave propagation in soils

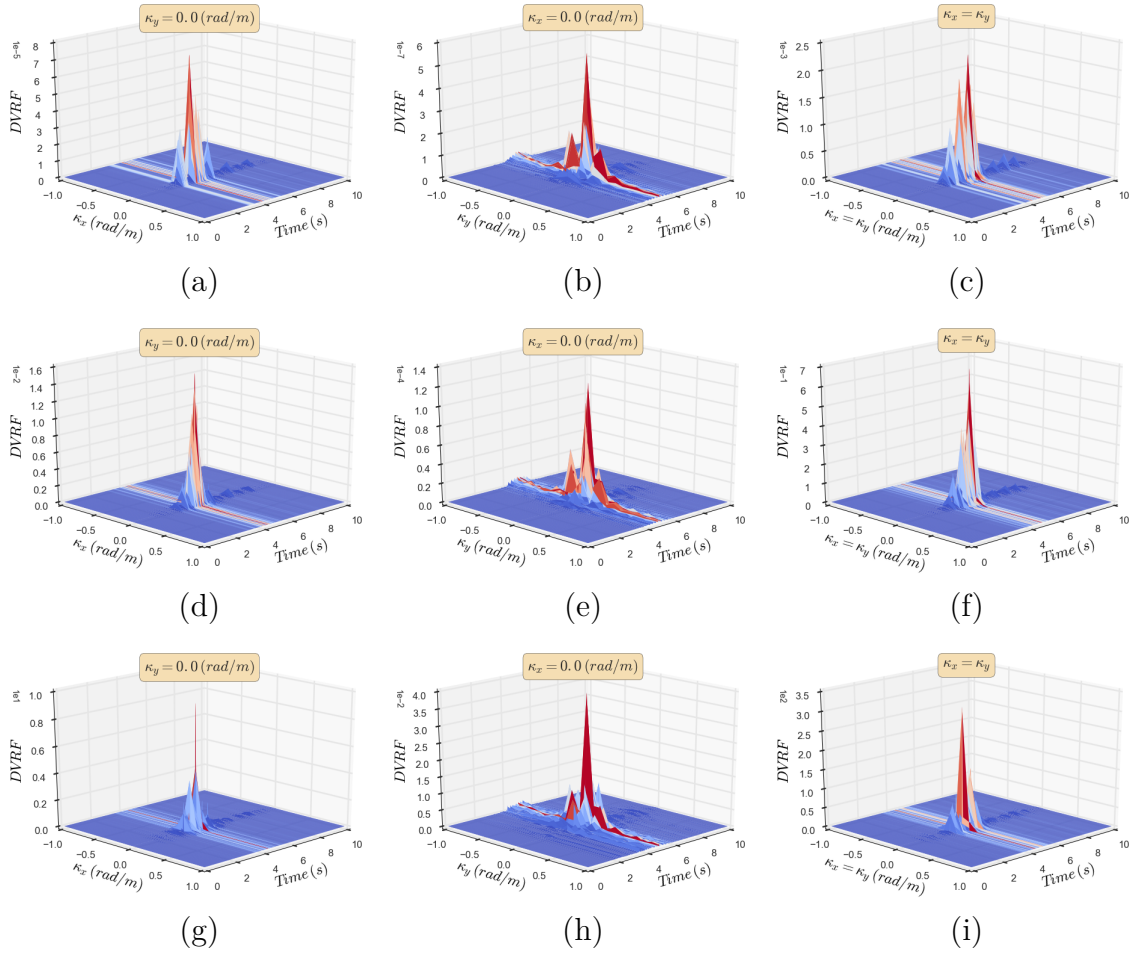


Figure 7.12. DVRF of ground response for incoming earthquake motion for $\sigma_{ff} = 0.2$: (a) displacement DVRF for $\kappa_y = 0.0 (rad/m)$, (b) displacement DVRF for $\kappa_x = 0.0 (rad/m)$, (c) displacement DVRF for $\kappa_x = \kappa_y$, (d) velocity DVRF for $\kappa_y = 0.0 (rad/m)$, (e) velocity DVRF for $\kappa_x = 0.0 (rad/m)$, (f) velocity DVRF for $\kappa_x = \kappa_y$, (g) acceleration DVRF for $\kappa_y = 0 (rad/m)$, (h) acceleration DVRF for $\kappa_x = 0.0 (rad/m)$ and (i) acceleration DVRF for $\kappa_x = \kappa_y$.

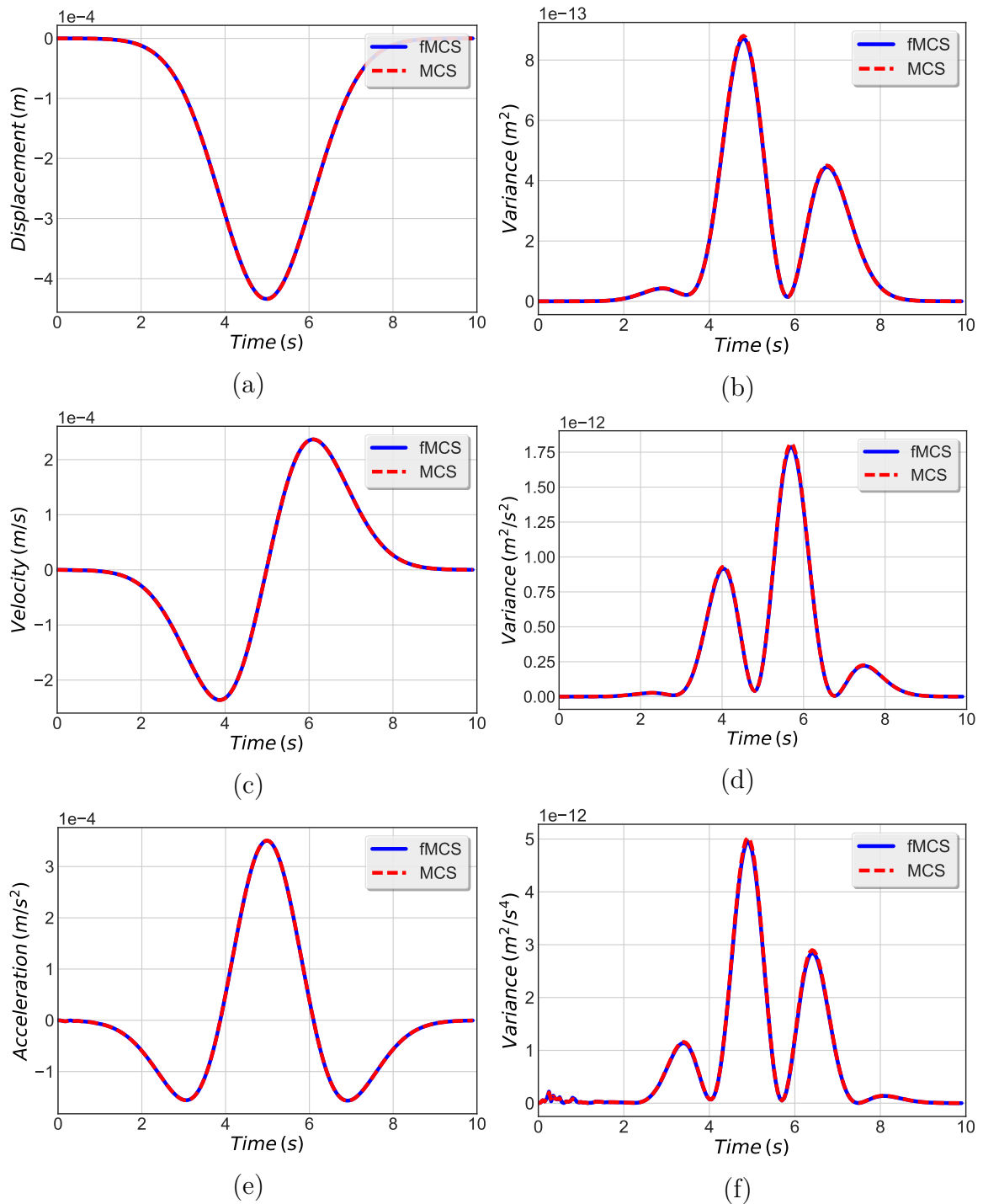


Figure 7.13. Mean and variance of ground response for Ricker wavelet for a Gaussian field with $\sigma_{ff} = 0.2$ and correlation parameters $b_x = b_y = 100$ m: (a) displacement mean, (b) displacement variance, (c) velocity mean, (d) velocity variance, (e) acceleration mean and (f) acceleration variance.

Dynamic variability response functions for shear wave propagation in soils

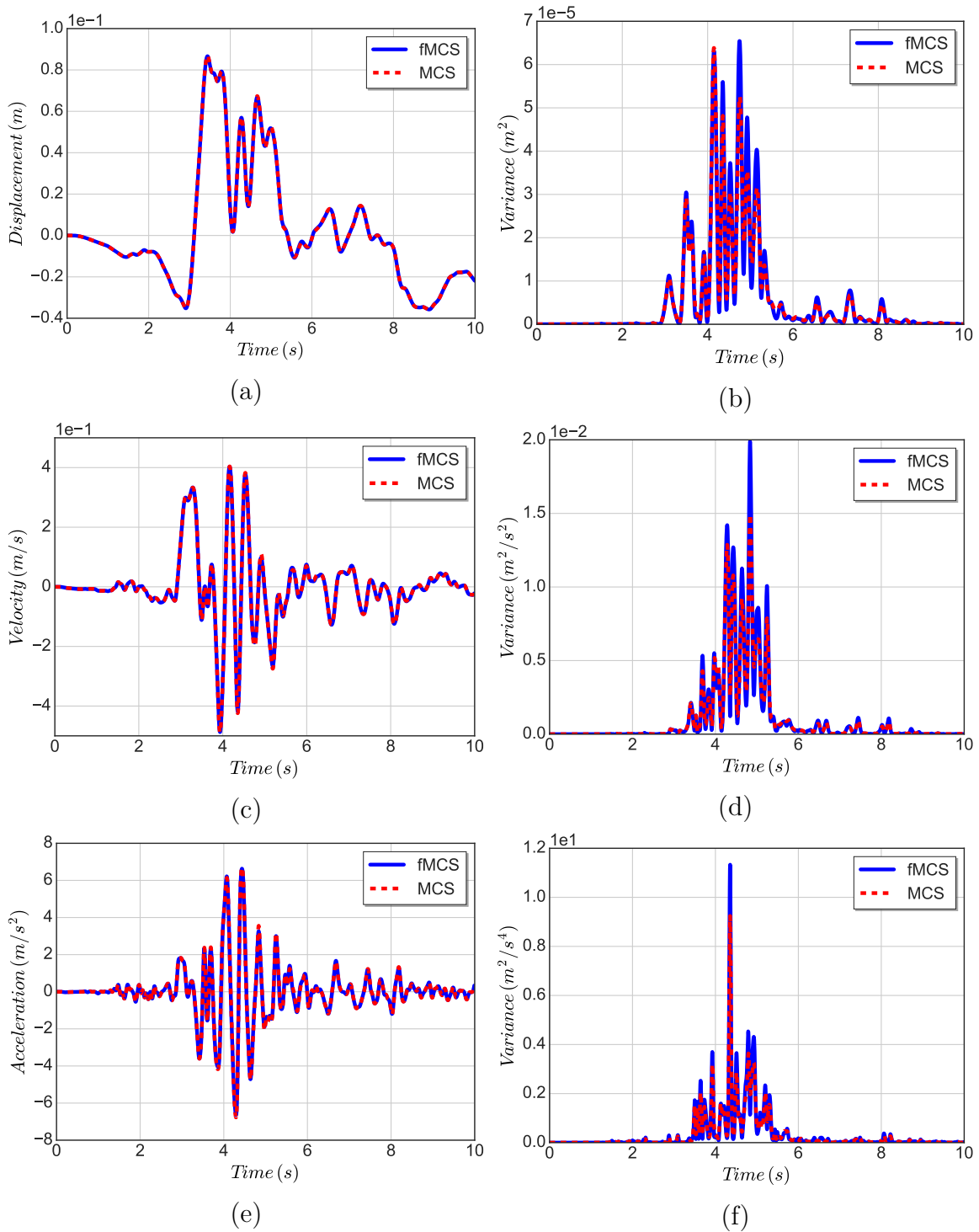


Figure 7.14. Mean and variance of ground response for Gilroy motion for a Gaussian field with $\sigma_{ff} = 0.2$ and correlation parameters $b_x = b_y = 100 m$: (a) displacement mean, (b) displacement variance, (c) velocity mean, (d) velocity variance, (e) acceleration mean and (f) acceleration variance.

7.5 Concluding remarks

In this study, it was shown that, according to the DMRF/DVRF methodology, the variance and mean of the ground response quantities, namely displacement, velocity and acceleration, are accurately calculated for shear wave propagation problems in soils. Errors regarding the system response are negligible when considering the mean of the response quantities, while the error of the calculated response variance based on the DVRF increases with larger values of standard deviation, as well as skewness of the underlying fields, but stays nevertheless within reasonable bounds. It was also demonstrated that the phenomenon of shear wave propagation in 1D soil is sensitive to underlying random field representations of $1/G$, which exhibit large correlation lengths. The DVRF spread is much more significant in the frequency axis corresponding to the vertical direction, as was demonstrated by 2D wave propagation analyses. Thus, in 2D problems and in the vertical dimension, the range of sensitive wave numbers is much larger. Finally, it was proven that the DMRF/DVRF functions are extremely useful when considering the incorporation of uncertain material parameters, revealing the system sensitivity to uncertainty; what's more, the DMRF/DVRF functions can be calculated effectively via the FMCS method. This fact alone leads to significant computational savings, since the spectral density and probability distribution free nature of the DMRF/DVRF functions allows the direct calculation of the mean and variance of the ground response quantities for any underlying correlation structure of $1/G$, without the need for further finite element simulations.

Chapter 8

Dynamic variability response functions for stochastic consolidation of soils

In this chapter, the case study of soil consolidation analyzed in chapter 6 is revisited using the DMRF/DVRF methodology used in chapter 7 to quantify the mean and variance of the response quantities of the footing-soil system. The FMCS method is again employed to numerically evaluate the DMRF/DVRF functions for the response quantities of interest. The results obtained via the DMRF/DVRF functions are then compared with the corresponding statistics obtained via the direct Monte Carlo simulation, in order to demonstrate the accuracy and effectiveness of the proposed methodology.

8.1 Revisiting the stochastic consolidation problem

As mentioned above, the problem consists of a rigid rough strip footing resting on a consolidating soil layer with uncertain permeability k and Young's modulus E . The corresponding permeability/Young's modulus at each spatial point (x, y) of the soil domain are given via the following relations:

$$k(x, y) = k_0(1 + f(x, y)) \quad (8.1)$$

$$E(x, y) = E_0(1 + f(x, y)) \quad (8.2)$$

where k_0 and E_0 are the mean values of permeability and Young's modulus respectively. As was the case in chapter 7, $f(x, y)$ corresponds to the random sinusoid used when

the FMCS is considered, while representing a zero mean homogeneous Gaussian random field in the case of the MCS. The geometry of the model, as well as the finite element discretization, are the same as the ones used in chapter 6 and are illustrated in fig. 6.3. Furthermore, the material properties used in the numerical model are the same with the corresponding ones used in chapter 6. Thus, the mean values of the uncertain k and E remain the same, but are nevertheless repeated here, i.e. $k_0 \equiv \mu_k = 1.22 \cdot 10^{-5} m^4 \cdot kN^{-1}/day$, $E_0 \equiv \mu_E = 622.7 kPa$.

Both footing settlement and pore pressure response statistics are studied. In particular, in terms of footing settlements, referring to fig. 6.4 ν_A , ν_C , as well as $\nu_{AD} = \nu_A - \nu_D$ are considered, while in terms of pore pressures, representative soil points below the footing center C at depths $B/10$, $B/5$, $B/2$ and B are studied denoted as $p_{B/10}$, $p_{B/5}$, $p_{B/2}$ and p_B respectively.

Finally, in order to demonstrate the accuracy of the methodology, direct comparison between the results obtained through the FMCS-based DMRF/DVRF functions and the ones from the direct MCS is made. For both methodologies, the standard deviation of both k and E is $\sigma_k = \sigma_E = 0.2$. Furthermore, in the MCS case, the underlying correlation structure has a spectral density of exponential type given by:

$$S_{ff}(\kappa_x, \kappa_y) = \frac{\sigma^2 b_1 b_2}{4\pi} \exp\left(-\left(\frac{b_1 \kappa_x}{2}\right)^2 - \left(\frac{b_2 \kappa_y}{2}\right)^2\right) \quad (8.3)$$

Isotropic correlation lengths $b_{1_k} = b_{2_k} = b_{1_E} = b_{2_E} = 10.0 m$ are used for both permeability and Young's modulus. The spectral representation method is employed to generate realizations of the random fields for each stochastic material property needed for the MCS method.

8.2 Footing settlement statistics

In this section, we study the response statistics of the footing settlements. Specifically, ν_A and ν_C , as well as ν_{AD} are considered. Comparison between the results obtained via the DMRF/DVRF methodology and the MCS method is made. The DMRF/DVRF functions are calculated according to the FMCS method analyzed in section 5.4.

Figures 8.1 and 8.2 illustrate the results of mean and variance for ν_A , ν_C and ν_{AD} . Due to the symmetry of the problem, the statistics of ν_D are the same with the statistics of ν_A and are therefore omitted. It is clear that in all cases, the mean value is in complete agreement for the FMCS and MCS. It is important to note though, that the mean value of ν_{AD} is theoretically zero due to the symmetry of the studied problem.

The values shown both for the FMCS and MCS are non-zero, but being minute, they are attributed to the finite accuracy available and therefore should not be taken into account. In terms of variance, only for very high values a difference between the FMCS and MCS is seen, although the error stays within the acceptable range of 3-5%.

In fig. 8.3, the DVRF function of the settlement ν_{AD} for stochastic k is illustrated. By inspecting the DVRF with respect to wave number axes κ_x and κ_y respectively, it can be clearly seen that the DVRF values corresponding to κ_x are many magnitudes larger than the corresponding ones for κ_y , namely $1.0e^{-7}$ compared to $1.0e^{-15}$. According to these observations, the variance of ν_{AD} is much more sensitive to the variability of k on the horizontal direction compared to the vertical.

The same observation can be made by inspecting fig. 8.4 where the DVRF function for stochastic E is illustrated. In this case, the corresponding values of the DVRF for κ_x and κ_y are $1.0e^{-4}$ and $1.0e^{-12}$ respectively.

Considering all the above, it can be said that the differential settlement variance is mostly governed by the variability of k and E with respect to the horizontal axis. In addition, in both k and E , the predominant wave numbers governing the variance lie in the vicinity of $\kappa_x = 0.25$ (rad/m). It is also obvious that the values of the DVRF for the case of E are much larger than the ones of the k case, this being in agreement with the results obtained for the same problem in chapter 6.

The DMRF/DVRF functions for the settlement of the footing center, i.e. ν_C , are illustrated next in figs. 8.5 and 8.6 for k and E respectively. In both cases, the DMRF is constant with respect to κ_x and κ_y . What's more, the contribution of κ_x and κ_y wave numbers is of the same order of magnitude, namely $1.0e^{-6}$ for k and $1.0e^{-4}$ for E . To conclude, the significant wave numbers for the DVRF in all cases lie close to $\kappa_x = 0.0$ (rad/m) and $\kappa_y = 0.0$ (rad/m), suggesting that the variance of ν_C is sensitive to strongly correlated random fields in both x and y dimensions.

Dynamic variability response functions for stochastic consolidation of soils

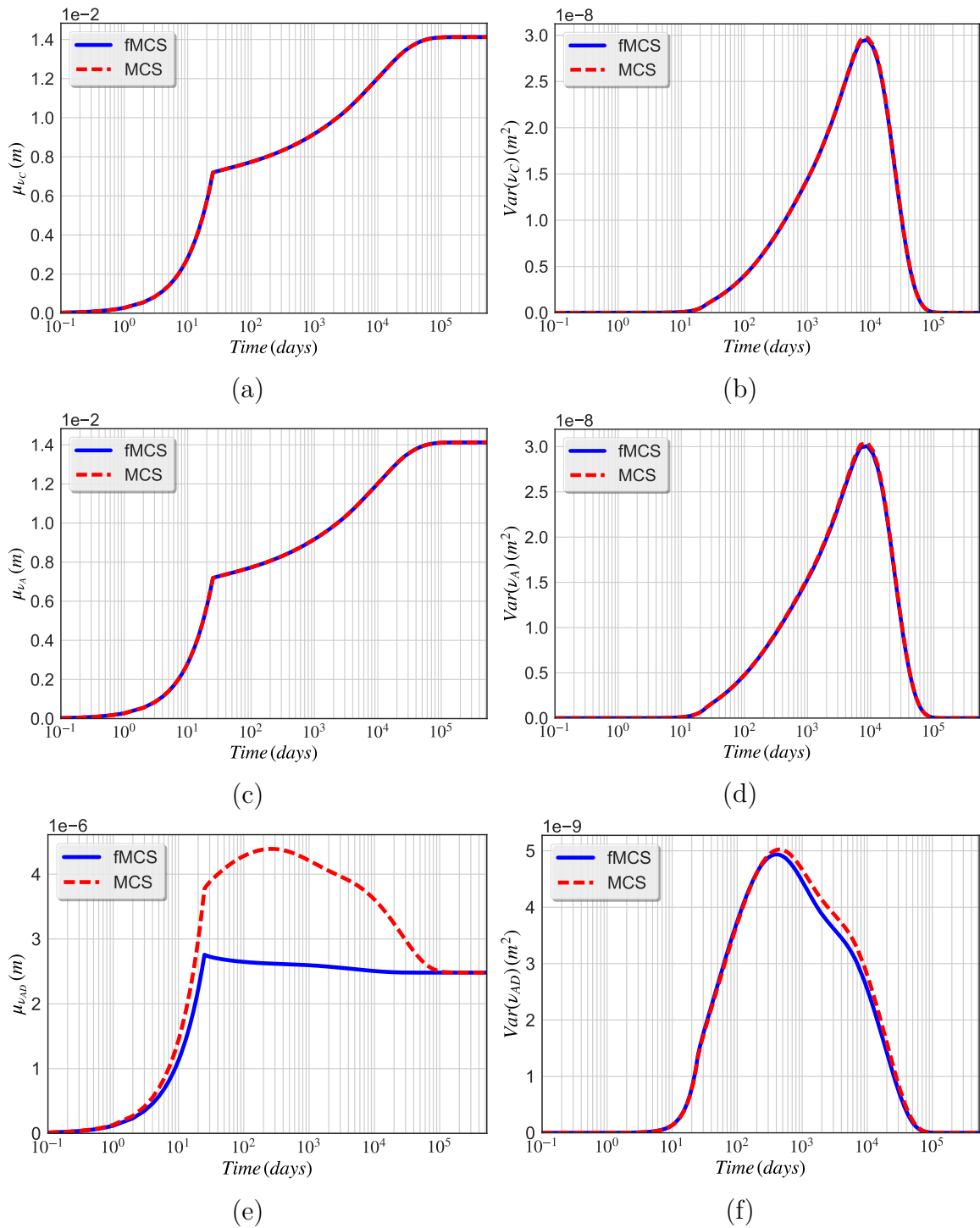


Figure 8.1. Mean and variance for various footing settlement for stochastic permeability with $\sigma_k = 0.2$ and correlation length $b = 10\text{ m}$: (a) μ_{ν_C} , (b) $Var(\nu_C)$, (c) μ_{ν_A} , (d) $Var(\nu_A)$, (e) $\mu_{\nu_{AD}}$ and (f) $Var(\nu_{AD})$.

8.2 Footing settlement statistics

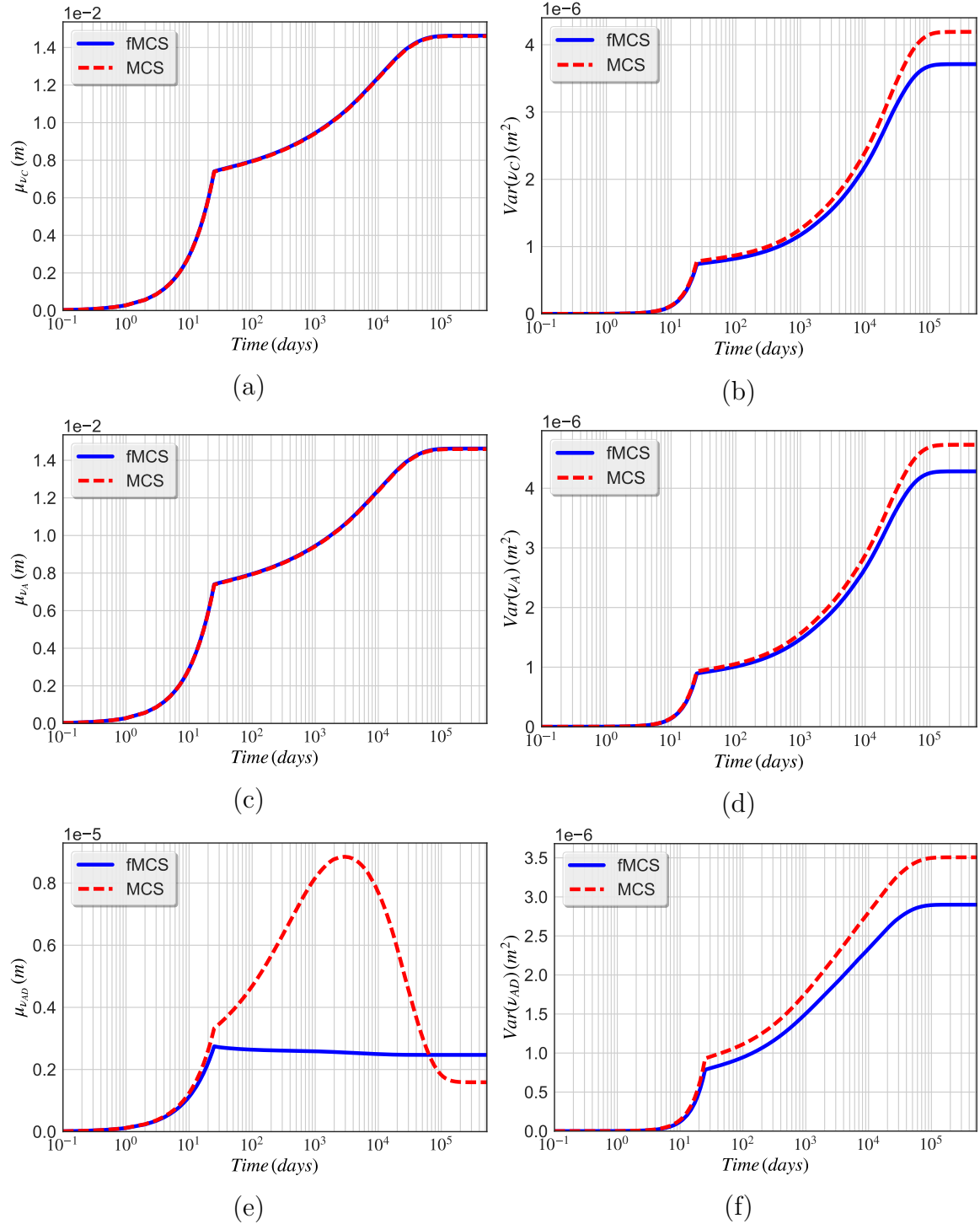


Figure 8.2. Mean and variance for various footing settlement for stochastic Young's modulus with $\sigma_E = 0.2$ and correlation length $b = 10$ m: (a) μ_{ν_C} , (b) $Var(\nu_C)$, (c) μ_{ν_A} , (d) $Var(\nu_A)$, (e) $\mu_{\nu_{AD}}$ and (f) $Var(\nu_{AD})$.

Dynamic variability response functions for stochastic consolidation of soils

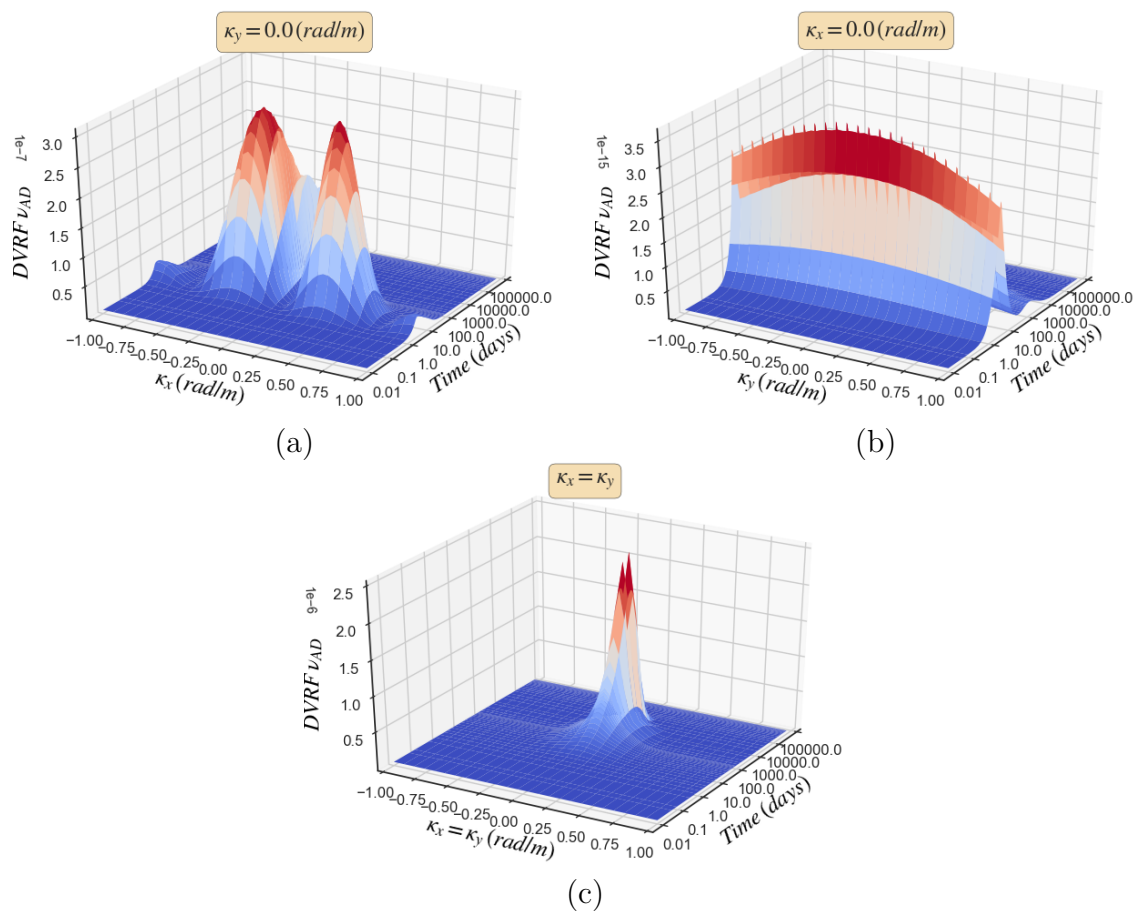


Figure 8.3. DVRF functions for settlement ν_{AD} of the footing for permeability with $\sigma_k = 0.2$ for: (a) $\kappa_y = 0.0$ (rad/m), (b) $\kappa_x = 0.0$ (rad/m) and (c) $\kappa_x = \kappa_y$.

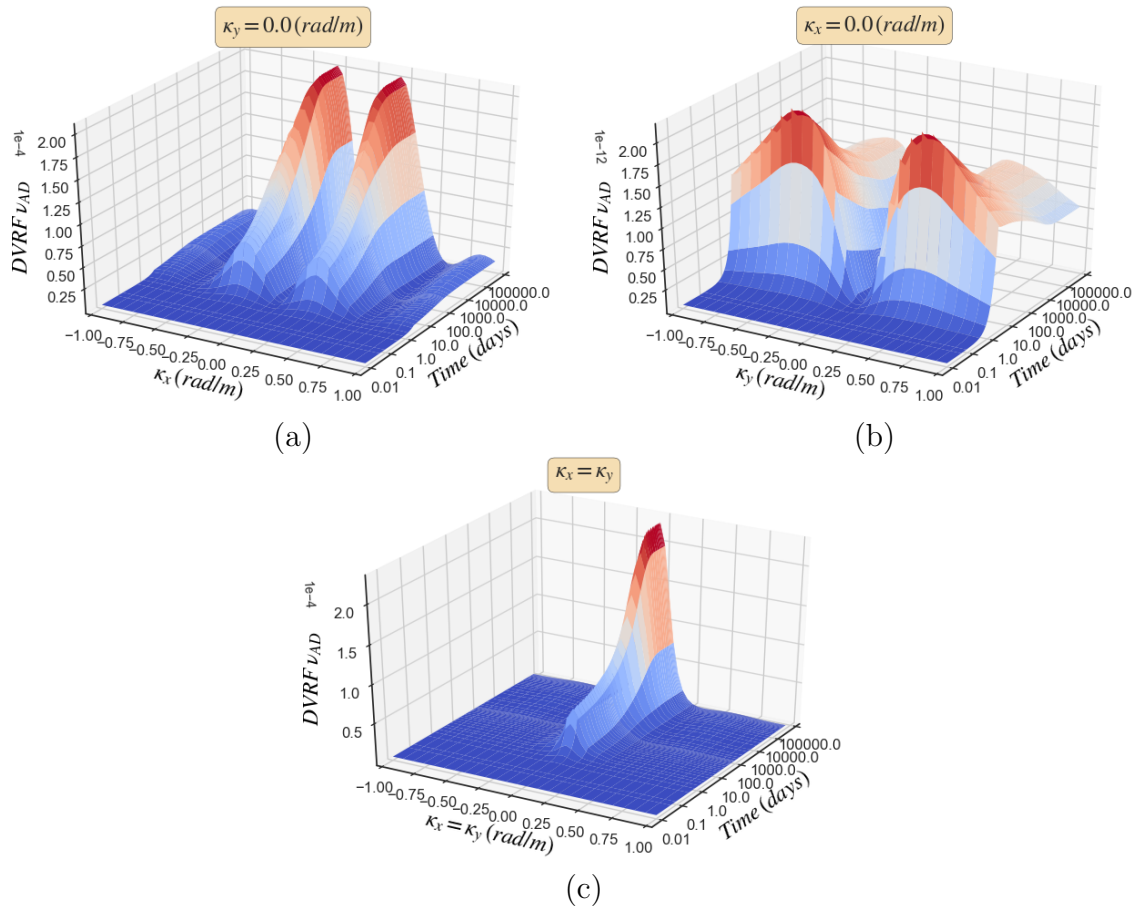


Figure 8.4. DVRF functions for settlement ν_{AD} of the footing for stochastic Young's modulus with $\sigma_E = 0.2$ for: (a) $\kappa_y = 0.0$ (rad/m), (b) $\kappa_x = 0.0$ (rad/m) and (c) $\kappa_x = \kappa_y$.

Dynamic variability response functions for stochastic consolidation of soils

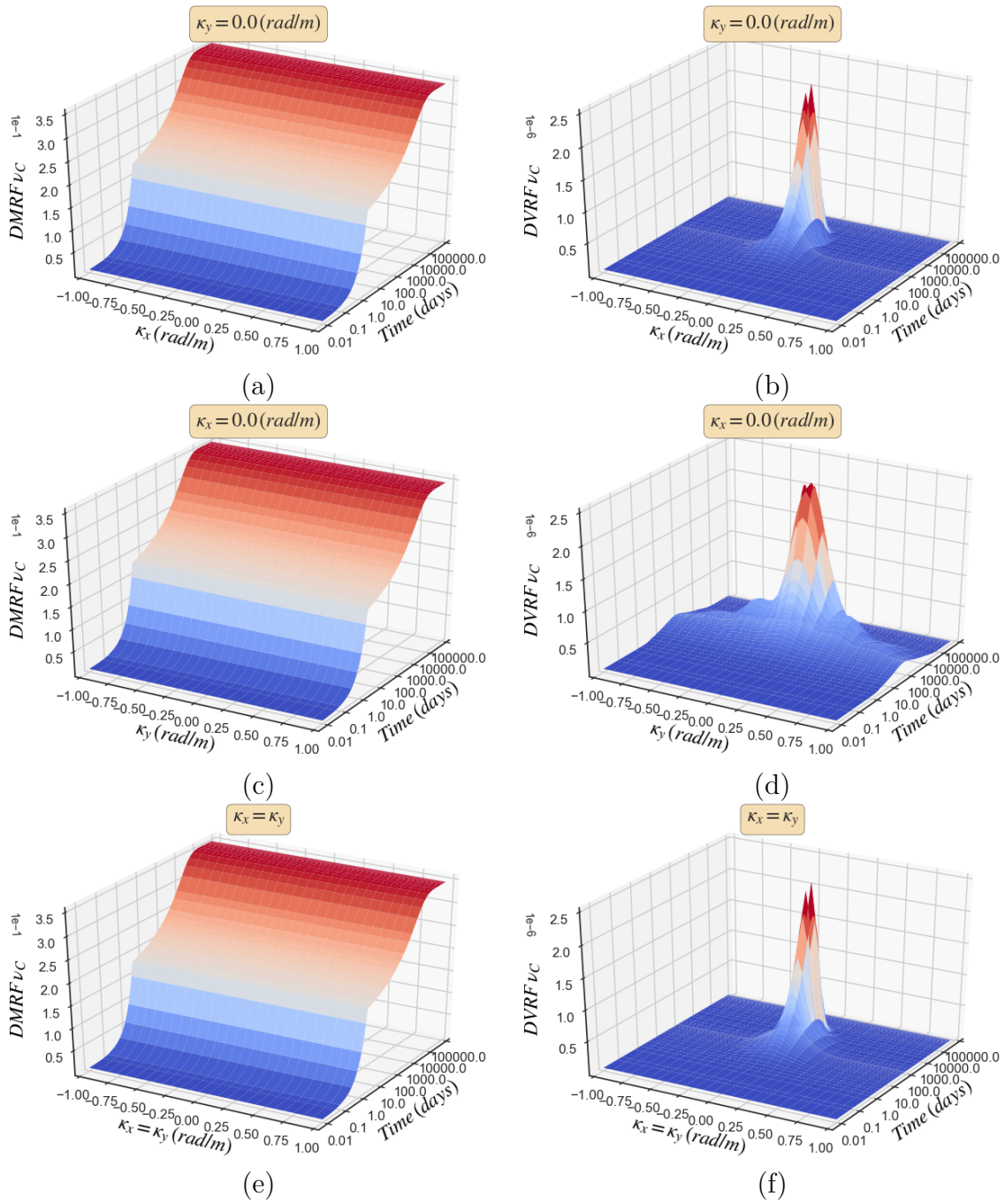


Figure 8.5. DMRF and DVRF functions for settlement ν_C of the footing center for permeability with $\sigma_k = 0.2$: (a) DMRF for $\kappa_y = 0.0$ (rad/m), (b) DVRF for $\kappa_y = 0.0$ (rad/m), (c) DMRF for $\kappa_x = 0.0$ (rad/m), (d) DVRF for $\kappa_x = 0.0$ (rad/m), (e) DMRF for $\kappa_x = \kappa_y$ and (f) DVRF for $\kappa_x = \kappa_y$.

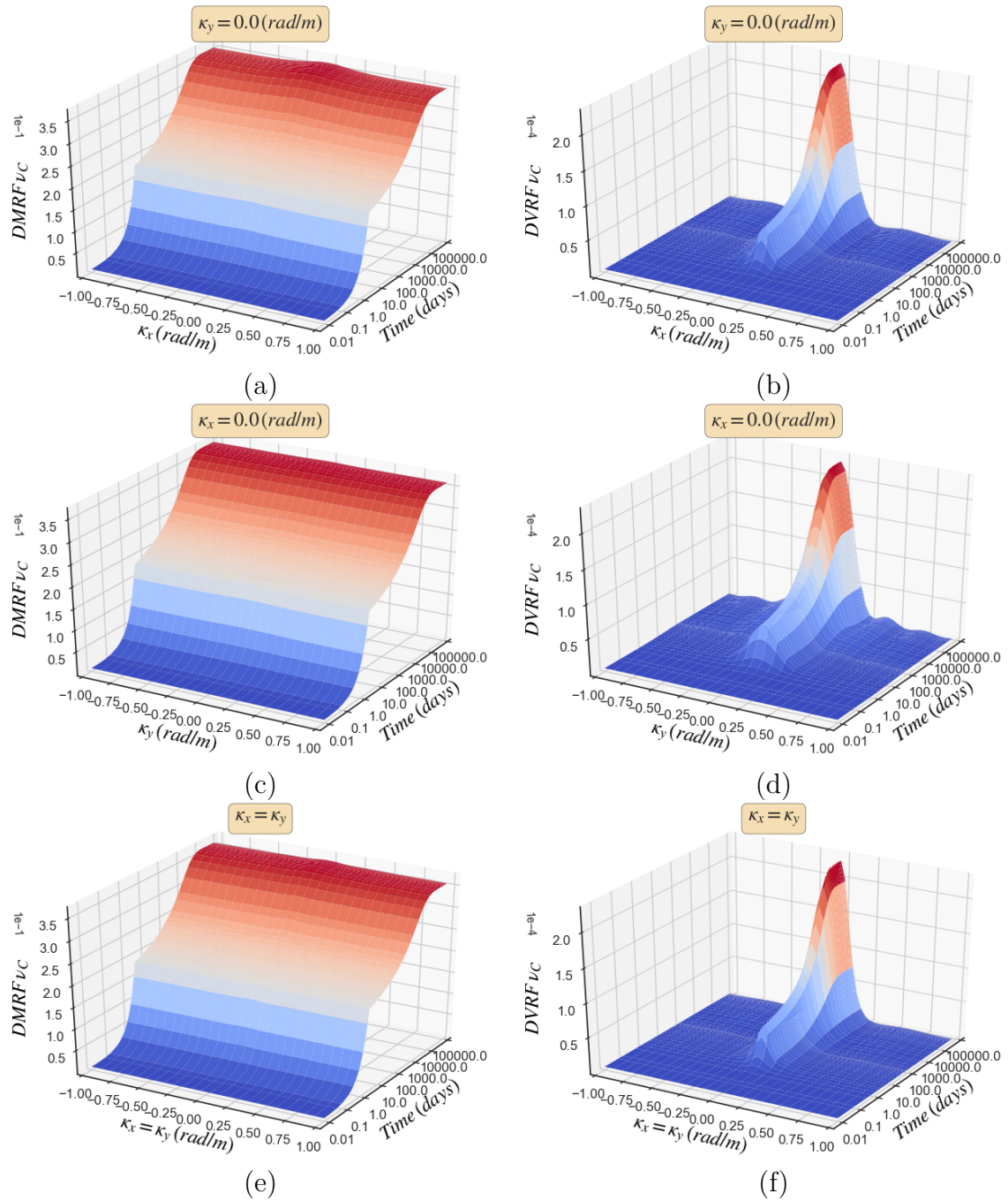


Figure 8.6. DMRF and DVRF functions for settlement ν_C of the footing center for stochastic Young's modulus with $\sigma_E = 0.2$: (a) DMRF for $\kappa_y = 0.0$ (rad/m), (b) DVRF for $\kappa_y = 0.0$ (rad/m), (c) DMRF for $\kappa_x = 0.0$ (rad/m), (d) DVRF for $\kappa_x = 0.0$ (rad/m), (e) DMRF for $\kappa_x = \kappa_y$ and (f) DVRF for $\kappa_x = \kappa_y$.

8.3 Excess pore pressure statistics

In this section, the statistics of the excess pore pressure generated in the soil below the center of the footing are studied. In order to demonstrate the accuracy of the DMRF/DVRF methodology, the pore pressures at depths $B/10$, $B/5$, $B/2$ and B (B denoting the footing width), namely $p_{B/10}$, $p_{B/5}$, $p_{B/2}$ and p_B , are used.

Figures 8.7 to 8.10 illustrate the time evolving mean and variance of the pore pressures mentioned above. Comparing the mean and variance of the pore pressures examined for both spatially variable k and E , it is clear that the FMCS-based DMRF/DVRF results coincide with the ones obtained through the MCS method. This fact is also true for all the studied pore pressures at various depths. As was the case for footing settlements, the advantage of the DMRF/DVRF method lies in the insight provided by the DMRF/DVRF functions on the sensitivity of the pore pressure statistics on the correlation structure characteristics of the underlying uncertain material properties. Figures 8.11 to 8.18 illustrate the DMRF/DVRF functions for pore pressures at all the depths mentioned above. Studying these, it is clear that in all depths and for both k and E , the DMRF functions are constant with respect to κ_x , as well as κ_y . The situation is different though, when considering the DVRF functions. Examining the DVRF functions in figs. 8.11 and 8.12 for $p_{B/10}$, it is obvious that, in the case of k , slight differences are visible with respect to κ_x and κ_y , while in the E case, predominant wave numbers exist for both κ_x and κ_y axes.

The DVRF function for $p_{B/5}$ is plotted in fig. 8.13 for k . Now, the DVRF appears to be definitely more sensitive to small κ_x wave numbers, i.e. strongly correlated permeability in the horizontal direction, whereas being affected more or less equally by a wide range of wave numbers κ_y . The DVRF function for $p_{B/5}$ for E is plotted in fig. 8.14, where it becomes clear that the predominant wave numbers for both κ_x and κ_y lie in the $(-0.50, -0.25) \cup (0.25, 0.50)$ (rad/m) range. Finally, the DVRF for $p_{B/2}$ and p_B depicted in figs. 8.15 and 8.17 for k is examined. In this case, the DVRF is significant only for small κ_x and κ_y wave numbers, i.e. for strongly correlated k values in the horizontal and vertical dimensions. In contrast, for spatially variable E the DVRF functions shown in figs. 8.16 and 8.18 terms, the predominant wave numbers lie in the vicinity of $\kappa_x = -0.75$ (rad/m), $\kappa_x = 0.75$ (rad/m) and $(-1.0, -0.75) \cup (0.75, 1.00)$ (rad/m) for κ_y .

To conclude, it can be said that with increasing depth, the variance of excess pore pressures is sensitive to strongly correlated values of k , while in the case of E , there is significant contribution for a wide range of wave numbers κ_x and κ_y .

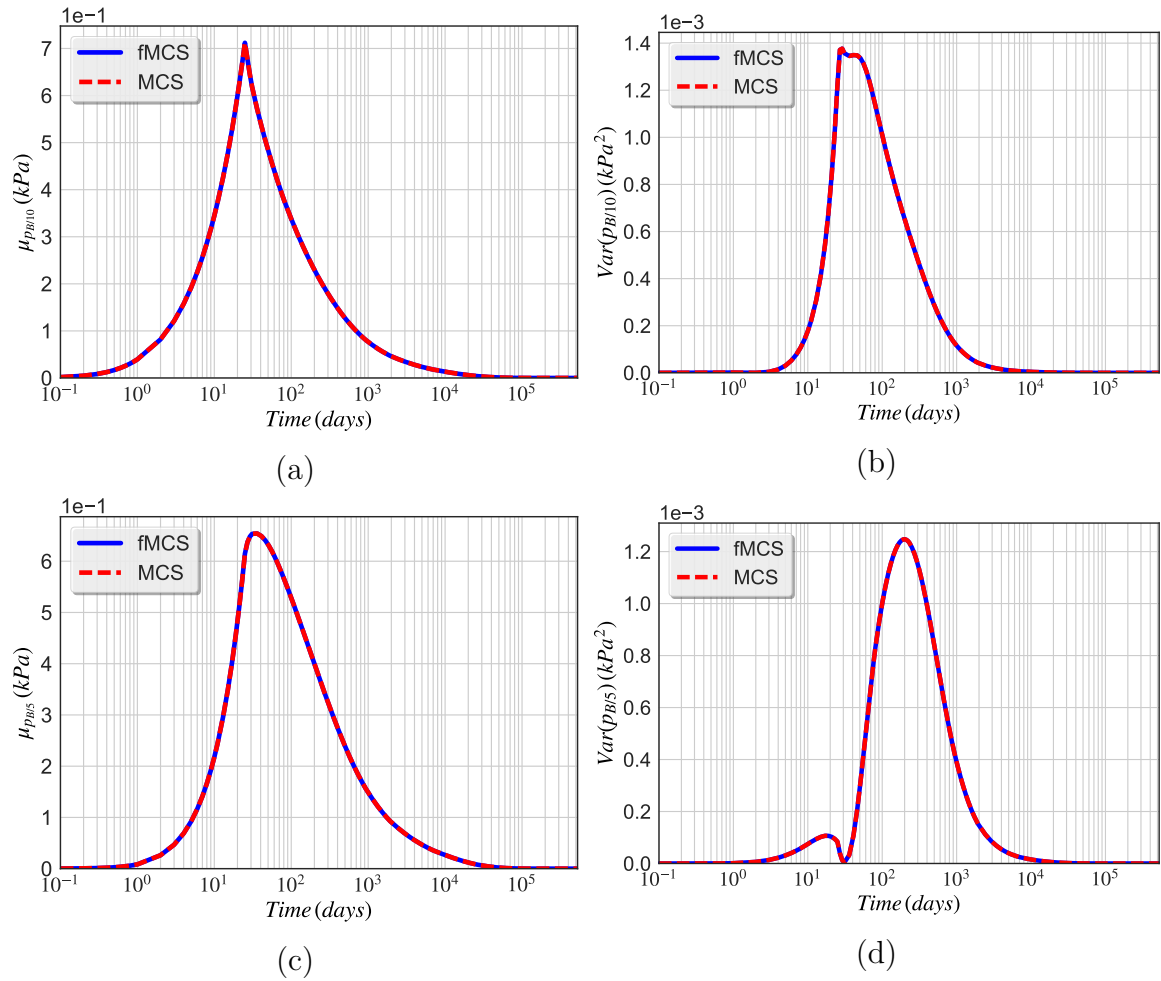


Figure 8.7. Mean and variance for excess pore pressure at depths $B/10$ and $B/5$ for stochastic permeability with $\sigma_k = 0.2$ and correlation length $b = 10 m$: (a) $\mu_{p_{B/10}}$, (b) $Var(p_{B/10})$, (c) $\mu_{p_{B/5}}$ and (d) $Var(p_{B/5})$.

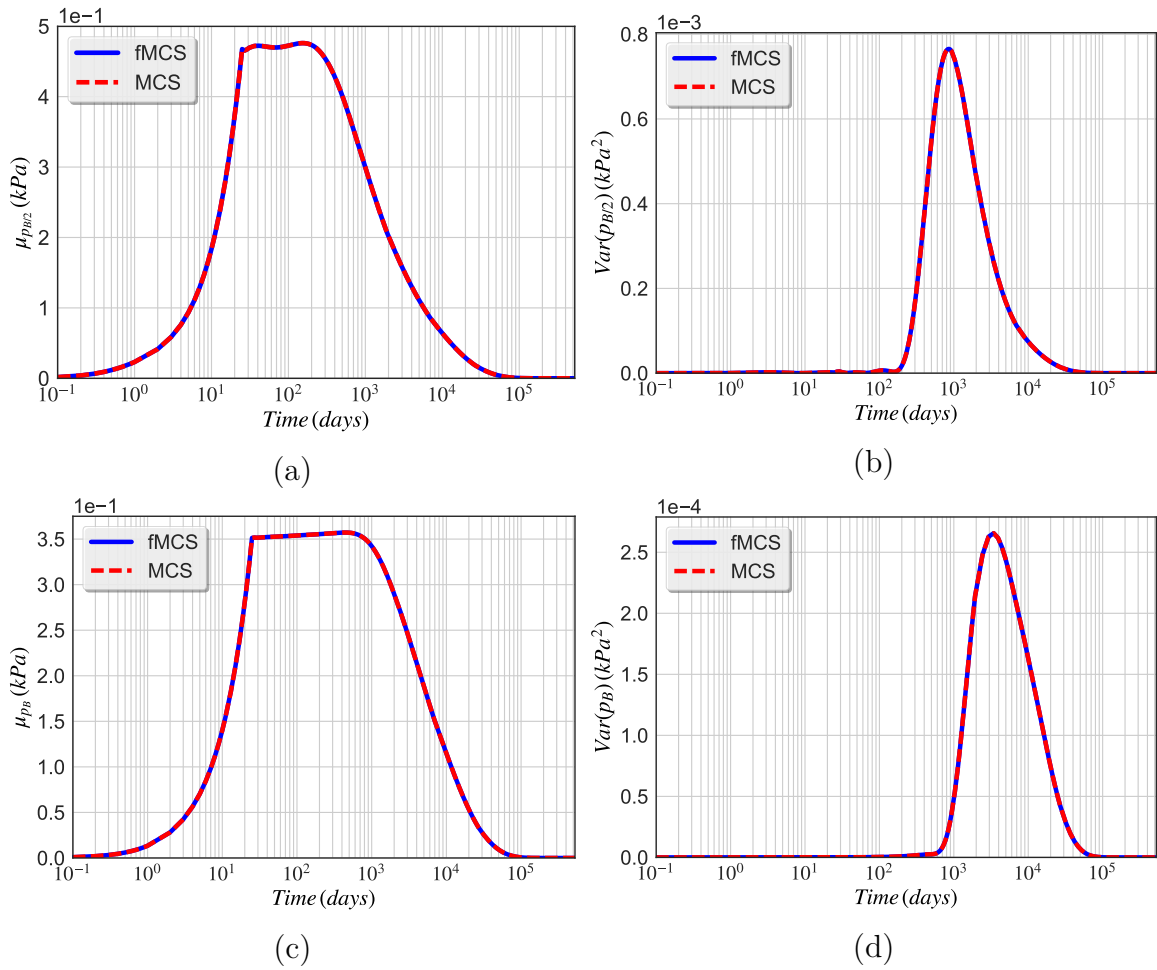


Figure 8.8. Mean and variance for excess pore pressure at depths $B/2$ and B for stochastic permeability with $\sigma_k = 0.2$ and correlation length $b = 10\text{ m}$: (a) $\mu_{p_{B/2}}$, (b) $Var(p_{B/2})$, (c) μ_{p_B} and (d) $Var(p_B)$.

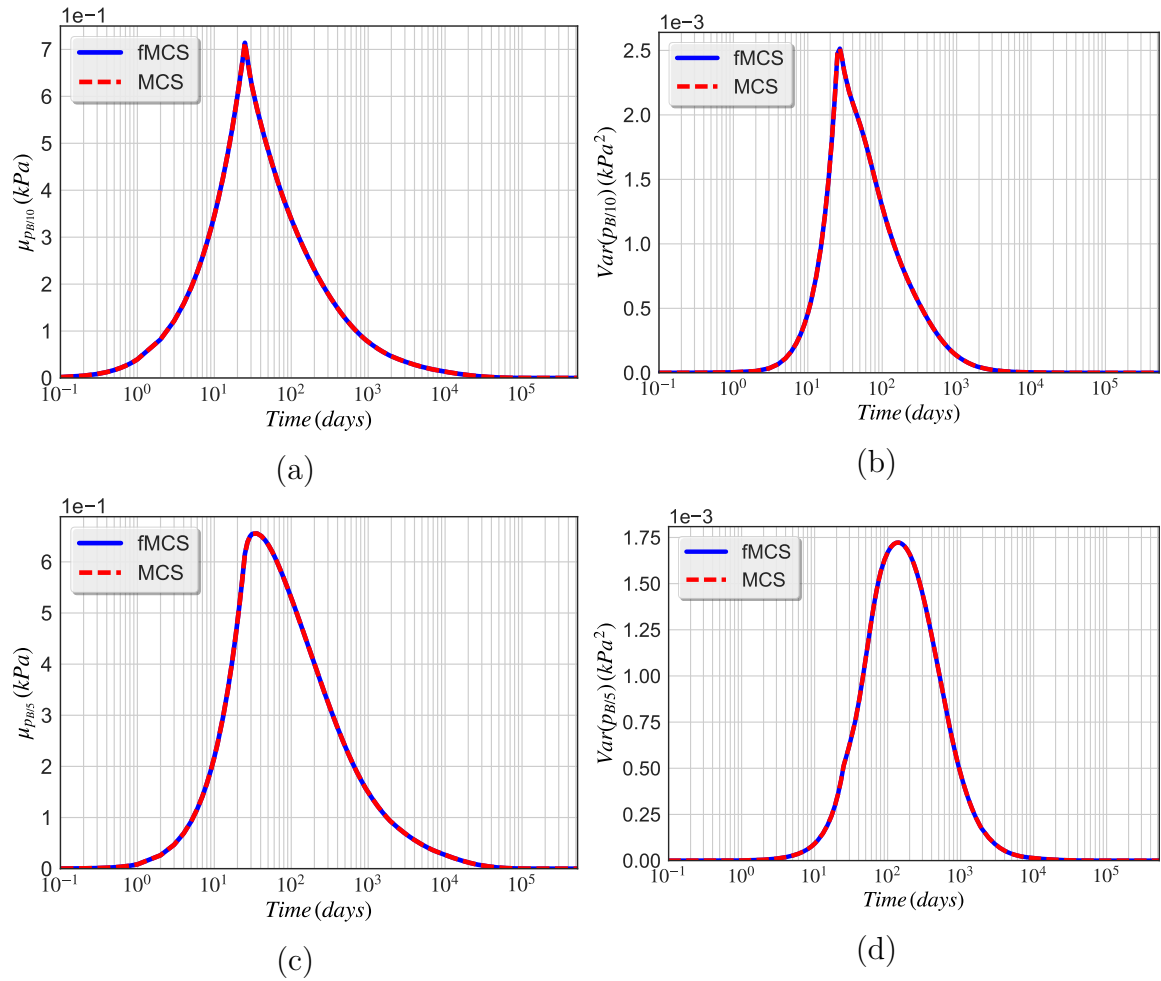


Figure 8.9. Mean and variance for excess pore pressure at depths $B/10$ and $B/5$ for stochastic Young's modulus with $\sigma_E = 0.2$ and correlation length $b = 10 m$: (a) $\mu_{p_{B/10}}$, (b) $Var(p_{B/10})$, (c) $\mu_{p_{B/5}}$ and (d) $Var(p_{B/5})$.

Dynamic variability response functions for stochastic consolidation of soils

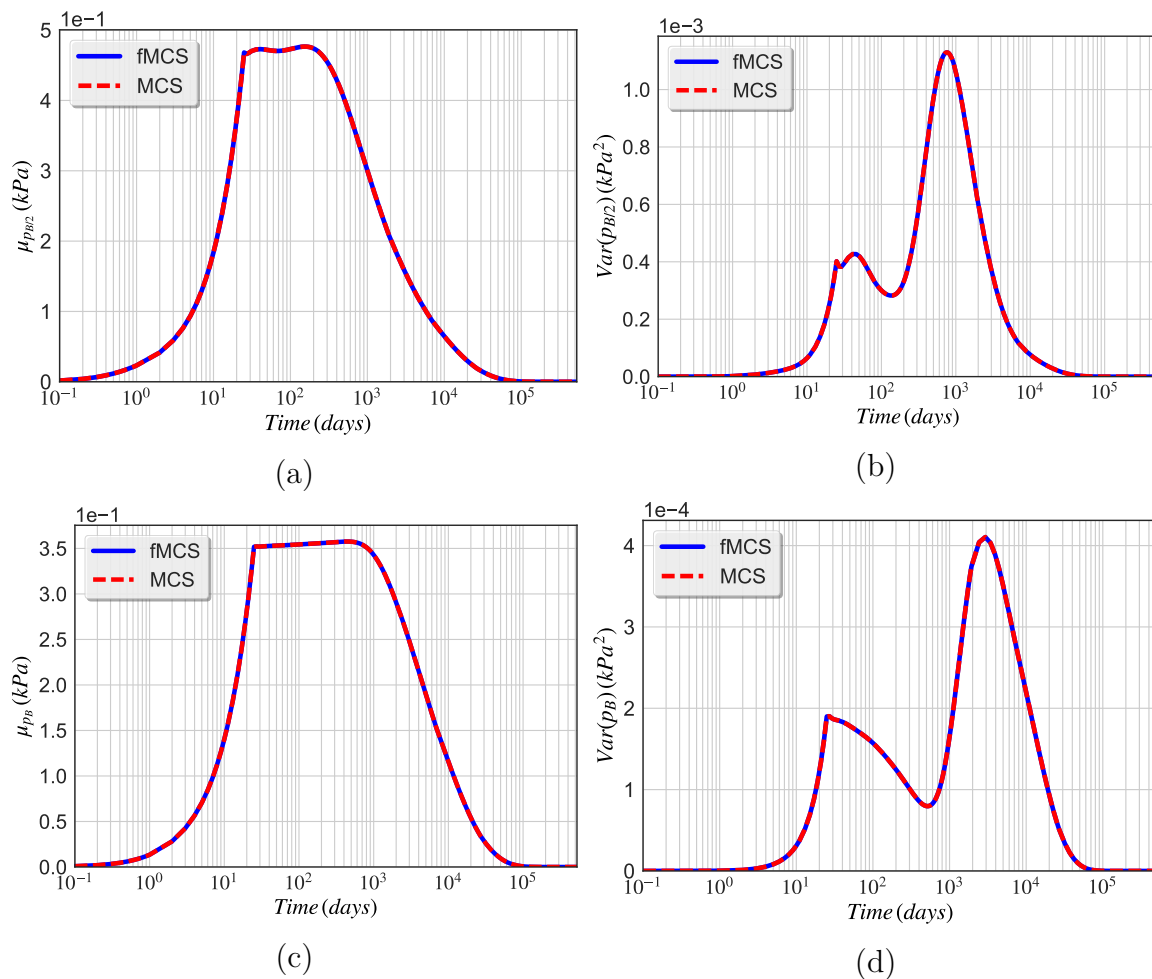


Figure 8.10. Mean and variance for excess pore pressure at depths $B/2$ and B for stochastic Young's modulus with $\sigma_E = 0.2$ and correlation length $b = 10$ m: (a) $\mu_{p_{B/2}}$, (b) $Var(p_{B/2})$, (c) μ_{p_B} and (d) $Var(p_B)$.

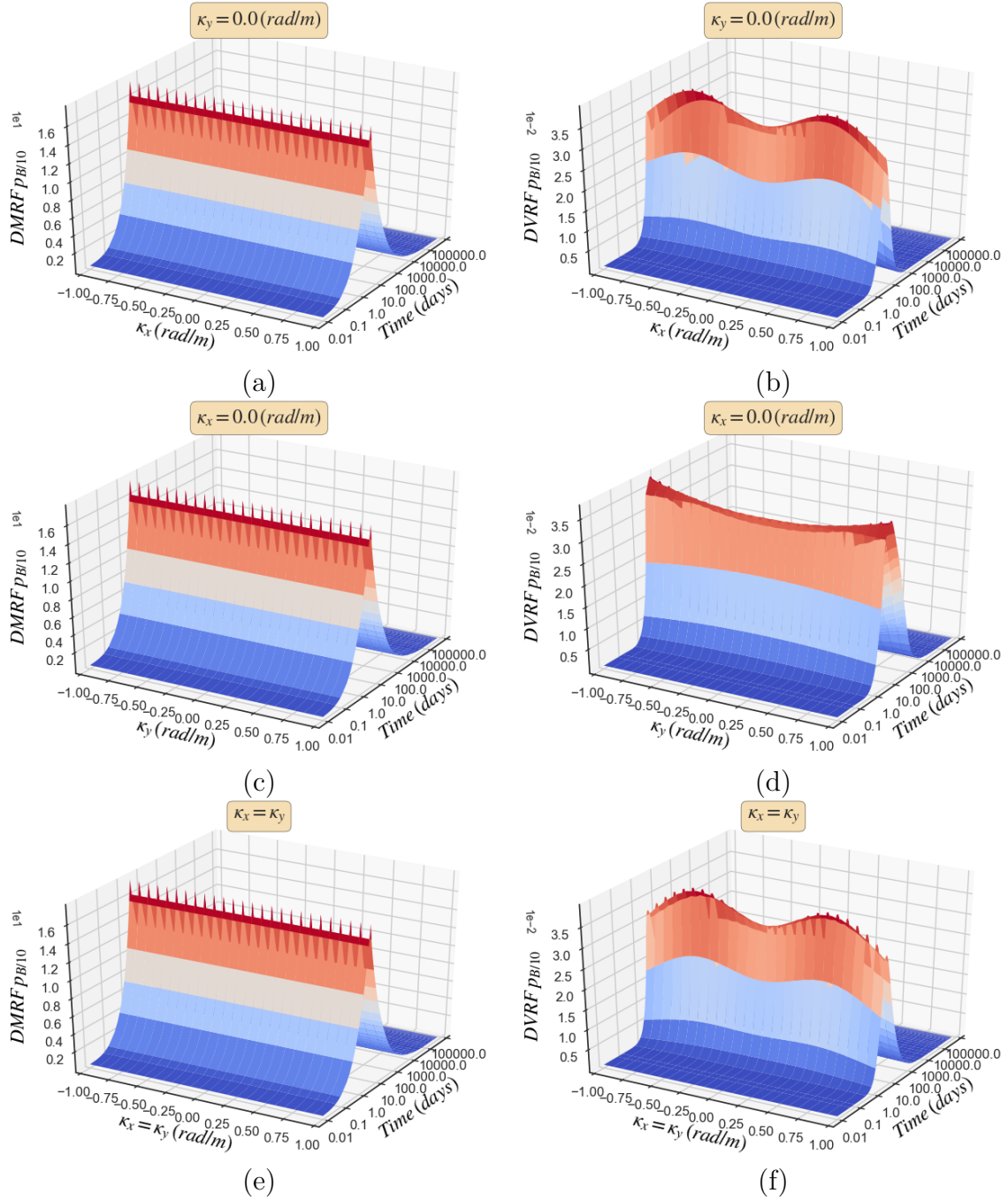


Figure 8.11. DMRF and DVRF functions for pore pressure $p_{B/10}$ for stochastic permeability with $\sigma_E = 0.2$: (a) DMRF for $\kappa_y = 0.0$ (rad/m), (b) DVRF for $\kappa_y = 0.0$ (rad/m), (c) DMRF for $\kappa_x = 0.0$ (rad/m), (d) DVRF for $\kappa_x = 0.0$ (rad/m), (e) DMRF for $\kappa_x = \kappa_y$ and (f) DVRF for $\kappa_x = \kappa_y$.

Dynamic variability response functions for stochastic consolidation of soils

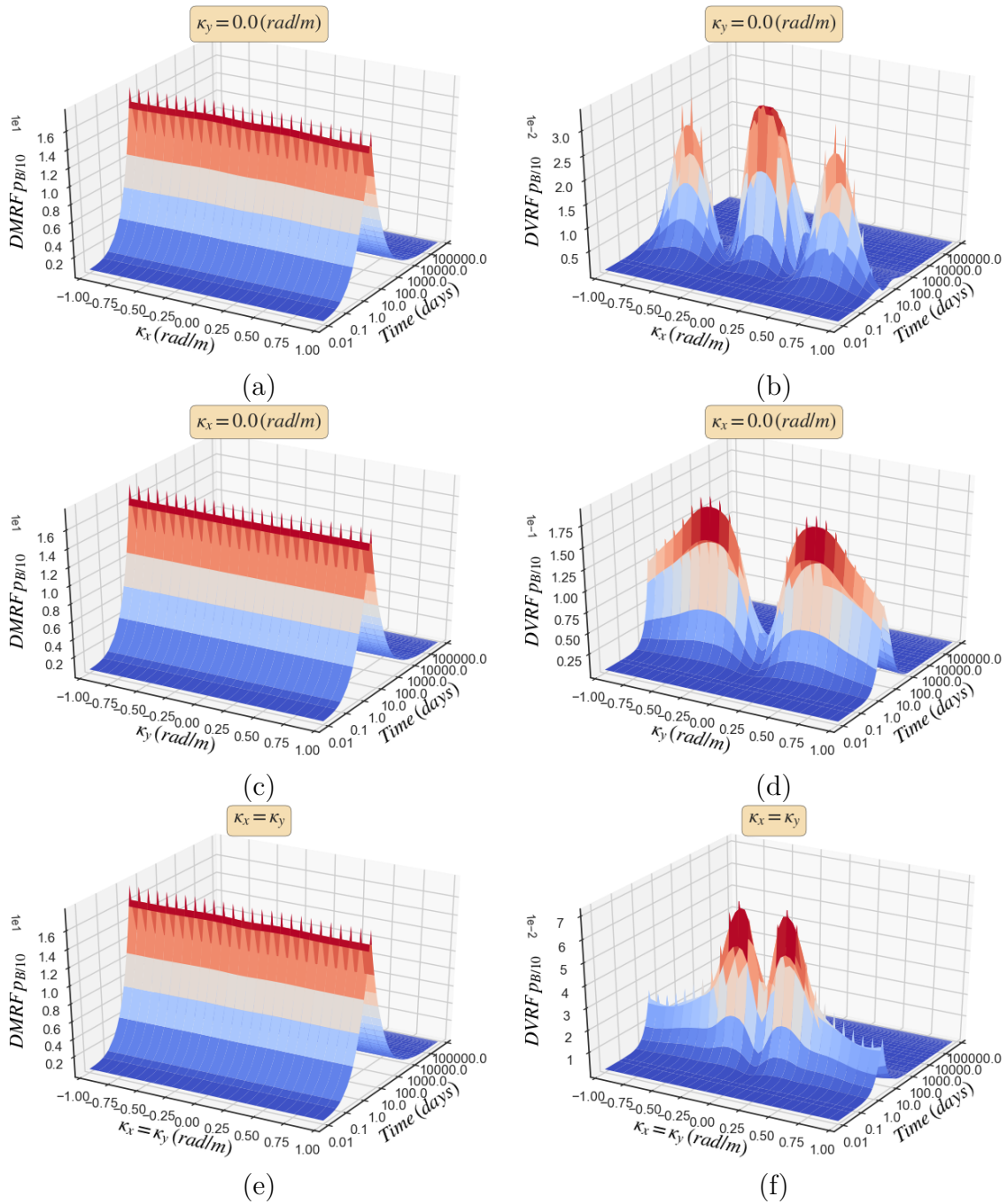


Figure 8.12. DMRF and DVRF functions for pore pressure $p_{B/10}$ for stochastic Young's modulus with $\sigma_E = 0.2$: (a) DMRF for $\kappa_y = 0.0 (rad/m)$, (b) DVRF for $\kappa_y = 0.0 (rad/m)$, (c) DMRF for $\kappa_x = 0.0 (rad/m)$, (d) DVRF for $\kappa_x = 0.0 (rad/m)$, (e) DMRF for $\kappa_x = \kappa_y$ and (f) DVRF for $\kappa_x = \kappa_y$.

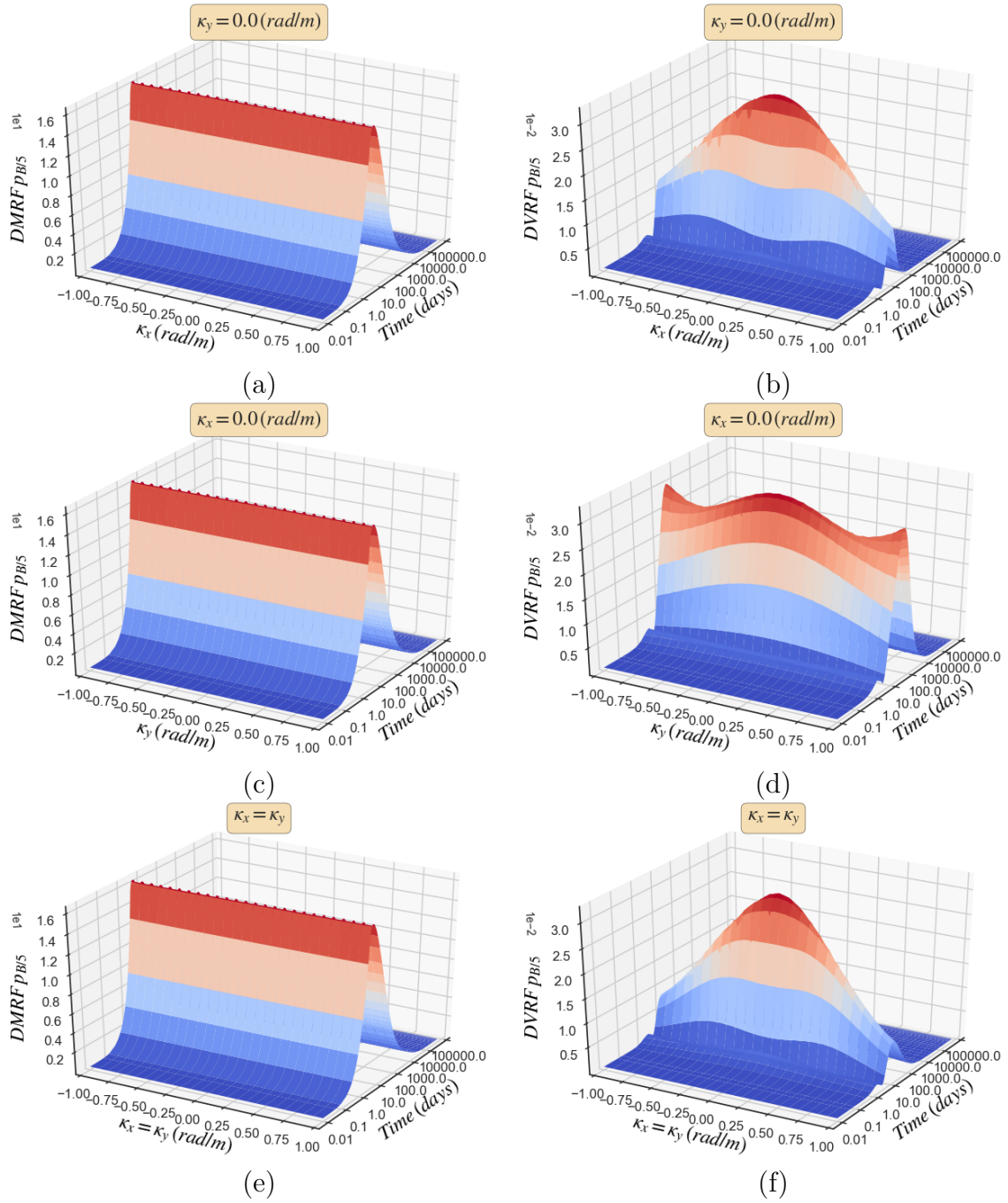


Figure 8.13. DMRF and DVRF functions for pore pressure $p_{B/5}$ for stochastic permeability with $\sigma_k = 0.2$: (a) DMRF for $\kappa_y = 0.0 \text{ (rad/m)}$, (b) DVRF for $\kappa_y = 0.0 \text{ (rad/m)}$, (c) DMRF for $\kappa_x = 0.0 \text{ (rad/m)}$, (d) DVRF for $\kappa_x = 0.0 \text{ (rad/m)}$, (e) DMRF for $\kappa_x = \kappa_y$ and (f) DVRF for $\kappa_x = \kappa_y$.

Dynamic variability response functions for stochastic consolidation of soils

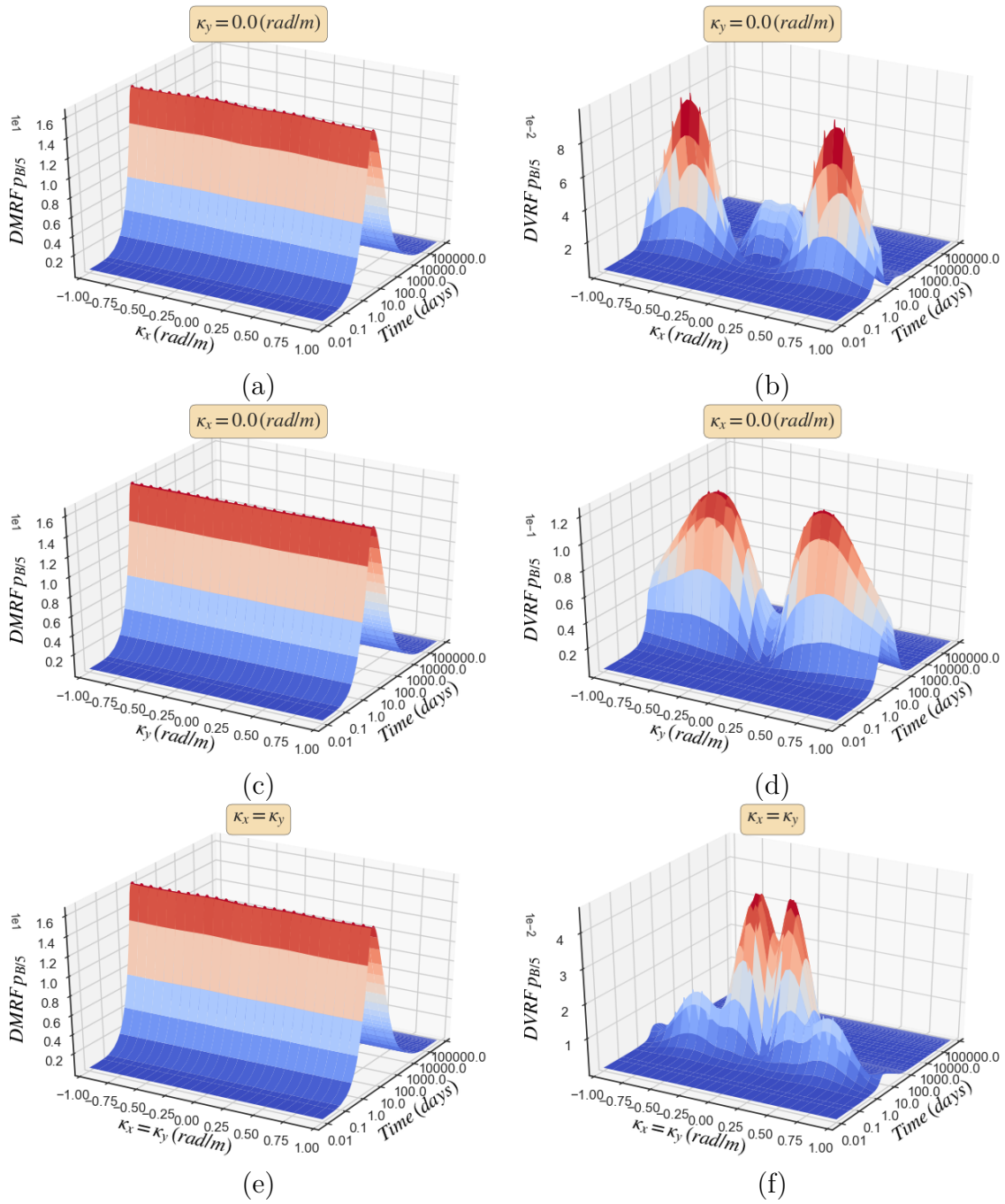


Figure 8.14. DMRF and DVRF functions for pore pressure $p_{B/5}$ for stochastic Young's modulus with $\sigma_E = 0.2$: (a) DMRF for $\kappa_y = 0.0$ (rad/m), (b) DVRF for $\kappa_y = 0.0$ (rad/m), (c) DMRF for $\kappa_x = 0.0$ (rad/m), (d) DVRF for $\kappa_x = 0.0$ (rad/m), (e) DMRF for $\kappa_x = \kappa_y$ and (f) DVRF for $\kappa_x = \kappa_y$.

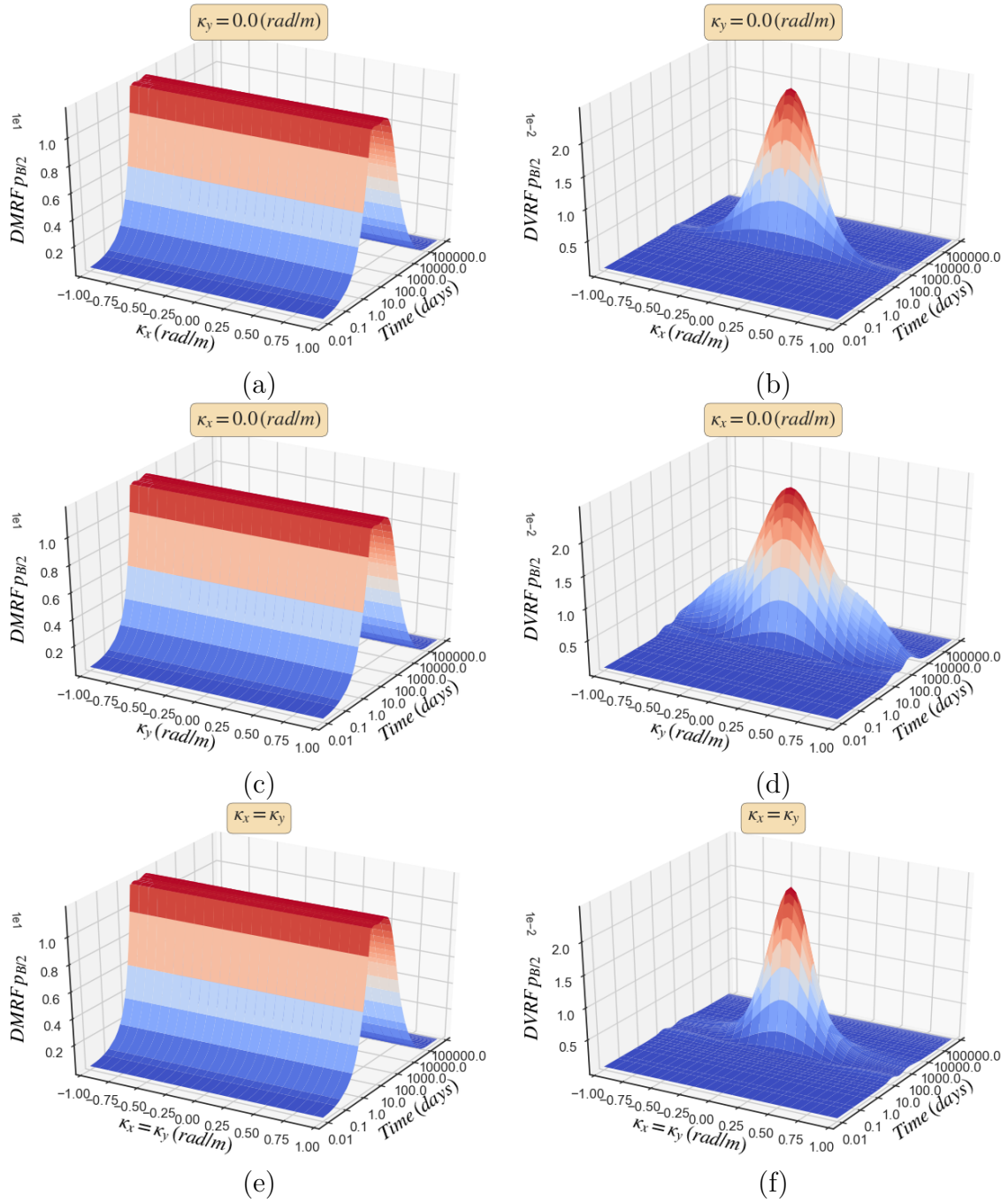


Figure 8.15. DMRF and DVRF functions for pore pressure $p_{B/2}$ for stochastic permeability with $\sigma_k = 0.2$: (a) DMRF for $\kappa_y = 0.0$ (rad/m), (b) DVRF for $\kappa_y = 0.0$ (rad/m), (c) DMRF for $\kappa_x = 0.0$ (rad/m), (d) DVRF for $\kappa_x = 0.0$ (rad/m), (e) DMRF for $\kappa_x = \kappa_y$ and (f) DVRF for $\kappa_x = \kappa_y$.

Dynamic variability response functions for stochastic consolidation of soils

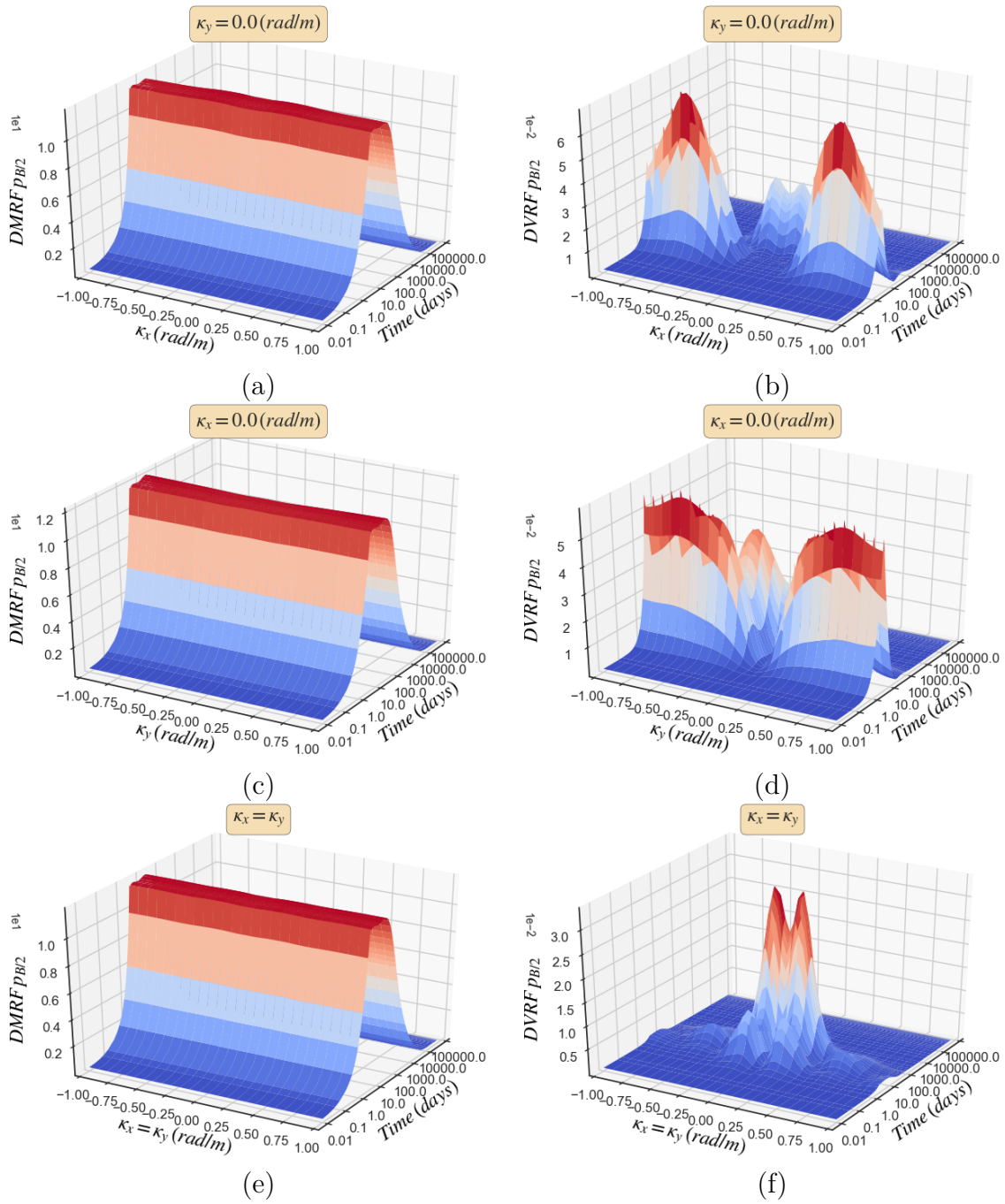


Figure 8.16. DMRF and DVRF functions for pore pressure $p_{B/2}$ for stochastic Young's modulus with $\sigma_E = 0.2$: (a) DMRF for $\kappa_y = 0.0$ (rad/m), (b) DVRF for $\kappa_y = 0.0$ (rad/m), (c) DMRF for $\kappa_x = 0.0$ (rad/m), (d) DVRF for $\kappa_x = 0.0$ (rad/m), (e) DMRF for $\kappa_x = \kappa_y$ and (f) DVRF for $\kappa_x = \kappa_y$.

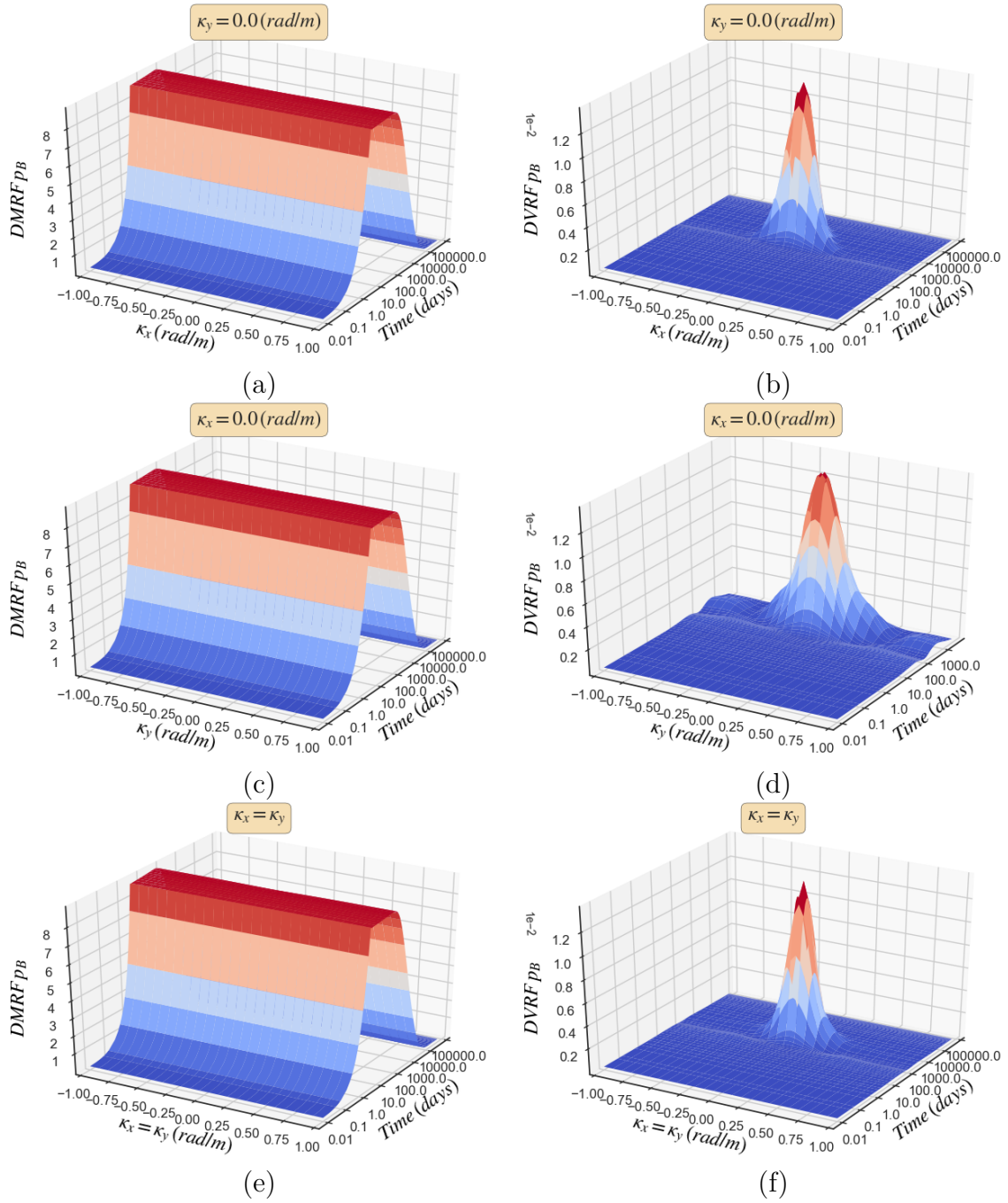


Figure 8.17. DMRF and DVRF functions for pore pressure p_B for stochastic permeability with $\sigma_k = 0.2$: (a) DMRF for $\kappa_y = 0.0$ (rad/m), (b) DVRF for $\kappa_y = 0.0$ (rad/m), (c) DMRF for $\kappa_x = 0.0$ (rad/m), (d) DVRF for $\kappa_x = 0.0$ (rad/m), (e) DMRF for $\kappa_x = \kappa_y$ and (f) DVRF for $\kappa_x = \kappa_y$.

Dynamic variability response functions for stochastic consolidation of soils

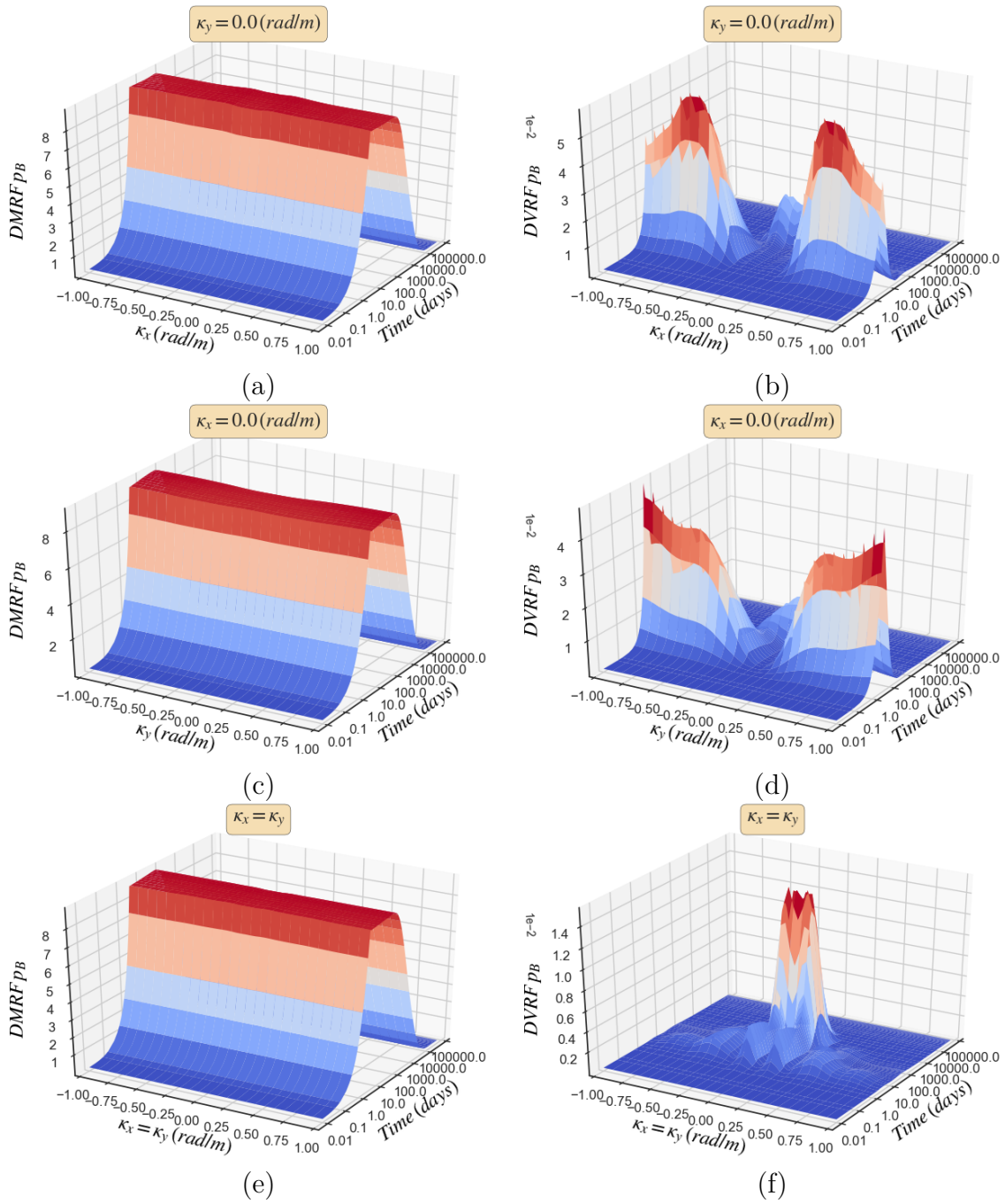


Figure 8.18. DMRF and DVRF functions for pore pressure p_B for stochastic Young's modulus with $\sigma_E = 0.2$: (a) DMRF for $\kappa_y = 0.0$ (rad/m), (b) DVRF for $\kappa_y = 0.0$ (rad/m), (c) DMRF for $\kappa_x = 0.0$ (rad/m), (d) DVRF for $\kappa_x = 0.0$ (rad/m), (e) DMRF for $\kappa_x = \kappa_y$ and (f) DVRF for $\kappa_x = \kappa_y$.

8.4 Conclusion

In this chapter, the validity and accuracy of the DMRF/DVRF methodology was again demonstrated for a coupled problem of soil consolidation. The importance of the insight provided by the DMRF/DVRF functions was once again noted and the computational efficiency of the FMCS method shown. Comparison between the DMRF/DVRF-based statistics and the ones obtained via the direct MCS also showed that the proposed method is suitable for uncertainty quantification of coupled problems involving uncertain soil parameters.

Chapter 9

Concluding remarks and recommendation for further research

9.1 Conclusions and recommendations for further research

9.1.1 Summary and conclusions of the research developed

In this dissertation, use of the stochastic finite element method was promoted, rendering it an indispensable tool for quantifying the effect of variability of soil properties in geotechnical problems. The incorporation of the SFEM is a realistic goal nowadays due to the ever-increasing computing power available to engineers. In view of this, the present dissertation is a major step forward on the detailed description of the required methodologies to successfully incorporate uncertain soil properties in geotechnical studies. Emphasis was given on the recently established concepts of the DMRF/DVRF functions, which offer a reliable alternative methodology for calculation of the response statistics of interest. To this purpose, the FMCS was shown to be the method of choice for the efficient estimation of the DMRF/DVRF of general finite element systems.

Specifically, chapter 2 introduced the basic set theory along with probability theory and random variables.

In chapter 3, the main concepts of random processes and random fields were discussed and the spectral representation method steps needed for successful computer generation of random field realizations outlined.

Concluding remarks and recommendation for further research

In chapter 4, the alternative methodologies of the SFEM family were presented.

In chapter 5, the concepts of MRF/VRF and their dynamic equivalents DMRF/DVRF were analyzed and the use of the FMCS for their numerical calculation illustrated in a step by step fashion.

In chapter 6, the direct MCS was applied to solve a problem of geotechnical nature. To specify, the problem of the loading of a rigid rough strip footing resting on a consolidating soil layer with spatially variable permeability and Young's modulus was thoroughly studied. Response statistics for footing settlements, as well as the generated excess pore pressures were obtained.

In chapter 7, shear wave propagation analyses were performed in 1D and 2D soil domains with uncertain shear modulus. The FMCS was again employed to calculate the DMRF/DVRF functions, which were used to obtain response statistics of displacement, velocity and acceleration of the ground surface.

Finally, in chapter 8 the consolidation problem was revisited on the basis of the DMRF/DVRF methodology. It was also proven that the FMCS is a powerful and efficient technique for numerically acquiring the DMRF/DVRF functions, which are then used to calculate the response statistics in a spectral and probability distribution free manner.

9.1.2 Contributions of the dissertation

The contributions of this dissertation can be summarized in the following key points:

- Demonstration of the importance of adopting the stochastic finite element method in geotechnical engineering problems. In particular, incorporation of spatial variability of soil parameters in the analysis via the SFEM reveals response characteristics such as the differential settlement in the footing loading case, which are absent if the soil is considered homogeneous.
- Validation of the accuracy and applicability of the DMRF/DVRF methodology for calculation of response statistics in porous problems, as well as site response analyses on the basis of shear wave propagation.
- Re-establishment of the FMCS as an efficient and accurate procedure to numerically calculate the DMRF/DVRF functions for general finite element systems, regardless of complexity.
- Highlight of the spectral and probability distribution free nature of the DMRF/DVRF functions. This allows to effectively assess the sensitivity of the model concerned

to uncertainty of the stochastic soil parameters taken into consideration, without the need to perform further finite element analyses.

9.1.3 Proposed future research

The research conducted throughout this dissertation is a major step forward on the use of the SFEM in geotechnical problems. However, the following topics are proposed for further research, which could enhance the applicability of the methodologies discussed:

- Extension of footing settlement test case in full three-dimensional analyses. It would be really interesting to investigate the same problem considering correlated values of permeability and Young's modulus. Furthermore, different footing shapes, as well as cases with more than one footing, would offer further insight on the stochastic consolidation problem.
- Investigation of the effect of additional soil properties such as cohesion and friction angle. To this purpose, nonlinear stochastic consolidation analyses have to be performed allowing failure of the footing-soil system to be simulated.
- Extension of the DMRF/DVRF methodology for nonlinear constitutive soil models. This development is considered crucial, since more realistic numerical simulations would be possible. A proposed direction could as well be the study and application of the recently proposed generalized variability response function (GVRF) concept developed in Teferra and Deodatis (2012); Teferra et al. (2014).
- Incorporation of multiple soil layers in wave propagation analyses. In addition, consideration of uncertainty regarding the orientation and thickness of each soil layer in three-dimensional analyses would provide further insight on the wave propagation phenomenon.
- Development of an adaptive version of the fast Monte Carlo simulation that would take into account the importance of wave numbers of the problems concerned. In this case, sampling of the wave number axes would be automatically refined in the vicinity of predominant wave numbers, allowing for further computational efficiency of the FMCS.
- Extension of the variability response function theory for statistical moments of higher order; this would make the VRF methodology essential for reliability analyses.

Bibliography

- J. D. Achenbach. *Wave propagation in elastic solids*. North-Holland Pub. Co.; American Elsevier Pub. Co., Amsterdam; New York, 1973. ISBN 0-444-10465-8 978-0-444-10465-6 0-7204-0325-1 978-0-7204-0325-1 978-0-7204-2367-9 0-7204-2367-8 0-7204-2350-3 978-0-7204-2350-1.
- T. Al-Bittar and A.-H. Soubra. Bearing capacity of strip footings on spatially random soils using sparse polynomial chaos expansion. *International Journal for Numerical and Analytical Methods in Geomechanics*, 37(13):2039–2060, Sept. 2013. ISSN 03639061. doi: 10.1002/nag.2120. URL <http://doi.wiley.com/10.1002/nag.2120>.
- J. D. Arregui-Mena, L. Margetts, and P. M. Mummery. Practical Application of the Stochastic Finite Element Method. *Archives of Computational Methods in Engineering*, 23(1):171–190, Mar. 2016. ISSN 1134-3060, 1886-1784. doi: 10.1007/s11831-014-9139-3. URL <http://link.springer.com/10.1007/s11831-014-9139-3>.
- S. R. Arwade, G. Deodatis, and K. Teferra. Variability response functions for apparent material properties. *Probabilistic Engineering Mechanics*, 44:28–34, Apr. 2016. ISSN 02668920. doi: 10.1016/j.probengmech.2015.10.010. URL <http://linkinghub.elsevier.com/retrieve/pii/S0266892015300576>.
- M. Badaoui, A. Nour, A. Slimani, and M. K. Berrah. Consolidation Statistics Investigation via Thin Layer Method Analysis. *Transport in Porous Media*, 67(1):69–91, Mar. 2007. ISSN 0169-3913, 1573-1634. doi: 10.1007/s11242-006-0021-0. URL <http://link.springer.com/10.1007/s11242-006-0021-0>.
- M. W. Bari, M. A. Shahin, and A.-H. Soubra. Probabilistic analyses of soil consolidation by prefabricated vertical drains for single-drain and multi-drain systems: Probabilistic Analyses of Soil Consolidation by PVDs. *International Journal for Numerical and Analytical Methods in Geomechanics*, 2016. ISSN 03639061. doi: 10.1002/nag.2535. URL <http://doi.wiley.com/10.1002/nag.2535>.
- K.-J. Bathe. *Finite element procedures*. s.n., S.l., 2006. ISBN 978-0-9790049-0-2 0-9790049-0-X.
- K.-J. Bathe. Conserving energy and momentum in nonlinear dynamics: A simple implicit time integration scheme. *Computers & Structures*, 85(7-8):437–445, Apr. 2007. ISSN 00457949. doi: 10.1016/j.compstruc.2006.09.004. URL <http://linkinghub.elsevier.com/retrieve/pii/S0045794906003099>.

Bibliography

- K.-J. Bathe and G. Noh. Insight into an implicit time integration scheme for structural dynamics. *Computers & Structures*, 98-99:1–6, May 2012. ISSN 00457949. doi: 10.1016/j.compstruc.2012.01.009. URL <http://linkinghub.elsevier.com/retrieve/pii/S0045794912000107>.
- D. M. Beazley, author. *Python cookbook*. Jones, Jones,. O'Reilly, Beijing, 2013. ISBN 1-4493-4037-7 978-1-4493-4037-7.
- D. P. Bertsekas and J. N. Tsitsiklis. *Introduction to probability*. Number 1 in Optimization and computation series. Athena Scientific, Belmont, Mass, 2. ed edition, 2008. ISBN 978-1-886529-23-6. OCLC: 259962612.
- T. Bong, Y. Son, S. Noh, and J. Park. Probabilistic analysis of consolidation that considers spatial variability using the stochastic response surface method. *Soils and Foundations*, 54(5):917–926, Oct. 2014. ISSN 00380806. doi: 10.1016/j.sandf.2014.09.005. URL <http://linkinghub.elsevier.com/retrieve/pii/S0038080614001048>.
- K. S. Bose and R. H. Sarma. Delineation of the intimate details of the backbone conformation of pyridine nucleotide coenzymes in aqueous solution. *Biochem. Biophys. Res. Commun.*, 66(4):1173–1179, Oct. 1975. ISSN 0006-291X.
- C. G. Bucher and M. Shinozuka. Structural Response Variability II. *Journal of Engineering Mechanics*, 114(12):2035–2054, Dec. 1988. ISSN 0733-9399, 1943-7889. doi: 10.1061/(ASCE)0733-9399(1988)114:12(2035).
- S. E. Cho and H. C. Park. Effect of spatial variability of cross-correlated soil properties on bearing capacity of strip footing. *International Journal for Numerical and Analytical Methods in Geomechanics*, 34(1):1–26, 2010. ISSN 1096-9853. doi: 10.1002/nag.791. URL <http://dx.doi.org/10.1002/nag.791>.
- A. K. Chopra. *Dynamics of structures: theory and applications to earthquake engineering*. Pearson/Prentice Hall, Upper Saddle River, N.J, 3rd ed edition, 2007. ISBN 0-13-156174-X.
- M. P. Coleman. *An introduction to partial differential equations with MATLAB*. Chapman & Hall/CRC applied mathematics & nonlinear science. Chapman and Hall/CRC, Boca Raton, second edition edition, 2013. ISBN 978-1-4398-9846-8.
- A. Collette. *Python and HDF5*. O'Reilly, Beijing, first edition edition, 2014. ISBN 1-4493-6783-6.
- M. Crisfield. *Non-linear finite element analysis of solids and structures. Volume 1, Volume 1.*. John Wiley & Sons, Chichester; New York, 1991. ISBN 0-471-97059-X 978-0-471-97059-0.
- B. M. Das. *Principles of soil dynamics*. Cengage Learning, Stamford, CT, 2nd ed edition, 2012. ISBN 978-0-495-41135-2.
- A. Der Kiureghian and J.-B. Ke. The stochastic finite element method in structural reliability. *Probabilistic Engineering Mechanics*, 3(2):83–91, June 1988. ISSN 02668920. doi: 10.1016/0266-8920(88)90019-7. URL <http://linkinghub.elsevier.com/retrieve/pii/0266892088900197>.

- C. S. Desai and M. Zaman. *Advanced geotechnical engineering: soil-structure interaction using computer and material models*. CRC Press/Taylor & Francis, Boca Raton, [Florida], 2014. ISBN 978-1-4665-1560-4.
- I. S. Doltsinis and International Centre for Mechanical Sciences. *Advances in computational nonlinear mechanics*. Springer-Verlag, Wien; New York, 1989. ISBN 0-387-82113-9 978-0-387-82113-9 3-211-82113-9 978-3-211-82113-8.
- J. F. Doyle. *Nonlinear structural dynamics using FE methods*. Cambridge University Press, Cambridge, 2014. ISBN 978-1-107-04570-5.
- M. Eiermann, O. G. Ernst, and E. Ullmann. Computational aspects of the stochastic finite element method. *Computing and Visualization in Science*, 10(1):3–15, Feb. 2007. ISSN 1432-9360, 1433-0369. doi: 10.1007/s00791-006-0047-4. URL <http://link.springer.com/10.1007/s00791-006-0047-4>.
- G. A. Fenton and D. V. Griffiths. Three-Dimensional Probabilistic Foundation Settlement. *Journal of Geotechnical and Geoenvironmental Engineering*, 131(2):232–239, Feb. 2005. ISSN 1090-0241, 1943-5606. doi: 10.1061/(ASCE)1090-0241(2005)131:2(232).
- G. A. Fenton and D. V. Griffiths. *Risk assessment in geotechnical engineering*. John Wiley & Sons, Hoboken, N.J., 2008. ISBN 0-470-17820-5 978-0-470-17820-1.
- M. Georgioudakis. *Stochastic Analysis and Optimum Design of Structures Subjected to Fracture*. PhD thesis, National Technical University of Athens, 2014.
- R. Ghanem and P. D. Spanos. *Stochastic finite elements: a spectral approach*. Dover Publications, Minneola, N.Y., rev. ed edition, 2003. ISBN 0-486-42818-4.
- D. G. Giovanis and V. Papadopoulos. Spectral representation-based neural network assisted stochastic structural mechanics. *Engineering Structures*, 84:382–394, Feb. 2015. ISSN 01410296. doi: 10.1016/j.engstruct.2014.11.044. URL <http://linkinghub.elsevier.com/retrieve/pii/S0141029614007408>.
- D. Giovannis. *Advanced Stochastic Finite Element Simulations and Reliability Analyses*. PhD thesis, National Technical University of Athens, 2014.
- M. Gorelick and I. Ozsvald. *High performance Python*. 2014. ISBN 978-1-4493-6159-4 1-4493-6159-5.
- K. F. Graff. *Wave motion in elastic solids*. Dover Publications, New York, 1991. ISBN 0-486-66745-6.
- L. Graham and G. Deodatis. Variability response functions for stochastic plate bending problems. *Structural Safety*, 20(2):167–188, Jan. 1998. ISSN 01674730. doi: 10.1016/S0167-4730(98)00006-X. URL <http://linkinghub.elsevier.com/retrieve/pii/S016747309800006X>.
- G. Gratzer. *Practical latex*. Springer, New York, 2014. ISBN 978-3-319-06424-6.

Bibliography

- A. Greenbaum and T. P. Chartier. *Numerical methods: design, analysis, and computer implementation of algorithms*. Princeton University Press, Princeton, N.J, 2012. ISBN 978-0-691-15122-9. OCLC: ocn761850909.
- D. V. Griffiths and G. A. Fenton. Three-Dimensional Seepage through Spatially Random Soil. *Journal of Geotechnical and Geoenvironmental Engineering*, 123(2):153–160, Feb. 1997. ISSN 1090-0241, 1943-5606. doi: 10.1061/(ASCE)1090-0241(1997)123:2(153).
- D. V. Griffiths and G. A. Fenton. Probabilistic Slope Stability Analysis by Finite Elements. *Journal of Geotechnical and Geoenvironmental Engineering*, 130(5):507–518, May 2004. ISSN 1090-0241, 1943-5606. doi: 10.1061/(ASCE)1090-0241(2004)130:5(507).
- D. V. Griffiths, G. A. Fenton, and N. Manoharan. Bearing Capacity of Rough Rigid Strip Footing on Cohesive Soil: Probabilistic Study. *Journal of Geotechnical and Geoenvironmental Engineering*, 128(9):743–755, Sept. 2002. ISSN 1090-0241, 1943-5606. doi: 10.1061/(ASCE)1090-0241(2002)128:9(743).
- D. V. Griffiths, G. A. Fenton, and N. Manoharan. Undrained Bearing Capacity of Two-Strip Footings on Spatially Random Soil. *International Journal of Geomechanics*, 6(6):421–427, Nov. 2006. ISSN 1532-3641, 1943-5622. doi: 10.1061/(ASCE)1532-3641(2006)6:6(421).
- D. V. Griffiths, J. Huang, and G. A. Fenton. Influence of Spatial Variability on Slope Reliability Using 2-D Random Fields. *Journal of Geotechnical and Geoenvironmental Engineering*, 135(10):1367–1378, Oct. 2009. ISSN 1090-0241, 1943-5606. doi: 10.1061/(ASCE)GT.1943-5606.0000099.
- M. Grigoriu. *Applied non-Gaussian processes: examples, theory, simulation, linear random vibration, and MATLAB solutions*. PTR Prentice Hall, Englewood Cliffs, NJ, 1995. ISBN 978-0-13-367095-0.
- M. Grigoriu. *Stochastic calculus: applications in science and engineering*. Birkhäuser, Boston, MA, 2002. ISBN 978-0-8176-4242-6 978-3-7643-4242-5.
- K. R. Gurley. *Modelling and Simulation of Non-Gaussian Processes*. PhD thesis, University of Notre Dame, 1997.
- J. Har. *Advanced computational dynamics of particles, materials, and structures: a unified approach*. Wiley, Hoboken, 2012. ISBN 978-0-470-74980-7.
- J. Ho Lee, J. Kwan Kim, and J. L. Tassoulas. Stochastic dynamic analysis of a layered half-space. *Soil Dynamics and Earthquake Engineering*, 48:220–233, May 2013. ISSN 02677261. doi: 10.1016/j.soildyn.2013.01.003. URL <http://linkinghub.elsevier.com/retrieve/pii/S0267726113000055>.
- M. Hori. *Introduction to computational earthquake engineering*. Imperial College Press, London, 2nd ed edition, 2011. ISBN 978-1-84816-397-3.
- C. S. Horstmann and G. Cornell. *Core Java*. Prentice Hall, Upper Saddle River, NJ, ninth edition edition, 2013. ISBN 978-0-13-708189-9 978-0-13-708160-8 0-13-708160-X.

- Y. Houmadi, A. Ahmed, and A.-H. Soubra. Probabilistic analysis of a one-dimensional soil consolidation problem. *Georisk: Assessment and Management of Risk for Engineered Systems and Geohazards*, 6(1):36–49, Mar. 2012. ISSN 1749-9518, 1749-9526. doi: 10.1080/17499518.2011.590090. URL <http://www.tandfonline.com/doi/abs/10.1080/17499518.2011.590090>.
- J. Huang, D. V. Griffiths, and G. A. Fenton. Probabilistic Analysis of Coupled Soil Consolidation. *Journal of Geotechnical and Geoenvironmental Engineering*, 136(3): 417–430, Mar. 2010. ISSN 1090-0241, 1943-5606. doi: 10.1061/(ASCE)GT.1943-5606.0000238.
- T. J. R. Hughes. *The finite element method: linear static and dynamic finite element analysis*. Dover Publications, Mineola, NY, 2000. ISBN 0-486-41181-8.
- R. Jimenez and N. Sitar. The importance of distribution types on finite element analyses of foundation settlement. *Computers and Geotechnics*, 36(3):474–483, Apr. 2009. ISSN 0266352X. doi: 10.1016/j.compgeo.2008.05.003. URL <http://linkinghub.elsevier.com/retrieve/pii/S0266352X0800058X>.
- A. Johari and A. Khodaparast. Analytical stochastic analysis of seismic stability of infinite slope. *Soil Dynamics and Earthquake Engineering*, 79:17–21, Dec. 2015. ISSN 02677261. doi: 10.1016/j.soildyn.2015.08.012. URL <http://linkinghub.elsevier.com/retrieve/pii/S0267726115002079>.
- A. Johari and M. Momeni. Stochastic analysis of ground response using non-recursive algorithm. *Soil Dynamics and Earthquake Engineering*, 69:57–82, Feb. 2015. ISSN 02677261. doi: 10.1016/j.soildyn.2014.10.025. URL <http://linkinghub.elsevier.com/retrieve/pii/S0267726114002279>.
- W. B. Joyner and A. T. F. Chen. Calculation of nonlinear ground response in earthquakes. *Bulletin of the Seismological Society of America*, 65(5):1315–1336, Oct. 1975.
- A. Kardara, C. G. Bucher, and M. Shinozuka. Structural Response Variability III. *Journal of Engineering Mechanics*, 115(8):1726–1747, Aug. 1989. ISSN 0733-9399, 1943-7889. doi: 10.1061/(ASCE)0733-9399(1989)115:8(1726).
- O. Kokkinos. *Stochastic dynamic response and optimization structures with Finite elements*. PhD thesis, National Technical University of Athens, 2015.
- O. Kokkinos and V. Papadopoulos. Robust design with Variability Response Functions; an alternative approach. *Structural Safety*, 59:1–8, Mar. 2016. ISSN 01674730. doi: 10.1016/j.strusafe.2015.10.001. URL <http://linkinghub.elsevier.com/retrieve/pii/S0167473015000818>.
- H. Kolsky. *Stress waves in solids*. Dover Publications, New York, 1963. ISBN 0-486-61098-5 978-0-486-61098-6.
- S. L. Kramer. *Geotechnical earthquake engineering*. Prentice-Hall international series in civil engineering and engineering mechanics. Prentice Hall, Upper Saddle River, N.J, 1996. ISBN 0-13-374943-6.

Bibliography

- R. W. Lewis, B. A. Schrefler, and R. W. Lewis. *The finite element method in the static and dynamic deformation and consolidation of porous media*. John Wiley, Chichester ; New York, 2nd ed edition, 1998. ISBN 0-471-92809-7.
- G. J. Lord, C. E. Powell, and T. Shardlow. *An introduction to computational stochastic PDEs*. Number 50 in Cambridge texts in applied mathematics. Cambridge University Press, New York, NY, USA, 2014. ISBN 978-0-521-89990-1 978-0-521-72852-2.
- J. Lysmer and R. L. Kuhlemeyer. Finite Dynamic Model For Infinite Media. *Journal of the Engineering Mechanics Division*, 95(4).
- P. Maheshwari and P. P. Kumar. Probabilistic Analysis and Design of a Strip Footing on Layered Soil Media. *Geotechnical and Geological Engineering*, 29(6):1099–1108, Nov. 2011. ISSN 0960-3182, 1573-1529. doi: 10.1007/s10706-011-9442-9. URL <http://link.springer.com/10.1007/s10706-011-9442-9>.
- Maurice A. Biot. General Theory of Three-Dimensional Consolidation. *American Institute of Physics*, 12(2):155–164, Feb. 1941.
- G. P. Mavroeidis and A. S. Papageorgiou. A Mathematical Representation of Near-Fault Ground Motions. *Bulletin of the Seismological Society of America*, 93(3): 1099–1131, June 2003. ISSN 0037-1106. doi: 10.1785/0120020100. URL <http://bssa.geoscienceworld.org/cgi/doi/10.1785/0120020100>.
- M. McQuaid. *Git in practice*. Manning, Shelter Island, NY, 2015. ISBN 978-1-61729-197-5.
- F. Mittelbach. *The LaTeX companion*. Addison-Wesley series on tools and techniques for computer typesetting. Addison-Wesley, Boston, 2nd ed edition, 2004. ISBN 0-201-36299-6.
- D. Muir Wood. *Geotechnical modelling*. Number v. 1 in Applied geotechnics. Spon Press, London ; New York, 2004. ISBN 0-415-34304-6.
- G. Noh, S. Ham, and K.-J. Bathe. Performance of an implicit time integration scheme in the analysis of wave propagations. *Computers & Structures*, 123:93–105, July 2013. ISSN 00457949. doi: 10.1016/j.compstruc.2013.02.006. URL <http://linkinghub.elsevier.com/retrieve/pii/S0045794913000540>.
- O. C. Zienkiewicz, A. H. C. Chan, M. Pastor, B. A. Schrefler, and T. Shiomi. *Computational Geomechanics with Special Reference to Earthquake Engineering*. Wiley, Feb. 1999. ISBN 978-0-471-98285-2.
- F. Oka. *Computational modeling of multi-phase geomaterials*. CRC Press, Boca Raton, FL, 2013. ISBN 978-0-415-80927-6.
- G. M. Paice, D. V. Griffiths, and G. A. Fenton. Finite Element Modeling of Settlements on Spatially Random Soil. *Journal of Geotechnical Engineering*, 122(9):777–779, Sept. 1996. ISSN 0733-9410, 1944-8368. doi: 10.1061/(ASCE)0733-9410(1996)122:9(777).

- V. Papadopoulos and G. Deodatis. Response variability of stochastic frame structures using evolutionary field theory. *Computer Methods in Applied Mechanics and Engineering*, 195(9-12):1050–1074, Feb. 2006. ISSN 00457825. doi: 10.1016/j.cma.2005.04.003. URL <http://linkinghub.elsevier.com/retrieve/pii/S0045782505001507>.
- V. Papadopoulos and O. Kokkinos. Variability response functions for stochastic systems under dynamic excitations. *Probabilistic Engineering Mechanics*, 28:176–184, Apr. 2012. ISSN 02668920. doi: 10.1016/j.probengmech.2011.08.002. URL <http://linkinghub.elsevier.com/retrieve/pii/S0266892011000488>.
- V. Papadopoulos and O. Kokkinos. Transient response of stochastic finite element systems using Dynamic Variability Response Functions. *Structural Safety*, 52:100–112, Jan. 2015. ISSN 01674730. doi: 10.1016/j.strusafe.2014.09.006. URL <http://linkinghub.elsevier.com/retrieve/pii/S0167473014000897>.
- V. Papadopoulos, G. Deodatis, and M. Papadrakakis. Flexibility-based upper bounds on the response variability of simple beams. *Computer Methods in Applied Mechanics and Engineering*, 194(12-16):1385–1404, Apr. 2005. ISSN 00457825. doi: 10.1016/j.cma.2004.06.040. URL <http://linkinghub.elsevier.com/retrieve/pii/S0045782504003986>.
- V. Papadopoulos, M. Papadrakakis, and G. Deodatis. Analysis of mean and mean square response of general linear stochastic finite element systems. *Computer Methods in Applied Mechanics and Engineering*, 195(41-43):5454–5471, Aug. 2006. ISSN 00457825. doi: 10.1016/j.cma.2005.11.008. URL <http://linkinghub.elsevier.com/retrieve/pii/S004578250500527X>.
- A. Papoulis and S. U. Pillai. *Probability, random variables, and stochastic processes*. McGraw-Hill, Boston, 2002. ISBN 0-07-366011-6 978-0-07-366011-0 0-07-112256-7 978-0-07-112256-6 0-07-122661-3 978-0-07-122661-5 0-07-281725-9 978-0-07-281725-6.
- D. Phillips. *Python 3 object oriented programming harness the power of Python 3 objects*. Packt Pub., Birmingham, U.K., 2010. ISBN 978-1-84951-127-8 1-84951-127-6. URL <http://public.eblib.com/choice/publicfullrecord.aspx?p=944028>.
- R. Popescu, G. Deodatis, and A. Nobahar. Effects of random heterogeneity of soil properties on bearing capacity. *Probabilistic Engineering Mechanics*, 20(4):324–341, Oct. 2005. ISSN 02668920. doi: 10.1016/j.probengmech.2005.06.003. URL <http://linkinghub.elsevier.com/retrieve/pii/S0266892005000184>.
- D. M. Potts. *Finite element analysis in geotechnical engineering: theory*. Telford ; Distributed by ASCE Press, London : Reston, VA, 1999. ISBN 0-7277-2753-2.
- D. M. Potts and L. Zdravkovic. *Finite element analysis in geotechnical engineering*. Thomas Telford, London, 2001. ISBN 0-7277-2783-4 978-0-7277-2783-1.
- W. H. Press, editor. *Numerical recipes: the art of scientific computing*. Cambridge University Press, Cambridge, UK ; New York, 3rd ed edition, 2007. ISBN 0-521-88068-8 978-0-521-88068-8 978-0-521-88407-5 0-521-88407-1 978-0-521-70685-8 0-521-70685-8.
- L. Ramalho. *Fluent Python*. O’Reilly, Sebastopol, CA, first edition edition, 2015. ISBN 978-1-4919-4600-8. OCLC: ocn884808025.

Bibliography

- M. B. Reed. An investigation of numerical errors in the analysis of consolidation by finite elements. *International Journal for Numerical and Analytical Methods in Geomechanics*, 8(3):243–257, May 1984. ISSN 0363-9061, 1096-9853. doi: 10.1002/nag.1610080304. URL <http://doi.wiley.com/10.1002/nag.1610080304>.
- W. Schroeder, K. Martin, B. Lorenzen, and I. Kitware. *The visualization toolkit: an object-oriented approach to 3D graphics*. Kitware, [Clifton Park, N.Y.], 2006. ISBN 978-1-930934-19-1 1-930934-19-X 978-1-930934-12-2 1-930934-12-2.
- J. F. Semblat. *Waves and vibrations in soils: earthquakes, traffic, shocks, construction works*. IUSS Press, Pavia, 2009. ISBN 978-88-6198-030-3.
- M. Shinozuka. Structural Response Variability. *Journal of Engineering Mechanics*, 113(6):825–842, June 1987. ISSN 0733-9399, 1943-7889. doi: 10.1061/(ASCE)0733-9399(1987)113:6(825).
- M. Shinozuka and G. Deodatis. Response Variability Of Stochastic Finite Element Systems. *Journal of Engineering Mechanics*, 114(3):499–519, Mar. 1988. ISSN 0733-9399, 1943-7889. doi: 10.1061/(ASCE)0733-9399(1988)114:3(499).
- M. Shinozuka and G. Deodatis. Simulation of Multi-Dimensional Gaussian Stochastic Fields by Spectral Representation. *Applied Mechanics Reviews*, 49(1):29, 1996. ISSN 00036900. doi: 10.1115/1.3101883. URL <http://AppliedMechanicsReviews.asmedigitalcollection.asme.org/article.aspx?articleid=1395651>.
- J. T. Simões, L. C. Neves, A. N. Antão, and N. M. C. Guerra. Probabilistic Analysis of bearing capacity of shallow foundations using three-dimensional limit analyses. *International Journal of Computational Methods*, 11(02):1342008, Mar. 2014. ISSN 0219-8762, 1793-6969. doi: 10.1142/S0219876213420085. URL <http://www.worldscientific.com/doi/abs/10.1142/S0219876213420085>.
- B. Slatkin. *Effective Python: 59 specific ways to write better Python*. Addison-Wesley, Upper Saddle River, NJ, 2015. ISBN 978-0-13-403428-7 0-13-403428-7.
- I. M. Smith. *Smith's elements of soil mechanics*. Blackwell Pub, Oxford ; Malden, MA, 8th ed edition, 2006. ISBN 978-1-4051-3370-8.
- I. M. Smith and D. V. Griffiths. *Programming the finite element method*. Wiley, Hoboken, NJ, 4th ed edition, 2004. ISBN 0-470-84969-X.
- P. D. Spanos and R. Ghanem. Stochastic Finite Element Expansion for Random Media. *Journal of Engineering Mechanics*, 115(5):1035–1053, May 1989. ISSN 0733-9399, 1943-7889. doi: 10.1061/(ASCE)0733-9399(1989)115:5(1035).
- G. Stavroulakis, D. G. Giovanis, M. Papadrakakis, and V. Papadopoulos. A new perspective on the solution of uncertainty quantification and reliability analysis of large-scale problems. *Computer Methods in Applied Mechanics and Engineering*, 276:627–658, July 2014. ISSN 00457825. doi: 10.1016/j.cma.2014.03.009. URL <http://linkinghub.elsevier.com/retrieve/pii/S0045782514000954>.

- G. Stefanou. The stochastic finite element method: Past, present and future. *Computer Methods in Applied Mechanics and Engineering*, 198(9-12):1031–1051, Feb. 2009. ISSN 00457825. doi: 10.1016/j.cma.2008.11.007. URL <http://linkinghub.elsevier.com/retrieve/pii/S0045782508004118>.
- G. Stefanou and M. Papadrakakis. Assessment of spectral representation and karhunen–loève expansion methods for the simulation of gaussian stochastic fields. *Computer Methods in Applied Mechanics and Engineering*, 196(21–24):2465 – 2477, 2007. ISSN 0045-7825. doi: <http://dx.doi.org/10.1016/j.cma.2007.01.009>. URL <http://www.sciencedirect.com/science/article/pii/S0045782507000254>.
- G. Strang. *Computational science and engineering*. Wellesley-Cambridge Press, Wellesley, MA, 2007. ISBN 0-9614088-1-2 978-0-9614088-1-7.
- M. Summerfield. *Python in practice: create better programs using concurrency, libraries, and patterns*. Developer’s library series. Addison-Wesley, Upper Saddle River, NJ, 2014. ISBN 978-0-321-90563-5 0-321-90563-6.
- K. Teferra. *Developments in the Theory and Applications of the Variability Response Function Concept*. PhD thesis, Columbia University, 2012.
- K. Teferra and G. Deodatis. Variability response functions for beams with nonlinear constitutive laws. *Probabilistic Engineering Mechanics*, 29:139–148, July 2012. ISSN 02668920. doi: 10.1016/j.probengmech.2011.11.007. URL <http://linkinghub.elsevier.com/retrieve/pii/S0266892011000993>.
- K. Teferra, S. R. Arwade, and G. Deodatis. Generalized variability response functions for two-dimensional elasticity problems. *Computer Methods in Applied Mechanics and Engineering*, 272:121–137, Apr. 2014. ISSN 00457825. doi: 10.1016/j.cma.2014.01.013. URL <http://linkinghub.elsevier.com/retrieve/pii/S0045782514000267>.
- R.-G. Urma, M. Fusco, and A. Mycroft. *Java 8 in action lambdas, streams, and functional-style programming*. Manning, Shelter Island, N.Y., 2015. ISBN 1-61729-199-4 978-1-61729-199-9. URL <http://proquest.safaribooksonline.com/?fpi=9781617291999>.
- E. Vanmarcke. *Random fields: analysis and synthesis*. World Scientific, Singapore ; Hackensack, NJ, rev. and expanded new ed edition, 2010. ISBN 978-981-256-297-5 981-256-297-4 978-981-256-353-8 981-256-353-9.
- F. Wang and K. Sett. Time-domain stochastic finite element simulation of uncertain seismic wave propagation through uncertain heterogeneous solids. *Soil Dynamics and Earthquake Engineering*, 88:369–385, Sept. 2016. ISSN 02677261. doi: 10.1016/j.soildyn.2016.07.011. URL <http://linkinghub.elsevier.com/retrieve/pii/S0267726116300896>.
- P. H. Wirsching, T. L. Paez, and K. Ortiz. *Random vibrations: theory and practice*. Dover Publications, Mineola, NY, 2006. ISBN 978-0-486-45015-5.
- J. P. Wolf. *Dynamic soil-structure interaction*. Prentice-Hall international series in civil engineering and engineering mechanics. Prentice-Hall, Englewood Cliffs, N.J, 1985. ISBN 0-13-221565-9.

Bibliography

- A. M. Yaglom and R. A. Silverman. *An introduction to the theory of stationary random functions*. Dover, New York, 1973. ISBN 978-0-486-64688-6. OCLC: 636786365.
- Y.-B. Yang and H. H. Hung. *Wave propagation for train-induced vibrations: a finite/infinite element approach*. World Scientific, Hackensack, NJ, 2009. ISBN 978-981-283-582-6 981-283-582-2.
- N. Yoshida. *Seismic ground response analysis*. Springer Berlin Heidelberg, New York, NY, 2014. ISBN 978-94-017-9459-6.
- S. Yuan and H. Zhong. Consolidation analysis of non-homogeneous soil by the weak form quadrature element method. *Computers and Geotechnics*, 62:1–10, Oct. 2014. ISSN 0266352X. doi: 10.1016/j.compgeo.2014.06.012. URL <http://linkinghub.elsevier.com/retrieve/pii/S0266352X14001207>.
- B. A. Zeldin and P. D. Spanos. On Random Field Discretization in Stochastic Finite Elements. *Journal of Applied Mechanics*, 65(2):320, 1998. ISSN 00218936. doi: 10.1115/1.2789057. URL <http://AppliedMechanics.asmedigitalcollection.asme.org/article.aspx?articleid=1413161>.
- O. C. Zienkiewicz. Basic Formulation of Static and Dynamic Behaviour of Soil and other Porous Media. In J. B. Martins, editor, *Numerical Methods in Geomechanics*, pages 39–55. Springer Netherlands, Dordrecht, 1982. ISBN 978-94-009-7897-3 978-94-009-7895-9. URL http://www.springerlink.com/index/10.1007/978-94-009-7895-9_2.
- O. C. Zienkiewicz. *The finite element method for solid and structural mechanics*. Elsevier Butterworth-Heinemann, Amsterdam ; Boston, 6th ed edition, 2005. ISBN 0-7506-6321-9.
- O. C. Zienkiewicz, R. L. Taylor, P. Nithiarasu, and J. Z. Zhu. *The finite element method*. Elsevier/Butterworth-Heinemann, Oxford; New York, 2005a. ISBN 978-0-7506-6431-8 0-7506-6431-2. URL <http://www.sciencedirect.com/science/book/9780750664318>.
- O. C. Zienkiewicz, R. L. Taylor, and J. Z. Zhu. *The finite element method its basis and fundamentals*. Elsevier Butterworth-Heinemann, Amsterdam; Boston, 2005b. ISBN 978-0-08-047277-5 0-08-047277-X.

Appendix A

Software used

In this appendix, all software used throughout the dissertation including programming languages, libraries, programming environments, operating systems and additional software is summarized. It is very important to emphasize though that most of the software used are open source projects, are freely available and anyone can contribute to their further development.

- The finite element analyses were performed using the Solverize inhouse finite element program developed by Alexander Karatarakis and Theofilos-Ioannis Manitaras. Solverize is an extension of the finite element code AnalyzerSharp written in the C# programming language by George Stavroulakis during his PhD. However, Solverize was written entirely in the Java programming language using the latest features available in Java 8. Both the Oracle Java Development Kit (JDK) available in: <https://www.oracle.com/>, as well as the open source alternative OpenJDK available through: <http://openjdk.java.net/>, were used. Java is an object-oriented programming language that runs on a virtual machine, namely the Java Virtual Machine (JVM). It has built-in language support for multithreaded execution and offers high-level programming constructs, enabling developers to take advantage of modern multicore processor architectures and reduce computing time (Horstmann and Cornell, 2013; Urma et al., 2015).
- Commons Math <http://commons.apache.org/proper/commons-math/> is a library of lightweight, self-contained mathematics and statistics components addressing the most common problems not available in the Java programming language and was used in many essential mathematical computations in Solverize.
- Google Guava <https://github.com/google/guava> is a set of core libraries that includes new collection types (such as multimap and multiset), immutable col-

Software used

lections, a graph library, functional types, an in-memory cache and APIs/utilities for concurrency, I/O, hashing, primitives, reflection, string processing and much more. It was a main component used in Solverize.

- Eclipse <https://eclipse.org/> is the integrated development environment (IDE) of choice for Java programming.
- Git <https://git-scm.com/> is a distributed version control system and was used throughout the Solverize project development. It has been essential for successful collaboration while developing and extending Solverize, in addition to finding bugs and introducing new features to the program (McQuaid, 2015).
- The output of the stochastic finite element computations was saved in HDF5 file format <https://support.hdfgroup.org/HDF5/>. HDF5 is a data model, library, and file format for storing and managing data. It is suitable for storing array-based numerical data and offers high-performance I/O operations. The numerical data are stored in binary format which results in no accuracy loss, while the HDF5 data model offers compatibility across a variety of operating systems and hardware. Wrappers for the Java programming language are officially supported. The h5py Python package <http://www.h5py.org/> is a pythonic interface that allows interaction with HDF5 files through the Python programming language (Collette, 2014).
- The Python programming language <https://www.python.org/> was used for all statistical calculations and post-processing of the stochastic finite element output. Note that Python is a high-level dynamic programming language which is easy to learn, while offering many useful software components in its standard library (Beazley, 2013; Gorelick and Ozsvald, 2014; Phillips, 2010; Ramalho, 2015; Slatkin, 2015; Summerfield, 2014).
- Python was combined with Numpy <http://www.numpy.org/>, the de facto standard Python package for scientific computing with arrays.
- Scipy was also used <https://www.scipy.org/>, which works aside Numpy offering many mathematical routines used in scientific computing.
- Matplotlib was also used <http://matplotlib.org/> to produce the plots and figures of the PhD dissertation. Furthermore, using Seaborn <http://seaborn.pydata.org/> on top of Matplotlib gives better quality plots especially for visualizing statistical data.

-
- Pandas <http://pandas.pydata.org/> offers high level data-structures and operations for data analysis with Python.
 - Jupyter <http://jupyter.org/> has been an additional tool allowing for interactive computing and visualization essential for scientific research, whenever alternative numerical recipes, algorithms and clear perspective of data were needed.
 - Paraview <http://www.paraview.org/> is a high performance parallel visualization software based on the Visualization Toolkit (VTK) <http://www.vtk.org/>, Schroeder et al. (2006). It was used to visualize all the finite element models and their resulting time dependent response.
 - Inkscape <https://inkscape.org/en/> was the software of choice for high quality vector drawings for this dissertation, as well as scientific articles and conference presentations.
 - During the present PhD dissertation, the author has also used Windows, Linux, macOS operating systems, while all the software mentioned above are able to work in all these operating systems.

Appendix B

Validation of the software used

In order to validate the correctness and accuracy of the in-house finite element suite **Solverize**, a 1D benchmark problem of coupled soil consolidation is simulated. Specifically, the problem corresponds to the example program 9.3 studied in (Smith and Griffiths, 2004) and thus, a comparison between the resulting settlements and excess pore pressures between **Solverize** and the ones supplied with the finite element code provided in (Smith and Griffiths, 2004) is made.

The finite element mesh is shown in fig. B.1 and consists of 4 quadrilateral 8-node plane strain elements with equal edges of 0.25 m for a total model height of 1.00 m . Note that all element nodes have displacement degrees of freedom (u), while only the four vertices contain pore pressure dofs (p). Young's modulus, as well as permeability of the soil, have unit values, i.e. $E = 1.0$ and $k/\gamma_w = 1.0$ and Poisson's ratio $\nu = 0.0$. A ramp load p , increasing linearly from 0.0 to $p_{max} = 1.0$ at time $t_0 = 0.5$ and then remaining constant is applied at the top edge of the model. The timestep chosen is $\Delta t = 0.01$ and a total number of 300 timesteps is used. The vertical sides of the model are constrained with respect to horizontal displacements, whereas the bottom of the model is fixed. Finally, the hydraulic boundary conditions consist of undrained conditions at the bottom and the sides of the model, while free drainage is allowed at the top edge of the mesh.

In fig. B.2, the vertical settlement of node 1 and the excess pore pressure of node 21 are illustrated. It is therefore clear that, the results obtained by **Solverize** are in perfect agreement with the corresponding ones calculated by the finite element code supplied in (Smith and Griffiths, 2004), confirming the accuracy and correctness of our in-house developed software.

Validation of the software used

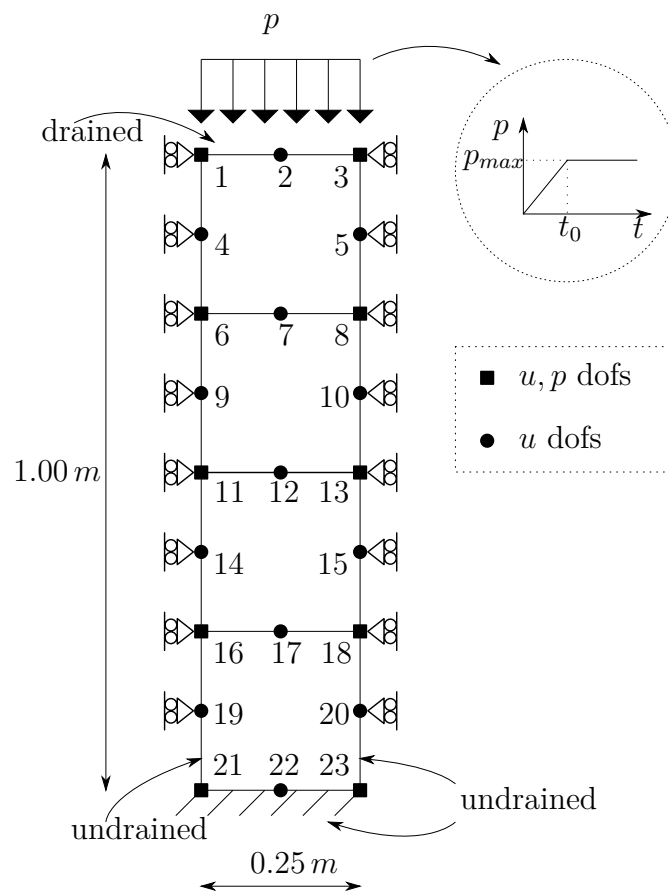


Figure B.1. Finite element mesh of the model.

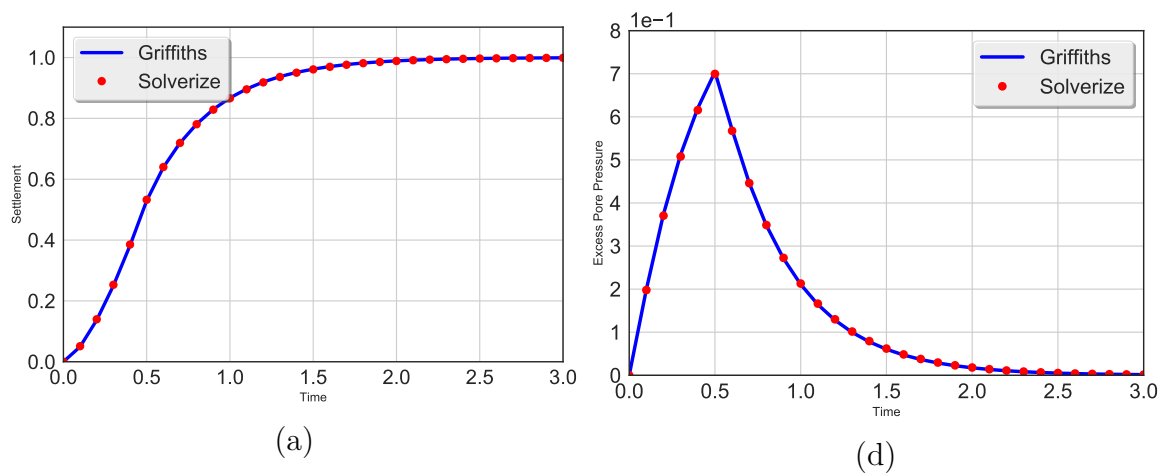


Figure B.2. Comparison between the results obtained by **Solverize** and (Smith and Griffiths, 2004) for a benchmark 1D consolidation problem, where: (a) Vertical displacement of node 1 and (b) Excess pore pressure of node 21.